Earth Observation-Based Operational Estimation of Crop Water Requirements in a Mediterranean context

Politecnico di Bari

Department of Civil, Environmental, Land, Construction and Chemistry

RISK AND ENVIRONMENTAL, TERRITORIAL, AND BUILDING DEVELOPMENT PhD Program

SSD: ICAR/02 – HYDRAULIC STRUCTURES, MARITIME ENGINEERING AND HYDROLOGY

Earth Observation-Based Operational Estimation of Crop Water Requirements in a Mediterranean context

---

Peschechera Giuseppe

Referees:

Prof. Juan Antonio Rodríguez Díaz

Prof. Ioannis L. Tsirogiannis

Supervisors:

Prof. Umberto Fratino

Prof. Nicola Lamaddalena

Prof. Miguel Ángel Moreno Hidalgo

Coordinator of PhD Program:
Prof. Michele Mossa

Course n. 33, 01/11/2017-31/12/2020

LIBERATORIA PER L'ARCHIVIAZIONE DELLA TESI DI DOTTORATO

Al Magnifico Rettore
Del Politecnico di Bari

Il sottoscritto PESCHECHERA GIUSEPPE nato a MILANO il 12/01/1990 residente a TRANI in via DELLE FORZE ARMATE 2/E e-mail giuseppe.peschechera@poliba.it iscritto al 3° anno di Corso di Dottorato di Ricerca in RISCHIO, SVILUPPO AMBIENTALE, TERRITORIALE ED EDILIZIO ciclo XXXIII ed essendo stato ammesso a sostenere l'esame finale con la prevista discussione della tesi dal titolo: "**Earth Observation-Based Operational Estimation of Crop Water Requirements in a Mediterranean context"**

DICHIARA

1) di essere consapevole che, ai sensi del D.P.R. n. 445 del 28.12.2000, le dichiarazioni mendaci, la falsità negli atti e l'uso di atti falsi sono puniti ai sensi del codice penale e delle Leggi speciali in materia, e che nel caso ricorressero dette ipotesi, decade fin dall'inizio e senza necessità di nessuna formalità dai benefici conseguenti al provvedimento emanato sulla base di tali dichiarazioni;
2) di essere iscritto al Corso di Dottorato di ricerca RISCHIO, SVILUPPO AMBIENTALE, TERRITORIALE ED EDILIZIO ciclo XXXIII, corso attivato ai sensi del "*Regolamento dei Corsi di Dottorato di ricerca del Politecnico di Bari"*, emanato con D.R. n.286 del 01.07.2013;
3) di essere pienamente a conoscenza delle disposizioni contenute nel predetto Regolamento in merito alla procedura di deposito, pubblicazione e autoarchiviazione della tesi di dottorato nell'Archivio Istituzionale ad accesso aperto alla letteratura scientifica;
4) di essere consapevole che attraverso l'autoarchiviazione delle tesi nell'Archivio Istituzionale ad accesso aperto alla letteratura scientifica del Politecnico di Bari (IRIS-POLIBA), l'Ateneo archivierà e renderà consultabile in rete (nel rispetto della Policy di Ateneo di cui al D.R. 642 del 13.11.2015) il testo completo della tesi di dottorato, fatta salva la possibilità di sottoscrizione di apposite licenze per le relative condizioni di utilizzo (di cui al sito http://www.creativecommons.it/Licenze), e fatte salve, altresì, le eventuali esigenze di "embargo", legate a strette considerazioni sulla tutelabilità e sfruttamento industriale/commerciale dei contenuti della tesi, da rappresentarsi mediante compilazione e sottoscrizione del modulo in calce (Richiesta di embargo);
5) che la tesi da depositare in IRIS-POLIBA, in formato digitale (PDF/A) sarà del tutto identica a quelle **consegnate**/inviate/da inviarsi ai componenti della commissione per l'esame finale e a qualsiasi altra copia depositata presso gli Uffici del Politecnico di Bari in forma cartacea o digitale, ovvero a quella da discutere in sede di esame finale, a quella da depositare, a cura dell'Ateneo, presso le Biblioteche Nazionali Centrali di Roma e Firenze e presso tutti gli Uffici competenti per legge al momento del deposito stesso, e che di conseguenza va esclusa qualsiasi responsabilità del Politecnico di Bari per quanto riguarda eventuali errori, imprecisioni o omissioni nei contenuti della tesi;
6) che il contenuto e l'organizzazione della tesi è opera originale realizzata dal sottoscritto e non compromette in alcun modo i diritti di terzi, ivi compresi quelli relativi alla sicurezza dei dati personali; che pertanto il Politecnico di Bari ed i suoi funzionari sono in ogni caso esenti da

responsabilità di qualsivoglia natura: civile, amministrativa e penale e saranno dal sottoscritto tenuti indenni da qualsiasi richiesta o rivendicazione da parte di terzi;

7) che il contenuto della tesi non infrange in alcun modo il diritto d'Autore né gli obblighi connessi alla salvaguardia di diritti morali od economici di altri autori o di altri aventi diritto, sia per testi, immagini, foto, tabelle, o altre parti di cui la tesi è composta.

Bari, 25/02/2021 Firma 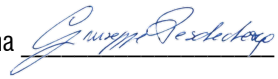

Il sottoscritto, con l'autoarchiviazione della propria tesi di dottorato nell'Archivio Istituzionale ad accesso aperto del Politecnico di Bari (POLIBA-IRIS), pur mantenendo su di essa tutti i diritti d'autore, morali ed economici, ai sensi della normativa vigente (Legge 633/1941 e ss.mm.ii.),

CONCEDE

- al Politecnico di Bari il permesso di trasferire l'opera su qualsiasi supporto e di convertirla in qualsiasi formato al fine di una corretta conservazione nel tempo. Il Politecnico di Bari garantisce che non verrà effettuata alcuna modifica al contenuto e alla struttura dell'opera.
- al Politecnico di Bari la possibilità di riprodurre l'opera in più di una copia per fini di sicurezza, back-up e conservazione.

Bari, 25/02/2021 Firma 

EXTENDED ABSTRACT

Irrigation is essential for global agricultural production and food security since irrigated land represents 20% of the world's cultivated area but supply about 40% of the world's food production. Even if agriculture is the greatest consumer of water (it is estimated that over 70 % of global freshwater is consumed by irrigation) and irrigation represents the most important intervention on the hydrological cycle, we have only partial knowledge on the areas irrigated and on the amount of water applied.

Currently, agriculture is facing a great dilemma: on the one hand, a growing world population demands more food and biomass. On the other hand, natural resources (such as water) are only available in limited quantities and their excessive use often leads to the degradation of ecosystems, which in turn has adverse effects on agricultural production and local livelihoods. Thus, efficient agricultural water management is a major issue that even more involves not only in traditionally water-scarce regions. However, water use rationalization is especially needed for regions suffering from water scarcity and that probably would suffer from water restrictions according to climate change scenarios. The Mediterranean region is one of these areas and is considered of the most prominent "hot spots" in future climate change projection. Here are expected larger warming than the global average and a pronounced increase in precipitation interannual variability which will lead to a further reduction of resources available and to exacerbate the conflicts among users and sectors for the use of the resources.

To enable sustainable water management two measures are necessary:

- Water demand and availability at the regional level must be known to identify possible overuse and adjust water allocation rights.
- Adopt intelligent irrigation management, which reduces water losses to the minimum, providing the right amount of water at the right time.

The present work demonstrates as in both aspects, investigated the possibility offered by the present Remote Sensing (RS) model and dataset to estimate the Crop Water Requirements (CWR) and the Irrigation Water Requirements (IWR) at different

temporal and spatial scale. The EO-based FAO-PM method was selected and adopted to estimate in an operative way the CWR using a combination of in situ classical agro-meteorological data with optical RS-derived crop biophysical parameters. The application of the method over two different test site and over both herbaceous and woody crops highlighted the necessity of adjustment to consider the actual (and not the potential or standard) status of the crops considering the water deficit condition.

The adjusted EO-based FAO-PM, in combination with the use of Sentinel2-derived information (Leaf Area Index and Surface Albedo), demonstrates its ability to retrieve at field scale CWR coherent with the international adopted FAO-PM method. The procedure was then extended to the CWR estimation at the irrigation district scale.

Lastly, the retrieved CWR information was used to estimate the extension of the irrigated areas and the irrigation volume applied both at field and irrigation district-scale over the two selected study area.

key words Irrigation Water Accounting; Irrigation Water Management; Penman-Monteith; Remote Sensing.

CONTENTS

INTRODUCTION

Background and Research motivation

Irrigation is essential for global agricultural production and food security since irrigated land represents 20% of the world's cultivated area but supply about 40% of the world's food production. Even if agriculture is the greatest consumer of water (it is estimated that over 70 % of global freshwater is consumed by irrigation) and irrigation represents the most important intervention on the hydrological cycle, we have only partial knowledge on the areas irrigated and on the amount of water applied.

Currently, agriculture is facing a great dilemma: on the one hand, a growing world population demands more food and biomass. On the other hand, natural resources (such as water) are only available in limited quantities. Moreover, excessive use often leads to the degradation of ecosystems, which in turn has adverse effects on agricultural production and local livelihoods. Thus, efficient agricultural water management is a major issue that even more involves not only in traditionally water-scarce regions. However, water use rationalization is especially needed for regions suffering from water scarcity and that probably would suffer from water restrictions according to climate change scenarios. The Mediterranean region is one of these areas and is considered of the most prominent "hot spots" in future climate change projection. Here are expected larger warming than the global average and a pronounced increase in precipitation interannual variability which will lead to a further reduction of resources available and to exacerbate the conflicts among users and sectors for the use of the resources.

The present work demonstrates the possibility offered by remote sensing to the two fundamentals measures necessary to enable sustainable water management:

- Mapping the water demand and availability at the regional level to identify possible overuse and adjust water allocation rights.

- Adopt intelligent irrigation management, which reduces water losses to the minimum, providing the right amount of water at the right time.

General and specific objectives

The aim of the entire work is to develop and test an operative remote sensing-based method to determine Crop and Irrigation Water Requirements in the Mediterranean context which is typically characterized by:

- Arid or semi-arid climate conditions.
- Water scarcity, which leads the farmers to apply deficit irrigation strategies.
- A high fragmented and heterogeneous landscape

Since the overall objective requires an *operative* approach to the problem, the specific criteria used for the model's design are:

- easy implementation
- modularity which leads the possibility to apply the model at different temporal and spatial scales
- limited (and even no) use of crop-specific parameters, since they are depending on a large number of crop-climate combinations that can be described only by expensive field measurements. Moreover, in this way it is possible to use the ET model also in contexts where a detailed and updated crop map is not available.
- representativity of the actual crop conditions considering the crop development stage and status.
- coherent with the internationally adopted FAO standards for Crop Water Requirements (CWR) and Irrigation Water Requirements (IWR) estimation. The procedure overpasses the two biggest weakness of the FAO's procedures:
    1. the necessity of a crop map.
    2. considers the actual condition instead of the "standard" optimal condition.

The primary objective was achieved through the following sub-objectives:

- Define optimal trade-off in terms of spatial, temporal and, spectral resolution, of the satellite data for CWR assessment
- Select and test the most suitable RS-based method for the ET estimation in the Mediterranean context

Research questions

The following research questions are formulated to achieve the above objective:

- What are the characteristics (in term of temporal, spatial, spectral resolution) that the satellite data should have to be applied for the CWR estimation and monitoring?
- Which category of existing RS-method is the most appropriate for the CWR estimation (at different spatial scales) in the Mediterranean context?
- It is possible to use the RS-derived CWR to estimate the IWR over heterogeneous and fragmented landscape as the Mediterranean context?

Hypothesis

- The existing assessment method for the CWR estimation can be improved using remote sensing data.
- Optical satellite data can be used for the estimation of the actual evapotranspiration.

Structure of the thesis

The first Chapter introduces and describes theoretically the main processes and components of the soil water balance for agriculture applications: evapotranspiration and irrigation. Since efficient agricultural water management requires reliable estimation of the Crop and Irrigation Water Requirements, particular attention is dedicated to the descriptions of the different methods for the evapotranspiration and irrigation estimation using both in-situ and RS-derived data.

Among the methods for retrieving the ET using RS-derived data available in the literature, the “one-step” FAO-56 method was retained as the most suitable procedure

for the CWR's estimation in an operative way and over large areas in a Mediterranean semi-arid context characterized by a very fragmented and heterogeneous landscape with a mosaic of rainfed and irrigated crops. Chapter 2 describes the internationally accepted standard FAO Penman-Monteith (FAO-PM) method and the possibility offered by the EO-based "one-step" approach to use a combination of in-situ meteorological data with crop characteristics as retrieved from optical satellite images directly integrated into the P-M equation to estimate the (potential) crop ET also over large areas. Together with the full description of the method and its applications, are presented both its mains advantages and limitations.

In Chapter 3 were described the improvements operated on the EO-based "one-step" approach for retrieve, instead of the potential crop ET, an estimation of the ET coherent with the values of ET retrieved using the classical "two-steps" approach using literature Kc's values. The overall scope of the modified method is to determine the crop water requirements in an operative way and over large areas in a context of a very fragmented and heterogeneous landscape with a mosaic of rainfed and irrigated crops. Moreover, the intent was to develop a method that can work over different crop types (both full cover herbaceous and sparse woody crops) without the necessity of adjustments of the model's parameter for each crop class. In this way is possible to use the model also in a context where the crop/land cover map is not available and/or updates. To address this objective were analysed the two resistance terms of the PM equation: the aerodynamic and surface resistance.

Chapter 4 provides a full and detailed description of the input data and the step-by-step procedure to handle the "one-step" FAO-56 RS-based method using as input the biophysical variables retrieved from the Sentinel-2 (S-2) satellites. Moreover, to justify the use of the S-2 derived products, a brief description of the mission and of characteristics of the data is provided.

The prosed methodology was then applied, in Chapter 6, for the estimation of the Crop Water Requirements at both plot and irrigation district-scale over the selected study areas described and characterized in the previous Chapter 5. In absence of direct field measurements of evapotranspiration, the CWR estimated were compared with the CWR estimated adopting the classical FAO-56 Kc approach (also called the "two-steps" approach).

Finally, in Chapter 7, the estimated CWR was used to feed a simple FAO56-based Soil Water Balance to estimate the Irrigation Water Requirements (IWR) at both plot and irrigation district scale. The estimates IWR were compared with the metered volumes applied by the framers.

1. CROP AND IRRIGATION WATER REQUIREMENT ASSESSMENT: THE FIRST STEP FOR SUSTAINABLE WATER MANAGEMENT

Overview

The determination of water fluxes at the Soil-Plant-Atmosphere (SPA) interface is of fundamental interest for agro-hydrological management purposes especially for irrigation planning and crop water stress monitoring both at the field and regional scales. A complete description of these fluxes can be done by analysing the soil water balance which can also quantify the processes and interaction of the SPA system.

This chapter introduces and describes theoretically the main processes and components of the soil water balance for agriculture applications: evapotranspiration and irrigation. Since efficient agricultural water management requires reliable estimation of the Crop Water Requirements (CWR - represented by the ET losses) and the corresponding Irrigation Requirement to meet CWR complementary to rainfall, particular attention is dedicated to the descriptions of the different methods for the evapotranspiration and irrigation estimation using both in-situ and RS-derived data.

1.1. Soil water balance components

The water balance computation consists in describing the evolution of the stock of water available in the root zone soil. Schematically, the root zone can be presented using a container in which the water content may fluctuate. A common and useful way to express the water content in terms of root zone depletion because it makes the adding and subtracting of losses and gains straightforward as the various parameters of the soil water budget are usually expressed in terms of water depth. Rainfall (P), irrigation (I) and capillary rise (CR) of groundwater towards the root zone add water to the root zone and decrease the root zone depletion. ET and percolation losses (DP) remove water from the root zone and increase the depletion. The daily water balance, expressed

in terms of depletion at the end of the day (i) with referment to the root zone at the end of the previous day (i-1), is expressed by Equation (1).

$$D_{r,i} = D_{r,i-1} - (P - RO)_i - I_i - CR_i + ETc_i + DP_i \quad (1)$$

Since it is often very difficult to accurately measure all terms of Eq. (1), some simplifications are generally made considering the standard conditions for agricultural application and looking for the local condition in term of soil depth, slope, permeability and surface storage. CR can normally be assumed to be zero when the water table is more than about 1 m below the bottom of the root zone (Allen et al., 1998). Deep percolation, which is a major unknown of Eq. (1) can be neglected in dry regions, as suggested by some researchers (Maselli et al., 2020). Lastly, also the RO term could be neglected for application over flat terrain, a condition that prevails in many agricultural regions, but here the decision should be considered also the characteristics of precipitation (amount, duration and intensity), the type of soil (and in particular its hydraulic conditions and antecedent moisture content) and the land use and cover. Generally, the impact of the runoff component can be ignored, otherwise, RO can be predicted using standard procedures from hydrological literature. Under these hypotheses, the daily water balance of Eq. (1) can assume the following simplified form:

$$D_{r,i} = D_{r,i-1} - P_i - I_i + ETc_i \quad (2)$$

The precipitation term can be estimated from a network of rainfall stations (rain gauge measurements) or weather radar data. Therefore, the evapotranspiration and irrigation terms become the key terms of the water balance equation.

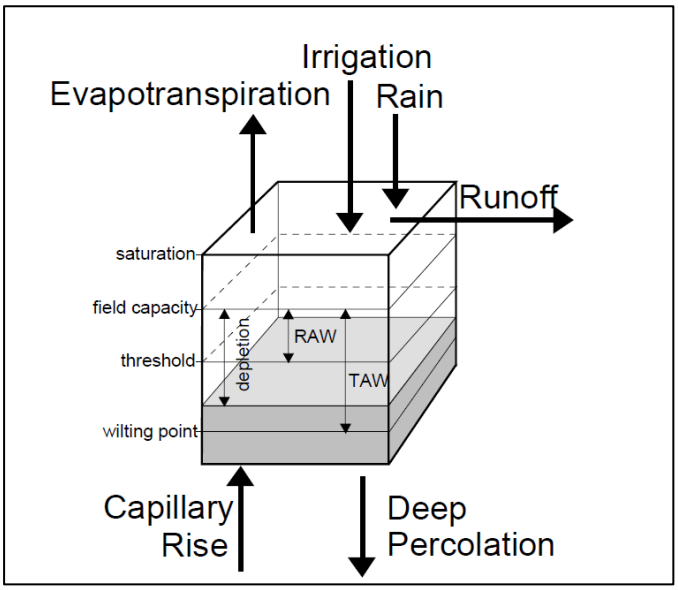

Figure 1.1. Water balance of the root zone (Source: Allen et al. (Allen et al., 1998)).

The soil water content can fluctuate between the soil *Field Capacity* (FC) and the permanent wilting point (WP) in the root zone. The FC (or drained upper limit) is defined as the water content of a soil that has reached equilibrium with gravity after several days of drainage. When the root zone is at FC, following heavy rain or irrigation, the minimum value for the depletion $Dr_{,i}$ is zero. As a result of percolation and evapotranspiration, the water content in the root zone will gradually decrease and the root zone depletion will increase. In the absence of any wetting event, the water content will steadily reach its minimum value. The WP (or lower limit of available water) is defined as the water content at which plants can no longer extract a sustainable quantity of water from the soil and begin to wilt. At that moment, no water is left for evapotranspiration in the root zone, and the root zone depletion has reached its maximum value. Typical suction values associated with the FC and WP are -3.3 kPa (-0.33 bars) and -1500 kPa (-15 bars) respectively. Like water content, FC and WP are defined as a volume of water per volume of soil.

The limits imposed on $D_{r,i}$ consequently range between:

$$0 \leq D_{r,i} \leq TAW \tag{3}$$

Where TAW represents the Total Available soil Water in the root zone. Although water is theoretically available until WP, the crop water uptake is reduced before the wilting point is reached because, as the soil water content decreases, water becomes more strongly bound to the soil matrix and is more difficult to extract. When the soil water content drops below a threshold value, soil water can no longer be transported quickly enough towards the roots to respond to the transpiration demand and the crop begins to experience stress. The fraction of TAW that a crop can extract from the root zone without suffering water stress is the Readily Available soil Water (RAW). The fraction of TAW that can be depleted from the root zone before moisture stress identified whit the factor *p* into the FAO-56 Soil Water Balance model, differs from one crop to another.

$$RAW = p * TAW \tag{4}$$

After the root zone depletion exceeds RAW, the crop starts to suffer water stress even more severe as the soil water content decreases. The root zone depletion is high enough to limit evapotranspiration to less than potential values and the crop evapotranspiration begins to decrease in proportion to the amount of water remaining in the root zone. The rate of water stress can be estimated by introducing the *water stress coefficient* (Ks), a dimensionless transpiration reduction factor dependent on available soil water:

$$K_s = \frac{TAW - D_r}{TAW - RAW} = \frac{TAW - D_r}{(1-p)\,TAW} \tag{5}$$

The Ks ranging between 0 and 1: for soil water limiting conditions, $Ks < 1$ while when there is no soil water stress, $Ks = 1$.

1.2. Evapotranspiration

After precipitation, evapotranspiration (ET) is one of the most significant components in terrestrial water budget and describes the transport of water into the atmosphere as the sum of water leaving the land surface and entering the atmosphere from soil, vegetation, and water surfaces through Evaporation (E) and from a vegetation canopy via Transpiration (T) (Hu et al., 2015). ET estimations are required for a wide range of problems in hydrology, land and water management (water balance, floods, and droughts), and studies on global and regional climate change and biogeochemical processes and cycles (Hu et al., 2015; Jung et al., 2019). Monitoring the spatial and temporal distribution of ET is critically important for water management, particularly in water-scarce regions (Gowda et al., 2008).

Since evaporation from soil and transpiration by the plant occur simultaneously and constitute the majority of the ET (especially for agriculture applications), the term evapotranspiration is used to describe the total loss of water from vegetated land surfaces to the atmosphere. *Crop Water Requirement* (CWR) refers to the water transpired by the plant, the water evaporated from the soil and the water stored by the plant for its metabolic processes. Since the water used for the plant metabolism is substantially negligible as compared to E and T, the term CWR is frequently alternative to evapotranspiration in standard/optimum conditions. Although the values for ETc and CWR are identical, crop evapotranspiration refers to the amount of water that is evaporated and transpired while CWR refers to the amount of water that needs to be available in the soil for making such crop consumption possible. The CWR always refers to a crop grown under optimal conditions and thus reaches its full production potential under the given environment and can be supplied to the crops by rainfall, by irrigation or by a combination of irrigation and rainfall.

ET plays a key role in the redistribution of water and energy at the soil–vegetation–atmosphere interface, and due to its complex interactions, it is considered the most difficult and complicated component of the hydrologic cycle to model (Xu and Singh, 2005) because of the complex controlling factors and heterogeneity of landscape (McCabe et al., 2016). Evaporation and transpiration occur simultaneously and both processes depend on several factors. Allen et al. (Allen et al., 1998) regrouped

and schematized these factors into three classes: weather parameters, crop characteristics, management, and environmental aspects (Figure 1.2).

The principal weather parameters affecting evapotranspiration are solar radiation, air temperature and humidity, and wind speed. While the energy supply from the sun and the surrounding air is the main driving force for the vaporization of water, the difference between the water vapour pressure at the evapotranspiring surface and the surrounding air is the determining factor for the vapour removal which depends to a large extent on wind and air turbulence which transfers large quantities of air over the evaporating surface. Several procedures have been developed to assess the evaporation rate from these parameters. The evaporation power of the atmosphere is expressed, adopting a standardized vegetated surface, by the *reference crop evapotranspiration* (ETo).

Transpiration rate is also influenced by crop characteristics, environmental aspects, and cultivation practices: different kinds of plants may have different transpiration rates. The crop type, variety and development stage should be considered when assessing the evapotranspiration from crops grown in large, well-managed fields. Differences in resistance to transpiration, crop height, crop roughness, reflection, ground cover and crop rooting characteristics result in different ET levels in different types of crops under identical environmental conditions. Crop *evapotranspiration under standard conditions* (ETc) refers to the evaporating demand from crops that are grown in large fields under optimum soil water, excellent management, and environmental conditions, to achieve full production under the given climatic conditions.

Following the procedure proposed by FAO-56 guidelines, reference and standard evapotranspiration are linked by the *crop coefficient* (Kc) and the following relation (Allen et al., 1998):

$$ET_c = K_c \, ET_o \tag{6}$$

Thanks to the Kc it is possible considering all the biophysical differences between the standard crop adopted for the definition of the standard ET and the specific crop or natural vegetation considers.

Moreover, it is necessary to consider other factors that can limit crop development and reduce evapotranspiration. Among these possible factors, there are the management and environmental aspects such as soil salinity, poor land fertility, limited application of fertilizers, the presence of hard or impenetrable soil horizons, the absence of control of diseases and pests and poor soil management. Other factors to be considered when assessing ET are ground cover, plant density and the soil water content. The effect of soil water content on ET is conditioned primarily by the magnitude of the water deficit and the type of soil. On the other hand, too much water will result in waterlogging which might damage the root and limit root water uptake by inhibiting respiration.

The effects of soil water availability on (evapo)transpiration can be estimated by allowing a reduction of the crop coefficient by the crop stress coefficient (Ks). In this way the ETc adjusted for water stress, and management and environmental constraints can be estimated as:

$$ET_{c,adj.} = K_c \, K_s \, ET_o \tag{7}$$

When assessing the ET rate, additional consideration should be given to the range of management practices that act on the climatic and crop factors affecting the ET process. Cultivation practices and the type of irrigation method can alter the microclimate, affect the crop characteristics, or affect the wetting of the soil and crop surface. For example, a windbreak reduces wind velocities and decreases the ET rate of the field directly beyond the barrier. The effect can be significant especially in windy, warm, and dry conditions although evapotranspiration from the trees themselves may offset any reduction in the field. Soil evaporation in a young orchard, where trees are widely spaced, can be reduced by using a well-designed drip or trickle irrigation system. The drippers apply water directly to the soil near trees, thereby leaving a major part of the soil surface dry and limiting the evaporation losses. The use of mulches, especially when the crop is small, is another way of substantially reducing soil evaporation. Anti-transpirants, such as stomata-closing, film-forming or reflecting material, reduce the water losses from the crop and hence the transpiration rate.

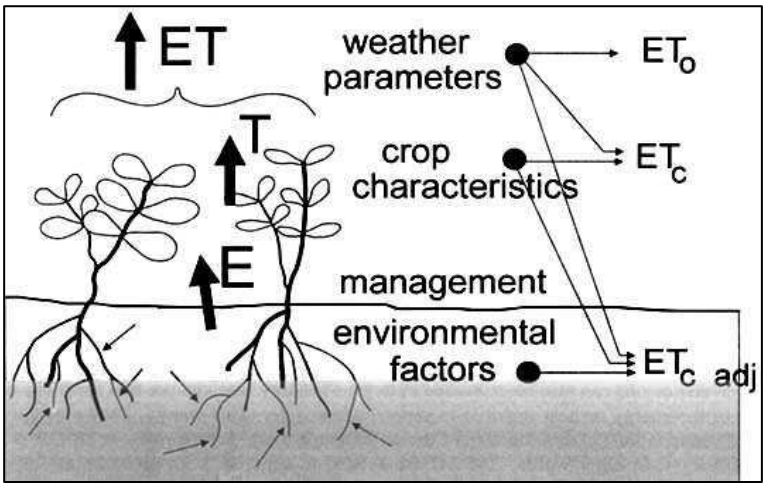

Figure 1.2 Factors affecting the Evapotranspiration process.

1.2.1. Evapotranspiration from orchards

The ETc from an orchard is more complex than from a uniform herbaceous crop because different components contribute to the water loss from an orchard (Steduto et al., 2012). In addition to tree transpiration (Tr), there could be transpiration losses from a cover crop or from weeds (Tr_{cc}), and there are E losses from the soil. In the case of micro-irrigation, two E has two components: one is the E from the soil areas wetted by the emitters, and the other is the E from the rest of the soil surface which is only wetted by rainfall (respectively E_{wz} and E_{dz}).

$$ET_c = Tr + Tr_{cc} + E_{wz} + E_{dz} \quad (8)$$

This method needs to estimate the four ETc components and therefore is not yet widely used. In general, orchards with cover crops have higher ET rates than orchards that are cleanly cultivated but the water-use rate of cover crops in orchards is difficult to measure and has not been thoroughly investigated. Either cover crops are planted in strips of variable width between tree rows or, sometimes, weeds can grow in these areas if not controlled periodically by cutting or with herbicides. Instead, as there are now methods available to measure tree Tr independently of ETc. Several factors affect the seasonal Tr values of mature orchards or vineyards well supplied with

water. In addition to the level of intercepted radiation, whether the species is deciduous or evergreen, the stomatal responses to the environment, the presence or absence of fruit, are factors that influence the Tr, and even some cultivar differences within a species have been described. If it is not possible to calculate Tr separately, is possible to use the overall crop coefficient (Kc) that embodies all the components of ETc.

1.3.ET estimation methods

Three biophysical processes in the Earth system are significantly affected by ET (Figure 1.3) and thus have been exploited to estimate ET:

1. Land Surface Energy Balance (SEB): the basic physics of determining water use is the principle of energy conservation at the evaporating surface. Evapotranspiration is a process governed by energy exchange at the vegetation surface and is limited by the amount of energy available either in the form of sensible heat or radiant energy. Thanks to this limitation, it is possible to predict the evapotranspiration rate by applying the principle of energy conservation.

$$(R_n - G) - \lambda ET - H = 0 \quad (9)$$

The energy arriving at the surface, the *net radiation* (R*n*), must equal the energy leaving the surface for the same period constituted by the *sensible heat* (H), the *soil heat flux* (G) and the latent heat flux (λET). λET representing the evapotranspiration fraction can be derived from the energy balance equation if all other components are known. While the net radiation and the soil heat fluxes can be measured or estimated from climatic parameters, measurements of the sensible heat are complex and cannot be easily obtained because requires measurement of temperature gradients above the surface. It is important to notice that only vertical fluxes are considered in Equation (9) and the net rate at which energy is being transferred horizontally, by advection, is ignored. Therefore, the equation is to be applied to large, extensive surfaces of homogeneous vegetation only. Moreover, in Equation (9) other energy terms, such as heat stored or released in the plant, or the energy

used in metabolic activities, are not considered because they account for only a small fraction of the daily net radiation and can be considered negligible when compared with the other four components.

2. Soil water balance: the soil moisture balance equation, based on the mass conservation equation, is “likely to be the fundamental equation in hydrology” (Rodriguez-Iturbe, 2000) and was yet described in the previous Paragraph 1.1.

3. Plant growth and the carbon cycle: plant transpiration depends on the leaf level energy balance and the leaf area, and it is controlled by stomatal conductance. The dependence of the latter on environmental conditions can be cast in the form of semi-empirical relationships and used to parameterize leaf-level fluxes of water and carbon dioxide and biomass accumulation by photosynthesis (Jarvis et al., 1976).

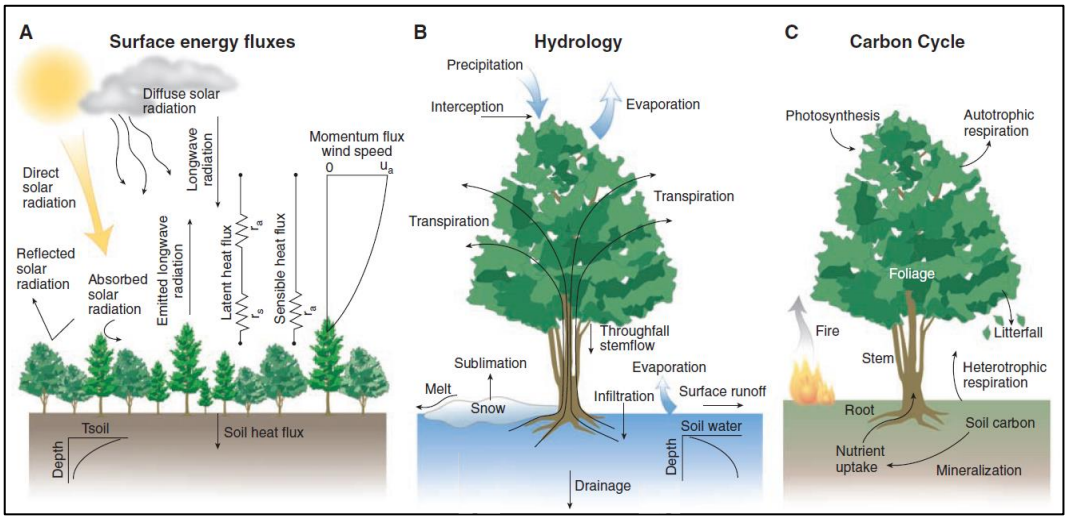

Figure 1.3. Biophysical processes in the Earth system are significantly affected by ET (Source: (Bonan, 2008), adapted).

The land surface energy balance is considered in all cases as a constraint, cast often in the form of the Penman-Monteith combination equation, or a simplified form of it (Jia et al., 2018). Independently of the biophysical process, a measure must be established

of the reduction in the rate of evapotranspiration below the maximum rate under unrestricted water availability, given radiative and boundary layer forcing.

1.4.In-situ direct measurements of ET

Hydrological approach: Weighing lysimeters

Weighing lysimeters have been developed to give a direct measurement of ET exploiting the principle of mass conservation. The lysimeter is a tank or container (of many different possible designs, sizes and, shapes) able to define the lateral and deep-water movement across a boundary (Allen et al., 1991). The main advantage of the lysimeter is that water consumption of vegetation can be performed based on the direct measurement of mass. However, a lysimeter measurement requires elaborate preparation and its application is typically limited to only a few individual trees or a small surface area of crops (Verstraeten et al., 2008). Majors limitation of lysimeters are the root extension is sometimes limited and that the capillary rise is not taken into consideration because the water table can be supposed to be at a considerable depth.

Plant physiology approaches

Methods based on plant physiology either measure the water loss from a whole plant or a group of plants. The two the most common methods of this category are:

1. the *sap flow method* can measure only plant transpiration using two possible simple accurate basic methods: the *heat pulse* and the *heat balance*. The heat balance method is the most popular sap flow method to estimate the plant transpiration by determining the sap mass flow using gauges that are attached to or inserted in the plant stem as proposed by Čermák et al. (Čermák et al., 1973) and improved by Steinberg et al. (Steinberg et al., 1990). While, in the heat balance method, a heater element is placed around the plant stem to provide energy to the system and thermocouples are used to determine how much heat is lost by conduction up, down, and radially in the stem from the heater element. The difference between the heat input and these losses is assumed to be

dissipated by convection with the sap flow up the stem and may be directly related to water flow.

Sap flow methods are a good alternative to lysimeter experiments, but the operation of sap-flow sensors requires a vast technical input and maintenance effort.

2. The *chamber system method* was described for the first time by Reicosky and Peters (Reicosky and Peters, 1977). The ET rate was calculated as a difference (latent heat storage) between two measurements by a psychrometer: one acquisition before the chamber was lowered on the plot and another one minute later. Chambers system is easier to implement than the weighing lysimeter, but it is not suitable for long term ET measurements. The most serious problem of almost all chambers is the microclimate modification during the measurement period.

Micrometeorological approaches

Micrometeorological methods require accurate measurements of meteorological parameters with high temporal resolution and their accuracy depends on the validity of some hypothesis (such as the flux conservation) which implies that measurements are performed over a large flat area with uniform vegetation. In this category of methods are included:

1.1. Aerodynamic method

Assuming that a flux density can be related to the gradient of the concentration in the atmospheric surface layer, the latent heat flux by the aerodynamic technique can be determined directly utilizing measurements of the vapour pressure at different heights above the crop. The major difficulty with this technique is the correct measurement of the vapour pressure. For this reason, latent heat flux can be derived indirectly by the energy balance where the sensible heat flux can be determined by the flux-gradient relation for temperatures. In this way, it is possible to avoid complex high-frequency humidity measurements,

but the obtained accuracy depends on the number of measurement levels for wind speed and temperature profiles (Wiernga, 1993).

1.2. *Eddy covariance*

The transport of vapour, heat, carbon dioxide (CO_2) and momentum in the lower atmosphere in contact with the canopies is mostly governed by air turbulence. The eddy covariance (EC) method is considered as the standard method for measuring surface turbulent fluxes to get the surface fluxes of sensible and latent heat and of (CO_2) with high accuracy (Dyer, 1961), and very good performances both at hourly and daily scale, also in semi-arid environments (Er-Raki et al., 2009).

The EC method requires the synchronized acquisition of vertical wind fluctuations (measured by the sonic anemometer) and vapour density fluctuations (by fast response hygrometer with a typical frequency of 10–20 Hz. Despite problems linked to the correct management of the sensors, complex data processing, and the management of 'closure error' of the energy balance of about 10-30% (Foken, 2008).

1.3. Scintillometer

Aerodynamic and eddy covariance methods can be applied only on small homogeneous surfaces and therefore large-scale turbulent fluxes are difficult to evaluate because the heterogeneity of most landscapes generates large flux variability, which is difficult to measure with the conventional techniques. Among the techniques developed to indirect turbulent flow measurement, the most promising and widely used is the scintillometery (Brunsell et al., 2011). Scintillometer consists of a transmitter and a receiver at both ends of an atmospheric propagation path (measurement transect). Depending on the wavelengths (λ) of the signal it is possible to distinguish among *optical scintillometer* (λ of about 1μm) and *microwave scintillometers* (λ is ranged between 1 and 10 mm). Scintillometery exploits the fact that fluxes of sensible heat and

momentum cause atmospheric turbulence close to the ground, and creates, with surface evaporation, refractive index fluctuations due mainly to air temperature and humidity fluctuations. The receiver detects and evaluates the intensity fluctuations of the transmitted signal, called scintillations, which are linked to surface fluxes of sensible and latent heat. The magnitude of these fluctuations is usually measured in terms of a structural parameter of the refractive index of air integrated along the optical path and are related to the measure sensible and latent heat fluxes (H and LE) through the Monin Obukhov stability parameters. Temperature fluctuations are the dominant cause of scintillation in the optical wavelengths, and therefore optical scintillometers can be applied to measure H without making measurements of, or assumptions on, humidity fluctuations. Scintillometers can provide average H estimates over areas comparable to those observed by satellites along a path length ranging from a few hundred meters to 5 km of the case of large aperture scintillometers (LAS) and 10 km reached by the extra-large aperture scintillometers (XLAS) (Hemakumara et al., 2003). Since the optical scintillometer provides spatially averaged H, LE can be computed as the energy balance residual term assuming 100% energy balance closure. The estimation of a representative value for the available energy across the transect is therefore crucial for the accuracy of LE retrieved values.

1.5. Remote sensing-based method for ET estimation

The conventional techniques for the direct measurement of the energy balance components' are on the one hand extremely expensive in term of time and cost and on the other and are representative only of local scales and cannot be extended to large areas because of the heterogeneity of the land surface, of the dynamic nature and the spatial distribution of heat transfer(Jia et al., 2018). Thus, direct measurements of ET is only possible at the local scale (for a single plot mostly) and are unable to provide

estimates of spatially distributed ET at larger scales (irrigated perimeter or watershed) (Gao et al., 2008; van Dijk and Renzullo, 2011).

Remote Sensing (RS) is the only feasible means of spatially estimating actual ET over large areas or continents (Yebra et al., 2013). First attempts to estimate ET by remote sensing started at the end of '80 (Jackson et al., 1987) and during these lasts three decades this has become a very active field of research as a new source of data were available at a lower cost and higher temporal and spatial resolution. Multiples remote sensing ET approaches have been developed and tested (Glenn et al., 2007). However, each method was specifically designed to work using different source (airborne, satellite or UAV) and type (optical, thermal or radar) of data, with a particular type of crops and climate and over different temporal (from the daily scale to the annul scale) and spatial scale (from the single plot to the regional scale until the global scale). As result, since there are few intercomparison studies, nowadays there is not a consensus on which of them should be preferred (French et al., 2018). A comprehensive global water resource monitoring program will utilize satellite information at multiple scales and wavelengths merging optical, Thermal Infrared (TIR) and microwaves data retrieved from polar and geostationary platforms (Anderson et al., 2012) as well in-situ and proximal (UAV) dataset.

Numerous are also the literature review of the methods during the years. A recent and extensive overview of various methods and model approaches to derive crop evapotranspiration and agricultural yield state from remote sensing data are presented by Toulios et al. (Toulios et al., 2020). According to Courault et al. (Courault et al., 2005), these methods can be classified into four mains categories:

1. *Empirical direct methods* where remote sensing data are introduced directly in semi-empirical models to estimate ET (for example, the simplified relationship using Thermal Infra-Red (TIR) remote sensing and meteorological data).
2. *Residual methods of the Surface Energy Budget (SEB)* combining some empirical relationships and physical modules.

3. *Deterministic methods* generally based on more complex models, such as Soil–Vegetation–Atmosphere Transfer models (SVAT), and where remote sensing data are used at different modelling levels.
4. *Vegetation Index (VI) methods*, which are based on the use of optical remote sensing data.

Considering the different type of remote sensing data exploited, two major categories of approach for the ET estimation are discussed in the following: the SEB (TIR-based) and the VI (Optical-based) approach.

SEB approaches (TIR-based)

Land Surface radiometric Temperature (LST) is the result of the thermodynamic equilibrium dictated by the energy balance at the atmosphere, surface, and subsurface interface, and the efficiency by which the surface transmits radiant energy into the atmosphere (Kustas and Norman, 1996). LST is highly variable in space and time mainly due to the meteorological forcing variability and to surface properties heterogeneity in terms of topography, vegetation cover (density, phenology), surface and root zone soil moisture, soil hydrodynamic properties (texture, porosity) and the radiative properties (albedo, emissivity) (Prata et al., 1995). LST is highly sensitive to local moisture conditions and the effects of evaporative cooling and plays a key role in diagnosing many of the major SEB components (Anderson et al., 2012). Remote sensing provides the possibility of retrieving the LST in the spectral range of TIR (8 to 14 μm) with varying temporal and spatial resolutions using a thermal camera on different platforms: UAV, airborne and satellite.

Following the classical approach of SEB, LST is used to compute the sensible heat (H) from the aerodynamic temperature (T_{AERO}) (which is related to the LST) and the above-canopy air temperature (T_{AIR}):

$$H = \rho C_p \frac{T_{AERO} - T_{AIR}}{R_A} \tag{10}$$

where:

- ρC_p is the heat capacity of the air.
- R_A is the aerodynamic resistance to turbulent transport between the heights above ground level associated with the quantity T_{AERO} and T_{AIR}. It depends on local wind speed, surface roughness and stability in the atmospheric surface layer.

Then the flux of latent heat (λET) is derived, at the instant of the satellite overpass, as a residual term of the SEB, described by Equation (9). There are several practical issues related to the computation of the sensible heat using the expression of Equation (10) especially related to the LST and the T_{AERO} (which is a theoretical construct but is not directly measurable) but different studies have demonstrated that TIR data can be effectively integrated into SEB modelling to mapping ET over large areas.

Two types of methods are currently used to compute LE: the so-called *"single-pixel"* and *"contextual"* methods. In the first case, the information from each pixel is used independently of any other pixel in the image and the balance is solved independently of the rest of the image, while the "contextual" methods take advantage of thermal contrasts in the image. Calculation of atmospheric resistances distributed over large areas is, therefore, a major challenge for the *"single-pixel"* models, partly because of the difficulties encountered in the spatialized estimation of the roughness properties of the surface. To circumvent this problem, the "contextual" methods exploit the spatial variability of the surface properties, placing each pixel in its context and locating it with respect to endmembers.

Remote sensing-based SEB models are reviewed in different work present in literature (Kalma et al., 2008; Li et al., 2009; Liou and Kar, 2014; Mohan et al., 2020). The majority considers the land surface as an electrical analogue, which means that the rate of exchange of a quantity (heat or mass) between two points is driven by a difference in potential (temperature or concentration) and controlled by a (variable) number of resistances that depend on the local

atmospheric environment and internal properties of the land surface and vegetation.

VI-based approaches (Optical-based)

The strong contrast of absorption and scattering of the red and near-infrared bands can be combined into different quantitative indices of vegetation conditions. The Vegetation Indices (VIs) are an integrated product of LAI, chlorophyll content, leaf angles, fractional cover, and canopy architecture over vegetated surfaces (Nagler et al., 2004) and are strongly correlated with physiological processes that depend on photosynthetically active radiation absorbed by a canopy, such as transpiration and photosynthesis (Sellers et al., 1992). Moreover, several studies showed that VIs are nearly scale-invariant in going from leaf-level ground measurements to large-area satellite/areal measurements.

VI-based approaches are increasingly being explored, partially because SEB methods have been difficult to implement due to the number of satellite sensors that have thermal infrared bands is still limited (Yebra et al., 2013) and the coarser spatial resolution of the TIR dataset. Among the TIR datasets available, is necessary to set a trade-off between temporal and spatial resolution. Landsat satellites provide TIR information characterized by high-spatial (100 meters) and low-temporal resolution (16 days) while the National Oceanic and Atmospheric Administration-Advanced Very High-resolution Radiometer (NOAA-AVHRR) the Terra/Aqua-Moderate Resolution Imaging Spectrometer (MODIS) and the Geostationary Operational Environmental Satellite (GOES) are characterized by low-spatial (ranging from 1 to 4 km) and high-temporal resolution (ranging from daily to hourly scale). Also, with the recent lunch od Sentinel-3, this trade-off is not solved because the Sea and Land Surface Temperature Radiometer (SLSTR) provides TIR data at the kilometre scale with revisit time equal to 1.9 days at the equator (one operational spacecraft) or 0.9 days (in constellation with a 180° in-plane separation between the two spacecraft). To solve this trade-off it possible also to combine optical and TIR satellites for high-resolution evapotranspiration estimations (Guzinski and Nieto, 2019). Therefore, even if to detect and quantify the crop water

stress it is preferable to utilise satellite observations both in visible/near-infrared (VIS-NIR) and TIR parts of the electromagnetic spectrum (Kullberg et al., 2017), numerous methods have been developed to estimate et ET using optical data since, by contrast, there are several satellites with bands in the Visible, Near Infra-Red (NIR) and Short-wavelength infrared (SWIR) spectrum over a wide range of temporal and spatial resolutions (Glenn et al., 2010). In particular, the spatial resolution of the retrieved ET maps plays a key role in the selecting of the most suitable RS-based ET estimation method because it should be comparable with the spatial scale of the predominant landscape feature (Kustas et al., 2004). This condition must be accurately considered when working in a context characterized by high fragmentation agriculture landscape (as the Mediterranean area) with field sizes ranging from hundreds to thousands of meters square, as better described in Paragraph 4.1.

Although working with optical data is not possible to detect soil evaporation nor vegetation stress (except long term effects) several studies have found VI-based ET methods provide a good estimation of ET (Cleugh et al., 2007; Kalma et al., 2008). Moreover, since VI-based methods cannot estimate bare soil evaporation or differences in stomatal conductance among species and as affected by environmental factors, these must be approximated from ground data or additional remote sensing data (Glenn et al., 2010).

There are 3 typical ways to use the VI retrieved from optical data for ET estimation:

1. To derive the crop coefficient and therefore the ET in the so-called *"two-steps"* or *"Kc-VI" approach.*
2. To parameterize the terms of the classical ET equation into the so-called *"one-step"* or *"analytical"* approach.
3. In combination with LST data into the *"dual-source" approach* (Moran et al., 1994).

Here only the first two listed categories of approaches were analysed while the "dual-source" approach, since requiring the use of LST data, was not considered.

1. **Kc-VI Approach**

Similarities between the crop coefficient (Kc) curve and a satellite-derived vegetation index showed potential for modelling a crop coefficient as a function of the vegetation index (Kamble et al., 2013). These similarities were exploited to derive empirical relationships between ground measurements of ET (typically from flux towers) or evaporative fraction (EF) and the crop coefficient estimated from the statistical regression of data, following the relation of Equation (6).

$$ET_c = K_c(VI) * ET_o \tag{11}$$

A recent review on spectral vegetation indices approaches is provided by Pôças et al. (Pôças et al., 2020). Commonly used VIs include:

- the *Normalized Difference Vegetation Index* (NDVI)

$$NDVI = \frac{\rho_{NIR} - \rho_{Red}}{\rho_{NIR} + \rho_{Red}} \tag{12}$$

  The NDVI is a normalized ratio of the near-infrared (NIR) and red bands and is sensitive to chlorophyll (Rouse, 1974). It has been used extensively for vegetation monitoring, crop yield assessment and drought detection and is also the VI most used to retrieve the Kc (Fisher et al., 2008).

  Despite its many successful uses, it exhibits scaling problems, asymptotic (saturated) signals over high biomass conditions, and is very sensitive to canopy background variations with brighter canopies negatively-biasing NDVI values (Huete et al., 2002).

- the *Enhanced vegetation index* (EVI)

$$EVI = \frac{\rho_{NIR} - \rho_{Red}}{\rho_{NIR} + \rho_{Red}} \tag{13}$$

  The EVI is an 'optimized' vegetation index designed to enhance the vegetation signal with improved sensitivity in high biomass regions and

improved vegetation monitoring through a de-coupling of the canopy background signal and a reduction in atmosphere influences (Yuan et al., 2010). Consequently, EVI is more responsive to canopy structural variations, including LAI, canopy type, plant physiognomy, and canopy architecture (Nagler et al., 2013).

- the *Normalized Difference Water Index* (NDWI)

$$NDWI = \frac{\rho_{NIR} - \rho_{SWIR}}{\rho_{NIR} + \rho_{SWIR}} \quad (14)$$

The NDWI is sensitive to changes in the liquid water content of vegetation canopies (Gao, 1996). Like the NDVI, also the NDWI does not completely remove the effects of background soil reflectance (Lu and Zhuang, 2010).

In addition to these VIs also modelled satellite products, such as Leaf Area Index (LAI) and the Fraction of Absorbed Photosynthetically Active Radiation (fPAR), and the fraction of ground covered by the canopy (f_c), were intensively used to map the ET (Cleugh et al., 2007; Leuning et al., 2008; Mu et al., 2007; van Dijk and Renzullo, 2011; Pereira et al., 2020) exploiting the well-known relationship between these variables and the crop coefficient developed studied in the 1970s, for annual crops, and later, in the last decennia, for perennial crops such as tree and vineyards.

Several studies have used multispectral VIs derived from remote sensing to estimate the ET on agricultural crops including corn (Bausch, 1995), wheat (Duchemin et al., 2006; Farg et al., 2012, 2012; Garatuza-Payan et al., 2003), cotton (Hunsaker et al., 2003), potato (Jayanthi et al., 2007), maize (Toureiro et al., 2017), sugarbeet crops (González-Dugo and Mateos, 2008) and vineyards (Balbontín et al., 2017; Vanino et al., 2015b).

Analysing the results of these study it is possible to notice that (Anderson et al., 2012) VI methods:

- tend to work best in irrigated and riparian areas that perennial unstressed, or over longer timescales where vegetation indices have time to adjust to local moisture conditions. In these cases, VI approaches have good capability to estimate water use requirements by managed crops.
- are less well-suited for routine satellite monitoring of actual water use for natural and agricultural landscapes characterized by stress conditions because in these contexts, which are of most interest, VI and ET are not well correlated. VIs tend to overestimate ET when stress develops most rapidly than the adjustment adopted by the crops in terms of biomass and spectral response.
- (in most cases) underestimate actual seasonal ET because during the pre-emergence phase, where VI are not significant, and evaporation from the soil is the major contribution to the ET. Precipitation events and irrigation water applied during this phase is neglected and leads to underestimation.

However, the major limitation to the use of the VI-Kc approach over large areas, especially over heterogeneous landscapes, is the necessity of use ET measurements to build the Kc-VI relationship for each crop/vegetation type. Moreover, even if empirical relationships are available in the literature before to be applied it is necessary to verify if the context where they were retrieved has the same characteristics as the context where will be applied. This is another limitation to the diffusion of the methods because the possible combinations of crop/climate types are more numerous than the combination available in the literature.

These considerations relative to Kc-VI approaches for estimating crop coefficients were recently resumed by Pôças et al. (Pôças et al., 2020) in a SWOT analysis reviewing the spectral vegetation indices approaches (Figure 1.4).

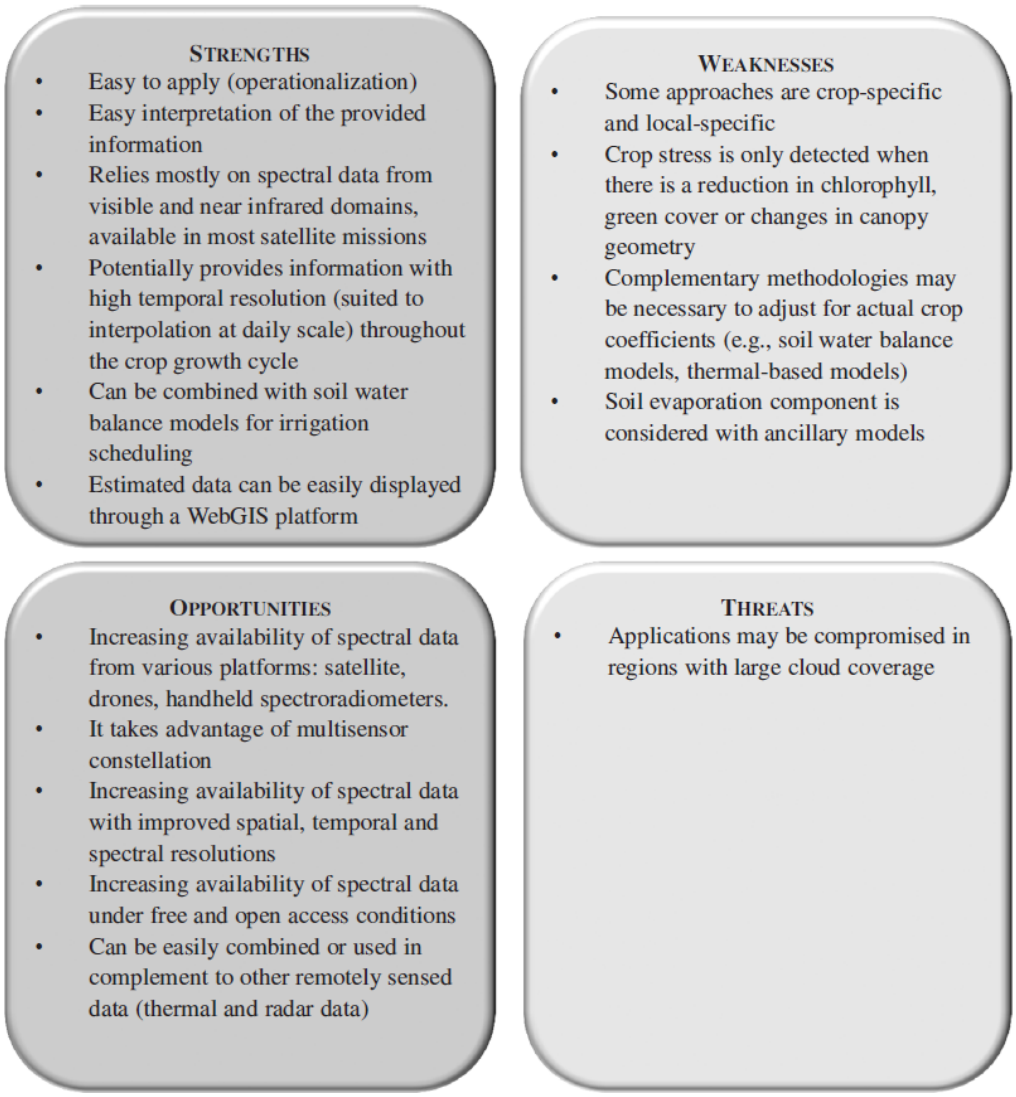

Figure 1.4. SWOT analysis relative to Kc-VI approaches for estimating crop coefficients (Source: (Pôças et al., 2020)).

2. "One-step" (or "Analytical") approach

The "one-step" approach consists in the force directly remote sensing crop parameters (such as albedo, LAI) and VIs into an ET combination equation such as Penman-Monteith, Priestly-Taylor (Priestley and Taylor, 1972) or Shuttleworth-

Wallace (Shuttleworth and Wallace, 1985; Zhou et al., 2006) avoiding the use of empirical relationships between optical properties and crop coefficients. However, to estimate actual ET is necessary to account for water stress in crop resistance using optical VIs (alone or in conjunction with TIR or microwave data) to parameterize the resistance terms of the Penman-Monteith equation or the empirical α coefficient of the Priestly-Taylor.

The Priestley-Taylor (PT) equation is similar to the Penman-Monteith method but simplified through the introduction of an empirical constant (α) accounting for the vapour pressure deficit and resistance values. Fisher et al. (Fisher et al., 2008), working on the global scale, preferred to adopt the Priestley–Taylor equation because, even if it is theoretically less accurate than the Penman-Monteith equation, not requires parameters that are difficult to characterize globally such as aerodynamic resistance, stomatal resistance, and wind speed. They proposed a model driven by 5 inputs (net radiation, NDVI, Soil Adjusted Vegetation Index (SAVI), maximum air temperature, and water vapour pressure) to reduce potential LE to actual LE. The model was developed to work on a monthly scale with MODIS satellite data and was compared with 16 FLUXNET sites with different climate conditions and crops.

Numerous are the application of the "one-step" approach developed to work with the FAO Penman-Montheit equation.

D'Urso and Menenti (D'Urso and Menenti, 1995) introduced an operative approach based on the direct integration into the P-M equation of Leaf Area Index (LAI), the crop heigh (h_c) and the Surface Albedo (α). A complete description of this method is reported in Chapter 2.

The Penman-Monteith equation is on the basis of the algorithm of the global MODIS Evapotranspiration/Latent Heat Flux product for the estimation of the actual ET (Mu et al., 2007). This 8-day composite product, provided at the global scale with a nominal spatial resolution of 500 meters, is calculated on daily basis by summing daytime and the nighttime ET and using as inputs daily meteorological reanalysis data with MODIS remotely sensed data products such as vegetation

property dynamics (described by LAI and Fraction of Photosynthetically Active Radiation (FPAR)), albedo, and land cover. Canopy conductance for plant transpiration was calculated by using LAI to scale stomatal conductance up to the canopy level. For many plant species during growing seasons, stomatal conductance is controlled by vapour pressure deficit (VPS) and daily minimum air temperature (Tmin): Tmin controls dormant and active growing seasons for evergreen biomes while high temperatures are often accompanied by high *VPD*s, leading to partial or complete closure of stomata. Under this hypothesis, for a given biome type, two threshold values for T_{min} and *VPD* was fixed and the stomatal conductance is estimated using a Biome-Property-Look-Up-Table. The MODIS ET product was validated worldwide with observed latent heat flux from field-based eddy covariance towers, displaced in 232 watersheds (Mu et al., 2011) and provides key information for water resource management and to calculate regional water and energy balance and soil water status from the regional to the global scale.

1.6. Irrigation Water Requirement

The Irrigation Water Requirement (IWR) includes several components, with the major component being the replacement of soil water depleted by crop ET (ETc). Other components provide water for leaching or controlling the soil salinity level, and for various miscellaneous purposes such as ensuring germination of seeds, controlling soil crusting, controlling frost, and conditioning the soil to enable harvesting root crops. Only part of the water for these other components is consumed by ET, therefore the IWR of the crop is defined as the amount of irrigation water required to be delivered in the field, in addition to the rainfall, to meet the CWR. Under this definition, the IWR is considered strictly as the difference between the CWR and effective precipitation, without considering additional water for leaching of salts and to compensate for non-uniformity of water application. In such cases, IWR is computed as a residual term of the water balance equation as the difference between the CWR and the effective rainfall ($Rain_{Eff}$) defined as the fraction of the total amount of rainwater retained in the root zone and which is effectively used by the plants for meeting the water need (Equation (15)).

$$IWR = CWR - Rain_{Eff} \quad (15)$$

While the IWR defines the amount of irrigation water required to be delivered in the field and therefore is also indicated as *"Net" Irrigation Water Requirement*s (NIWR), the *irrigation schedule* indicates how much irrigation water must be given to the crop, and how often or when this water is given to either maximize the production or to maximize the benefit. The scheduling is influenced by the soil type (influences the maximum amount of water which can be stored in the soil per meter depth), the root depth (frequent – but small – irrigation applications shallow root system and less frequently and more water for deep rooting crops) and the irrigation method (surface, sprinkler, or drip irrigation).

The crop coefficient method, as introduced by the FAO-56 guidelines (Allen et al., 1998), is currently the method most used for water requirements estimation and scheduling irrigations (Glenn et al., 2007). The large diffusion of the method was possible also thanks to the release of two tools developed by the FAO:

- CROPWAT: software for the calculation of crop water and irrigation requirements based on soil, climate, and crop data (Smith and Nations, 1992).
- CLIMWAT: a complementary database for CROPWAT providing agroclimatic information from over 5.000 stations distributed around the world.

1.6.1. Irrigation efficiencies

The term *irrigation* efficiency *(e)* expresses the performance of a complete irrigation system or components of the system. Not considering the salt balance in the crop root zone, the irrigation efficiency is defined as the ratio between the amount of water used to meet the consumptive use requirement of the crop to the total volume of water diverted, stored, or pumped for irrigation. Thus, the losses that can occur during the transport and the distribution as well as the water applied by the irrigation system and not being made available to be taken up by plant roots is considered wasted and reduces irrigation efficiency.

The scheme irrigation efficiency is that part of the water pumped or diverted through the scheme inlet which is used effectively by the plants and it can be subdivided into:

- the *conveyance efficiency* (e_c) which represents the efficiency of the transport and distribution scheme.
- the *field application efficiency* (e_a) which represents the efficiency of water application in the field. It mainly depends on the irrigation method and the level of farmer discipline. Efficient irrigation is achieved when most of the water applied is consumed as transpiration and the losses in evaporation, runoff and percolation are kept to a minimum. Some indicative values of the average field application efficiency are reported in the following Table.

Table 1-1. Average field application efficiency (e_a) (Source: FAO).

Irrigation methods	Field application efficiency
Surface irrigation (border, furrow, basin)	60%
Sprinkler irrigation	75%
Drip irrigation	90%

Once the conveyance and field application efficiencies have been determined, the scheme irrigation efficiency can be calculated as:

$$e = \frac{e_c \, e_a}{100} \tag{16}$$

Information on irrigation efficiency is necessary to be able to transform NIWR into Gross Irrigation Water Requirement (GIWR), which is the quantity of water to be applied, considering also water losses.

$$GIWR = \frac{NIWR}{e} = \frac{CWR - Rain_{eff}}{e} \tag{17}$$

1.6.2. Factors affecting irrigation management

Irrigation management depends on several factors, most of which are interrelated. Fernández García et al. resumed the principal factor which affected the irrigation scheduling, as described below (Fernández García et al., 2020):

- *Crop*: is the main driver of irrigation scheduling as irrigation is intended to satisfy the fraction of CWR, equivalent to the amount of water lost by crop evapotranspiration (ETc), that cannot be satisfied with rainwater during the crop season.
- *Soil characteristics:* such as soil condition, slope, texture, structure, depth, organic matter content, bulk density, salinity, acidity drainage, fertility and chemical parameters affect soil water distribution and root water absorption.
- *Irrigation scheduling criteria* used to establish irrigation scheduling. Several "irrigation criteria" have been developed including:
    1. A farmer's perception/experience of crop irrigation needs, which usually results in less-than-optimal irrigation scheduling (lack of water during some crop stages and over-irrigation in others) and hence, lower production and profits. However, worldwide, irrigation management decisions are based primarily on local experience, with very limited technical input.
    2. Rational estimation of daily crop irrigation requirements using historical climate data that are daily updated during the irrigation season.
    3. Rational estimation of daily crop irrigation requirements based on both climate information and on daily soil water balance.
    4. Estimation of daily irrigation needs using soil water data collected from soil moisture sensors.
    5. Irrigation needs to be estimated from plant water status monitoring.

    The above criteria define the daily irrigation program once the irrigation strategy is established.

- *Irrigation strategy* is influenced by several factors:

- water allocation for the whole season (from full irrigation to different levels of deficit irrigation).
- the type of irrigation system and its hydraulic characteristics.
- water availability at the field scale, according to the management of the irrigation district (on-demand irrigation in which farmers can irrigate 24 h a day or by irrigation turns) and the kind and quality of water source. For example, groundwater is a more reliable water source and less vulnerable to drought compared to surface water which is dependent on climatic variables.

- *Water distribution system and irrigation system*. Pressurized irrigation networks show higher water use efficiency but also increased energy requirements than open channel water distribution networks. The operating conditions in these kinds of networks must ensure that hydrant service conditions are adequate for the proper functioning of on-field irrigation systems, applying the expected water depth and avoiding inadequate irrigation schedules that lead to inefficient use of water. Moreover, the hydraulic features of the on-farm irrigation system must be considered to establish irrigation programming. These features depend on the type of system (surface, sprinkler, or trickle) and its design (layout) and hydrant operation (sectoring).

- *Energy source and its management*. Pressurized water distribution and application systems, which have become common in recent decades, are generally more efficient in the use of water than open channel systems. However, improved water efficiency leads to the augmentation of energy costs. The operation of the main hydraulic networks designed to reduce energy costs may limit the available irrigation time for farmers conditioning the irrigation schedule of their fields. Even in the case of the use of renewable energy sources (wind, solar photovoltaic and micro hydropower) irrigation must be scheduled around the availability of renewably

sourced energy since the generation of energy depends on suitable weather conditions (sufficient wind or solar radiation for pumping).

- *Economy and farmer's behaviour*. The costs of current irrigation scheduling systems (e.g., ICs, sensors, apps, web platforms, etc.) are generally falling. However, the adoption of these systems can be justified only by the (significantly) increase in farmer income. Therefore, for moderate to low-profit crops, and for small scale farms (as usual in the Mediterranean context characterized by a great number of small-medium, often familiar, farms) these technologies may still be cost-prohibitive.

1.6.3. Irrigation monitoring

Even if agriculture is recognized to be the biggest water consumer sector, detailed, and updated spatiotemporal information about the location and extension of irrigated areas are still missing. Global datasets, as the FAO global information system on water resources and agricultural water management (AQUASTAT), provide information at the Country level based on the information collected during the agricultural census. Therefore, the so-called *Informal irrigation* is not considered in these datasets.

However, the information available from these datasets are different because multiple definitions for the term "irrigated areas" were developed for different application and contexts (Thenkabail, 2015):

- Areas equipped for irrigation.
- Areas that receive irrigation at least once during their crop growing period.
- Areas that receive irrigation to meet at least half their crop water requirements during the growing season.
- Areas that are irrigated throughout the growing season.
- those areas which are irrigated one or more time during crop growing season.

Following different definitions, the obtained irrigated area extent will vary, therefore the key to effective mapping is to set a precise and clear definition of what is mapped.

If the definition and identification of the irrigated areas is a difficult task, estimate the spatiotemporal pattern of Irrigation Water Applied (IWA) over large areas (like irrigation schemes) is even more complex, because of the great variety of agricultural practices applied, particularly for schemes that utilize both surface and groundwater. However, the availability of accurate information about the water consumed for irrigation is the first and key step to support the development and monitoring of policies and regulations able to support and promote the sustainable management of the water resources, especially in water-scarce regions. Conventional ground-based metering methods are costly, in terms of time and labour, and need to be repeated regularly to obtain temporal patterns (Ursitti et al., 2018). Therefore they can provide only a partial solution only for assessing crop irrigation over relatively small areas and for brief periods (Maselli et al., 2020).

Remote sensing methods can be of assistance in estimating irrigation water usage in irrigated agricultural areas and can in some cases be the only way to identify the spatiotemporal evolution of the irrigated areas and to close the water budget. Since IRW cannot be directly assessed from satellite, statistical RS-based approaches to classify the irrigated crops have obtained good results at field scale but are less suitable to be applied over large areas were ground-truth samples are missing. Over large areas, IWR is mainly estimated using a more deterministic strategy. The first possibility is based on the identification of water deficit conditions which are presumably corresponding to irrigation, assuming implicitly that the water used for irrigation approximately correspond to the not-rain water consumed by the crop (Steduto et al., 2012). Under this hypothesis, which can be considered as reasonable in all cases when the cost of extracting and distributing irrigation requires the improvement of farmer's water use efficiency (as common in many Mediterranean regions), (net) IWR can be estimated as the difference between the Crop Water Requirements, represented by the actual ET (ETc) and the net rainfall (Rn):

$$IW = \sum_{i} ET_{c,i} - \sum_{i} R_{n,i} \tag{18}$$

In an even more deterministic way, irrigated field and IWR could be estimated using RS-SWB (RS-SWB) models can provide a continuous and predictive estimation of water balance components, including irrigation. In large scale RS-SWB models, the spatial and temporal pattern of actual ET (or equivalently the LE) is derived from RS and irrigation is estimated as a residual term of the SWB equation. In a recent approach introduced by Brocca et al. (Brocca et al., 2018) even satellite soil moisture product was exploited, inverting the SWB model, to quantify the amount of water applied for irrigation. However, due to the coarse spatial resolution of the satellite products used, this method has low performance when applied over small, irrigated fields. Different RS-SWB models were developed to assess the IWR over large areas developed with different specific objectives:

- *monitoring of the irrigated area* (almost in real-time)
- *management of illegal irrigation:* combining information about plots with water rights for irrigation with the modelled IWR can help to detect anomalies related to possible unregulated irrigations and agricultural plots with water rights that were not irrigated.
- *monitoring groundwater use patterns* (Hunink et al., 2015).
- *precision irrigation* defined as "the accurate and precise application of water to meet the specific requirements of individual plants or management units and minimize the adverse environmental impact" (Raine et al., 2007). Monitoring water use and crop water status in the field is important for developing effective precautions, and for this purpose, some indicators are required.
- *Irrigation performance* in water user association (Karatas et al., 2009).
- *green-blue water accounting.*

Among these models, the most significant retrieved in literature is reported below.

- The *Simulation and Management of On-Demand Irrigation Systems* (SIMODIS) estimate the actual irrigation water demand in a district in Sicily (Italy) (Minacapilli et al., 2008) solving the one-dimensional water flow equation with vegetation parameters derived from EO data. The irrigation schedule is set using

two crop and soil specific irrigation parameters: the threshold value of soil water pressure head in the root zone and the fraction of soil water deficit to be refilled. Together with a spatial distribution of the soil hydraulic properties and the vegetation conditions throughout the irrigation season, potential ET was estimated using a Kc obtained from LandSat TM derived canopy parameters such as the leaf area index, LAI, the fractional vegetation cover, the surface albedo, and crop height. Under the tested agro-climatic conditions typical for the Mediterranean region, was concluded that the spatial variability of the crop conditions had much more influence to assess the irrigation water demand than the soil hydraulic spatial variability.

- Piedelobo et al. (Piedelobo et al., 2018) developed an open-sours tool for irrigation almost in near-real-time monitoring and management using free satellite imagery (HidroMap) developed and validated in Duero Hydrographic Basin (Spain) (Piedelobo et al., 2018). HidroMap was developed to support Hydrological Planning Offices as a decision support tool including all actors involved in water management and water policymakers at the field level.
- HYDROMore is an FAO-56 SWB-based model which integrates RS derived products and local data (meteorology, soil hydrology, and crop characteristics) gathered from direct observations and geodatabase in the dual crop coefficient approach (Sanchez et al., 2010). Its innovative features are on the one hand the assimilation of multispectral RS data using the NDVI-Kcb and NDVI act relations; on the other hand, the spatial distribution of the FAO-56 model using a distributed hydrological model. The model runs at a daily time-step and pixel-based scale. The spatial coverage and resolution are defined by the footprint of the satellite images over the terrain and their pixel size, respectively. Therefore, the model is can be applied over different spatial and water resource scales, ranging from the plot and the Water User Association (WUA) to larger scales like the aquifer and river basins (Garrido Rubio et al., 2020).

However, in the field of irrigation scheduling, there are very few concrete outcomes with respect to the number of works and model retrieved in the literature. Vuolo et al. summarized some initiatives implementing satellite-based irrigation advisory services developed and working in different contexts (Vuolo et al., 2015):

- Southern Italy, with the "*Irrigation assisted by Satellite"* – IRRISAT (http://www.irrisat.it).
- Lower Austria, with *"Earth Observation for Water resources management"* - EO4Water (http://eo4water.com).
- Southern Australia, with the *"South Australian Trial for a Satellite Irrigation Advisory Service"* – IRRiEYE (, http://www.irrieye.com).
- The Iberian Peninsula with the "*System of Participatory Information, Decision Support and Expert knowledge for irrigation River basin water management"* (SPIDER). Its first prototype has been developed in 2005 by the Remote Sensing and GIS Lab of the University of Castilla-La Mancha from and it is currently providing time series of Sentinel-2 and Landsat 8 imagery and derived products (Eto maps, colour composition RGB, NDVI, Kcb and CWR) for the whole Spain and Portugal in near real-time mode, 24 hours after image delivery in the web-portals of Landsat 8 and Sentinel 2A by USGS and Copernicus, respectively.
  The previously introduced HydroMORE software is used for operative applications providing distributed spatio-temporal thematic cartography (ETc, NIR…) on a monthly time scale in the framework of two EU funded projects aimed respectively to generate services on water management to water users at different levels ("*SIRIUS EU project*", sirius-gmes.es/) and to detect non-authorized irrigation water abstractions in comparison with the local water authorities data (*"DIANA EU project", diana-h2020.eu*).

2. THE EO-BASED "ONE-STEP" FAO-56 METHOD

Overview

Among the methods for retrieving the ET using RS-derived data available in the literature and reported in the previous Chapter, the "one-step" FAO-56 method was retained as the most suitable approach for the CWR's estimation in an operative way and over large areas in a Mediterranean semi-arid context characterized by a very fragmented and heterogeneous landscape with a mosaic of rainfed and irrigated crops.

The present Chapter describes the internationally adopted standard FAO Penman-Monteith (FAO-PM) model and the possibility of feed it with a combination of in-situ meteorological data and crop characteristics retrieved from optical satellite images into the so-called EO-based "one-step" approach. Together with the full description of the method and its applications, are presented both its mains advantages and limitations.

2.1. The FAO-PM method

The FAO Irrigation and Drainage Paper No 56 "Crop Evapotranspiration" was introduced in 1998 by the Food and Agriculture Organization of the United Nations to revise guidelines for computing crop water requirements (Allen et al., 1998). The FAO-56 guidelines were a follow-on to the historic FAO paper No 24 (Doorenbos and Pruitt, 1977) which introduced the two-step crop coefficient–reference ET procedure to estimate CWRs practically and operatively. In this approach (Equation (6)), reference evapotranspiration (ETo) represents the primary weather-induced effects on water consumption, and the crop coefficient (Kc) scales the reference ET to account for crop-specific influences on ET and their variation during the crop growing season.

The FAO-56 introduced a more in-depth analysis and decomposition of the two-stage approach for estimating crop water use and the further expansion of Kc to

estimate crop ET under various crop growth and management conditions, accounting for the influences of:

- crop growth stage, amount of vegetation, and cultivar type.
- the planting date, crop season length, and termination.
- plant and row spacings, plant density, crop height and canopy architecture.
- the wetting frequency and its contribution to total ET.
- soil water availability and associated water stress.
- soil and water salinity.
- non-standard and sub-optimal cropping practices.

Besides, in the FAO-56 guidelines:

- the Kc was extended to natural vegetation to support hydrologic applications.
- was introduced the dual *Kc crop coefficient* that, instead of the Kc crop coefficient that incorporates both crop transpiration and soil evaporation, separates these two processes.

But the most important issue addressed by FAO-56 was the introduction of a standardized method for the reference ETo estimation. Indeed, before its introduction, there was many equations to estimate the ETo and therefore, for the same crop, different Kc values were existing depending on the ETo formulation adopted. The missing of a non-unique relation between crop type and Kc has the effect of limiting the spread of the method and the comparison of results worldwide. Therefore, a specific *Expert Consultation on Procedures for Revision of FAO Guidelines for Prediction of Crop Water Requirements* was nominated to select, through a comparative analysis, the most suitable method for the ETo estimation. The Expert consultation recommended the adoption of the Penman-Monteith (P-M) (Monteith, 1965) as a globally applicable reference method because it is a physics-based method and "physics are physics everywhere" (Pereira et al., 2015). The adoption of the P-M equation and single reference basis has effectively and substantially reduced the numerous discussions and research efforts of the past on the development and selection of ET reference crop methods and has

established one worldwide accepted procedure, now largely uncontested, to estimate reference crop evapotranspiration. The FAO P-M method has become a de-facto international standard method for reference evapotranspiration and has been incorporated into a variety of models used in irrigation scheduling, irrigation systems design, water resources planning (to estimate the water demand), and hydrologic modelling (to estimate the water consumption of vegetation and crop).

The P-M equation calculates ET by combining the surface energy balance equation with resistance-based methods.

$$\lambda ET = \frac{\Delta(R_n - G) + \rho\ c_p \frac{(e_s - e_a)}{r_a}}{\Delta + \gamma\left(1 + \frac{r_c}{r_a}\right)} \tag{19}$$

Where:

- ρ is air density.
- c_p is the specific heat (capacity) of air.
- γ is the psychrometric constant.
- e_s is the saturation vapour pressure at surface temperature (T_o).
- e_a is the actual vapour pressure or the saturation vapour pressure at dew-point temperature.
- r_a is the aerodynamic resistance.
- r_c is the canopy or bulk stomatal resistance of the vegetation (resistance to vapour diffusion).

The P-M equation introduces the so-called “big-leaf” approach for describing the plant canopy exchanges with the overlying atmosphere assuming that the exchanges of the whole canopy can be adequately represented and described ad they occurred at a single level: the effective source-sink height. At this level, the whole-canopy parallel-average values of stomatal resistance and the usually much smaller leaf-boundary-layer resistance control the exchange between the hypothetical big leaf and the surrounding air in the canopy, these resistances being appropriately scaled-

down from the resistances for individual leaves by dividing by the leaf area index. A further resistance for latent and sensible heat is then used to represent the turbulent transfer of energy fluxes upward to some reference level in the atmosphere above (Shuttleworth, 2006). In the big-leaf model, as represented schematically in Figure 2.1, the canopy-average leaf boundary layer resistance and the turbulent aerodynamic resistance act in series for both the latent and sensible heat transfer and are often combined as a single aerodynamic resistance between the surface of the big leaf and the reference height above the canopy where atmospheric variables are measured.

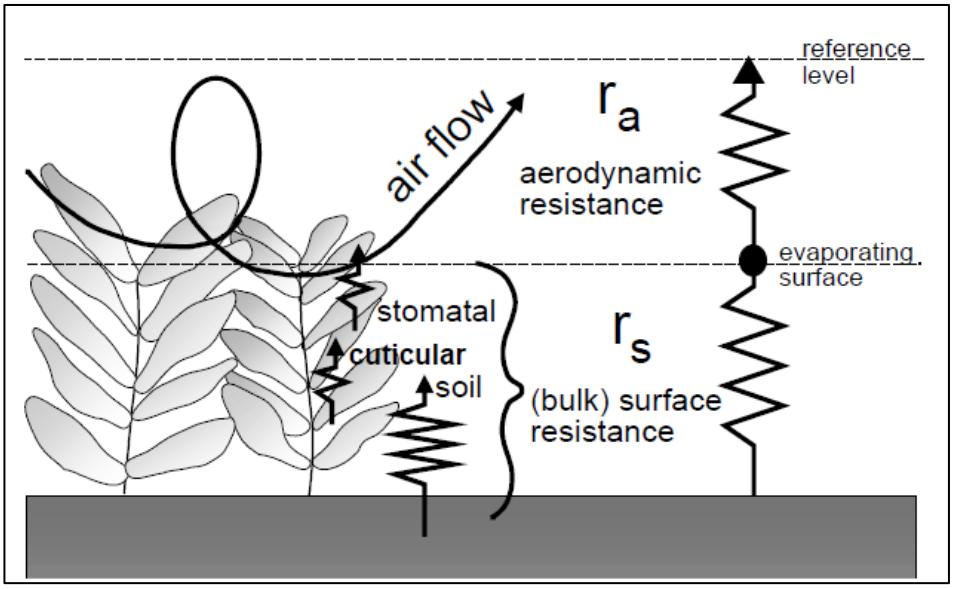

Figure 2.1. Simplified representation of the (bulk) surface and aerodynamic resistances for water vapour flow (Source: Allen et al. (Allen et al., 1998)).

The FAO-56 guidelines specified the standardized procedure to estimate each parameter of Equation (19). In particular:

- the *surface aerodynamic resistance* (r_a) determines the transfer of heat and water vapour from the evaporating surface into the air above the canopy. Under the hypothesis of neutral stability conditions, where temperature, atmospheric pressure, and wind velocity distributions follow nearly adiabatic conditions (no heat exchange), in FAO-56 it is estimated by the expression of the Equation (20):

$$r_a = \frac{ln\left[\frac{z_m - d}{z_{om}}\right] ln\left[\frac{z_h - d}{z_{oh}}\right]}{k^2 u_z} \quad (20)$$

Where:

- z_m height of wind measurements [m]
- z_h height of humidity measurements [m]
- d zero plane displacement height [m]
- z_{om} roughness length governing momentum transfer [m]
- z_{oh} roughness length governing the transfer of heat and vapour [m]
- k von Karman's constant, 0.41 [-]
- u_z wind speed at height z [m s^{-1}].

The factors d, z_{om} and z_{oh} depend upon the crop height (h_c) and architecture and are estimated by empirical equations. The expressions adopted in FAO-56 are the followings:

$$d = {}^2/_3 \; h_c$$
$$z_{om} = 0.123 \; h_c \quad (21)$$
$$z_{oh} = 0.1 \; z_{om}$$

- the *('bulk')* <u>*surface resistance*</u> (r_s), which describes the resistance of vapour flow through the transpiring crop and evaporating soil surface. Considering dense full cover vegetation, the surface resistance was estimated as:

$$r_s = \frac{r_1}{LAI_{active}} \quad (22)$$

Where:

- r_1 is the *bulk stomatal resistance* of the well-illuminated leaf [s m^{-1}].
- LAI_{active} is *active (sunlit) leaf area index*, a dimensionless quantity (expressed as m^2 leaf area per m^2 ground area), which quantify the leaf area

that actively contributes to the surface heat and vapour transfer. It is generally the upper, sunlit portion of a dense canopy.

The surface resistance is a key parameter of the P-M equation. It depends on numerous factors (including radiation intensity, temperature, and vapour pressure deficit) to be considered for its accurate estimation. In general, it is crop-specific and differs among crop varieties and crop management which can affect for example water stress. Yet in FAO-56 it is reported that, where the vegetation does not completely cover the soil, the resistance factor should indeed include the effects of the evaporation from the soil surface. If the crop is not transpiring at a potential rate, the resistance depends also on the water status of the vegetation.

To introduce the concept of reference evapotranspiration, which is affected only by the local climatic condition, was necessary to introduce a *reference crop.* In FAO-56 was selected a hypothetical grass reference with *"an assumed height (h_c) of 0.12 m having a surface resistance of 70 s m^{-1} and an albedo of 0.23, closely resembling the evaporation of an extension surface of green grass of uniform height, actively growing and adequately watered".*

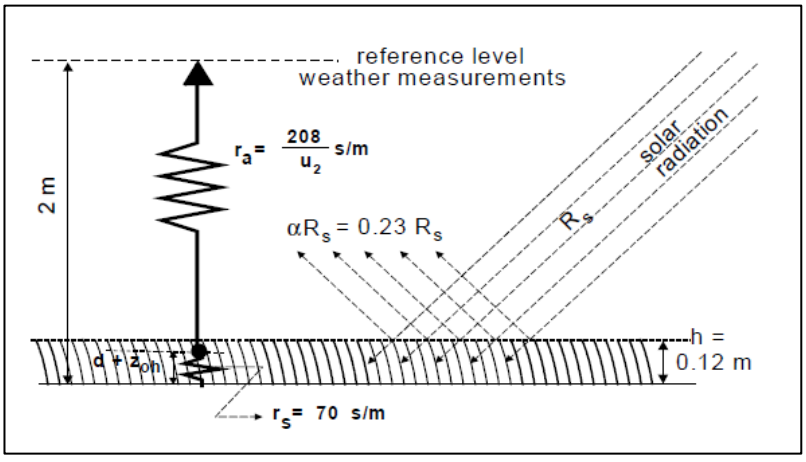

Figure 2.2. Characteristics of the hypothetical reference crop adopted by FAO-56 (Source: Allen et al. (Allen et al., 1998)).

Under these hypotheses, the expression of the aerodynamic and stomatal resistance was standardized ad assumed the following forms:

$$r_a = \frac{208}{u_z} \ [\mathrm{m\ s^{-1}}] \tag{23}$$

$$r_s = \frac{r_1}{LAI_{active}} = \frac{100}{0.5\ (24\ h_c)} \approx 70\ [\mathrm{m\ s^{-1}}] \tag{24}$$

From the original Penman-Monteith equation (Equation (19)) and the equations of the aerodynamic (Equation 4) and surface resistance (Equation (19) and (24)), the FAO Penman-Monteith method to estimate ETo on a daily scale assumes the following form:

$$ET_o = \frac{0.408\,\Delta(R_n - G) + \gamma\ \frac{900}{\mathrm{T} + 273}\ u_2(e_s - e_a)}{\Delta + \gamma(1 + 0.34\,u_2)} \ [\mathrm{mm\ day^{-1}}] \tag{25}$$

Where:

- R_n is the net solar radiation [MJ m^{-2} day^{-1}].
- G is the soil heat flux density [MJ m^{-2} day^{-1}].
- T mean daily air temperature at 2 m height [°C].
- u_2 wind speed at 2 m height [m s^{-1}].
- (e_s-e_a) represents the saturation vapour pressure deficit [kPa].
- Δ is the slope vapour pressure curve [kPa °C^{-1}].
- γ is the psychrometric constant [kPa °C^{-1}].

2.2. The EO-based FAO-PM method

FAO-56 did not provide specific means for estimating ET from satellite imagery. However, since it was published, substantial progress has been attained in remote sensing of ET, as described in Paragraph 1.5, and nowadays they are also directly applied in several irrigation scheduling services for farmers (Calera et al., 2017).

Among these methods, the Earth Observation (EO)-based FAO-PM method, as proposed by (D'Urso and Menenti, 1995), is an operative approach based on the direct application of the FAO Penman-Monteith Equation (19) using as input a combination of in-situ meteorological data with crop characteristics as retrieved from optical satellite images (the Leaf Area Index (LAI), the crop heigh (h_c) and the Surface Albedo (α)) directly integrated to estimate resistance factors of the P-M equation.

The method is also called "Kc-Analytical Approach" because, once the ET map is estimated, it is possible to perform the pixel-based Kc calculation for each satellite acquisition using the inverse relation of Equation (6):

$$K_c = \frac{ET_c}{ET_o} \tag{26}$$

In the second phase, following the "two-steps" approach, potential crop ET (ETc) between two satellite overpasses is estimated as the product of the corresponding daily reference evapotranspiration (ETo), depending only on atmospheric conditions, and the retrieved Kc maps assuming that the estimate Kc map is representative of the mean value of the ratio between ETc and ETo over around the date of satellite's passage. With the increased availability of satellite images, which allows reducing the time between two consecutive satellite overpasses, this hypothesis has even less influence on the estimated ET.

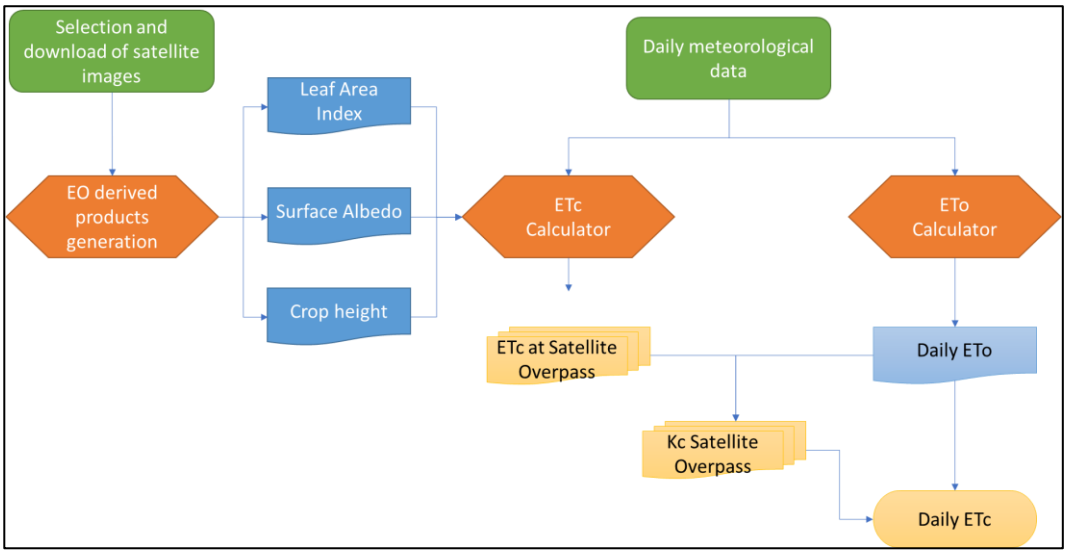

Figure 2.3. Flow chart of the EO-based FAO-PM method.

The works retrieved in literature where the EO-based FAO-PM method are summarized in Table 2-1.

Table 2-1. List of the works available in the literature on the application of the EO-based "one-step" FAO-56 model, with the indication of the scale and purpose of the work.

Scale	Crop	Purpose	References
Regional	various	irrigation management	(D'Urso et al., 2010)
Plot scale	Wheat	CWR	(Farg et al., 2012)
Irrigation scheme	-	CWR	(Akdim et al., 2014)
Regional scale	-	CWR	(Neugebauer and Vuolo, 2014)
Plot scale	vineyard	CWR	(Vanino et al., 2015b)
Irrigation scheme	-	water accounting	(Vanino et al., 2015a)
Plot scale	wheat	CWR	(Kadam et al., 2017)
Plot scale	tomato	CWR & IWR	(Vanino et al., 2018)

2.2.1. Main hypothesis and limitations

Two are the mains hypothesis adopted to estimate the resistance parameters:

1. the crop height, which compares in the aerodynamic resistance (r_a) calculation (Equation (20)) was assumed constant and independent from the specific crop map derived from satellite data.
2. the surface resistance (r_s) was set at its minimum value corresponding to set the bulk stomatal resistance at its minimum value ($r_{1,min}$). Kelliher et al. showed that a minimum value $r_{c,min}$ for most crops ranges between 50 to 70 [s m^{-1}] (Kelliher et al., 1995). Usually, following the FAO-PM methodology, the value of the stomatal resistance was set equal to 100 [s m^{-1}].

The assumption on the crop height has a limited effect on the retrieved ET because, as demonstrated by different sensitivity analysis, the radiation component in the SEB is dominant during the irrigation season at mid-latitude regions.

Instead, the hypothesis concerning the value of the surface resistance has a significant effect on the estimated ET. In particular, selecting and setting a minimum value of the stomatal resistance means that the method cannot estimate the actual evapotranspiration (ETa) but only the maximum (also called "potential") ET (Vanino et al., 2018). Therefore, the method can be implemented with good results especially over homogeneous landscapes represented by irrigated farmland under unstressed conditions (Anderson et al., 2012).

The unique case retrieved in the literature of a differ parametrization of the surface resistance applied to the EO-based "one-step" FAO-PM method was the work of D'Urso et al. (D'Urso et al., 2010). The Authors maintained the hypothesis of assuming a minimum value for the stomatal resistance, set equal to 100 [s m^{-1}], but exploited a different parametrization for the LAI active:

$$r_s = \frac{r_{1,min}}{LAI} \quad \text{for LAI} < 0.5\ \text{LAI}_{max}$$
$$r_s = \frac{r_{1,min}}{0.5\ LAI} \quad \text{for LAI} > 0.5\ \text{LAI}_{max} \qquad (27)$$
$$r_s = r_{1,min} \quad \text{for LAI} \geq 4$$

2.2.2. Advantages

The direct consequence of the assumption of constant (mean) value for the crop height is the independence from the availability of a detailed and updated crop map.

Other advantages offered by the EO-based FAO methods are that:

- it is easily implemented.
- the retrieved crop coefficients depend only on the effective cover and not on other variables such as planting date and density.
- the resulting ETc maps have the same spatial resolution of the satellite dataset exploited which can range from 10 meters (using the high-resolution Sentinel-2 data) to 500 meters (using the MODIS datasets). Therefore, it is possible to estimate ET at the field scale also in contexts extremely fragmented and heterogeneous. Conversely, the TIR-based datasets available for continuous crop monitoring during the crop season has a coarser spatial resolution: the highest spatial resolution is provided by the Landsat (100 meters).
- Thanks to the availability of several satellites and sensor with bands in the Visible, NIR and SWIR spectrum over a wide range of temporal and spatial resolutions it is possible to merge these constellations into a “virtual constellation” to increase the temporal resolution of the satellite data. This solution is valid also to solve possible problems of acquisition caused by the presence of cloud which makes impossible the acquisition in the optical spectrum.

3. TOWARDS THE ACTUAL EVAPOTRANSPIRATION ESTIMATION USING THE EO-BASED "ONE-STEP" FAO-PM METHOD

To estimate the actual ET using remote sensing derived data during last decades were developed several models even more realistic that are hindered by complex parameterization. The trend has been towards increasing complexity, as opposed to applicability because greater complexity requires detailed input parameters that limit the application to areas where the necessary data are available (Cleugh et al., 2007; Damm et al., 2018).

The use of EO-based "one-step" FAO-PM has the advantage of being easily implemented and has become more popular recently for assessing the potential ET under different hydro-climatic regions and crops such as wheat, cotton, tomato, grapes, and orchards. However, since for water management it is important to estimate the actual crop water consumption, it is necessary to analyse the assumption of the method to moving towards the actual ET estimation using the EO-based "one-step" FAO-PM method.

Despite the Penman-Monteith equation is universally accepted by the community concerned with estimating crop water requirements as the theoretically superior approach, as evidenced by Shuttleworth (Shuttleworth, 2006), the reluctance to use a so-called "one-step" estimation results from two outstanding issues:

1. no method has been yet defined to handle the problem that meteorological variables are commonly available only at 2 m above the ground while, when using the Penman-Monteith equation, they are required at some level above the crop to calculate the aerodynamic resistances to, and the vapour pressure deficit at, the blending height from climate variables at 2 m.
2. table of effective values currently no exists for the surface resistance of different crops equivalent to that for the crop coefficient. Usually, especially for herbaceous a minimum value of stomatal resistance is considered assuming that crop in standard conditions. But this assumption leads to estimate the maximum evapotranspiration and not the actual evapotranspiration (Vanino et al.,

2018), which can be very different especially in case of crop stress due to water shortage or plant disease. This approach, therefore, can be applied over homogeneous landscapes represented by irrigated farmland under unstressed conditions (Anderson et al., 2012).

In the following paragraphs, these two issues are addressed to define an improved procedure for the estimation of the ET, considering the overall objective of determining the crop water requirements in an operative way and over large areas in a context of a very fragmented and heterogeneous landscape with a mosaic of rainfed and irrigated crops.

3.1. Crop height and Aerodynamic resistance

The first obstacle to the direct application of the FAO-56 equation is the dependence of the factors of Equations (20) on the crop height, which is variable in time and space and is not commonly available, especially working on large, cultivated areas with a complex crop pattern. Even if some correlations between the crop height with vegetation indices are available (Anderson et al., 2004), the efforts to estimate the crop height using spectral reflectance data is quite difficult (Akdim et al., 2014).

In these cases, the most common solution adopted by different Authors is to work with a fixed value of crop height, considering its average spatial-temporal distribution for the considerate working scale. This assumption is considered valid for irrigated environments where the radiative component of the FAO-PM equation, at the daily scale, is dominant over the aerodynamic term (D'Urso, 2010). Moreover, it results to be consistent with sensitivity analysis published by several Authors which demonstrate as the variation of crop height adopted has a low influence on the estimated (potential) crop evapotranspiration. These sensitivity analyses were conducted both at a regional scale for herbaceous crops (Aghdasi, 2010), showing that a percentage change of 50% in crop height corresponds to a variation of the order of 5% of K_c, and at field scale for tomato (Vanino et al., 2018) (Figure 3.1) and orange orchards (Consoli et al., 2006) (Figure 3.2). Working on an irrigation scheme, Akdim et al. (Akdim et al., 2014) found

that ETc hardly depends on h_c especially in summer when high values of the vapour pressure deficit occur (Figure 3.3).

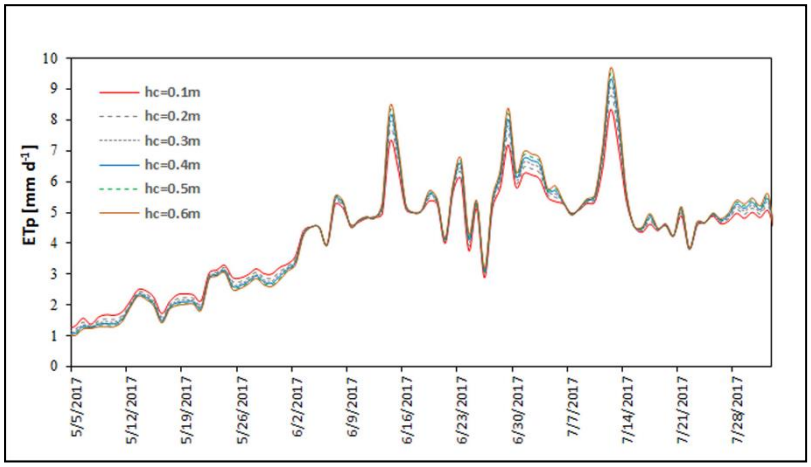

Figure 3.1. Relationship between potential crop evapotranspiration (ETp) and crop height (h_c) ranging from 0.1 and 0.6 meters estimated for a tomato field by (Vanino et al., 2018).

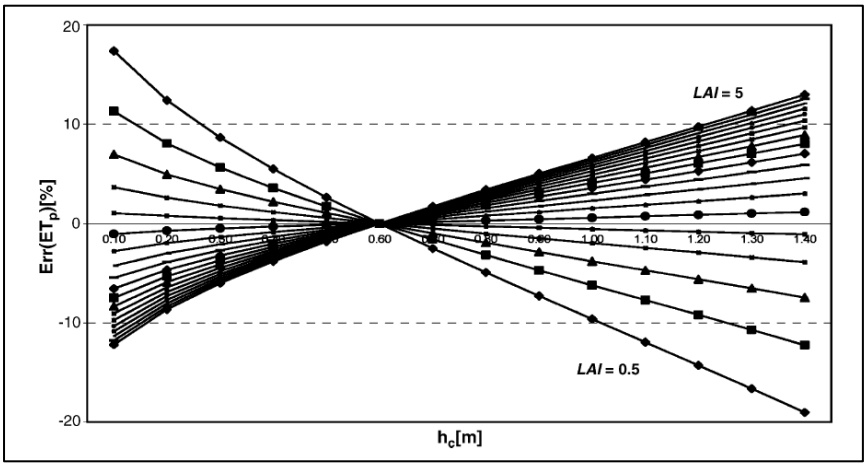

Figure 3.2 Error in potential crop evapotranspiration (ET_p) estimation for h_c and LAI values (Souce: (Consoli et al., 2006).

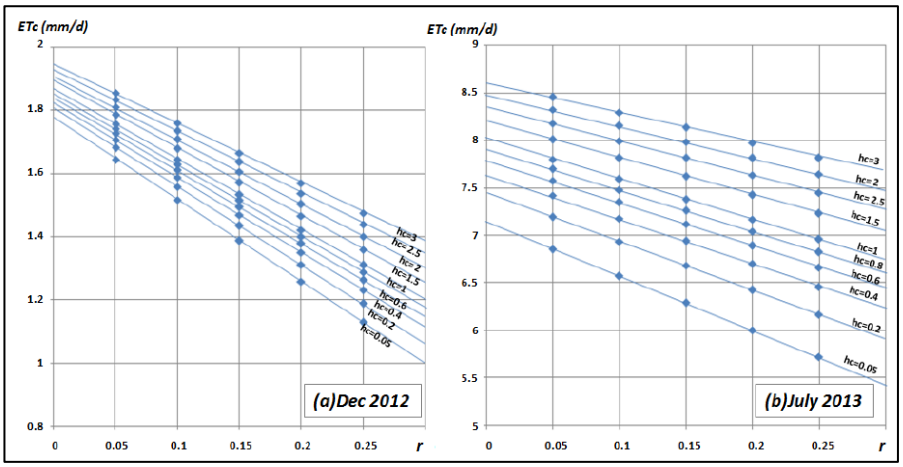

Figure 3.3. Relationship between crop evapotranspiration ETc (analytical method) and the surface albedo r for different values of h_c and LAI = 2, in December 2012 (a) and June 2013 (b) as found by Akdim et al. (Akdim et al., 2014).

Even if the assumption of constant value of crop height over for large areas (Consoli et al., 2006) make easier the application of the "one-step" approach because it eliminates the dependence from the crop pattern information, still are not fully investigated the influence of the crop height on the ET estimation for taller crops. The assumption of constant value of crop height was adopted also for tree crops like vineyards (Vanino et al., 2015b) but it was tested only over a little range of h_c values, not exceeding the 1.40 meters (Consoli et al., 2006), which is not represented of the crop trees height, that could easily reach the 3-4 meters. Moreover, for these taller crops, the meteorological variables are commonly only available at a fixed height (usually 2 m) above the ground while, when using the Penman-Monteith equation, these values are required at some level above the crop for which calculations are to be made (Allen et al., 1998).

Following the methodology proposed by Shuttleworth (Shuttleworth, 2006) which introduce a "blending height" in the *Atmospheric Boundary Layer* (ABL) where meteorological conditions are independent of the underlying crop, the validity of the assumption of a unique value of crop height independently from the crop pattern and its temporal evolution (which is fundamental especially for herbaceous crops) was tested if also for taller crops. For the test were considered different conditions of Leaf Area Index, surface

albedo, and crop heights. In particular, the crop heights selected range from the typical values for herbaceous crops (0.50, and 1.00 meter) and for woody crops (2.00, 3.00, 4.00 and 5 meters). Moreover, the crop height value of 10 meters was tested to assess the validity of the method. Were also selected 4 values of *blending height (Z)* (5, 10, 20 and 50 meters) to be compared against the standard FAO-56 blending height of 2 meters.

The test was conducted with the meteorological data retrieved at the *Cerignola CBC* station during the 15 days stared from the 5th until the 20th of July 2017 and reported in Table 3-1. This period was considered because was representative of the summer condition where the crop evapotranspiration is maximum. The analysis, to be not affected by the daily meteorological condition, was conducted considering the average values retrieved during the considered period.

Table 3-1. Meteorological data from the Cerignola CBC station metered during the 15 days stared from the 5th until the 20th of July 2017 and used for the analysis of the aerodynamic resistance.

	P	**T_{max}**	**T_{min}**	**RH_{max}**	**RH_{min}**	**Solar. Rad.**	**Wind speed**
	[mm]	[°C]	[°C]	[%]	[%]	[cal/cmq/g]	[Km/g]
05/07/2017	0.00	35.40	13.60	82.00	22.00	536.23	118.74
06/07/2017	0.00	36.00	18.20	70.00	22.00	540.70	130.38
07/07/2017	0.00	35.70	17.90	72.00	24.00	516.24	128.58
08/07/2017	0.00	37.00	17.90	83.00	23.00	518.31	139.80
09/07/2017	0.00	39.20	19.20	80.00	13.00	505.80	175.98
10/07/2017	0.00	39.30	18.20	74.00	9.00	533.57	131.04
11/07/2017	0.00	38.10	18.50	86.00	19.00	516.44	152.40
12/07/2017	0.00	36.50	22.30	76.00	27.00	527.68	224.40
13/07/2017	21.80	33.30	19.80	89.00	39.00	424.23	186.78
14/07/2017	0.00	30.20	20.40	87.00	35.00	478.54	314.34
15/07/2017	0.00	27.70	19.00	82.00	29.00	545.52	254.16
16/07/2017	0.00	28.90	15.70	75.00	30.00	534.86	215.64
17/07/2017	0.00	31.80	16.70	85.00	29.00	467.60	185.16
18/07/2017	0.00	32.10	15.50	88.00	32.00	527.82	132.72
19/07/2017	0.00	33.30	17.30	88.00	25.00	537.79	115.50
20/07/2017	0.00	35.10	18.00	81.00	29.00	515.02	141.18
Average		34.35	18.01	81.13	25.44	514.15	171.68

Assuming the absence of divergence of the momentum flux between 2 m and the blending height above a reference crop, then the friction velocity is constant with height and, in neutral atmospheric stability, the wind speed at any height Z *(u_z)* above an extensive area of reference was estimated as proposed by Shuttleworth (Shuttleworth, 2006):

$$u_Z = u_{Zm} \frac{\ln\left[\frac{Z - 0.08}{0.0148}\right]}{\ln\left[\frac{Z_m - 0.08}{0.0148}\right]} \tag{28}$$

The resulting wind profile follows the typical wind profile power law (Figure 3.4).

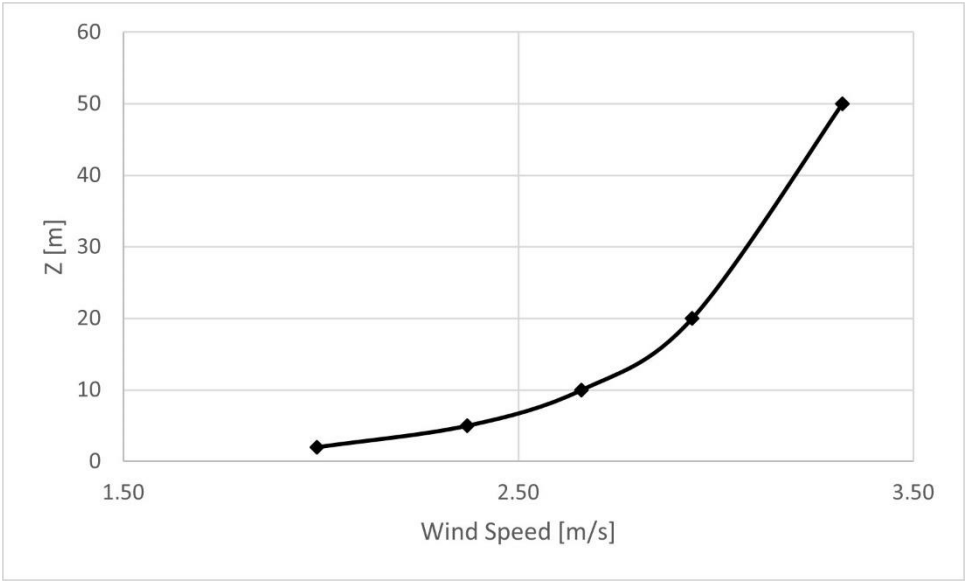

Figure 3.4. Wind speed estimated at the different blending heights (Z), from the wind speed measurements at $Z_m = 2$ meters, using the expression of Equation (28).

By replacing the expression of wind speed at any height Z into the expression of Equation (20), it is possible to estimate the aerodynamic resistance as:

$$r_a = \frac{R_c^Z}{u_{Zm}} \tag{29}$$

Where R_c^Z is a dimensionless variables defined as:

$$R_c^Z = \frac{\ln\left[\frac{z_m - d}{z_{om}}\right] \ln\left[\frac{z_h - d}{z_{oh}}\right]}{k^2} \frac{\ln\left[\frac{Z_m - 0.08}{0.0148}\right]}{\ln\left[\frac{Z - 0.08}{0.0148}\right]} \quad (30)$$

As shown in Table 3-2 and Table 3-3, the use of different crop heights following the proposed procedure and Equation (30), lead to small differences in the final estimated crop evapotranspiration. These differences increase with the increase of the LAI and crop height. However, in the ranges of the crop heights of the main agriculture crops (0,5 – 4,0 meters), these differences are very limited and allow to assume a unique crop-independent value for the crop height, as done by several Authors. In the rest of the present work, therefore, all the computation are performed assuming a crop height equal to 0.50 meters.

Table 3-2. Estimated crop evapotranspiration ETc [mm/day] (analytical method) for surface albedo equal to 0.15 and different values of blending height (Z), crop height (h_c) and Leaf Area Index (LAI) during summer season (July 2017).

			Albedo = 0.15				
	Z [m] =		**2**	**5**	**10**	**20**	**50**
LAI = 1	**hc** [m] =	0.50	4.15	4.05	3.99	3.95	3.90
		1.00	4.34	4.17	4.09	4.03	3.97
		2.00	4.71	4.34	4.21	4.13	4.05
		3.00	-	4.48	4.30	4.20	4.10
		4.00	-	4.61	4.38	4.25	4.14
		5.00	-	4.75	4.45	4.30	4.18
		10.00	-	-	4.77	4.48	4.30
LAI = 2	**hc** [m] =	0.50	5.73	5.41	5.24	.	4.98
		1.00	6.45	5.80	5.54	5.35	5.17
		2.00	8.13	6.42	5.96	5.67	5.41
		3.00	-	7.01	6.29	5.91	5.57
		4.00	-	7.64	6.60	6.10	5.71
		5.00	-	8.43	6.89	6.28	5.83
		10.00	-	-	8.55	7.04	6.28
LAI = 3	**hc** [m] =	0.50	6.60	6.12	5.89	5.72	5.54
		1.00	7.69	6.70	6.32	6.05	5.79
		2.00	10.89	7.66	6.93	6.50	6.13
		3.00	-	8.62	7.45	6.85	6.37
		4.00	-	9.77	7.93	7.15	6.56
		5.00	-	11.33	8.42	7.25	6.74
		10.00	-	-	11.60	8.69	7.43

Table 3-3. Estimated crop evapotranspiration ETc [mm/day] (analytical method) for surface albedo equal to 0.20 and different values of blending height (Z), crop height (h_c) and Leaf Area Index (LAI) during summer season (July 2017).

			Albedo = 0.20				
	Z [m] =		**2**	**5**	**10**	**20**	**50**
LAI = 1	**hc** [m] =	0.50	4.02	3.90	3.84	3.78	3.73
		1.00	4.24	4.04	3.95	3.88	3.81
		2.00	4.67	4.24	4.09	4.00	3.90
		3.00	-	4.40	4.20	4.08	3.96
		4.00	-	4.55	4.29	4.14	4.01
		5.00	-	4.71	4.37	4.19	4.05
		10.00	-	-	4.74	4.41	4.19
LAI = 2	**hc** [m] =	0.50	5.54	5.20	5.03	4.89	4.75
		1.00	6.29	5.62	5.34	5.14	4.95
		2.00	8.14	6.26	5.78	5.48	5.20
		3.00	-	6.87	6.13	5.72	5.38
		4.00	-	7.54	6.42	5.93	5.52
		5.00	-	8.36	3.89	6.11	5.64
		10.00	-	-	8.49	6.91	6.11
LAI = 3	**hc** [m] =	0.50	6.37	5.88	5.65	5.47	5.28
		1.00	7.49	6.48	6.08	5.81	5.54
		2.00	10.78	7.46	6.71	6.27	5.88
		3.00	-	8.45	7.24	6.63	6.13
		4.00	-	9.63	7.74	6.94	6.33
		5.00	-	11.23	8.24	7.22	6.51
		10.00	-	-	11.51	8.51	7.22

3.2. Modelling the (bulk) surface resistance (r_s)

The conception of bulk *surface resistance* originates from the "*big-leaf model"* introduced into the P-M equation (Monteith, 1965) for describing plant exchanges with the overlying atmosphere assuming the land surface as a uniform layer. It is closely related to leaf area index (LAI), soil moisture, temperature, atmospheric wetness, and leaf physical properties, but it is not directly measurable (Li et al., 2019). Surface resistance increases when the crop is water-stressed and when the soil water availability limits crop evapotranspiration.

Since r_s describes the resistance of vapour flow through the transpiring crop and evaporating soil surface when the vegetation does not completely cover the soil, in principle, it should be furtherly subdivided into canopy surface conductance and soil surface conductance (Shuttleworth and Wallace, 1985), while there is usually no distinction between bulk surface conductance and canopy surface conductance on the large scale since the transpiration typically is the primary component (Monteith and Unsworth, 2013).

The challenge of applying the Penman-Monteith model at a large scale is the parameterization of surface resistance. It can be quantified from two possible perspectives: understanding the relationship between stomatal/surface conductance and its controlling environmental factors or investigating the consequent effects, such as the changes in terms of surface temperature (Hu et al., 2018).

The first approach is valid and largely implemented at the field scale in ET estimation. Jarvis (1976) firstly employed meteorological observations (photon flux density, temperature, vapour pressure deficit, leaf water potential and ambient CO2 concentration) to parameterize stomatal conductance (C_L) because it is influenced by climate and water availability (however, the degree of influence varies by crop type and variety). As a logical consequence, Stewart (1988) further extended the stomatal conductance model to the canopy scale using LAI and including other meteorological variables (solar radiation, specific humidity deficit, temperature, and soil moisture deficit). The resulting *Jarvis-Stewart model* has been widely applied in ET estimation (Cleugh

et al., 2007) even in RS-based model as the MODIS and the LSA SAF (Satellite Application Facility on Land Surface Analysis) products.

In the MODIS ET algorithm (Mu et al., 2007) the biome-specific canopy resistance was estimated as a function of the mean potential conductance per unit leaf area (C_L) and two factors that limit stomatal resistance by minimum air temperature and vapour pressure deficit:

$$r_s = \frac{1}{LAI\ C_L\ m(T_{min})\ m(VDP)} \tag{31}$$

In the LSA SAF ET algorithm the canopy resistance ($r_{s,canopy}$) is parameterized as a function of the minimum stomatal resistance ($r_{s,stoma,min}$) and of the Jarvis functions (f_1, f_2, f_3) for the stomatal response to radiation, soil water content and atmospheric humidity demand, respectively using as input the downwelling surface shortwave flux (S), the average volumetric soil water content in the root zone (w) and the atmospheric moisture deficit (δq_a):

$$r_{s,canopy} = \frac{f_1(S)\ f_2(w)\ f_3(\delta q_a)\ r_{s,stoma(\min)}}{LAI} \tag{32}$$

The downwelling shortwave flux is derived from the Meteosat Second Generation (MSG) Spinning Enhanced Visible and Infrared Imager (SEVIRI) instrument, while the soil moisture and temperature in the four soil layers (7 cm for the top layer and then 21, 72, and 189 cm) are modelled as a solution to diffusion equations at the spatial scale of MSG/SEVIRI grid to compute the soil water content in the root-zone. The air temperature, air humidity and surface atmospheric pressure provided by the ECMWF interim reanalysis product (ERA-Interim) are used to calculate the atmospheric moisture deficit.

In the ETMonitor model developed by Hu and Jia (Hu and Jia, 2015) to estimate the daily actual ET, the canopy surface resistance was parameterized by a multiplicative response, described by limiting functions (f), to several environmental factors include the solar radiation (Ra), the air temperature (ta) and the vapour pressure deficit (VDP)

and the root zone soil moisture (θ_r). In addition, was introduced the leaf shadowing factor (F_s) linked to the LAI and the canopy structure.

$$r_{s,canopy} = \frac{F_s}{LAI} \frac{r_{s,stoma(\min)}}{f_1(R_s)\, f_2(t_a) f_3(VPD)\, f_3(\theta_r)} \tag{33}$$

Zhou et al. (Zhou et al., 2006) used the Shuttleworth and Wallace model (Shuttleworth and Wallace, 1985) and NDVI to estimate ET from sparse canopy adopting the P-M ETo with an increase of stomatal resistance based on the generic equation:

$$r_{s,canopy} = \frac{r_{stomatal,min}}{LAI_{eff}\, F_i(X_i)} \tag{34}$$

With $F_i(X_i)$ represents the stress function for the generic factor X_i (water, pests, nutrients, etc.).

Other similar models were proposed by Leuning (Leuning et al., 2008) and Irmak-Mutiibwa model (Irmak and Mutiibwa, 2010). Even if it is logical to parameterize r_s by meteorological data and LAI, there are several limitations to the application of these models on a large scale:

- the non-linearity of environmental stress functions increases the difficulty of acquiring model parameters.
- the interdependence of environmental variables (such as air temperature and vapour pressure deficit) may result in misestimates the model parameters (Wang et al., 2014).
- spatial meteorological data are not directly measured but interpolated with sparse station measurements, which introduces additional uncertainty.

The second possible approach to retrieve the r_s consists of the research of the effects of changing in r_s values. This approach was selected by Smith et al. (Smith et al., 1988) and Shuttleworth and Gurney (Shuttleworth and Gurney, 1990), since the r_s controls ET and eventually affects the land surface temperature, developed a theoretical relationship

between foliage temperature and canopy conductance for sparse crops based on Shuttleworth-Wallace model. The obtained relationship is over-complex and of therefore has limited applicability. Recently different Authors had proposed a simplified model (e.g. by introducing dry and wet reference temperatures and employed the temperature index to estimate stomatal conductance at the leaf scale) while others applied similar methods to the field-scale problem (Hu et al., 2018).

Due to these difficulties, a recent approach to address the estimation of the r_s over large areas is to exploit the capability of remote sensing to capture and to quantify the vegetation and soil properties through the synthetic information provided by indices sing optical, thermal and microwave sensors (Yebra et al., 2013; Bai et al., 2017; Hu et al., 2018; Barraza et al., 2015, 2017).
Since the visible, NIR and SWIR bands are sensitive to leaf chlorophyll concentration, and leaf turgor and structure, Yebra et al. studied an optical-based surface conductance model to estimate actual evapotranspiration using six different vegetation indices derived from the MODIS sensor and three contrasting estimation approaches: the first two approaches directly regressed various MODIS VIs (NDVI, EVI, Kc, NDWI) and products (the leaf area index and the fraction of photosynthetically active radiation) with ET *("direct regression"*) and the evaporative fraction (EF) (*"potential evapotranspiration scaling").* The EF was computed as the ratio between ET and the available energy assumed to be equal to the sum of the measured sensible and latent (λE) heat.

$$\begin{aligned} ET &= a + b\,VI \\ EF &= a + b\,VI \end{aligned} \tag{35}$$

In the third approach, the so-called *"PM conductance approach" (*PM-r_s approach*),* the PM equation was inverted to obtain surface conductance (for dry plant canopies). The PM-r_s uses an empirical relationship between r_s and different VIs to parameterize the conductance term of the PM equation. The remote sensed-derived r_s is subsequently used as input in the PM equation together with other key meteorological drivers to estimate ET. The PM-r_s approach is the most mechanistic VI–ET model and provides the

best conceptual basis for ET estimation since VIs are used to derive r_s, which is then combined with meteorological data within the PM framework

$$r_s = a \exp[\, b\, (VI - VI_{MIN})] \tag{36}$$

The estimated ET was compared with in-situ measurements from eddy covariance flux towers at 16 FLUXNET sites located over six different land cover types. They concluded that *the use of VIs to estimate r_s within the PM framework provides the best basis for ET estimation* when compared to direct regression or PET scaling approaches or the two MODIS vegetation products (LAI and fPAR). However, none of the three most successful VIs was uniformly superior across all land cover types.

Bai et al. proposed an approach to simulate water stress in a PM-based model (RS-WBPM) when estimating ET in areas having a Mediterranean climate using precipitation, vertical root distribution and satellite-retrieved vegetation information. A multilayer water balance module was employed to simulate the soil water stress factor of multiple soil layers at different depths. The RS-WBPM model was evaluated at 27 flux sites having a Mediterranean climate. Results show that incorporating recommended VI (NDVI for shrub and EVI for other biomes), the model can capture the variation of ET in summer at most sites. As all inputs of RS-WBPM are globally available, and therefore it can be implemented on a regional and global scale.

Barrazza et al. evaluated and compared optical and passive microwave index-based retrievals of r_s and ET following the P–M approach over forests (Barraza et al., 2015). The methodology was evaluated over the growing season at five FLUXNET sites, which provided the in-situ measurements of ET, using MODIS (MYD09A1) and AMSR-E passive microwave data to compute the Vis (EVI, NDWI and Frequency index).
From the analysis conducted, the Authors concluded that a combined optical-microwave approach produced the best ET estimates for evergreen forest and offered a robust approach for deciduous forest without sacrificing precision. A similar conclusion was found analyzing savannah vegetation (Barraza et al., 2017) where ET is mostly

driven by available water and the vegetation exerts strong control over the rate of transpiration. In this context, as in general for arid and semi-arid lands, optical Vis-based ET models tends to overestimate water fluxes. In water-limited ecosystems the microwave indices provided information about water availability and moisture stress (e.g. water content in leaves and shallow soil depths, atmospheric demand) at a high temporal resolution, thereby providing a scaling factor for potential r_s. The method combines multi-sensor derived with global meteorological data to estimate r_s. The comparison of the retrieved ET with the global MODIS LE product indicates that the model that they proposed could estimate ET at a regional scale using global meteorological data in arid and semi-arid biomes and could be further extended to continental scales providing equally robust estimates of LE.

Hu et al. compared and evaluate the performance across and within land cover types of three different (and contrasting) forms of r_s models, by using six optical-based vegetation index (derived from MODIS sensor), thermal-based Temperature Vegetation Difference Index (TVDI), and jointly using the optical and thermal index. The three proposed surface conductance models on remote sensing information and reduced the uncertainty of meteorological data originating from spatial interpolation and were designed to be an alternative approach to acquiring evapotranspiration estimation for large-scale application. The analysis was conducted over three-year evapotranspiration observation at three stations in the North China Plain. Generally, widely used vegetation index including *NDVI and EVI produced good estimation of surface conductance and evapotranspiration* because they were able to capture the growth process of leaf and describe the temporal variation trend of surface conductance. The empirical TVDI-based model performed poorly in quantifying surface conductance. The combination of vegetation index and TVDI generated the optimal surface conductance estimation for all sites.

3.2.1. The proposed (bulk) surface resistance (r_s) model

To meet the overall and the specific objectives of the present work, the proposed model for the estimation of the (bulk) surface resistance was designed to be:

- not crop-specific, to allows to use of the ET model also in contexts where a detailed and updated crop map is not available.
- coherent with the surface resistance model adopted by the FAO P-M equation.
- (sufficiently) representative of the actual crop conditions considering the crop water stress (even if by exploiting only optical satellite data).

Under these working hypotheses, the FAO P-M surface resistance (Equation (22)) was modified to include remote sensing derived information about the crop status, synthetically described by one vegetation index, into the expression of the resistance.

$$r_s = \frac{r_1(VI)}{LAI_{eff}} \tag{37}$$

Among the various remote sensing-based vegetation indices retrieved in literature, was selected the widely used for vegetation monitoring: the Normalized Difference Vegetation Index (NDVI). It is the most widely used proxy for live green vegetation cover, production, and yield. It is also largely applied for the estimation of phenological indicators such as the length of the growing season, the onset date of greenness, and the date of maximum photosynthetic. Moreover, as described before in Paragraph 1.5, it is the VI most applied to retrieve the crop coefficient in the “Kc-VI approach”.

The NDVI value can range between -1.0 and $+1.0$. and is functionally (but not linearly) equivalent to the simple infrared/red ratio (NIR/VIS). Negative values of NDVI (values approaching -1) correspond to water. Values close to zero (from -0.1 to 0.1) generally correspond to barren areas of rock, sand, or snow. Low, positive values represent shrub and grassland (approximately 0.2 to 0.4), while high values indicate temperate and tropical rainforests (values approaching 1).

A simple linear relation between the NDVI and the stomatal resistance was imposed maintaining the same structure of the P-M's surface resistance:

$$r_s = \frac{\alpha\ NDVI}{LAI_{eff}} \tag{38}$$

Following this empirical relation, as shown in Figure 3.5, the surface resistances decrease as the area of vegetation per unit ground area (LAI) increases as coherent with the well-known Shuttleworth and Wallace model (Shuttleworth and Wallace, 1985).

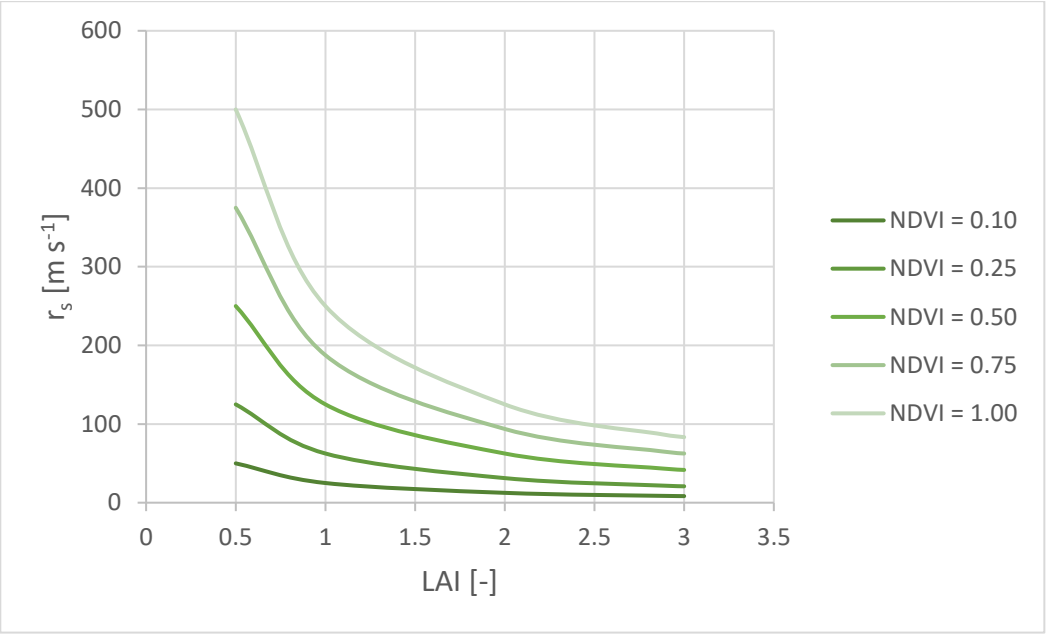

Figure 3.5. The empirical relationship between the LAI and NDVI with the surface resistance (r_s).

While the NDVI has a standardized definition and procedure of calculation, the LAI value depends on the method of estimation applied. Pasqualotto et al. (Pasqualotto et al., 2019) analysed the influence of the LAI parameter estimated with four different methodologies in the calculation of crop potential evapotranspiration (ETc) with the adapted FAO-PM, using a multi-temporal S-2 dataset. The tested LAI products ware retrieved using empirical (vegetation indices), semi-empirical (CLAIR model with fixed and calibrated extinction coefficient) and artificial neural network S2 products (ANN S2

LAI) derived from the Sentinel Application Platform Software (SNAP) biophysical processor. The analysis, conducted over four different test areas, showed that the crop potential evapotranspiration values estimated with the ANN S2 LAI product are the closest to those estimated with the in-situ LAI values using a dataset with seasonal information of wheat and tomato. Moreover, ANN S2 products are the only ones that do not produce saturation, demonstrating the great potential of ANN S2 products for operational use in the monitoring of agricultural areas.

The procedure used for the estimation of the coefficient α of Equation (38) is reported in detail in Chapter 6.

3.3. Masking no cropped areas

The FAO-PM ET model was designed to estimate the evapotranspiration from cropped areas, therefore whether the model is running at a large scale or field scale, it is important to identify the growing crop season and to mask for the rest of the time the no cropped areas. Even if this operation is important both at the local and at the regional scale, is right to the latter the most affected by overestimation in the crop and irrigation water requirements estimation because otherwise also the not cropped areas are contributing to the balance.

For this reason, in this improved version of the Analytical Approach, was introduced the preliminary masking of the no vegetated areas based on the values of the Vegetation Fraction Cover (VFC) as better described in Paragraph 4.4.

4. HANDLE THE EO-BASED "ONE-STEP" FAO-56 METHOD WITH SENTINEL-2 DATA

Overview

This Chapter provides a full and detailed description of the input data and the step-by-step procedure to follow to handle the "one-step" EO-based FAO-PM method using as input the biophysical variables retrieved from the Sentinel-2 (S-2) satellites. Moreover, to justify the use of the S-2 derived products, a brief description of the mission and a characterization in terms of spectral, temporal and, spatial resolution of the data is provided.

4.1. Why use Sentinel-2?

Sentinel-2 (S-2) is a polar-orbiting, multispectral high-resolution imaging mission for environment monitoring developed into the European Commission's Copernicus program (https://earth.esa.int/). It is based on a constellation of two identical satellites (S-2A launched on 23 June 2015 and S-2B 7 March 2017) in the same orbit, 180° apart for optimal coverage and data delivery capable able to cover all Earth's land surfaces The mission was designed to offer continuity and to expand the French SPOT *("Satellite Pour l'Observation de la Terre")* and the US LandSat *("Land Satellite")* missions (Drusch et al., 2012) proving free and open-access global coverage at an unprecedented spatial, temporal, and spectral resolution. These characteristics are described in detail in the following paragraphs with an especial focus on the land and agriculture applications.

4.1.1. Spectral Resolutions

Both Sentinel-2A and Sentinel-2B satellites have onboard the same Multi-Spectral Instrument (MSI) with 13 bands from the visible (VIS) and the near-infrared (NIR) to the shortwave infrared (SWIR) at different spatial resolutions ranging from 10 to 60 m: four bands at 10 m, the classical broadband visible blue, green, red, and near-

infrared; six bands at 20 m, four narrow bands in the vegetation red edge spectral-domain (705, 740, 775, and 865 nm), and two longer SWIR bands (1610 and 2190 nm); and three bands at 60 m dedicated to atmospheric correction (443 nm for aerosols and 940 nm for water vapour) and cirrus detection (1380 nm) (Table 4-1).

Table 4-1. Bands and resolutions of Sentinel-2 Multi-Spectral Instrument (MSI).

Sentinel-2 Bands		Central Wavelength [μm]	Resolution [m]
Band 1	Coastal aerosol	0.443	60
Band 2	Blue	0.490	10
Band 3	Green	0.560	10
Band 4	Red	0.665	10
Band 5	Vegetation Red Edge	0.705	20
Band 6	Vegetation Red Edge	0.740	20
Band 7	Vegetation Red Edge	0.783	20
Band 8	NIR	0.842	10
Band 8a	Vegetation Red Edge	0.865	20
Band 9	Water vapor	0.945	60
Band 10	SWIR- Cirrus	1.375	60
Band 11	SWIR	1.610	20
Band 12	SWIR	2.190	20

S-2 is the first optical Earth observation mission of its kind to include three bands in the 'red edge' which, combinate with the high resolution and frequent revisit times, can provide key information for vegetation health and growth monitoring for regional to a global scale, especially during the rapidly growing in the summer. Moreover, it is possible to distinguish between different crop types as well as data on numerous plant indices essential to accurately monitor plant growth parameters such as Leaf Area Index (LAI), Leaf Chlorophyll Content (LCC) and Leaf Cover (LC). The principal purpose for land application of each MSI band is reported in Table 4-2.

Table 4-2. Principal purpose for land applications of each MSI band.

Band	Principal purpose
Band 1	Atmospheric correction (aerosol scattering)
Band 2	Sensitive to vegetation senescing, carotenoid, browning and soil background. Atmospheric correction (aerosol scattering)
Band 3	Green peak, sensitive to total chlorophyll in vegetation
Band 4	Maximum chlorophyll absorption
Band 5	Position of the red edge. consolidation of atmospheric corrections/fluorescence baseline.
Band 6	Position of red edge, atmospheric correction, retrieval of aerosol load.
Band 7	Leaf Area Index (LAI), the edge of the Near-Infrared (NIR) plateau.
Band 8	LAI
Band 8a	NIR plateau, sensitive to total chlorophyll, biomass, LAI, and protein. Water vapour absorption reference; retrieval of aerosol load and type.
Band 9	Water vapour absorption, atmospheric correction.
Band 10	Detection of thin cirrus for atmospheric correction.
Band 11	Sensitive to lignin, starch, and forest above-ground biomass. Snow/ice/cloud separation.
Band 12	Assessment of Mediterranean vegetation conditions. Distinction of clay soils for the monitoring of soil erosion. The distinction between live biomass, dead biomass, and soil, e.g. for burn scars mapping.

4.1.2. Temporal Resolutions

Monitoring crop development and crop ET over the growing season for the purpose of irrigation management requires dense time series of multispectral imagery at a spatial resolution high enough to resolve within-field variability and delivered in real-time (Calera et al., 2017).

The orbit type and altitude of the S-2 mission were designed to provide a high temporal resolution with a 5-day global revisit frequency, and up to 2-day revisit in top northern and southern parts of the globe. Its sun-synchronous orbit guarantees a frequent and systematic coverage of all land surfaces needful for both land cover and land cover change mapping, and to support the assessment of bio-geophysical parameters (Drusch et al., 2012).

4.1.3. Spatial Resolutions

Focusing on the spatial resolution of S-2, it ranges between 10 and 60 meters (Table 4-1), but the agricultural dedicated bands are either 10 or 20 m, depending on the bandwidth, while the other bands at 60 m are for atmospheric aerosols and water vapour observations mainly for improved image calibration.

Due to their shorter revisit time and more detailed spatial resolution (compared, for example, to Landsat mission whit 16 days and mostly 30 m pixel size), more precision in sub-field monitoring can be performed using these paired satellite constellations, hence covering from agroecosystem to field scales more precisely and thus gaining relevance for use in agricultural contexts and even more specifically smallholder farming systems (Segarra et al., 2020).

As recently suggested by Blatchford et al. (Blatchford et al., 2020) it is important to compare the spatial resolution of the satellite dataset with the irrigation scheme characteristics. They suggested, for plots with average size ranges from 2 to 10 hectares, that:

- Spatial resolutions of 250 m, 100 m, and 30 m are suitable for inter-annual and inter-scheme assessments for adequacy, equity, and crop water productivity (CWP), regardless of plot size.
- Spatial resolutions of 250 m and 100 m should not be used for inter-plot comparison for adequacy, equity, or CWP on plots with extension inferior to 2 ha. The 30 m resolution may also be too coarse, and Sentinel-2 application should be considered.
- Spatial resolutions of 250 m and 100 m show general spatiotemporal trends for adequacy, equity, and CWP within a scheme, but not the full extent of plot-to-plot variation for all plot sizes tested.

However, they recommend further investigation into the resolution requirements to suitably undertake irrigation assessment in smaller plots.

4.2. Input data

The EO-based "one-step" FAO-PM approach requires as input a combination of in-situ meteorological data and crop characteristics estimated from satellite images. While the biophysical parameters necessary are described in Paragraph 4.3.2, the characteristics that the meteorological data should have, are discussed in detail in the following.

- Temperature

  The (average) daily maximum and minimum air temperatures in degrees Celsius (°C) are required. Where only (average) mean daily temperatures are available, the calculations can still be executed but some underestimation of ETo will probably occur due to the non-linearity of the saturation vapour pressure-temperature relationship. Using mean air temperature instead of maximum and minimum air temperatures yields a lower saturation vapour pressure es, and hence a lower vapour pressure difference (es - ea), and a lower reference evapotranspiration estimate.

- Air Humidity

  The (average) daily actual vapour pressure, e_a, in kilopascals [kPa] is required. The actual vapour pressure, when not available, can be derived from maximum and minimum relative humidity (%), psychrometric data (dry and wet bulb temperatures in °C) or dewpoint temperature (°C) according to the procedures reported in FAO-56 Guidelines (Allen et al., 1998).

- Radiation

  The daily net radiation expressed in megajoules per square metre per day [MJ m^{-2} day^{-1}] is required. These data are not commonly available but can be derived from the (average) shortwave radiation measured with a pyranometer or from the (average) daily actual duration of bright sunshine (hours per day) measured

with a (Campbell-Stokes) sunshine recorder using the procedures are outlined in Chapter 3 of FAO-56 Guidelines (Allen et al., 1998).

- Wind speed

  The (average) daily wind speed in metres per second [m s^{-1}] measured at 2 m above the ground level is required. It is important to verify the height at which wind speed is measured, as wind speeds measured at different heights above the soil surface differ.

As outlined in FAO-56 Guidelines (Allen et al., 1998), where data for some weather variables are missing, it is recommended to calculate ET using the standard FAO Penman-Monteith method after resolving the specific problem of the missing data with the procedures for estimating missing climatic data are outlined in Chapter 3 of FAO-56 Guidelines.

The use of an alternative ET calculation procedure, requiring only limited meteorological parameters, should generally be avoided. Differences between ET values obtained with the FAO-PM equation with, on the one hand, a limited data set and, on the other hand, a full data set, are expected to be smaller than or of similar magnitude to the differences resulting from the use of an alternative ET equation.

Altitude above sea level and the *latitude* (expressed in degrees north or south) of the location should be specified. These data are needed to adjust some weather parameters for the local average value of atmospheric pressure (a function of the site elevation above mean sea level) and to compute extra-terrestrial radiation (Ra) and, in some cases, daylight hours (N).

4.3. Flow chart of the S-2 based "one-step" FAO-PM approach

The methodology proposed follows the flow diagram of Figure 4.1. Each sub-step is detailed in the paragraphs below.

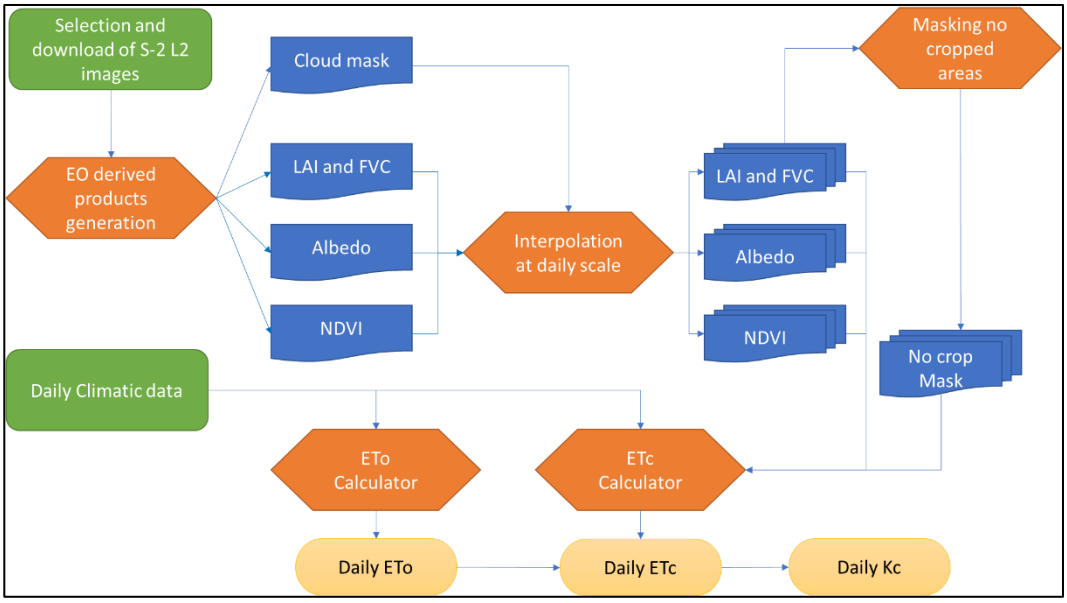

Figure 4.1 Flow chart for ET estimation with the one-step FAO approach.

4.3.1. Selection of images

The Bottom Of Atmosphere (BOA) reflectance (Level-2A) images were retrieved and downloaded from the Copernicus Open Access Hub (https://scihub.copernicus.eu/). Level-2A are calibrated and atmospherically corrected, from radiometric and geometric corrected (Level-1C), using the European Space Agency's (ESA) Sen2Cor processor (Main-Knorn et al., 2017). Among the available images, were selected only the images with a cloud coverage lower than 20%. In this way, it was possible to consider only the images with low cloud contamination over the entire 100 km^2 tile. Once selected the images were downloaded and clipped to the extension of the considered study area. Again, the cloud mask filter was applied to exclude the satellite images with cloud coverage higher than 20% over the considered area. In this way was ensured that only the satellite images with the lowest cloud contamination were selected and used

for the rest of the computation. For these last cloud filtering, was exploited the information contented into the *Scene Classification Map* (SCM) provided within the Level-2A product. Thanks to the SCM map were masked pixels flagged as “no data”, “saturated”, “dark features/shadows” and “cloud-covered” (Figure 4.2).

Label	Classification
0	NO_DATA
1	SATURATED_OR_DEFECTIVE
2	DARK_AREA_PIXELS
3	CLOUD_SHADOWS
4	VEGETATION
5	NOT_VEGETATED
6	WATER
7	UNCLASSIFIED
8	CLOUD_MEDIUM_PROBABILITY
9	CLOUD_HIGH_PROBABILITY
10	THIN_CIRRUS
11	SNOW

Figure 4.2. Scene Classification Values.

4.3.2. Computing biophysical parameters

4.3.2.1. Leaf Area Index (LAI) and Vegetation Fraction Cover (VFC)

Leaf Area Index (LAI) and Cover Fraction (FVC) maps were retrieved at each satellite overpass using the Biophysical Processor tool (L2B) of the ESA’s Sentinel-2 Toolbox. L2B is one of the tools of the Sentinel Application Platform (SNAP) provided for the visualization, analysis, processing, and exploitation of MSI data. L2B processor makes possible to create value-added products (Level-2B) with a special focus on agricultural vegetation monitoring (Drusch et al., 2012). It employs a neural network algorithm tailored for S-2 and trained using radiative transfer simulations from PROSAIL

(PROSPECT+SAIL) radiative transfer models (Jacquemoud et al., 2009) to estimate the canopy characteristics from the S-2 Top of Canopy (TOC) reflectance. The algorithm provides the biophysical variable product (FVC and LAI) values with a spatial resolution of 10 meters. Moreover, for each retrieved biophysical parameter, the algorithm provides the relative input/output quality flag. These flags were utilized for excluding the pixels with input and/or output out of range (and providing product outside tolerance) and pixels with bad quality of input values.

4.3.2.2. Surface albedo (α)

Albedo (α) is a dimensionless biophysical characteristic of the soil-plant canopy system over lands and represents the amount of solar energy reflected by the surface. Therefore, it is a key parameter for local and regional estimation of energy and mass exchanges between the Earth surface and the atmosphere because provides information on the radiative balance necessary to ET estimation.

Considering the limited spectral resolution of EO data normally available, the albedo was estimated as an approximation of the hemispherical and spectrally integrated surface albedo. Under this approximation, the albedo was calculated as a weighted sum of *surface spectral reflectance* ρ_λ derived from the atmospheric correction, with broadband coefficients ω_λ representing the corresponding fraction of the solar irradiance in each sensor band (D'Urso and Belmonte, 2006) as proposed by Menenti and Bastiaanssen (Menenti et al., 1989). For each satellite overpass, the broadband surface albedo was calculated as the integration of the Level-2A S-2 surface reflectance (ρ_λ) across the shortwave spectrum, as shown in equation (4).

$$\alpha = \sum_{\lambda_i=1}^{n} \rho_{\lambda_i}\, \omega_{\lambda_i} \tag{39}$$

$$\omega_{\lambda_i} = \frac{E_\lambda^0}{\sum_\lambda E_\lambda^0} \tag{40}$$

The broadband weights (w_λ) represent the corresponding fraction of the solar irradiance in each sensor band (E_λ^0) and are sensor dependent. They were calculated for the S-2 surface reflectance product (with a spatial resolution of 10 meters) and are reported in the following table:

Table 4-3. Weighting coefficients for the calculation of albedo.

Band Number	**Center (λ)** [μm]	**Spectral width (Δλ)** [μm]	E_λ^0 [W m^{-2}]	$\omega_{\lambda i}$ [-]
B1	0.443	0.02	1893	-
B2	0.49	0.065	1927	0.1836
B3	0.56	0.035	1846	0.1759
B4	0.665	0.03	1528	0.1456
B5	0.705	0.015	1413	0.1347
B6	0.74	0.015	1294	0.1233
B7	0.783	0.02	1190	0.1134
B8	0.842	0.115	1050	0.1001
B8a	0.865	0.02	970	-
B9	0.945	0.02	831	-
B10	1.375	0.03	360	-
B11	1.61	0.09	242	0.0231
B12	2.19	0.18	3	0.0003
			Sum	1.0000

4.4. Masking no cropped areas with Sentinel-2 VFC

As described in Paragraph 2.1, the FAO-PM model was designed to estimate the evapotranspiration from cropped areas and therefore it is necessary to mask and exclude all the not vegetated areas, occupied basically from build-up, bare soil, and water surfaces, present inside each satellite image acquired. For this operation, the Vegetation Fraction Cover layer was used to mask the pixels width FVC value less of a threshold value settled at 0.10. This value was accurately selected to avoid the to consider as not vegetated also areas with sparse vegetation, which are spread diffused especially in the “Sinistra Ofanto” study area.

5. DESCRIPTION OF THE SELECTED STUDY AREAS

5.1. Sinistra Ofanto (CBC - Italy)

The irrigation district "Sinistra Ofanto" (Figure 5.1) is a large, cultivated area situated in the North of the Apulian Region (Italy) and delimited by the Ofanto river at the southeast. It is characterized by an extremely heterogeneous and fragmented landscape with the presence of vineyards, olive trees, orchards, and cereals.

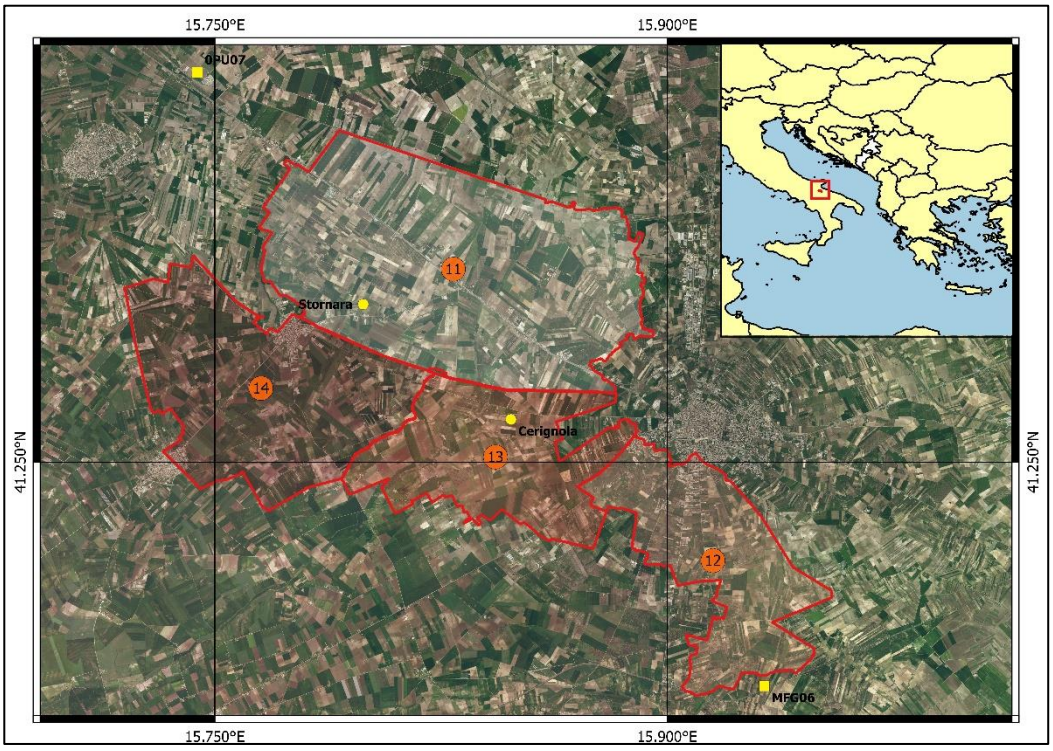

Figure 5.1. Satellite view of the "Sinistra Ofanto" irrigation scheme (S.R. WGS84) with the location of the agrometeorological station working on the study area and managed by the CBC and ARIF (respectively the circular and square point) and its overall position in the Italian Peninsula (upper right box).

The irrigation district is managed by the *"Capitanata" Irrigation Consortium (Consorzio per la Bonifica della Capitanata – CBC)*, one of the greatest and most important Water User Association (WUA) of the Mediterranean region (Lamaddalena et al., 2004). It covers a large, cultivated area (55.000 ha) served by a water distribution

network working since 1983 proving water for 40.000 ha organized in 21 command areas called "*districts*" each of that are sub-divided into smaller operational units called irrigation "*sectors*" that are composed of several grouped farms (Zaccaria et al., 2013). Water management in the study area is typical of semiarid regions with an upstream sub-catchment that transfers surface flows collected by the *Capaciotti* and *San Pietro sull'Osento* dams to the downstream plain supporting irrigated agriculture. The area serviced by the system is subdivided into the "Zona Bassa" ("Low zone"), where water is supplied to farms by gravity, and the "Zona Alta" ("High zone") where cropped fields are at higher elevations relative to the water source and irrigation water is conveyed and supplied using a lifting plant. In this work were considered the 4 districts which constitute the so-called "Zona Alta" that, for its relatively higher elevation, has an independent distribution network. The overall extension of the "Zona Alta" (sub-district: 11, 12, 13 and, 14) is 12,726 hectares and is fully equipped with a telemetry system (Acquacard) that, through a flowmeter installed in each hydrant (about 2,500), records the volume of water applied by the farmers. For this study area, the daily pattern of the water distributed is currently available only for a limited number of hydrants. However, the total seasonal volumes of water distributed for each sub-district are available.

The irrigation season, in accord with the amount of water stored in the 2 dams which served the area (Capaciotti and Osento), starts the 1st of April and ends the 30th November of each year, as happened for the 3 irrigation season considered in the present work (2017, 2018 and, 2019). The irrigation network usually works "on-demand" but, during the peak of the irrigation demand, it can be set to works "on-turn".

The climate of the study area is typically Mediterranean with strong seasonal and inter-annual variability. Annual precipitation ranges between 400 and 700 mm occurring predominantly during the winter while summers are generally hot and dry.

5.1.1. Satellite dataset

Following the procedure for the selection of the best quality satellite images available from the Copernicus Open Access Hub, as previously described in Paragraph 4.3.1, for the 3 considered irrigation seasons starting from March to October of each year. The complete scene list is reported in Annex 1. The annual number of available images ranges from a maximum of 24 for 2019 to a minimum of 14 for the 2017 first year of operativity of the Sentinel-2B satellite which was launched in the 7th March 2017.

The resulting effective temporal resolution of the images acquisition is in line with the theoretical "cloud-free" temporal resolution especially during the summers, where clouds are absent, and it is easily possible to retrieve an S-2 image every 5 days.

5.1.2. Meteorological data

The sub-irrigation scheme *"Zona Alta"* is covered by four agrometeorological weather station of two different networks. Two stations are managed directly by the Consortium CBC and are fully equipped for the measurements of the standard agrometeorological data. The other two are managed by the Regional Agency for the Irrigation (*"Agenzia Regionale per le Attività Irrigue e Forestali"* - ARIF). Among these lasts two weather station, only the station of "Ortanova" (0PU07) is fully equipped while for the station of *"Cerignola" (MFG06)* the solar radiation measurement is missing. The complete description of the 4 weather stations is provided in Table 5-1 while their position is represented in Figure 5.1.

Table 5-1. Weather stations used for the “Zona Alta” case study.

		Coordinate [S.R. WGS84]		Elevation	Data availability		
		N	E	[m]	2017	2018	2019
ARIF	Ortanova (0PU07)	41.347220	15.744167	52	x	x	x
	Cerignola (MFG06)	41.194168	15.932222	96	x	x	x
CBC	Cerignola	41.26070	15.84820	126	x	x*	
	Stornara	41.28940	15.79920	94		x*	

* data available starting from the 1st of June

All the stations are located on the edge of irrigated fields and sensors are mounted at standard sensor heights for agricultural weather data collection requirements. Daily agrometeorological measurements were spatially distributed using Inverse Distance Weighting (IDW) method.

Reference evapotranspiration and rainfall time series retrieved for each meteorological station during the three years are reported in Figure 5.2, Figure 5.3 and, Figure 5.4. Looking at the rainfall patterns, the three considered years appears to be completely different from 2017 characterized by a very low amount of rainfall. This can be further confirmed by confronting the average monthly rainfall over the study area with the long-term monthly rainfall registered. Unfortunately, the selected four agrometeorological stations are not able to provide a long-term series of data. Therefore, was used the long-term rainfall measurement (from 1950 to 2016) meteorological station of Cerignola of the network of the Region Civil Protection Agency (www.protezionecivile.puglia.it). From this comparison, it is evident as 2017 was a year characterized by very low precipitation, not only concerning the other 2 following years but also looking to the historic average trend. All the year was characterized by values of monthly precipitation lower than the average with the only exception for May. During the irrigation season, this trend was, even more, exacerbate with the total absence of precipitation during June and August.

The cumulated precipitation volumes occurring during the irrigation season period (April-September) for 2018 and 2019 were almost similar (respectively 278.6 and 292.7 mm) and in line with the long-term average value (equal to 223 mm). However, as shown in Figure 5.5, the temporal patterns of the rainfall are sensible different among these 2 years. Indeed while during the irrigation season 2018 the monthly rainfall follows the average long term pattern (with the only exception for rain deficit occurring during April, soon recovered during May), the irrigation season 2019 is characterized by an initial irrigation season with rainfall in line with the long-term average, an exceptional rainy July (with monthly rainfall almost equal to 2.5 times the expected average monthly rainfall) and closure of season with September and October with relatively limited rainfall (almost the 50% of the expected).

Even the monthly average values of reference evapotranspiration reflect the meteorological difference among the three years. As shown in Figure 5.6 for the agrometeorological station of Ortanova (the unique station equipped with the solar radiometer and working along the three considered years), the year 2017 has the highest values of ETo along all the year and especially during July and August where the average ETo was equal to almost 8 mm.

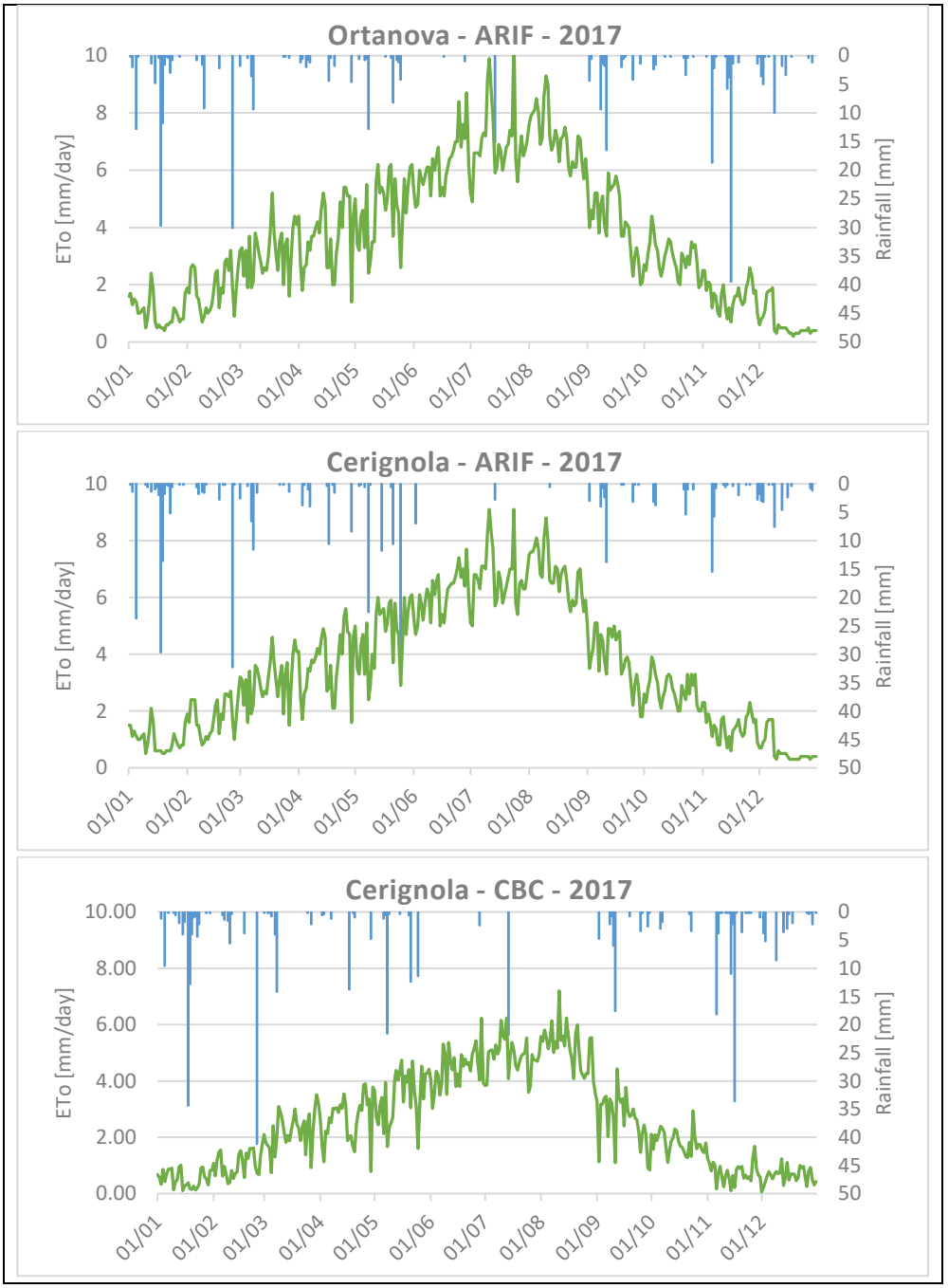

Figure 5.2. Annual time series of precipitation and potential evapotranspiration (ETo) during 2017.

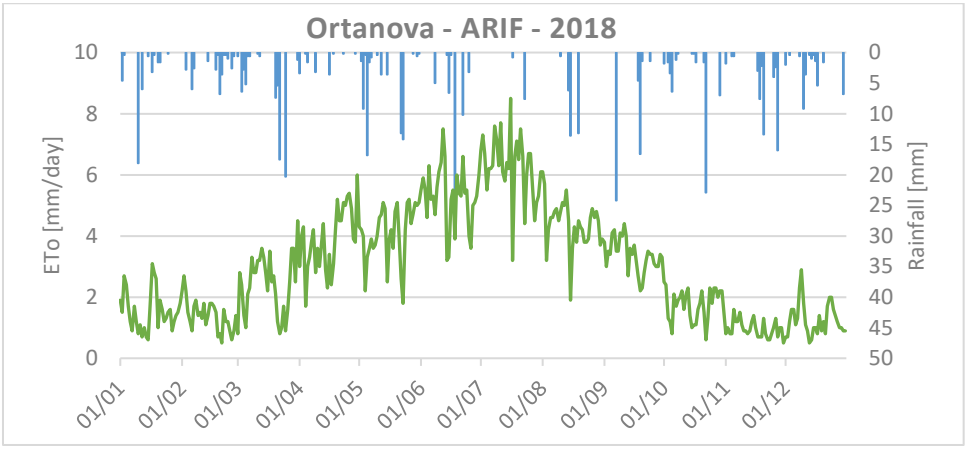
Ortanova - ARIF - 2018
ETo [mm/day]
Rainfall [mm]
0
2
4
6
8
10
0
5
10
15
20
25
30
35
40
45
50
01/01
01/02
01/03
01/04
01/05
01/06
01/07
01/08
01/09
01/10
01/11
01/12

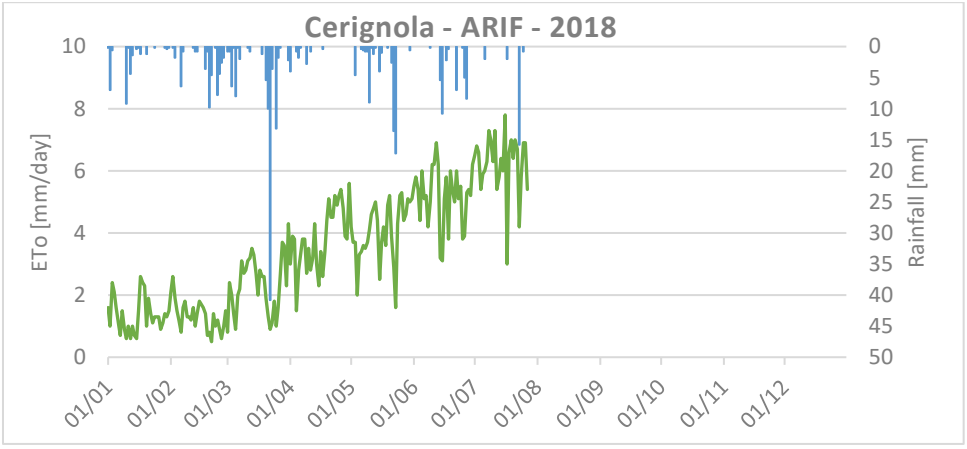
Cerignola - ARIF - 2018
ETo [mm/day]
Rainfall [mm]
0
2
4
6
8
10
0
5
10
15
20
25
30
35
40
45
50
01/01
01/02
01/03
01/04
01/05
01/06
01/07
01/08
01/09
01/10
01/11
01/12

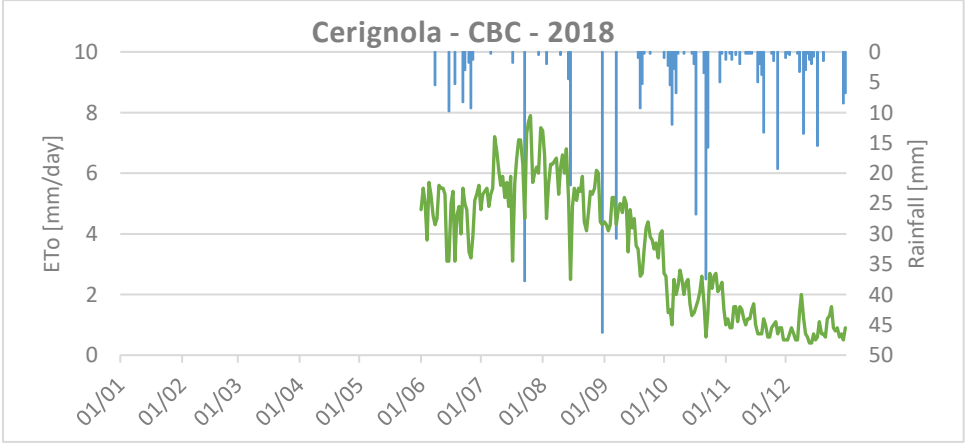
Cerignola - CBC - 2018
ETo [mm/day]
Rainfall [mm]
0
2
4
6
8
10
0
5
10
15
20
25
30
35
40
45
50
01/01
01/02
01/03
01/04
01/05
01/06
01/07
01/08
01/09
01/10
01/11
01/12

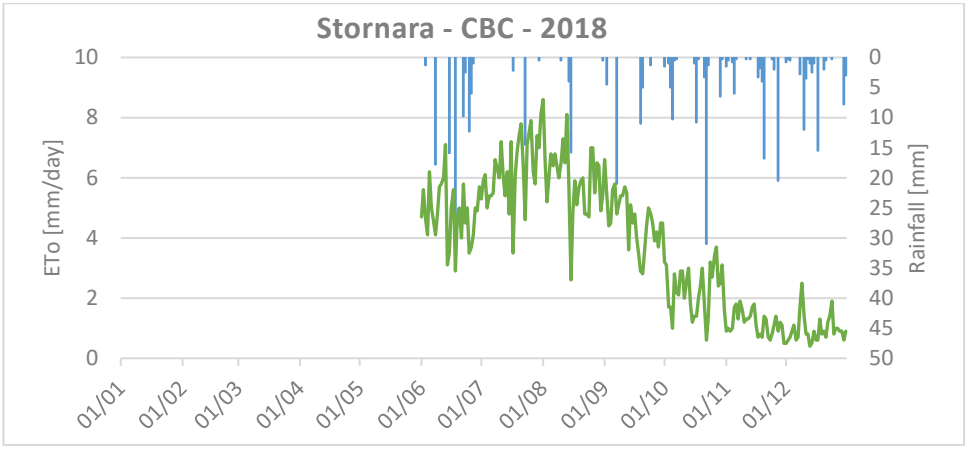

Figure 5.3. Annual time series of precipitation and potential evapotranspiration (ETo) during 2018.

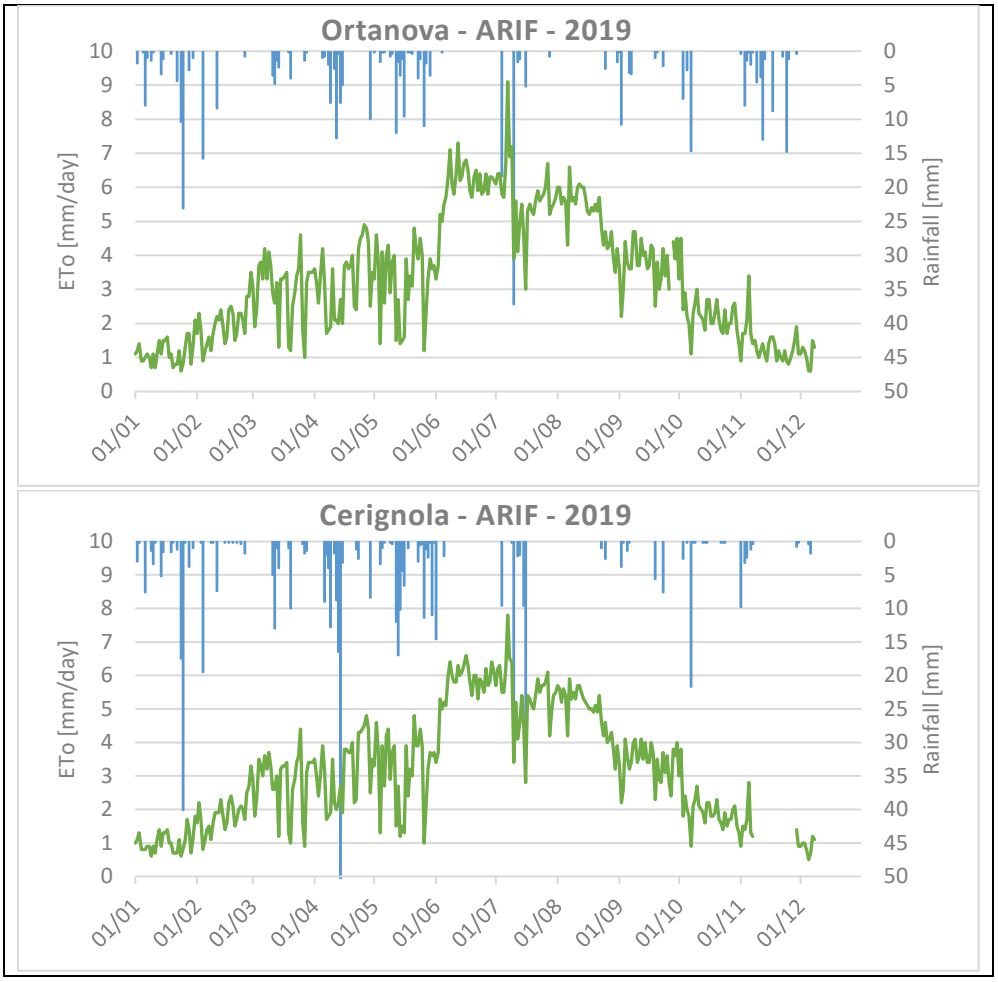

Figure 5.4. Annual time series of precipitation and potential evapotranspiration (ETo) during 2019.

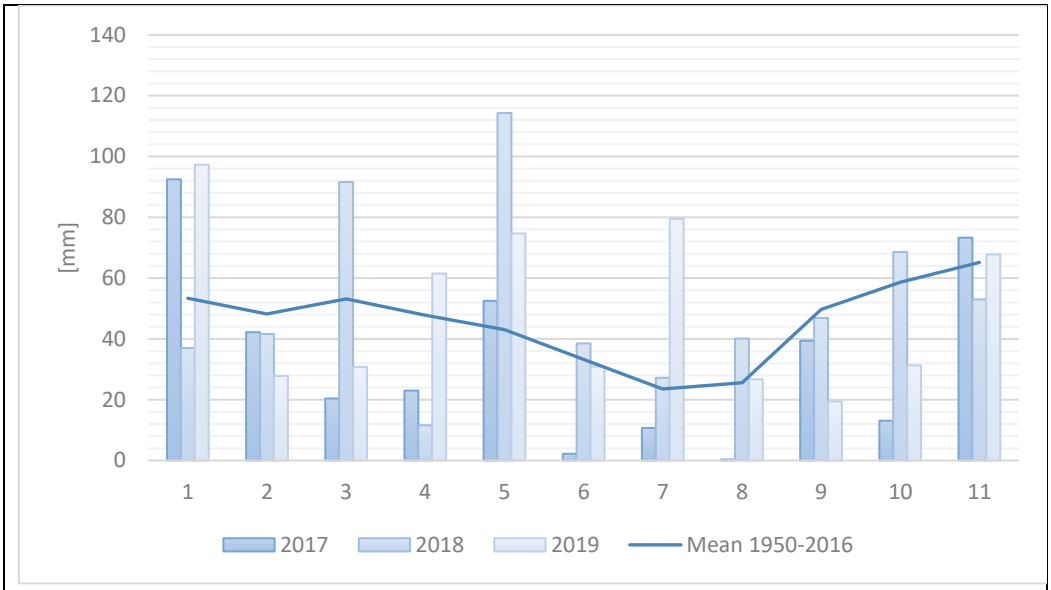

		Precipitation			Percentual variation		
Month	Mean 1950-2016	2017	2018	2019	2017	2018	2019
1	53.3	92.5	37	97.3	+74%	-31%	+83%
2	48.2	42.2	41.6	27.8	-12%	-14%	-42%
3	53.2	20.4	91.6	30.8	-62%	+72%	-42%
4	47.8	23	11.6	61.5	-52%	-76%	+29%
5	43.1	52.5	114.3	74.7	+22%	+165%	+73%
6	33.3	2.2	38.5	30.9	-93%	+16%	-7%
7	23.5	10.7	27.2	79.5	-54%	+16%	+238%
8	25.6	0.3	40.1	26.7	-99%	+57%	+4%
9	49.7	39.4	46.9	19.4	-21%	-6%	-61%
10	58.6	13.1	68.6	31.3	-78%	17%	-47%
11	65.2	73.3	53	67.8	+12%	-19%	+4%
Total	501.5	369.6	570.4	547.7			

Figure 5.5. Precipitation characterization of the Sinistra Ofanto scheme for the reference period 1950-2016 compared to the years of study (2017-2019) and the percentual variation against the long-term average monthly rainfall.

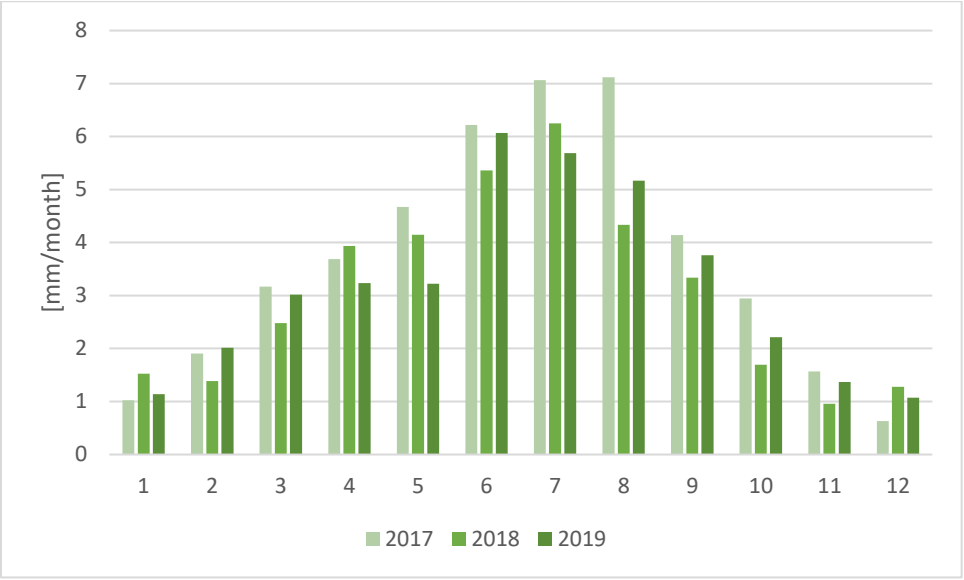

Figure 5.6. Monthly reference Evapotranspiration characterization of the Sinistra Ofanto scheme for the three years of study (2017-2019).

5.1.3. Crop pattern

Annually updated information about the crop pattern of the Sinistra Ofanto scheme is not currently available. The unique data available is, therefore, the *Regional Land Use Map* ("Carta dell'Uso Del Suolo" - UDS) even if it is referred to the year 2011. From the analysis of the Land Use Map, it was possible to estimate the mean crop pattern for each Irrigation District of the "Zona Alta" as reported in Table 5-2. It is important to notice that from the UDS maps it is not possible to estimate the exact extension of winter crops (mainly represented by wheat) and summer crops because they are reported in the unique crop class denominated as "annual crops". Moreover, their spatial distributions can change yearly as the farmers choice analysing a large set of parameters including the water availability and cost and the trend of the market. It is true also for the other crop classes (e.g., it is not possible to sub-divided table and wine vineyard) but in these cases, as the crops are plurennial, can be assumed that looking at the average crop pattern distribution, there are very little changes over consecutive years.

Table 5-2. Crop pattern, reported in hectares and in percentual terms, for each irrigation district of the "Zona Alta" irrigation scheme.

District	Olive	Stone Fruits	Vineyards	Annual Crops	Cropped Area	Total Area [ha]
11	1,323	87	1,611	1,790	4,812	5,262
12	984	1	663	349	1,997	2,097
13	838	18	548	704	2,107	2,172
14	445	17	698	1,971	3,131	3,228
11-14	3,590	122	3,521	4,814	12,047	12,759

District	Olive	Stone Fruits	Vineyards	Annual Crops	Cropped Area
11	25.2%	1.7%	30.6%	34.0%	93.1%
12	46.9%	0.0%	31.6%	16.7%	95.2%
13	38.6%	0.8%	25.2%	32.4%	97.0%
14	13.8%	0.5%	21.6%	61.1%	97.0%
11-14	28.1%	1.0%	27.6%	37.7%	94.4%

The average crop pattern over the entire "Zona Alta" shows that both olives and vineyards occupied almost 28% of the area and 38% is devoted to annual crops. This composition however is not respected considering each district individually (only District 11 follows the average crop mapping of the entire study area). It is possible to notice as the District 14 (located in the highest part of the scheme) shows the highest percentual of annual crops and vice versa the District 12 (the closest to the Ofanto river) it's mostly occupied by olive and vineyards and therefore has the lowest percentual of annual crops.

5.1.4. Selected crop classes and plots

The selected plots falling into the Irrigation District 12 which, as previously described, is mainly occupied by olive trees (46.9%) and vineyards (31.6%) which correspond to the selected crop classes. Since from the crop map available are not provided useful information about the crop variety, it was not possible to further subdivided these two crop class but it is important to notice that in the considered area there is the presence of both table and oil olive and wine and table grapes. These different varieties of course require different managerial cultivation strategies (also for the irrigation) but cannot be assessed unless field surveying that in this case are missing.

Tree crops and vines have more complex behaviour and have been less studied than the major annual crops. For these crop classes currently is not possible to define a simple and robust dynamic simulation model of the yield response to water, as AquaCrop is for the herbaceous crops (Steduto et al., 2012).

Olive (*Olea europaea L.*) is an evergreen tree grown primarily between 30 and 45° latitude in both hemispheres even if the almost total harvested area (95.5 %) was concentrated in ten countries surrounding the Mediterranean Sea: Spain, Italy and Greece are the main producers of virgin oil followed by Tunisia, Syria, Turkey, and Morocco. Although traditional groves vary in cultivar composition, tree density, training system, degree of mechanization and chemical inputs, they are still the most widespread production system and a landmark of Mediterranean landscapes. About 90 per

cent of the world production of olive fruit is for oil extraction, and the rest is for table olives. Olive trees have been sparsely planted for centuries (typical densities of traditional groves are between 50 and 100 tree/ha), without irrigation, on marginal lands in Mediterranean climate conditions because of their strong resistance to drought, lime and salinity. Intensive orchards have a higher density (ranging between 200 and 550 tree/ha) which translates into higher productivity per unit land area than traditional systems. In areas of annual rainfall higher than 600 mm, production can be maintained under rainfed conditions in soils with good water-holding capacity. However, irrigation plays an important role in the drier areas, and/or for soils with limited water storage. Elsewhere, irrigation plays an important role in stabilizing yields in the years of low rainfall. Irrigation is becoming common in the intensive orchards as it allows early onset of production (from the second to fourth year after planting), high yields (averages up to 10-15 tonne/ha) under optimal conditions and less variability because of alternate bearing. During the last years very high density, hedgerow type, olive orchards (from 1000 to 2000 tree/ha) have been developed to further reduce harvesting costs using over-the tree harvesting machines. In these systems, due to the higher ETc demand of the dense canopies and the low soil volume available for each tree, irrigation is needed. This last system is not yet adopted in the Sinistra Ofanto scheme.

Grapevine is a long-lived deciduous crop with temperature-driven phenology. The annual cycle of grapevine in temperate and cool environments includes a dormancy phase and a phase of active vegetative and reproductive development and growth. Grapevines are grown in Mediterranean-type climates in southern Europe, California, and parts of South Africa, Chile, and Australia. Winter rainfall often ensures soil water storage that allows for early growth, whereas a pattern of terminal drought is typical of rainfed vines in Mediterranean environments. Rainfall pattern and soil-water storage capacity are major drivers of the temporal pattern of water supply and water deficit in rainfed systems. Temporary water deficits are common in temperate, summer rainfall regions of western and central Europe where vineyards are established in shallow soils or soils with low water-holding capacity.

To compare the estimated with the Applied Irrigation Water volumes (as reported in Chapter 7.2) particular attention was paid to the selection of the plots to find a unique correspondence with the upstream hydrant. Indeed, as the average farm sizing is small, in general at each hydrant corresponds to more than one farm (and more crop types). Using this criterion, among the 505 hydrants present over District 12, only 18 olive and 7 vineyard plots were selected. Their spatial distribution is reported in Figure 5.7.

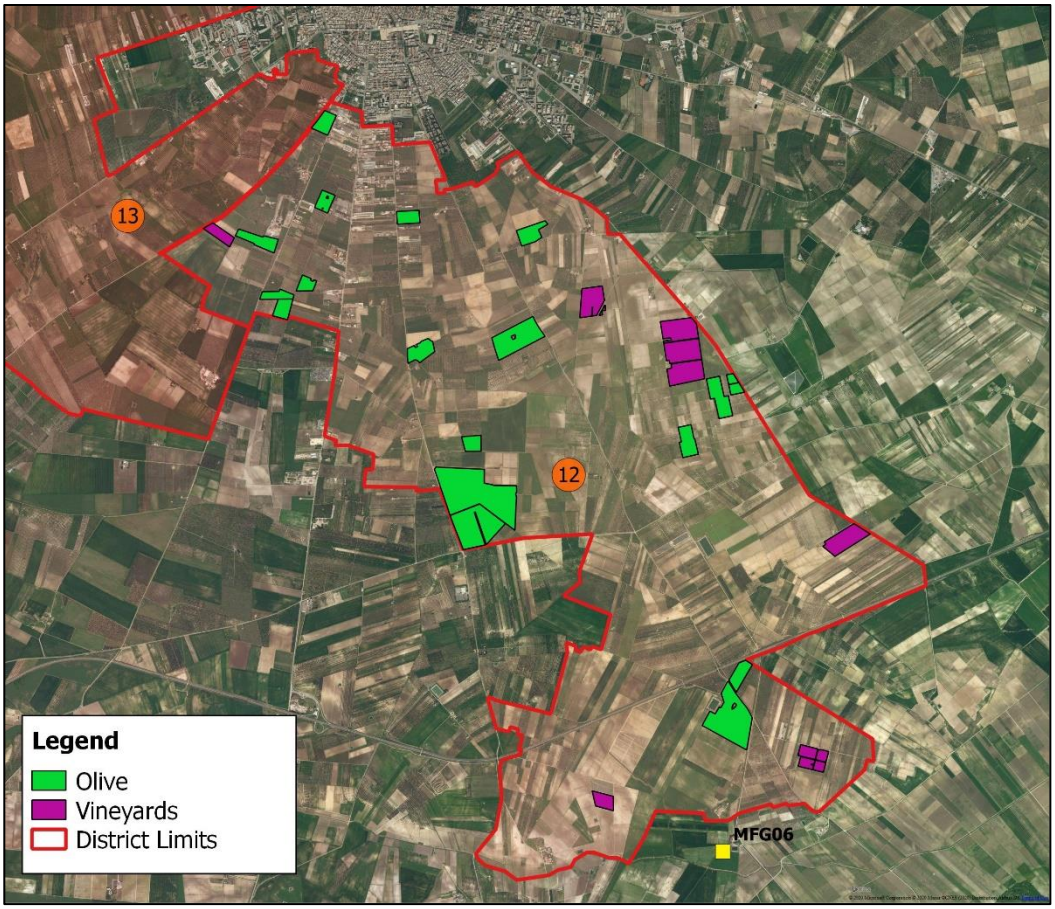

Figure 5.7. Spatial distribution of the selected Olive (green) and Vineyards (violet) plots.

5.2. The "Canal del Zujar Irrigation District" (CZID - Spain)

The *Canal del Zujar Irrigation District* (CZID) is a Water User Association (WUA) located in southwest Spain (Extremadura region) (Figure 5.8) covering a total area of 21,141 hectares organized in 10 independent hydraulic sectors. In particular, the *"Sector II"* of the CZID was selected for this work. It covers an irrigated area of 2,691 hectares and is composed of 1,466 hydrants. Sector II is equipped with a telemetry system that, through a flowmeter installed in each hydrant, records the volume of Irrigation Water Applied (IWA) at an hourly scale. The water consumption records were aggregated on daily basis in each hydrant for the 2017 irrigation season. Besides, for each hydrant, information about the type of crop and the farm size is also recorded.

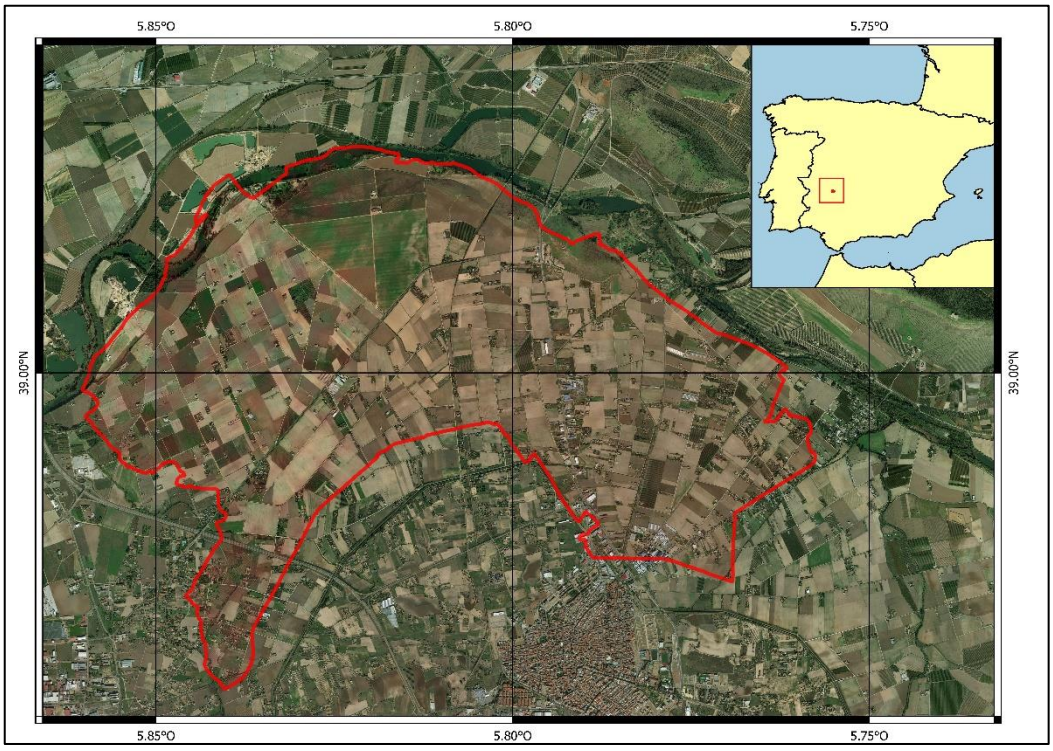

Figure 5.8. Identification of the Sector II of CZID (S.R. WGS84) and its position in the Iberian Peninsula (upper right box).

The main crops are tomato, maize, and rice. Drip irrigation is used for tomato and maize crops, while rice is flood irrigated. The average and standard deviation of the

area of the farms are 1.15 ha and 2.08 ha, respectively. However, a farm that covers an area of 26 ha can be found in this WUA.

The average temperature in the area ranges from 7.1 °C in January to 25 °C in July, and the average maximum temperature ranges from 13.2 °C to 35.1 °C. The average annual rainfall is 390 mm. The maximum evapotranspiration occurs in July, with a daily average value for this month of 7.03 mm. The average annual evapotranspiration is 1,296 mm.

5.2.1. Satellite dataset

Following the procedure for the selection of the best quality satellite images available, as previously described in Paragraph 4.3.1, 23 Sentinel-2 images (reported in Annex 2.) were retrieved from the Copernicus Open Access Hub (https://scihub.copernicus.eu/). Since the Level-2A became an operational product starting from the middle of March 2018, the first three images were generated from the Level-1C product using the Sentinel-2 Toolbox.

The resulting effective temporal resolution of the images acquisition is in line with the theoretical "cloud-free" temporal resolution and therefore adequate to crop monitoring. Only in the first part of the year can be observed a reduction in the number of available images, due to the presence of clouds and the limited operativity of the Sentinel-2 mission (the Sentinel-2B was launched only in the 7th March 2017).

5.2.2. Meteorological data

The daily climatic data used in this work were retrieved from the closest weather station, "Don Benito-EFA", of the *Sistema de Información Agroclimática para el Regadío* (SiAR). In particular, the following daily climatic data, recorded from 1st January 2017 until 31st December 2017, were used: maximum and minimum temperature (T) and relative humidity (RH), precipitation (P) and, average Wind Speed (WS) and Solar Radiation (SR). In the Figure 5.9 and Figure 5.10 are reported the annual pattern of Temperature, Precipitation and, potential evapotranspiration (ETo) recorded during

2017. More information about the weather station is available at http://redarexplus.go-bex.es/.

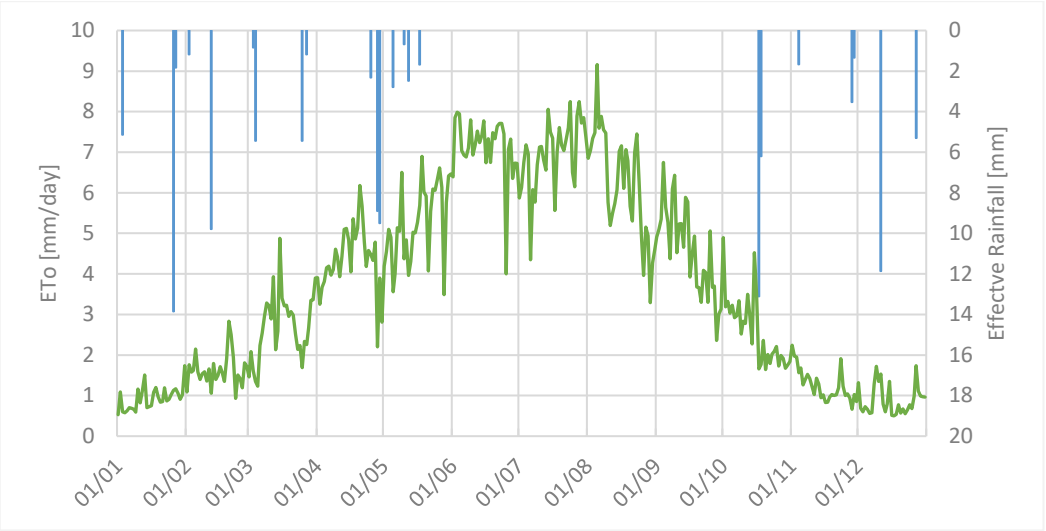

Figure 5.9. Annual time series of Effective Precipitation and potential evapotranspiration (ETo) during 2017 recorded and estimated at the weather station "Don Benito-EFA".

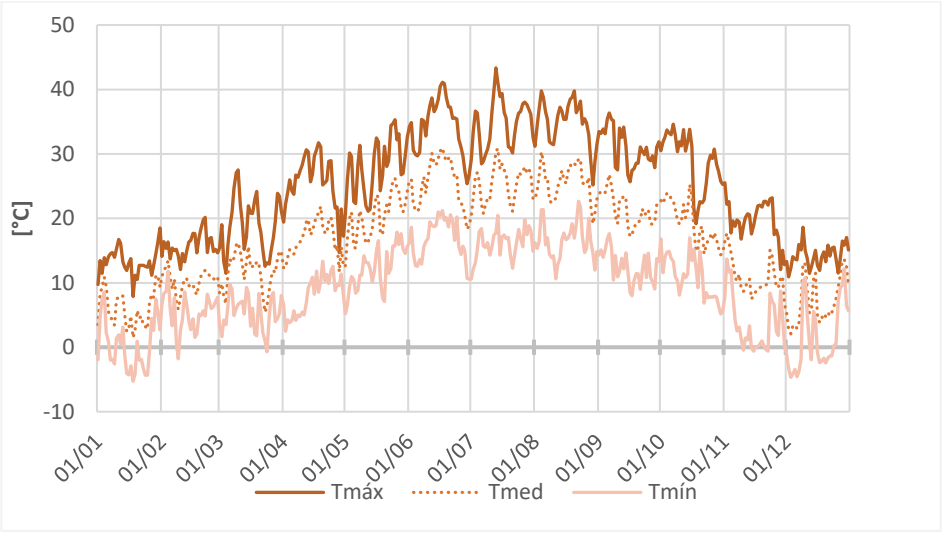

Figure 5.10 – Annual time series of daily maximum, mean and minimum Temperature (T) 2017 recorded and estimated at the weather station "Don Benito-EFA".

5.2.3. Selected crop classes and plots

Tomato and maize, the first two crop types for surface occupied in the CZID area, were selected. Respectively 67 and 18 plots were selected for each class. Even in this case, where the IWA data was available at daily scale for all the 1,466 hydrants, was necessary to effectuate a selection due to the mismatching between the crop cover map with the area served by each hydrant (which based on the cadastral map and does not consider the real extension of the farm).

The spatial distribution of the selected plots is reported in Figure 5.11 and covers almost uniformly all the CZID area.

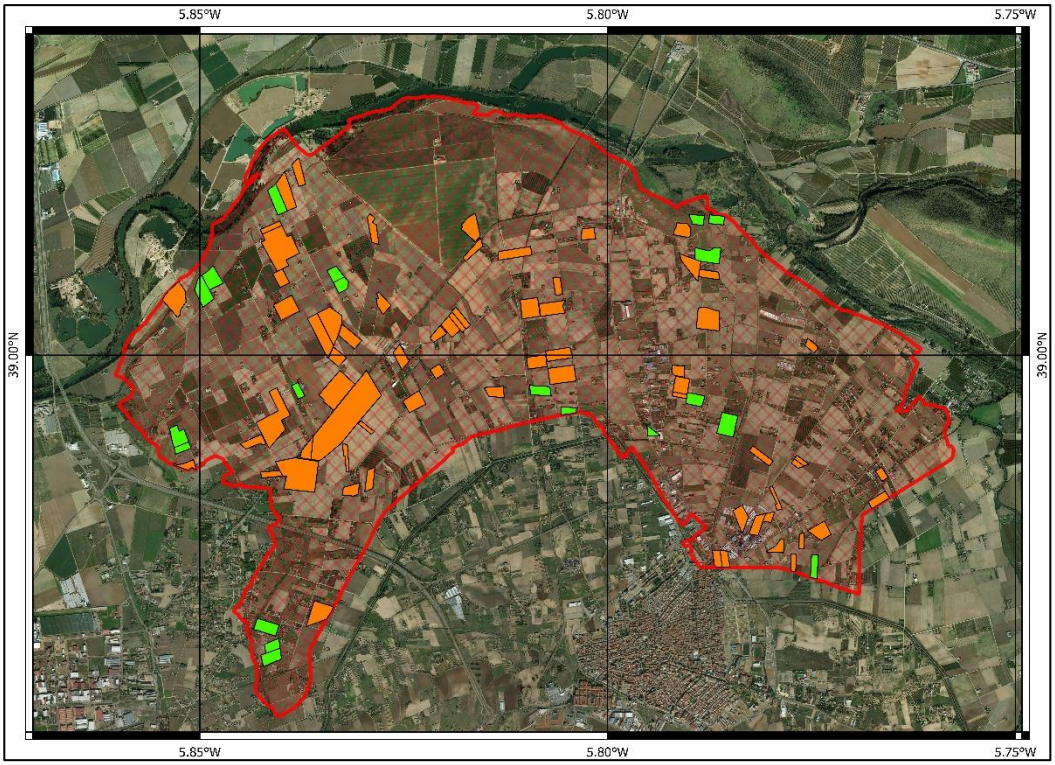

Figure 5.11. Spatial distribution of the selected tomato (red) and maize (green) plots.

Maize and tomato are not only the first two crop types for surface occupied in the CZID, but are twos of the most important cultivation in the Mediterranean context (Steduto et al., 2012).

Maize (Zea mays L.) ranks as the most important crop worldwide in terms of grain production. Although wheat and rice are the most important for direct human consumption, maize seeds are often the main component of animal feed. Moreover, it is used also to produce vegetable oil, sugar syrup, alcohol as biofuel, and feedstock for the manufacturing of plastic. Maize originated in a climate with warm summers. It is grown, however, extensively in temperate regions for grain as well as for silage. For the latter, the crop is harvested before full maturity, when the grains are in the late phase of filling and the vegetative material still mostly green, is coarsely chopped and partially fermented as animal feed. Even in areas with a growing season too short for grain to mature, maize is popular as a crop for silage and forage. Where rainfall amount and distribution are usually favourable and the soil is deep with a high water-holding capacity, maize is grown without irrigation or only with supplemental irrigation. In the more arid areas, maize is irrigated. Seasonal maize water use varies according to evaporative demand of the atmosphere, and hence according to climate, time of the season when the crop is grown, the life cycle length of the crop, and water availability. For well-watered situations, seasonal ET ranges from less than 500 to more than 800 mm, the typical seasonal ET of a cultivar of medium-season length grown in a temperate climate at a latitude of 35º to 40º being around 650 mm. These global values are in line with the standard CWRs values for grain and fodder maize provided from the SIAR for the considered crop season and which value respectively 800 and 565 mm.

Tomato is the second most valuable vegetable crop next to the potato. It requires soils with proper water-holding capacity and aeration and is intolerant to soil compaction and waterlogging. Well-drained, deep, sandy loam soils are preferred, but heavier soils can also be highly productive under proper management. At some locations tomato needs a 3-year rotation, with crops other than solanaceous (e.g., potato, pepper, eggplant, tobacco), to minimize nematodes, virus, and bacterial diseases. The life cycle varies from 95-115 days for processing tomato (cultivated in the CZID) or up to more than 145 days for undetermined fresh market tomato. Processing tomato consumes 400-800 mm of water from emergence/transplanting to harvest, depending on climate, plant type, soil, irrigation, and crop management. The reference value of CWR

provided by the SIAR for the growing season 2017 is 615 mm. Over the peak growing period, maximum water uses in average is equal to 4-7 mm/day in a sub-humid climate but can reach 8-9 mm/day in more arid areas. Tomato plants can tolerate drought to some degree; therefore, soil moisture levels can reach 50 per cent of the TAW without significant yield losses after the development of the canopy is completed. It is important to maintain adequate soil moisture levels early in the life cycle, at transplanting, and from the first flower until complete fruit setting (e.g., of the fifth truss on the main axes). Irrigation can stop a few weeks before harvest, depending on soil water storage and rainfall expectancy.

6. THE IMPROVED EO-BASED "ONE-STEP" FAO-56 METHOD: validation and application at the plot scale

6.1. Methodological approach

6.2. Statistical Performance metrics

The following types of metrics were calculated to assess the performance of the simulation for both CWR and IWR estimation. Assuming that O_i and P_i are the observed and the predicted values, and *n* the number of observations, the metrics used assumed can be written as:

Standard Deviation

$$SD = \sqrt{\frac{\sum_{i=1}^{n}(X_i - \bar{X})^2}{n}} \tag{41}$$

A disadvantage of the Standard Deviation is the unsuitability to determine inter-unit variation. Therefore, the SD is normalized into the **Coefficient of Variance**:

$$CV = \frac{SD}{\bar{X}}\,[\%] \tag{42}$$

Mean Error

$$ME = \frac{\sum_{i=1}^{n}(P_i - O_i)}{n} \tag{43}$$

Mean Percentage Error

$$MPE = \frac{1}{n}\sum_{i=1}^{n}\frac{(P_i - O_i)}{O_i} \tag{44}$$

Mean Absolute Error

$$MAE = \frac{\sum_{i=1}^{n}|P_i - O_i|}{n} \tag{45}$$

Mean Absolute Percentage Error

$$MAPE = \frac{1}{n}\sum_{i=1}^{n}\frac{|P_i - O_i|}{O_i} \tag{46}$$

Root Mean Square Error

$$RMSE = \sqrt{\frac{\sum_{i=1}^{n}(P_i - O_i)^2}{n}} \tag{47}$$

The RMSE is a difference-based evaluation giving an indication of the coincidence or lack of coincidence between simulated and measured value, was calculated. RMSE indicates the difference between measured and simulated values and has the advantage of producing a result in the same units as that used for measurement. The calculated RMSE can be compared with the size of the difference that is considered acceptable. A disadvantage of RMES lies in that the residual errors are calculated as squared values, which means that higher values in a time series are given greater weight than lower values.

Coefficient of determination - R^2

In the linear regression between observed and model-estimated values estimates of the intercept and the slope are good indicators of accuracy. Best values of intercept and slope are zero and 1, respectively.

6.3. Testing the classical EO-FAO56 approach to estimate the ET

As previously remarked, the assumption of setting the surface resistance (r_s) at its minimum value corresponding to set the bulk stomatal resistance at its minimum value, usually assumed equal to 100 ms^{-1} (as done in FAO P-M equation), allows to estimate the maximum (potential) crop ET. The ET estimated under this hypothesis was analysed and compared at the plot scale over the selected plots of the two selected study areas. However, due to the absence of field measurement of ET, the comparison was made in terms of crop coefficient (Kc) values using locally validated datasets: for the "Zona Alta" they were obtained from the last regional water accounting report ("*Bilancio Idrico Irriguo"* - www.sit.puglia.it); while, for the "CZID" the were retrieved, as the meteorological data, from the *Sistema de Información Agroclimática para el Regadío* (SiAR) website.

The Kc values for the Zona Alta were additionally corrected, as suggested into FAO-56 guidelines, to consider the effects of climate conditions (wind speed and the minimum relative humidity) and crop height:

$$K_{C,Corrected} = K_c + \ [0.04(u_2 - 2) + 0.004\ (RH_{min} - 45)] \left(\frac{h_c}{3}\right)^{0.3} \qquad (48)$$

The height of olive and vineyard was considered constant and the used values were fixed respectively to 4 and 2 meters. This correction was not applied to the CZID study area since the temporal evolution of the crop height for each plot is unknown.

As demonstrated respectively in Figure 6.1 - Figure 6.2, the direct application of the EO-based "one-step" FAO-PM approach leads to overestimating the Kc (and therefore ET) for olive and vineyards. For almost all the considered plots, the estimated Kc values are higher than the reference literature-based Kc, sometimes also 2 times higher. For vineyards plots, the Kc during the midseason growth phase, corresponding to its maximum value, range between 1.10 and 1.25 in almost all plots and during the three years, while the literature value for the study area is estimated at 0.70. However, the pattern of the temporal trend follows the phenology of the crop while for the olive it seems to be influenced also by the presence of weeds crops among the trees.

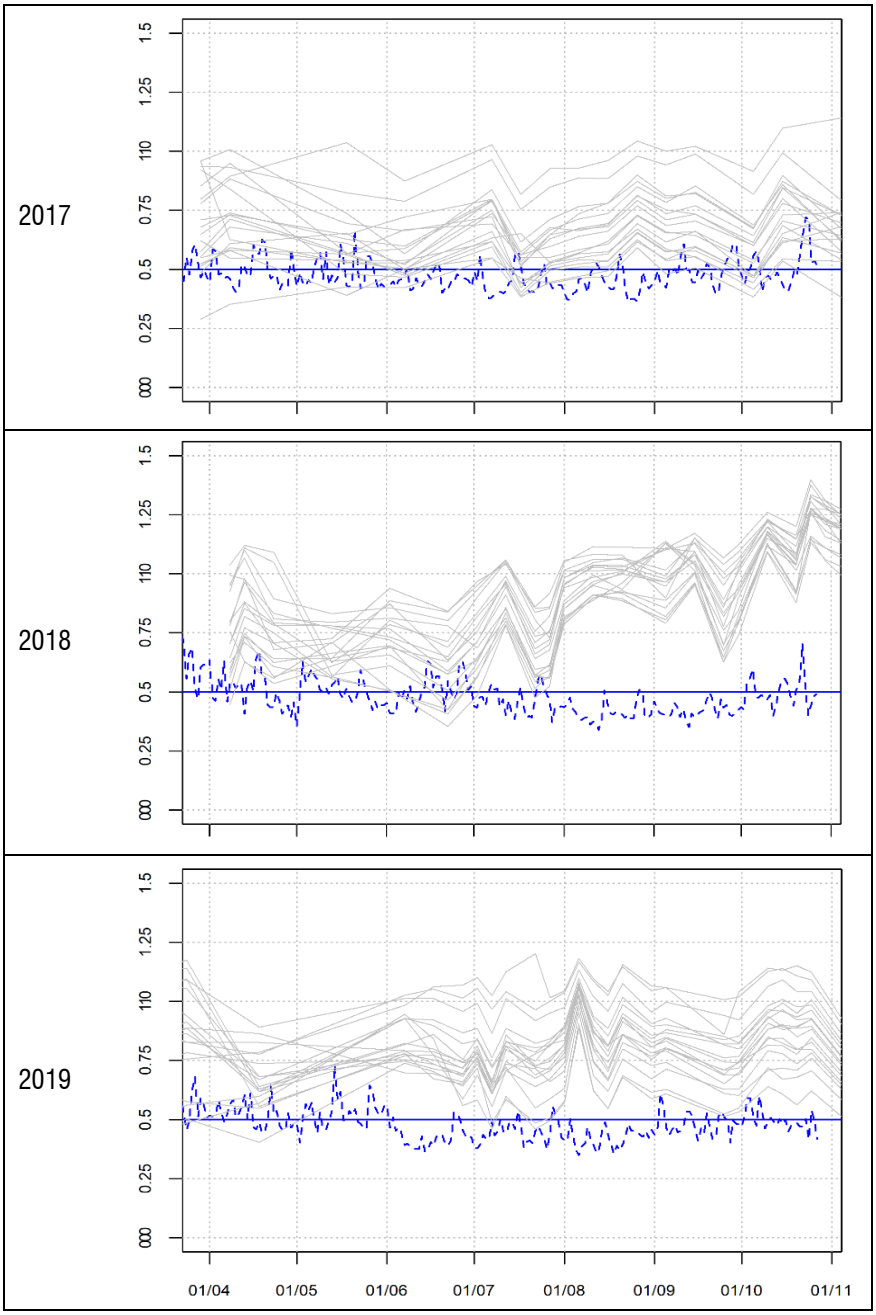

Figure 6.1. Olive's Kc estimated at plot scale (in grey) using the classical version of the EO-based "one-step" FAO-PM approach versus the "standard" Kc and $Kc_{Corrected}$ (respectively the solid and dashed lines).

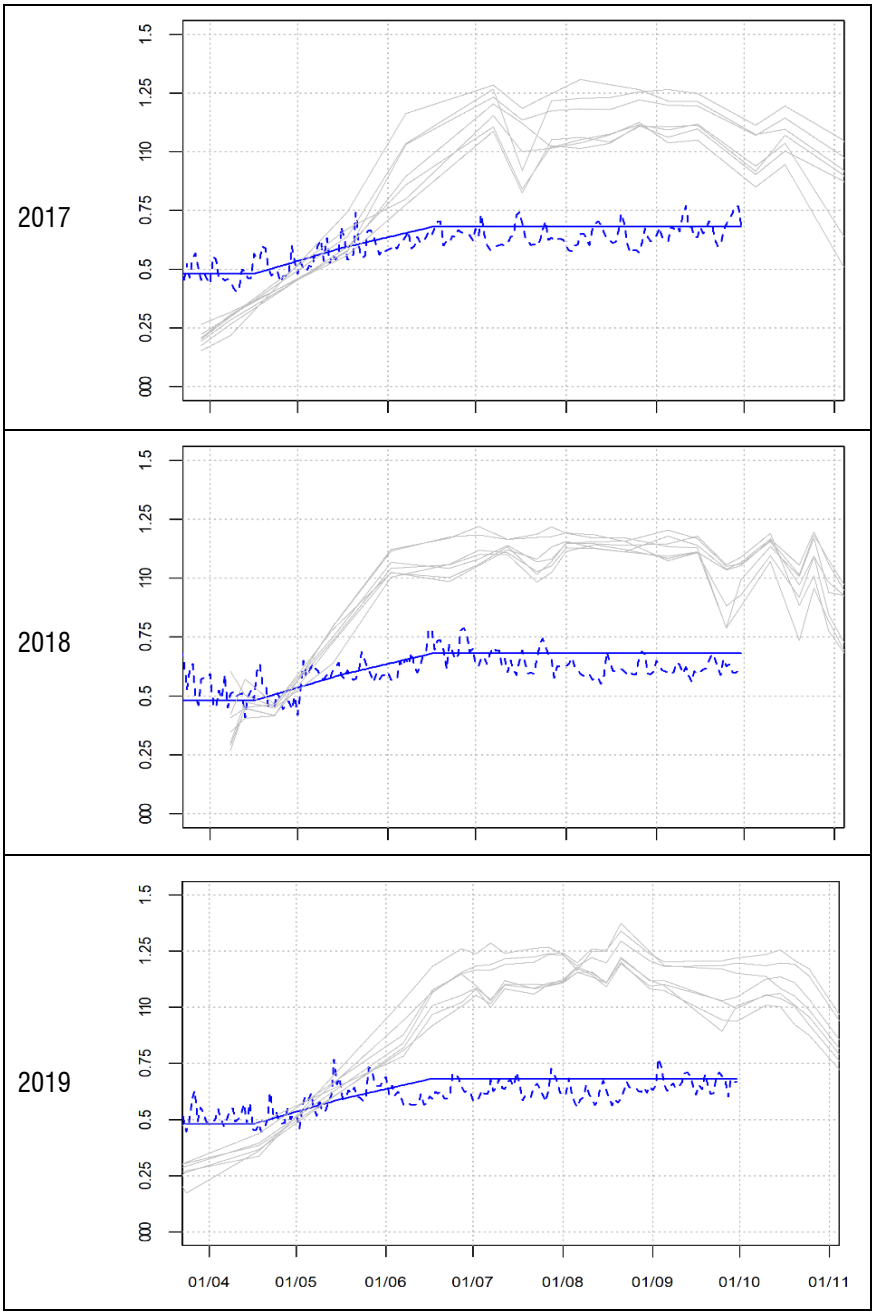

Figure 6.2. Vineyard's Kc estimated at plot scale (in grey) using the classical version of the EO-based "one-step" FAO-PM approach versus the "standard" Kc and $Kc_{,Corrected}$ (respectively the solid and dashed lines).

The Kc values estimated for the herbaceous crops (maize and tomato) results to be lower than the Kc values retrieved from the SiAR and valid for the CZID area. Even if the trend retrieved from each plot is almost the same, it appears to be shifted in time depending on the plantation date and on the crop growing cycle length, which is farm-specific. From Figure 6.3 it is also possible to notice that the direct use of EO-based "one-step" FAO-PM approach leads to estimate crop ET also before the seeding and after the harvesting when generally the vegetation is absent, and the soil is bare. Also in this case the ETc estimated could be estimated as potential evaporation from the soil (with Ke = 0.20, as usually assumed in literature (Allen et al., 1998)).

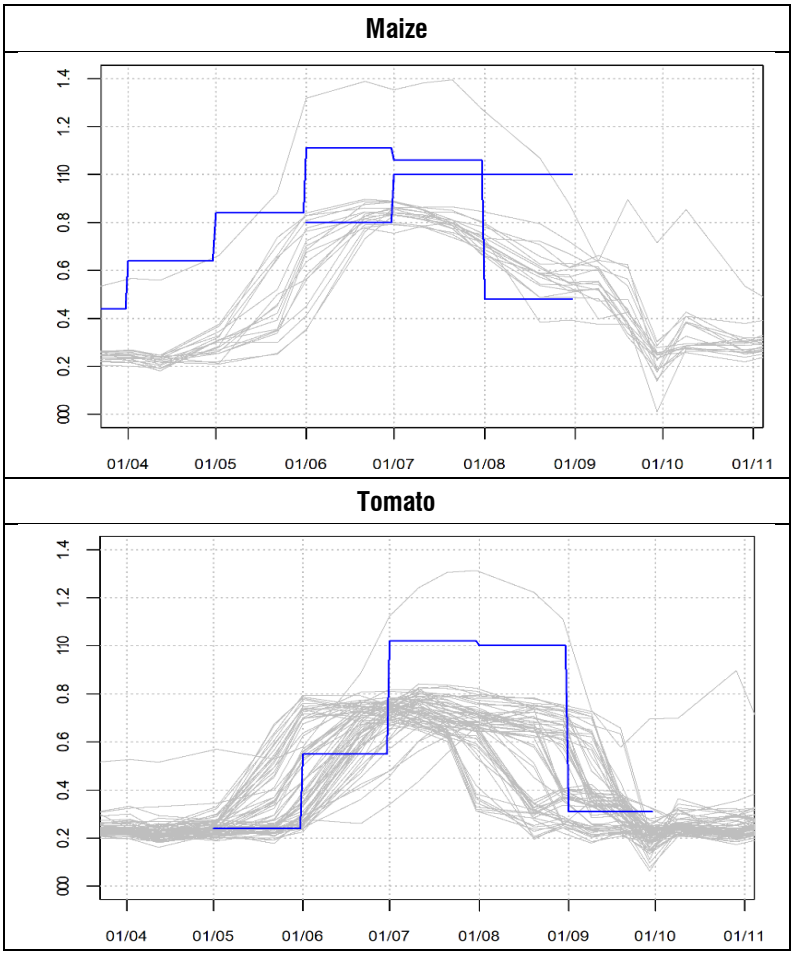

Figure 6.3. Maize and Tomato's Kc at plot scale (in grey) estimated using the classical version of the EO-based "one-step" FAO-PM approach versus the "standard" Kc.

To understand these differences in terms of surface resistance were compared the "standard" surface resistance estimated using the expression on Equation (22) and

adopting a minimum bulk resistance equal to 100 ms^{-1}, with the values retrieved by inverting the FAO P-M equation, as suggested by Shuttleworth (Shuttleworth, 2006), as a function of the Kc and of the dimensionless parameter (R_C^Z) used for the estimation of the aerodynamic resistance used in Equation (30):

$$r_s = \frac{1.056\ (R_C^Z + 144.4)}{K_c} - 1.3297\ R_C^Z \tag{49}$$

As demonstrated in Figure 6.4, Figure 6.5 and Figure 6.6 the assumption of a constant value for the stomatal resistance (assumed equal to 100 sm^{-1}) leads to a underestimate of the surface resistance for every crop class considered.

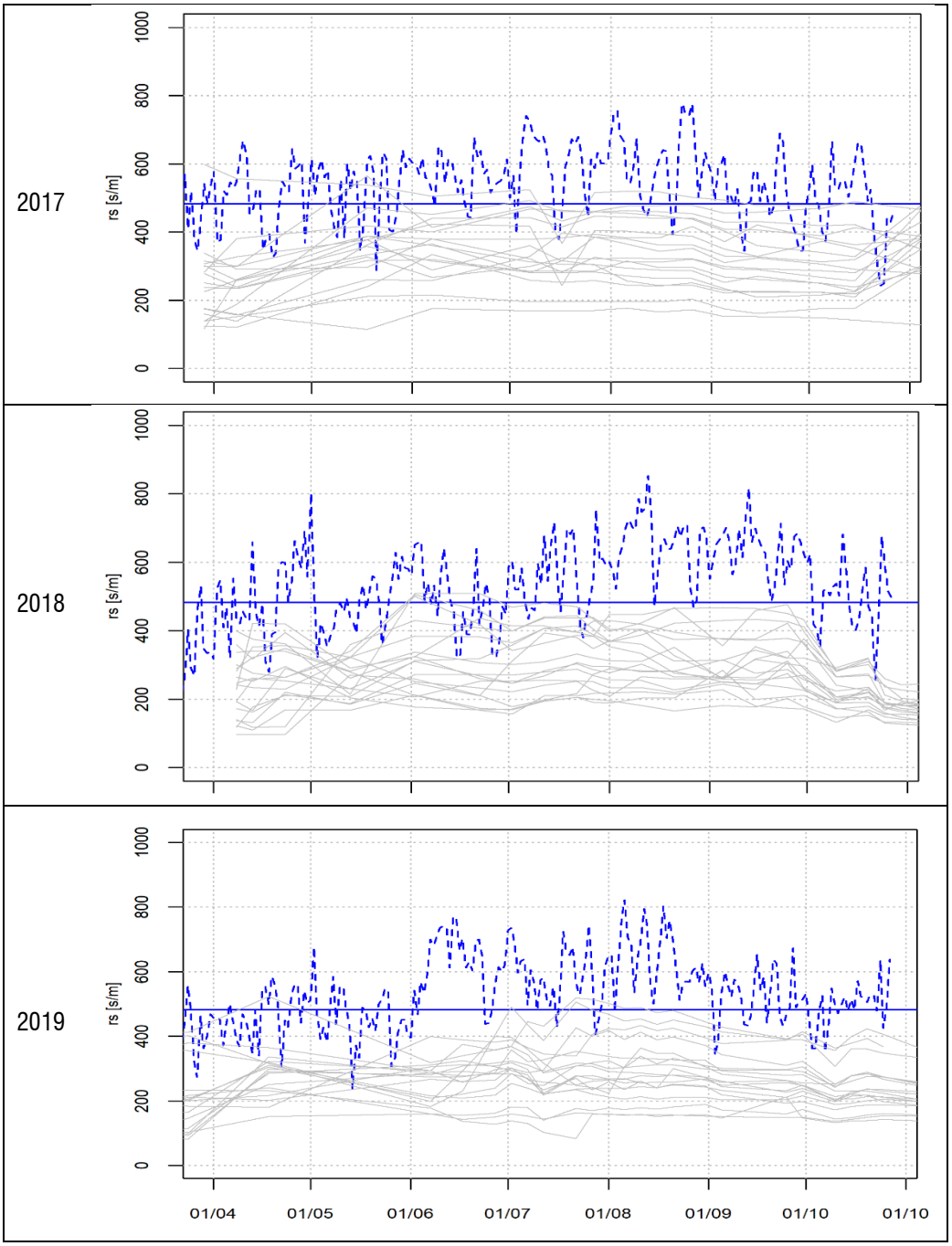

Figure 6.4. Estimated surface resistance (r_s) at plot scale (in grey) versus the "standard" surface resistance obtained for Olive from Equation (49).

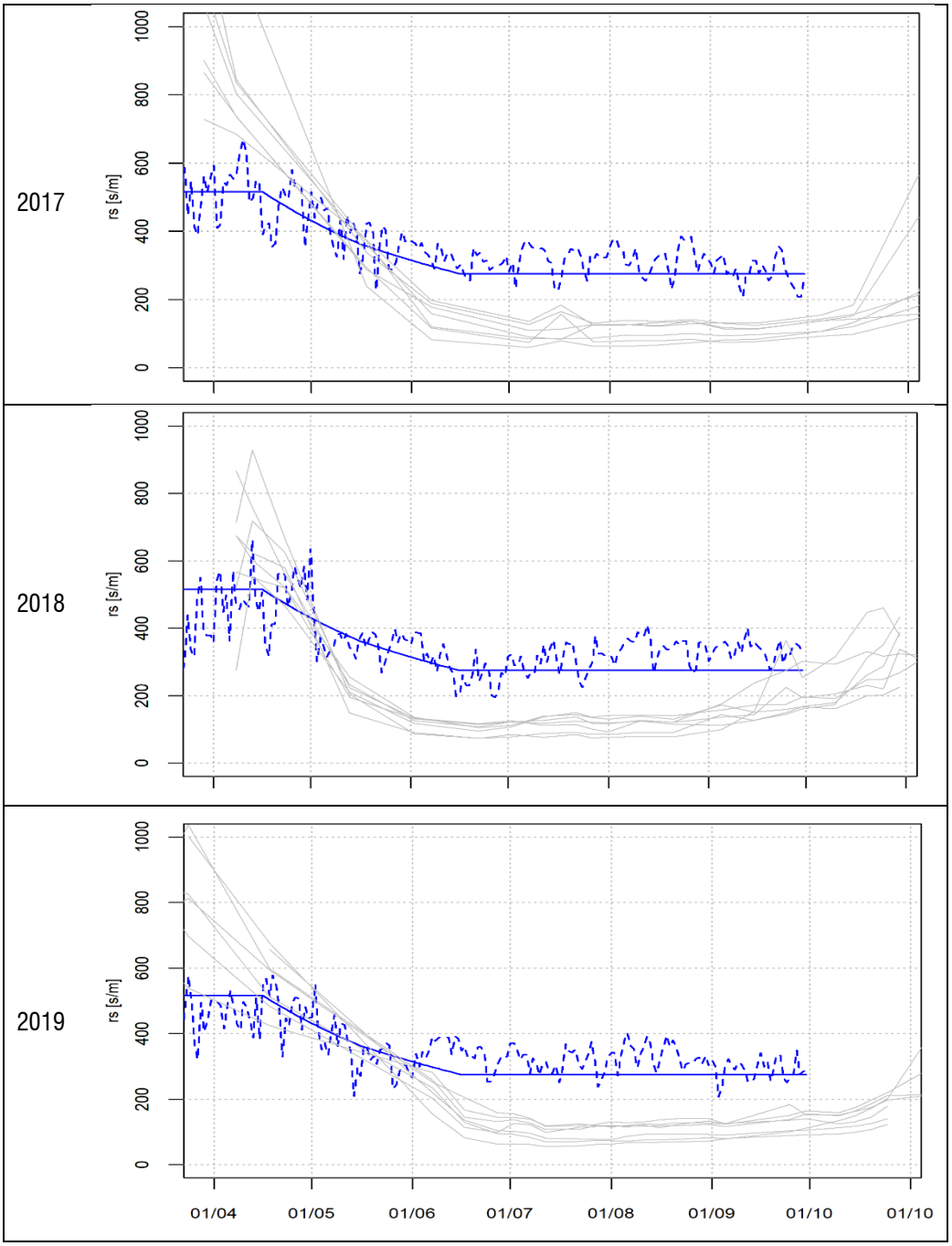

Figure 6.5. Estimated surface resistance (r_s) at plot scale (in grey) versus the "standard" surface resistance obtained for Vineyards from Equation (49).

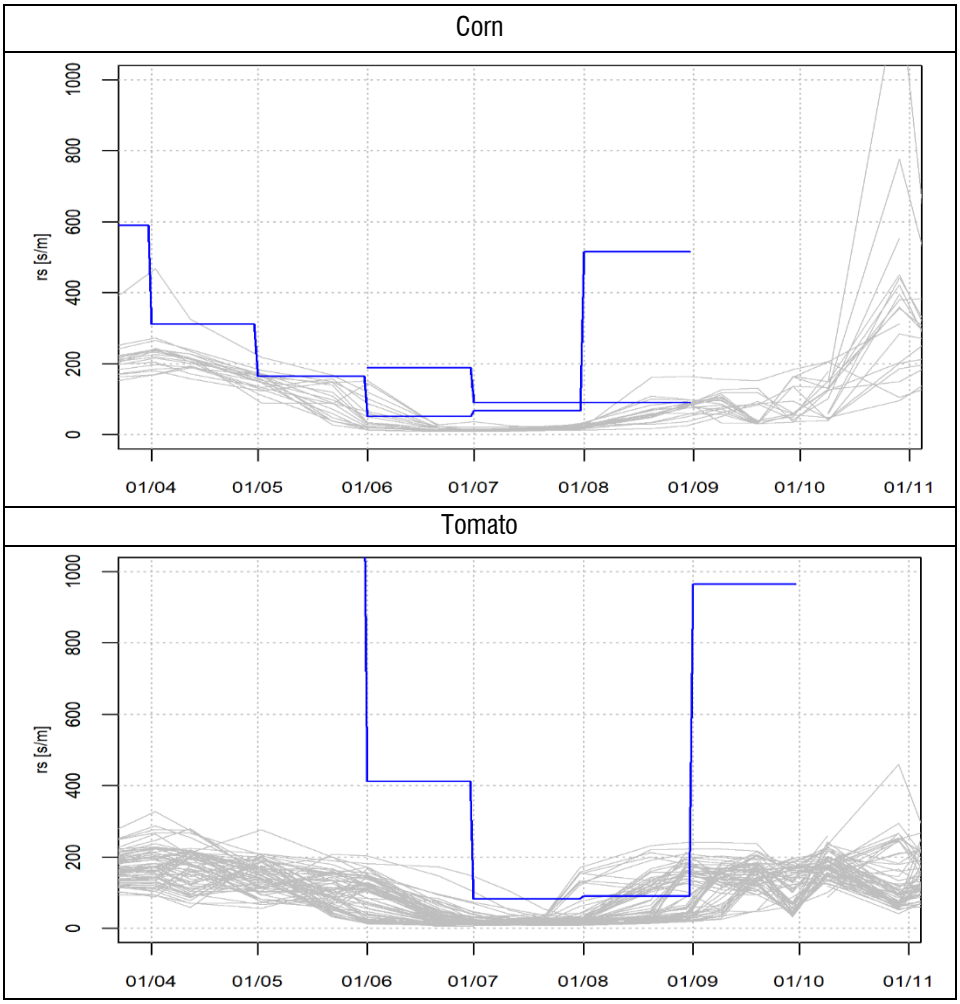

Figure 6.6. Estimated surface resistance (r_s) at plot scale (in grey) versus the "standard" surface resistance obtained for Maize and Tomato from Equation (49).

6.4. Calibrating the proposed expression for the (bulk) surface resistance (r_s) estimation

As demonstrated in the precedent Paragraph 6.3, the assumption of a constant value for the stomatal resistance (assumed equal to 100 sm^{-1}) leads to underestimating the surface resistance for every crop class considered, both for annual and perianal crops. However, even if the values of the surface resistance result always inferior to the FAO-Kc inverted surface resistance, the structure of Equation (22), thanks to the presence of the LAI at the denominator, allows following the phenology of the annual crops. For these crops, as reported in the FAO-56 handbook, the temporal evolution of the LAI is strictly correlated with the crop hight and the crop phenology. For perennial crops, like olives, this is not true because the seasonal variations of the LAI are much more limited.

Starting from these considerations were analysed the temporal patterns of the principal satellite-derived VIs: the Vegetation Fraction Cover (VFC), the NDVI and the LAI. As the NDVI is used, as previously described, in a great number of applications for vegetation monitoring and in many Kc-VI and surface resistance models, the idea was to include the NDVI into the FAO-56 expression of the surface resistance. Moreover, since the specific objectives of the present work, is to develop a not crop-specific surface resistance model, coherent with the surface resistance model adopted by the FAO P-M equation and (sufficiently) representative of the actual crop conditions considering the crop water stress, the simplest linear relation with the surface resistance was imposed:

$$r_s = \frac{\alpha\, NDVI}{LAI_{eff}} \tag{50}$$

For the selection of the value assumed by the coefficient α, different values were selected, and the retrieved surface resistance was compared with the values obtained from Equation (49). In the left column of Figure 6.7 - Figure 6.17 are reported these comparisons made with α assumed equal to 300, 400 and 500 (respectively reported with the letter *a*, *b*, and *c*).

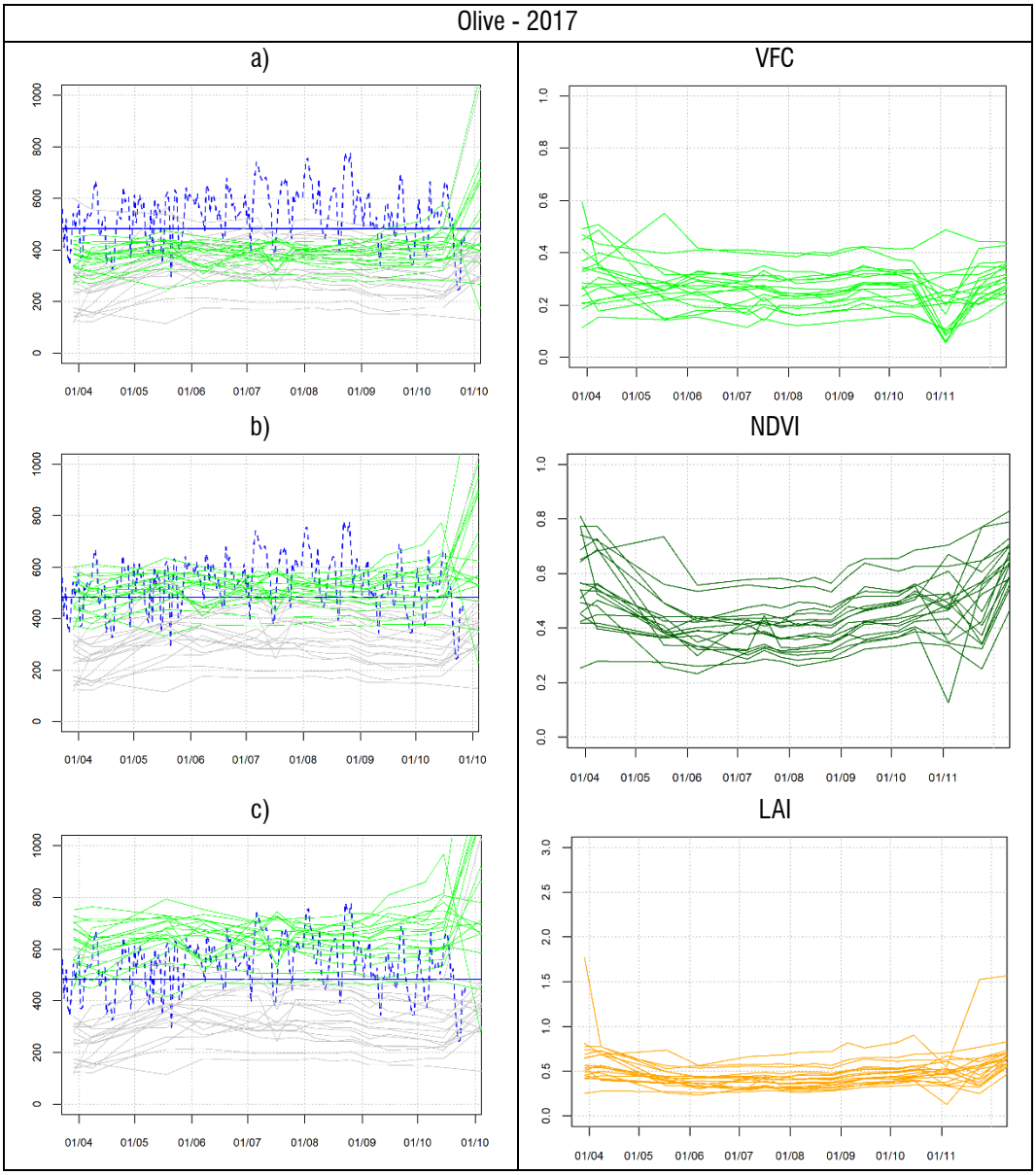

Figure 6.7. Surface resistance estimated for olive fields during the 2017 growing season (left column, using the relation of Equation (38) with α equal to 300 (a), 400 (b) and 500 (c)) and the Vegetation Fraction Cover (VFC), NDVI and LAI (right column).

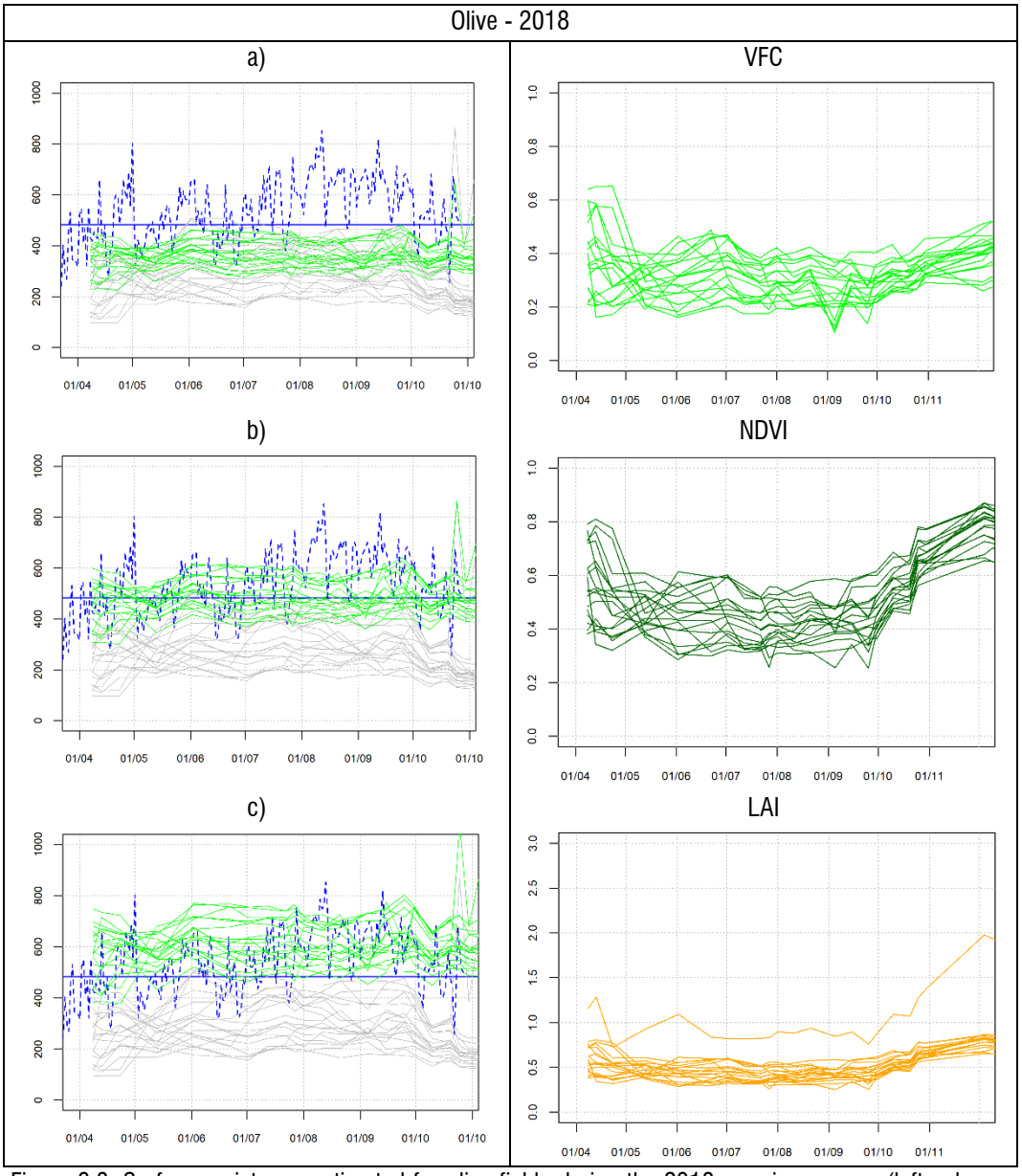

Figure 6.8. Surface resistance estimated for olive fields during the 2018 growing season (left column, using the relation of Equation (38) with α equal to 300 (a), 400 (b) and 500 (c)) and the Vegetation Fraction Cover (VFC), NDVI and LAI (right column).

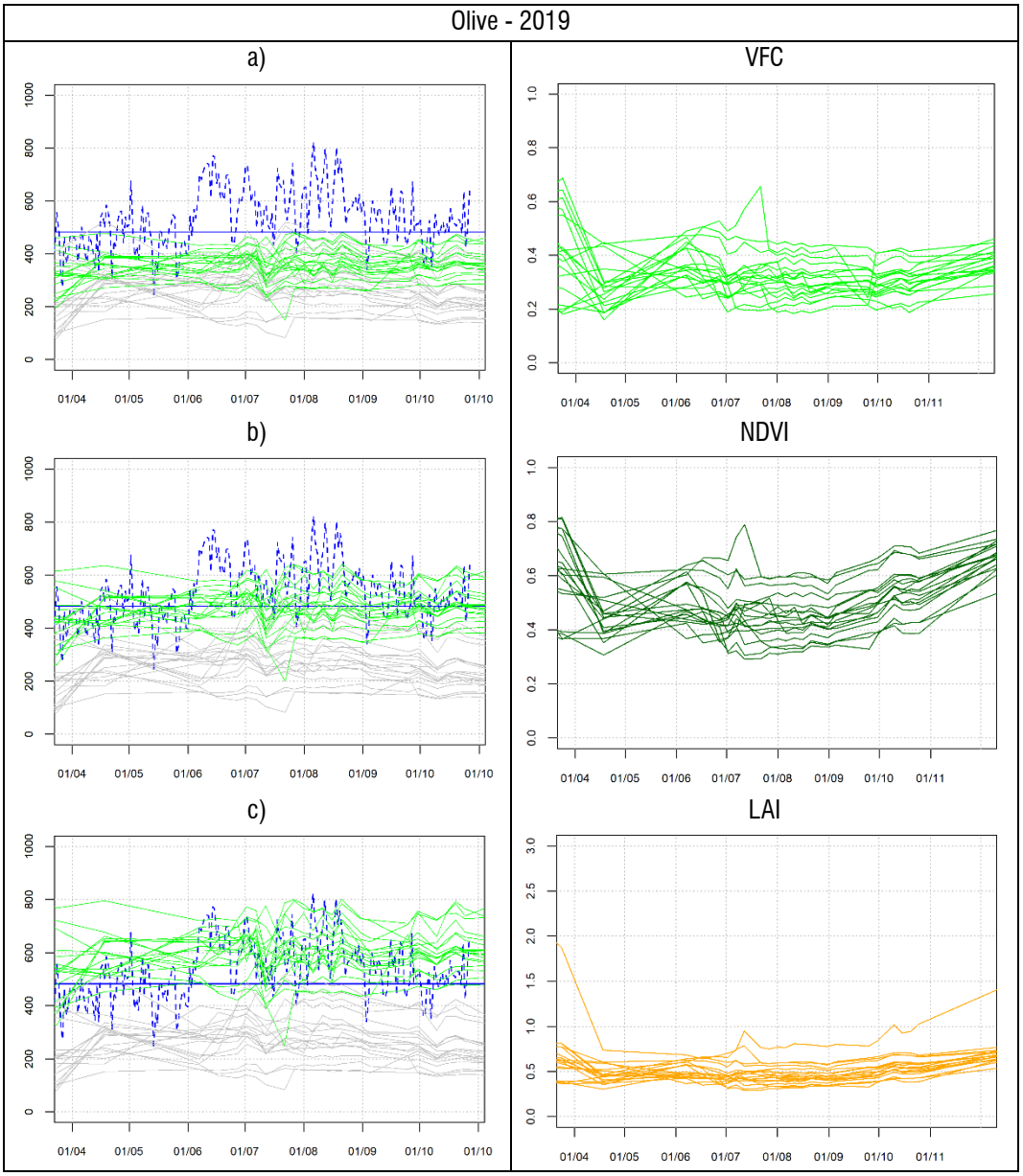

Figure 6.9. Surface resistance estimated for olive fields during the 2019 growing season (left column, using the relation of Equation (38) with α equal to 300 (a), 400 (b) and 500 (c)) and the Vegetation Fraction Cover (VFC), NDVI and LAI (right column).

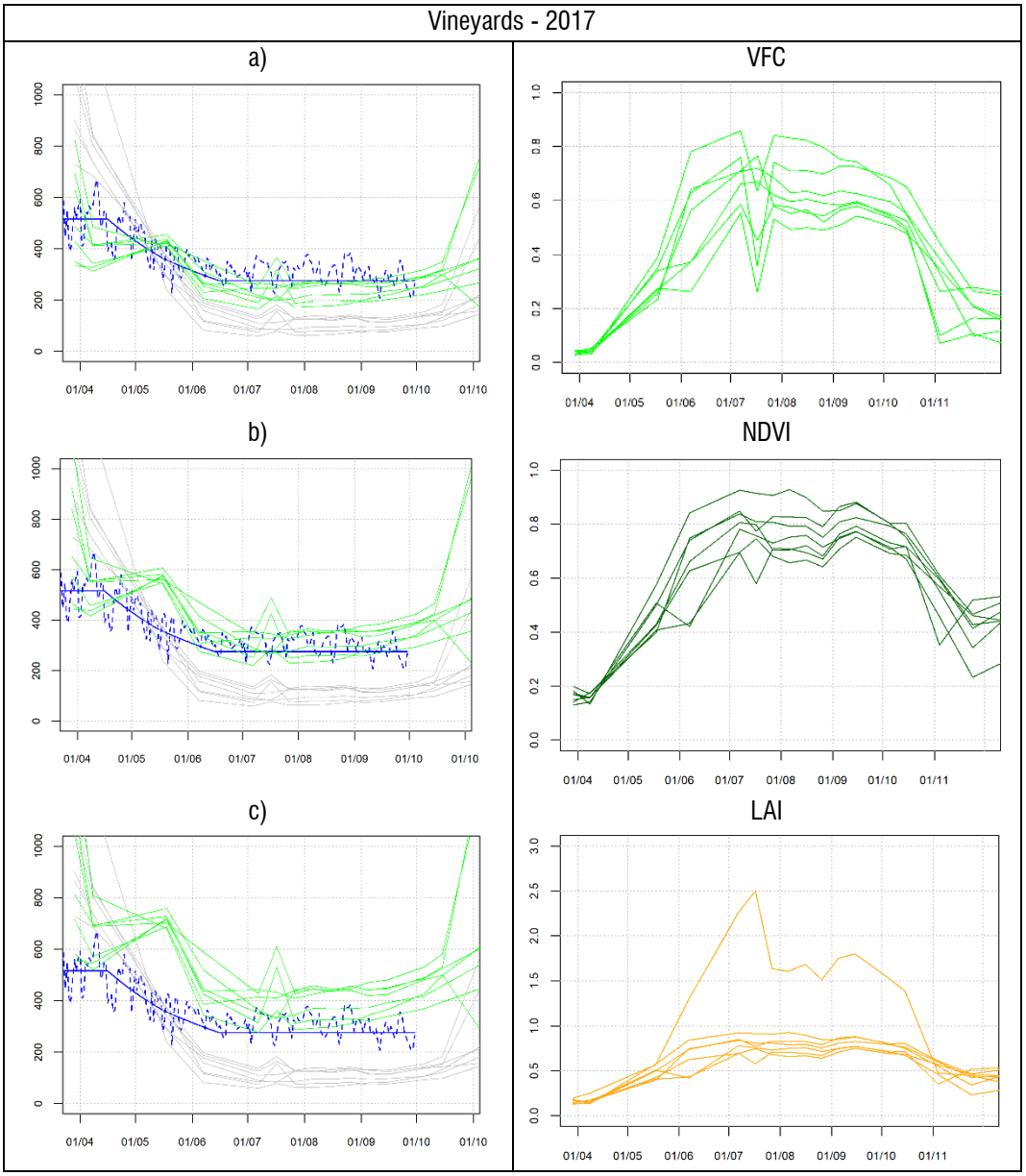

Figure 6.10. Surface resistance estimated for vineyard fields during the 2017 growing season (left column, using the relation of Equation (38) with α equal to 300 (a), 400 (b) and 500 (c)) and the Vegetation Fraction Cover (VFC), NDVI and LAI (right column).

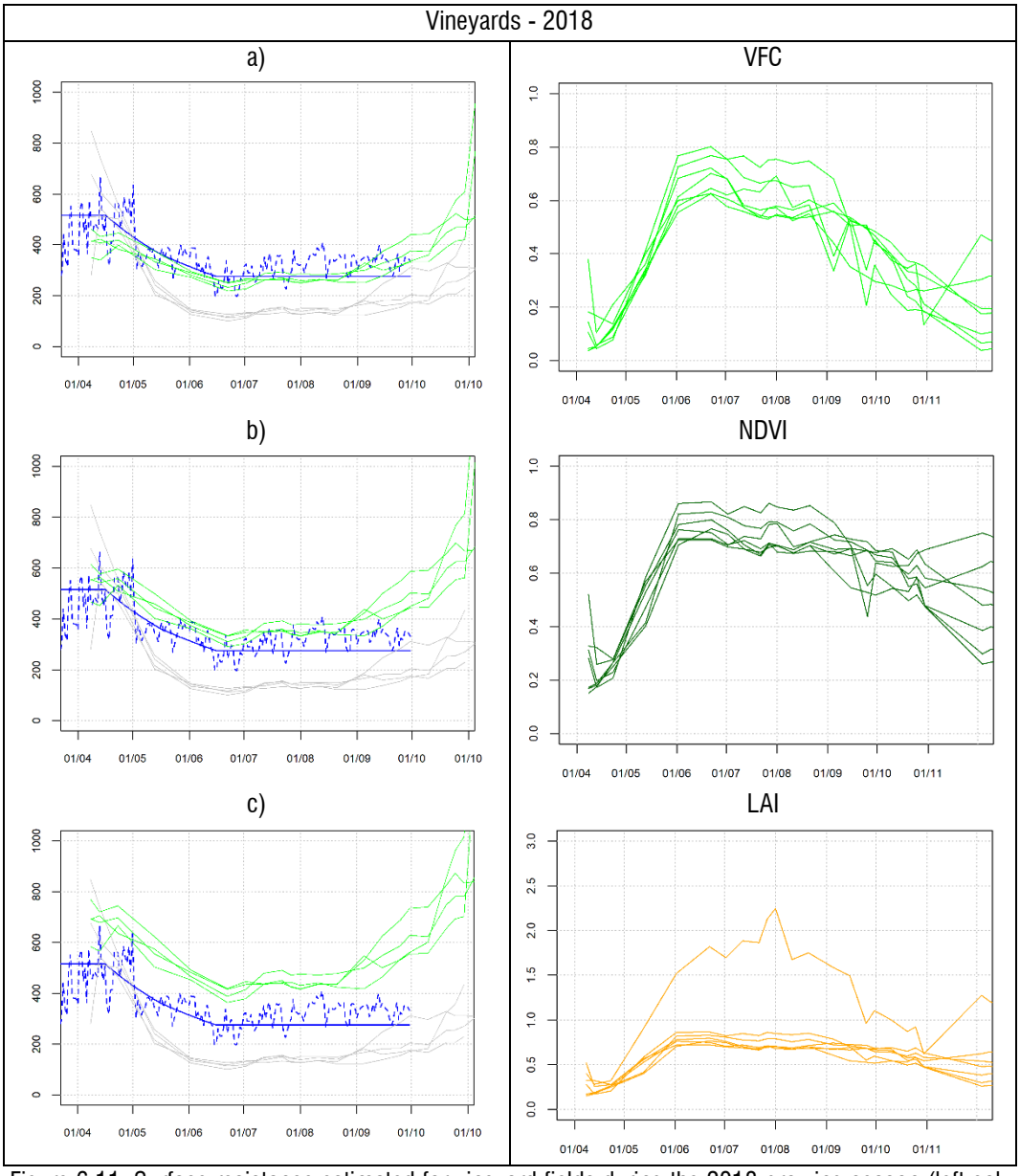

Figure 6.11. Surface resistance estimated for vineyard fields during the 2018 growing season (left column, using the relation of Equation (38) with α equal to 300 (a), 400 (b) and 500 (c)) and the Vegetation Fraction Cover (VFC), NDVI and LAI (right column).

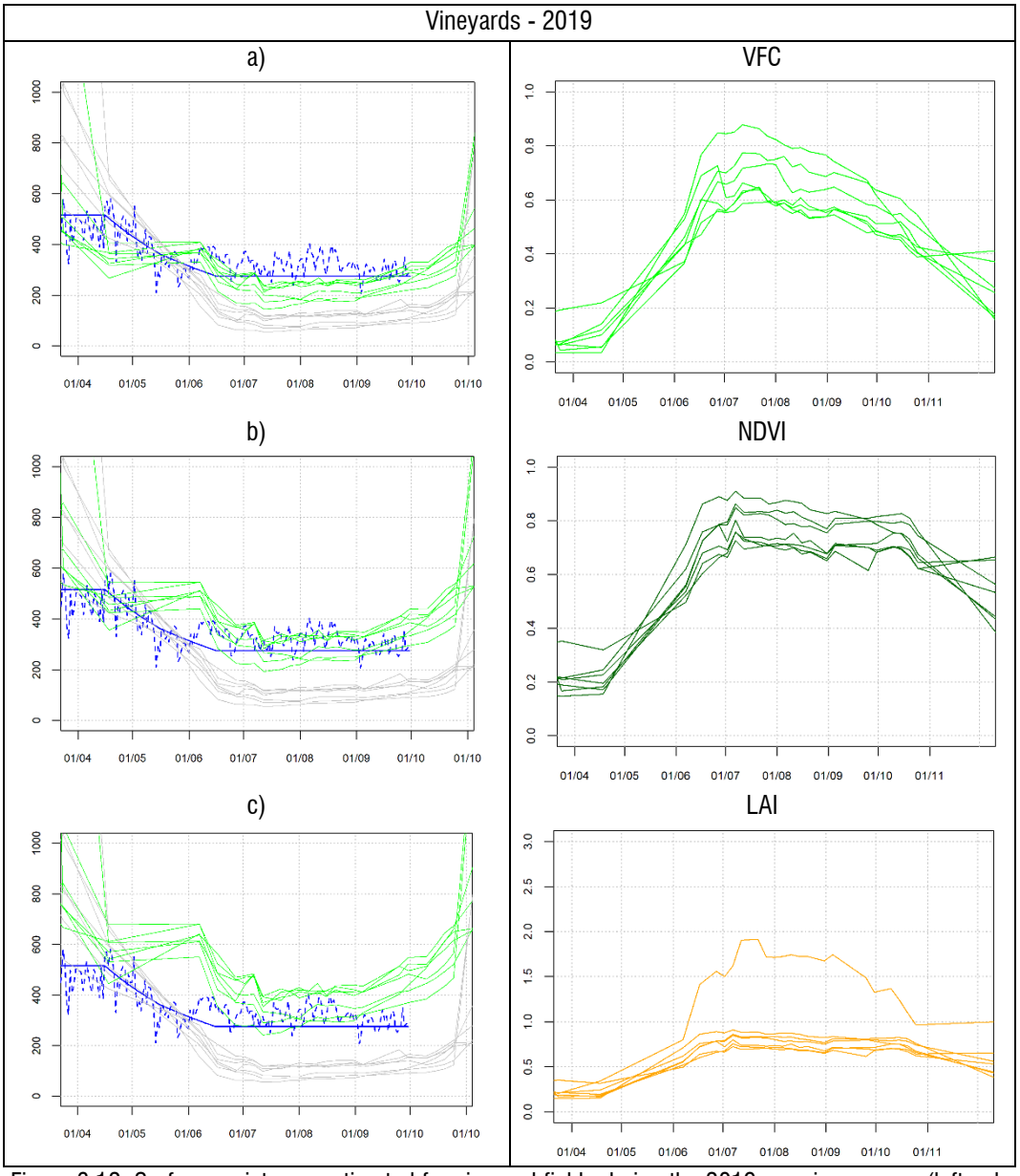

Figure 6.12. Surface resistance estimated for vineyard fields during the 2019 growing season (left column, using the relation of Equation (38) with α equal to 300 (a), 400 (b) and 500 (c)) and the Vegetation Fraction Cover (VFC), NDVI and LAI (right column).

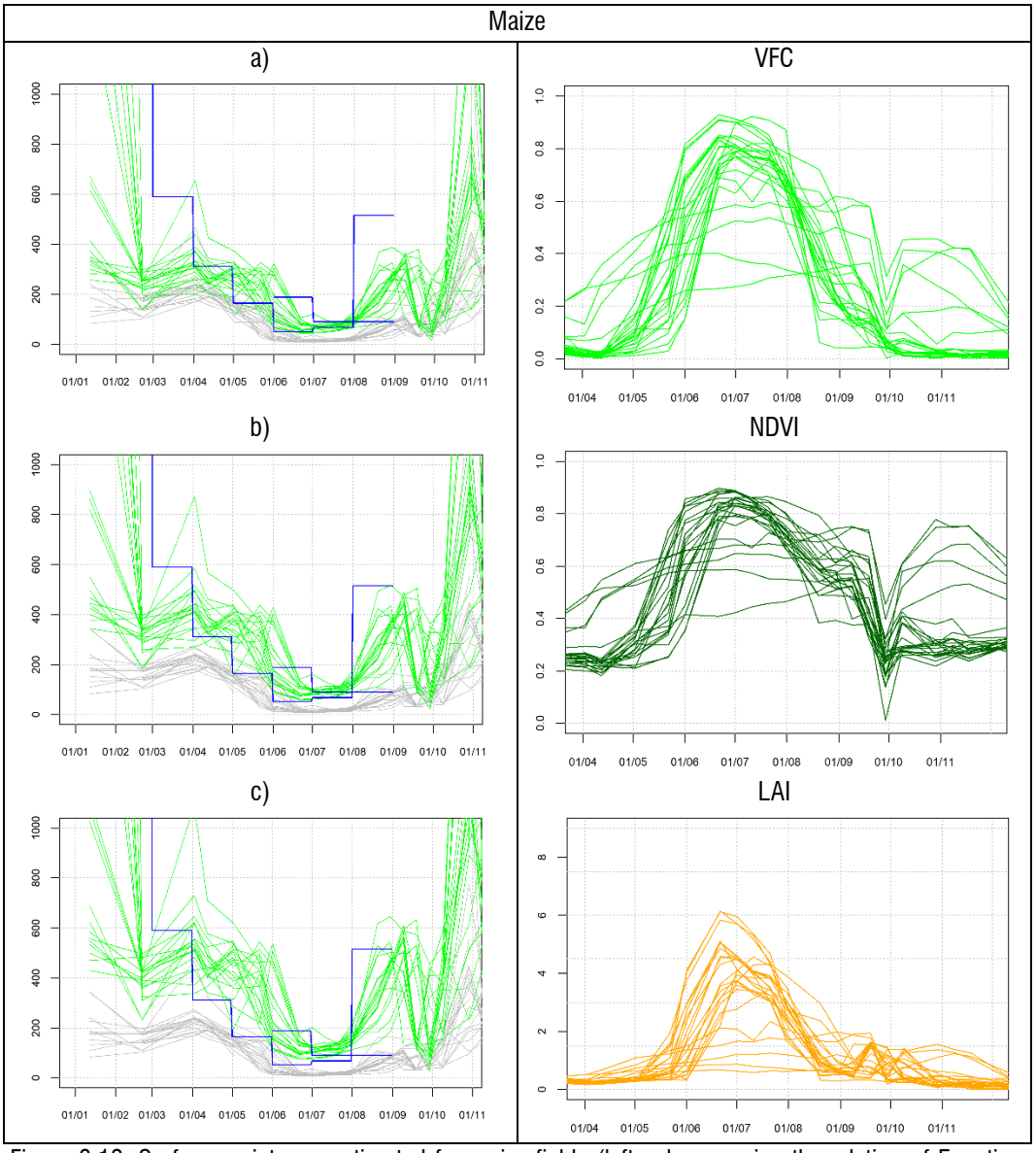

Figure 6.13. Surface resistance estimated for maize fields (left column, using the relation of Equation (38) with α equal to 300 (a), 400 (b) and 500 (c)) and the Vegetation Fraction Cover (VFC), NDVI and LAI (right column).

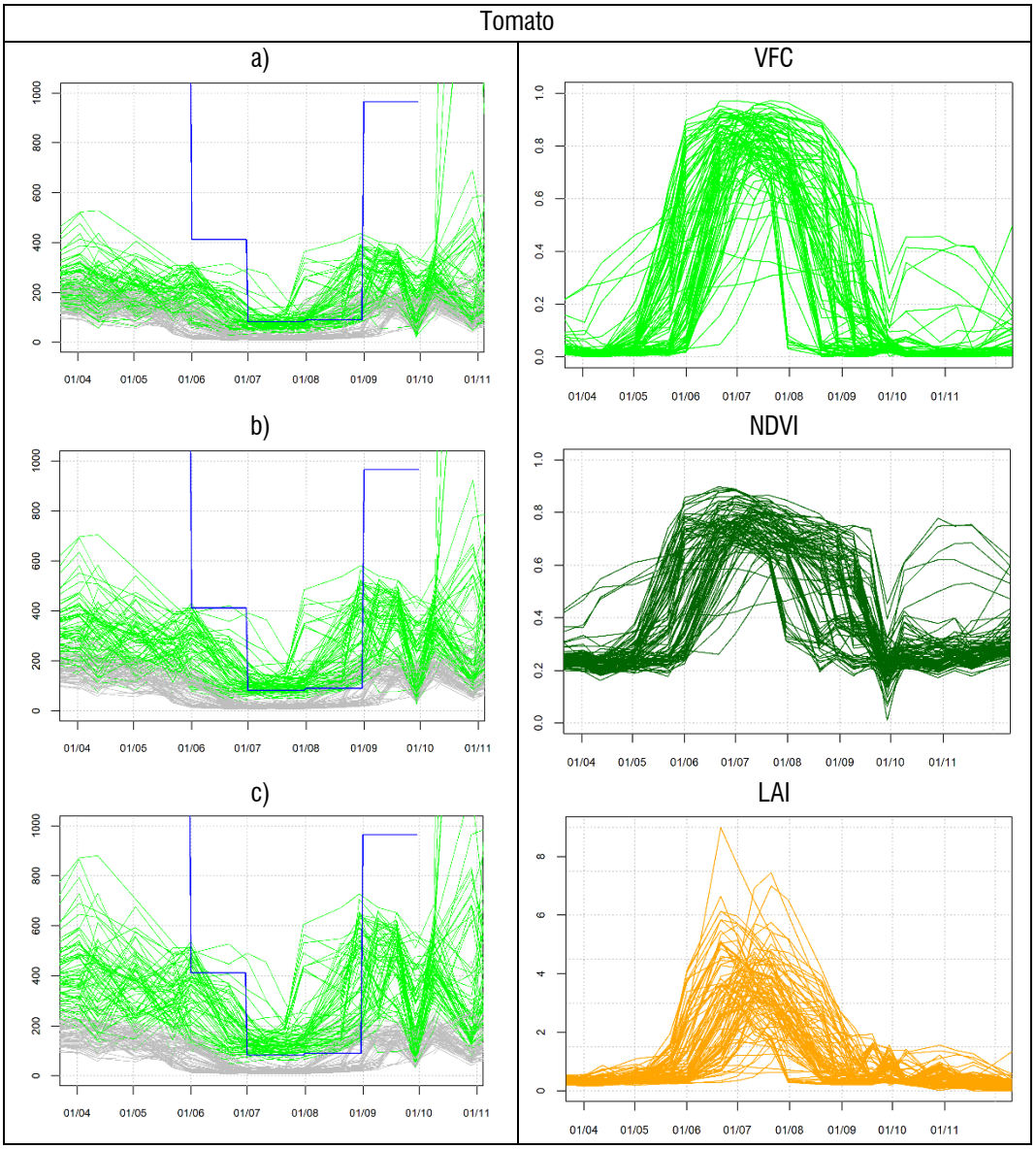

Figure 6.14. Surface resistance estimated for tomato fields (left column, using the relation of Equation (38) with α equal to 300 (a), 400 (b) and 500 (c)) and the Vegetation Fraction Cover (VFC), NDVI and LAI (right column).

Since measurements of surface resistance over the considered plots are missing, the use of the term “calibration” appears to have low (or none) significant if applied in rigours sense Instead, in this work “calibration” was intended as the qualitative research of a “one-fit” value of the parameter α valid for the most generic crop-climate conditions. In this sense, the calibration of the surface reflectance model proposed had as objective the research of the value of the parameter α valid for both the study areas and the extremely different crop considered (herbaceous, woody, and perennial crops) considering the different climate conditions between years.

Following these criteria, the best-fit value of the parameter was estimated to be 500. Therefore, the expression adopted for the surface resistance estimation is:

$$r_s = \frac{500\ NDVI}{LAI_{eff}} \tag{51}$$

In Figure 6.15 - Figure 6.17 were reported the temporal patterns for each crop class of the retrieved Kc estimated using Equation (51) compared with the literature-based values and with the Kc retrieved by the direct application of the EO-based FAO-PM approach. The comparison shows that for all the cases analysed, the obtained Kc curves follow the expected FAO-kc curves. If the model reduces the Kc value for the considered woody crops (olive and vineyard), for the herbaceous crops (maize and tomato) there is an increment of the Kc value achieved during the crop season. For these crops, the estimated Kc patterns are now more similar to the FAO-Kc pattern. Moreover, the FAO-Kc lines in these cases represent an upper limit border for the estimated Kc, in line with the definition of the “optimal” crop coefficient.

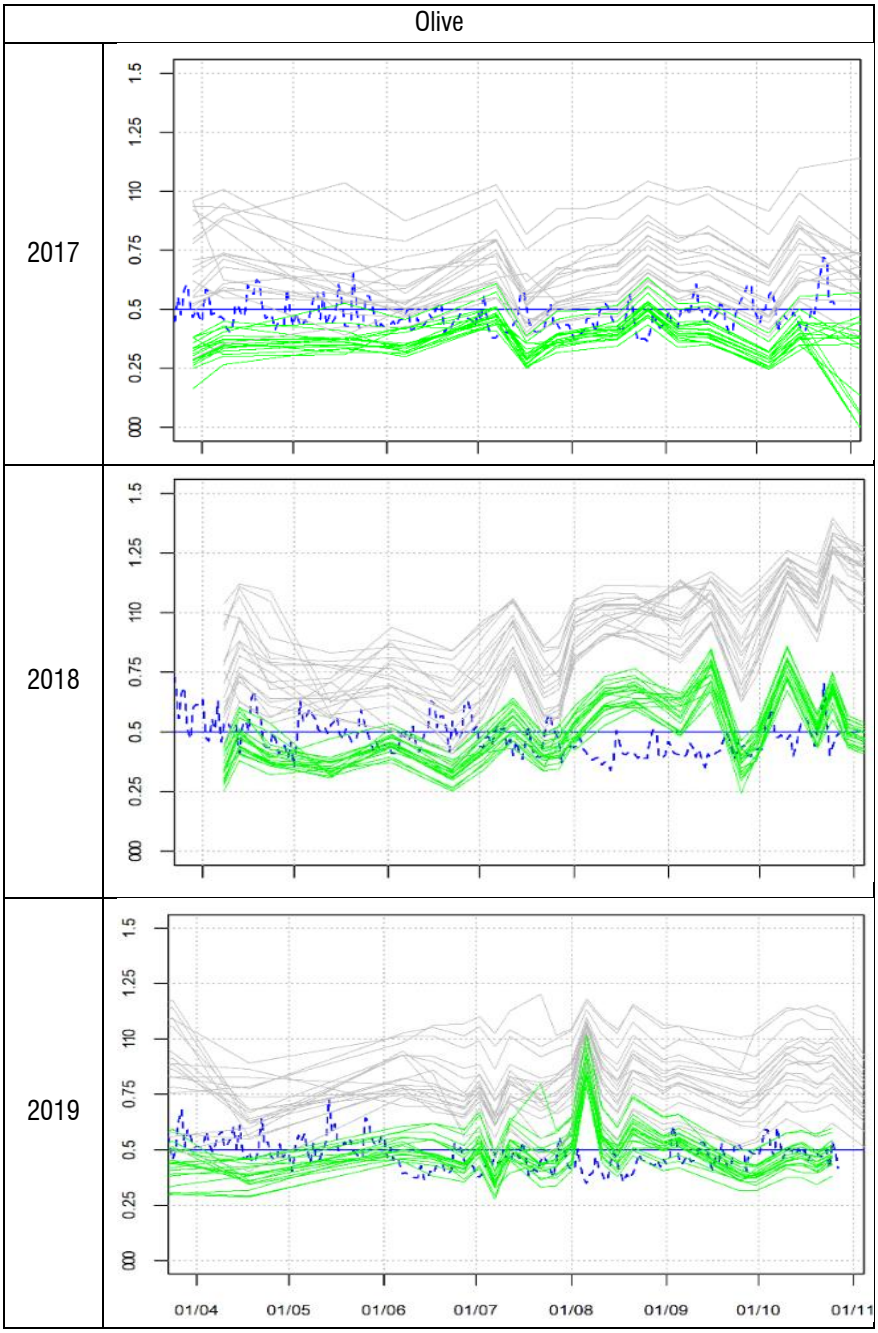

Figure 6.15. Olive's Kc estimated along the three crop seasons using the proposed EO-based "one-step" approach (green) and the reference FAO Kc and adjusted Kc FAO (respectively the continuous and dashed blue lines).

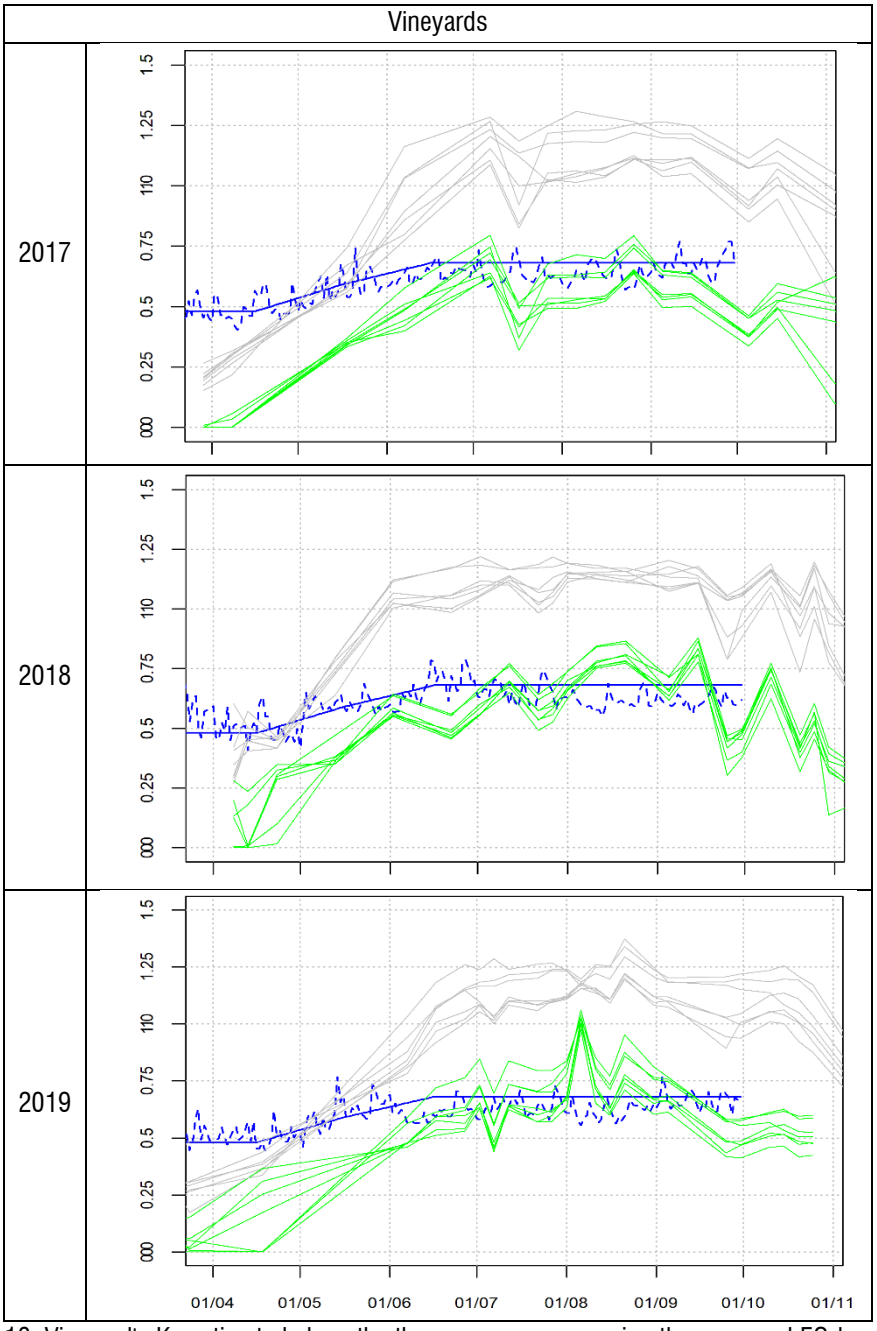

Figure 6.16. Vineyard's Kc estimated along the three crop seasons using the proposed EO-based "one-step" approach (green) and the reference FAO Kc and adjusted Kc FAO (respectively the continuous and dashed blue lines).

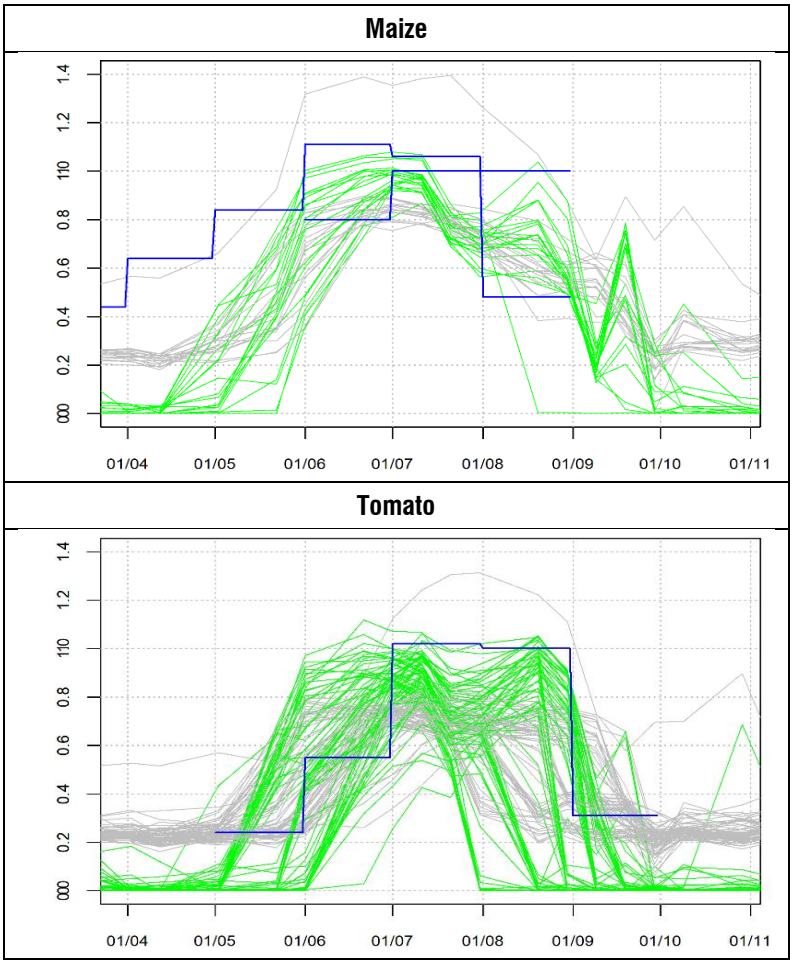

Figure 6.17. Maize and tomato's Kc estimated along the crop season using the classical and the proposed improved EO-based "one-step" approach (respectively the grey and green lines) and the reference FAO Kc (blue lines).

6.5. Seasonal CWR estimation at the plot scale

Adopting the proposed aerodynamic and surface resistance model, was possible to estimate the daily ETc using the procedure described in Chapter 4 during the period between the first and the last available S-2 overpass of every considered year. The seasonal CWR for each plot was estimated by summing the daily ET maps along the crop growing season. For vineyards and olive crops, the considered growth season follows the irrigation season of the "Sinistra Ofanto" study area and therefore ranges from April to the end of October. Instead for the annual crops considered, tomato and corn, since in general the planting date and the length of the crop cycle are farm-specific, the growing phase was retrieved using the procedure reported in Paragraph 4.4 opportunely modified to be applied with the average FVC value instead of the pixel-based value. In these case in fact, as the spatial information about the limits of each plot was available, was possible to follow the FVC trend at the plot scale.

6.5.1. Olive

Form Figure 6.18 it is possible to notice that the CWR using the standard two steps FAO56 approach reflects only the seasonal differences in terms of ETo described in Paragraph 5.1.2 with higher CWR for the year 2017 (equal to 4,282,0 m^3/ha) and lower for the others two years. The differences in terms of CWR among the plots are influenced only by the spatial interpolation of the meteorological data and does not reflect the differences existing among plots due to different spacing among threes or crop status (in terms of disease or water stress).

Instead, the CWR estimated using the proposed EO-based method can reproduce the differences among the plots as dictated by the expression of the surface resistance (Equation (38)) and the LAI and NDVI values over each plot. In absence of field surveying and measurements, it is not possible to correlate these differences to any variable able to affect the ETc. However, looking at the plots of Figure 6.18, for all the considered plots during 2017 the model detects a CWR inferior to the expected FAO-Kc CWR which is not influenced by the rainfall pattern and therefore is not able to

consider the rainfall deficit occurring during all the year and especially during the summer.

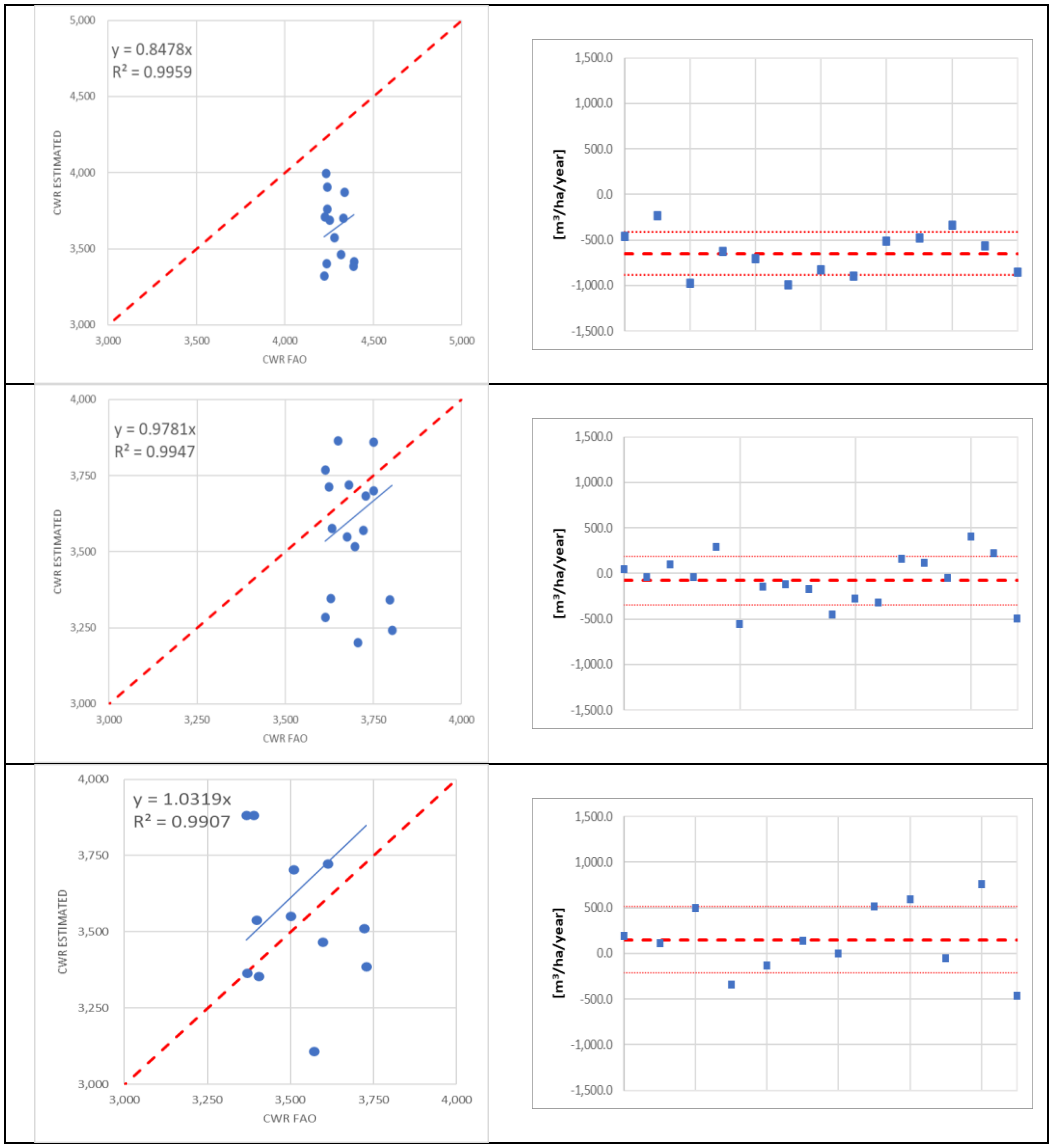

Figure 6.18. Scatter plot and differences plot between the estimated seasonal CWR and the standard FAO potential CWR (estimated using the $Kc_{,adj}$) for each olive plot and for the three considered irrigation seasons (2017-2019).

The extraordinary climatic conditions of 2017 were reflected in the synthetic quantitative description of the results provided from the statistical descriptors and

reported in Table 6-2. Indeed, on average the CWR estimated was 650 m^3/ha inferior to the expected using the FAO-kc method, with an MPE of -15.1 %. This result, however, could be justified with the fact that the Kc correspond to the "potential" or "optimal" crop condition and therefore the estimated ETc represent the upper limit value for the specific crop considered. The CWR estimated for the year 2018 and 2019 confirm this assumption because the values obtained are in line with the expected FAO-kc derived with MPE lower than equal respectively -2.1 and 3.6%.

Table 6-1. Summary statistics for the description of seasonal olive's CWR [m^3/ha/year] estimated using the standard "two-step" FAO approach and the EO-based "one-step" approach.

	CWR FAO [m^3/ha/year]			**CWR estimated** [m^3/ha/year]		
	2017	**2018**	**2019**	**2017**	**2018**	**2019**
Max	4,391.0	3,802.0	3,729.0	3,997.0	4,042.0	4,224.0
Min	4,222.0	3,613.0	3,366.0	3,325.0	3,202.0	3,108.0
Average	4,282.4	3,691.3	3,514.6	3,632.1	3,612.2	3,633.2
SD	59.0	60.7	124.8	211.2	249.0	306.4

Table 6-2. Summary statistics comparing seasonal olive's CWR estimated using the standard "two-step" FAO approach and the EO-based "one-step" approach for the three considered irrigation seasons.

	2017	**2018**	**2019**	
ME	-650	-79	119	[m^3/ha]
SE	237	264	349	[m^3/ha]
MPE	-15.1%	-2.1%	3.6%	[-]
MAE	650	224	290	[m^3/ha]
MAPE	15.1%	6.0%	8.3%	[-]
RMSE	692	276	369	[m^3/ha]

6.5.2. Vineyards

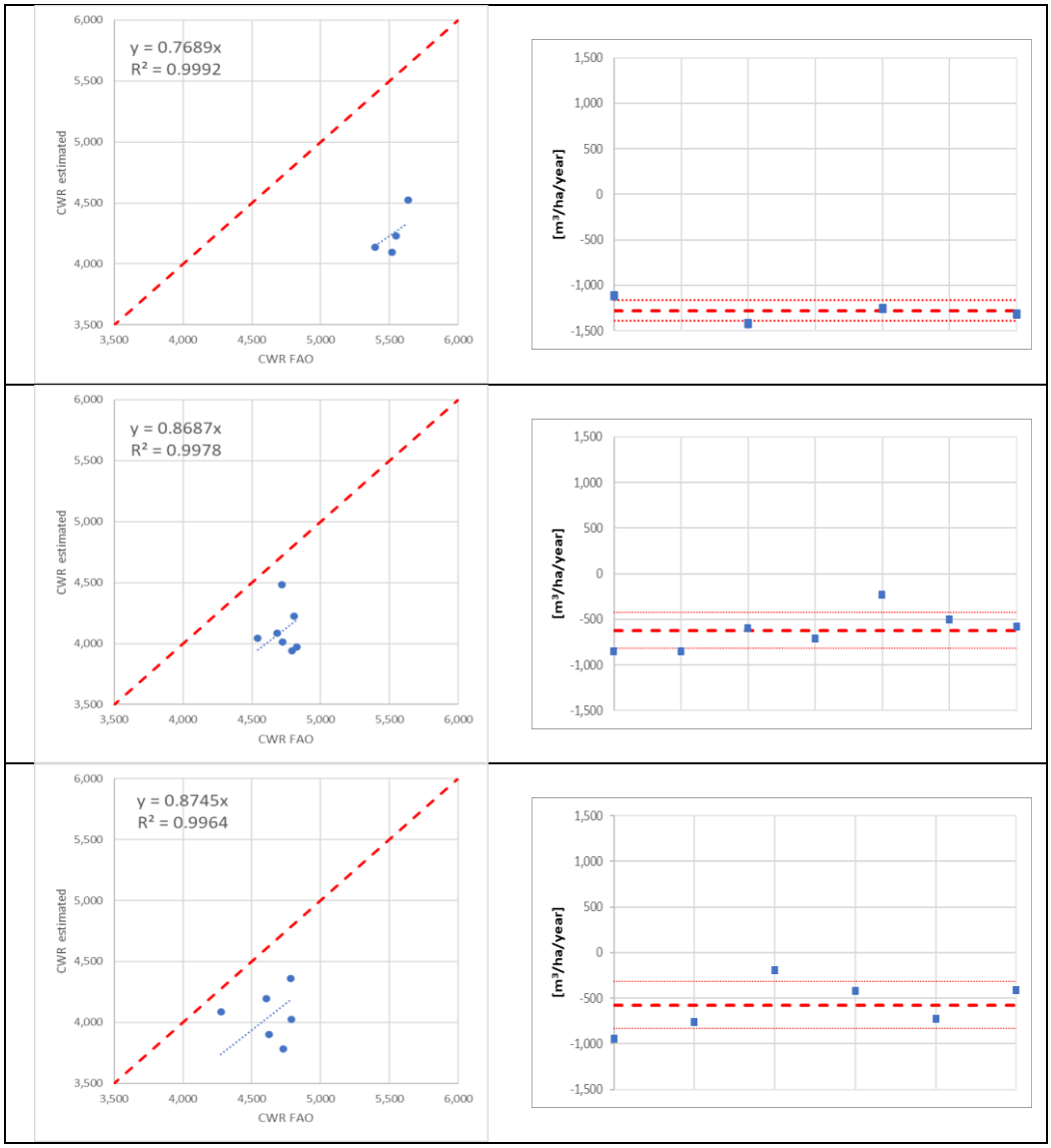

Figure 6.19. Scatter plot and differences plot between the estimated seasonal CWR and the standard FAO potential CWR (estimated using the $K_{c,adj}$) for each vineyard plot and for the three considered irrigation seasons (2017-2019).

Even the analysis of the vineyard's CWR confirms that the application of the classical FAO-Kc method to estimate the CWR leads to overestimating the CWR,

especially during rain scarce years (as was 2017 for the Sinistra Ofanto). Moreover, these differences are sensibly higher than the ones retrieved for olive. As expected, the maximum displacement was retrieved for the crop season 2017 where the ME was equal to -1,278 m^3/ha. During the other years, the differences between estimated and expected CWR decreased to 10-11 %, corresponding to a ME of -618 and - 576 m^3/ha/year.

Table 6-3. Summary statistics for the description of seasonal vineyard's CWR [m^3/ha] estimated using the standard "two-step" FAO approach and the EO-based "one-step" approach.

	CWR FAO			**CWR estimated**		
	2017	**2018**	**2019**	**2017**	**2018**	**2019**
Max	5,636	4,824	4,786	4,523.0	4,482	4,361
Min	5,397	4,544	4,277	4,098.0	3,943	3,781
Average	5,525	4,715	4,635	4,247.3	4,109	4,097
SD	86	90	174	166.1	174.7	204.3

Table 6-4. Summary statistics comparing seasonal vineyard's CWR estimated using the standard "two-step" FAO approach and the EO-based "one-step" approach for the three considered irrigation seasons.

	2017	**2018**	**2019**	
ME	-1,278	-619	-576	[m^3/ha]
SE	112	200	257	[m^3/ha]
MPE	-5.8%	-1.9%	-2.1%	[-]
MAE	1,278	619	576	[m^3/ha]
MAPE	5.8%	1.9%	2.1%	[-]
RMSE	1,283	651	630	[m^3/ha]

The underestimation of CWR was retrieved and confirmed for each plot for the three years which could indicate, besides an incorrect estimation of the parameter α used in the surface resistance expression, also the possibility that farmers apply a water management strategy that leads to controlled water stress reflected in the CWR estimated. Moreover, is necessary to consider as the seasonal dynamics of Kc is affected by crop age and the environment as demonstrated by different Authors (Figure 6.20).

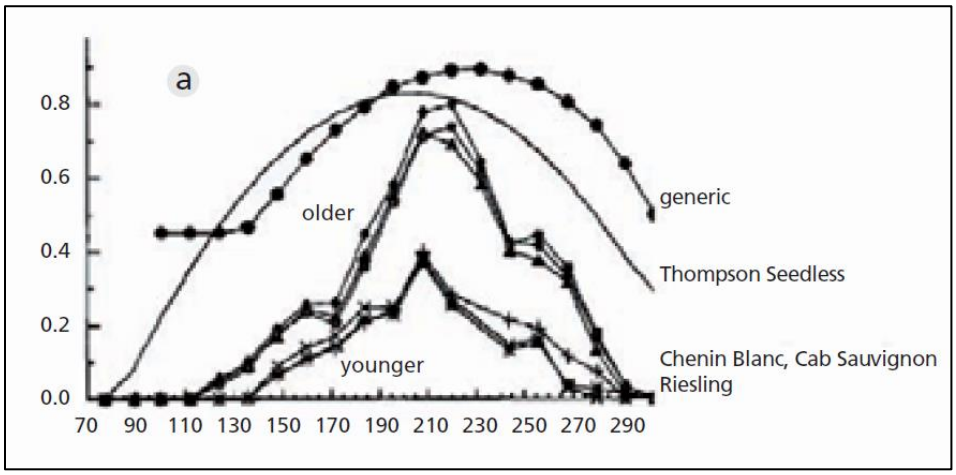

Figure 6.20. Seasonal dynamics of crop coefficients for vines in central Washington (USA) and São Francisco (Brazil). (Sources: (Steduto et al., 2012)).

6.5.3. Tomato

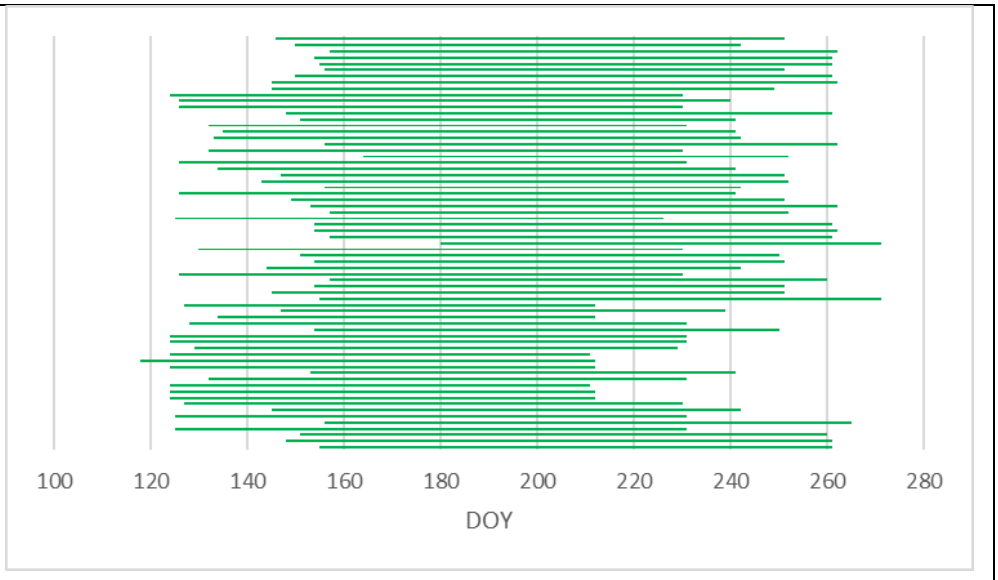

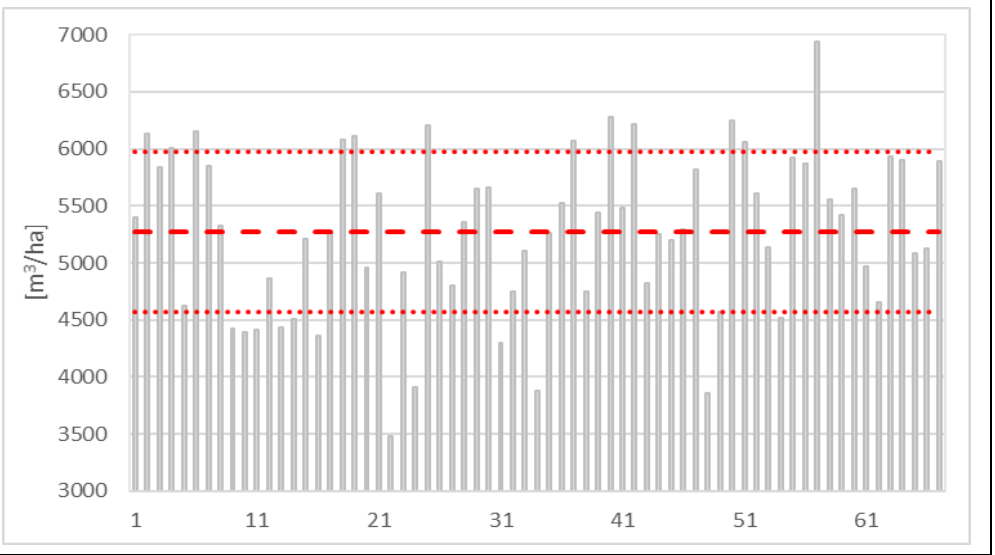

	CWR [m³/ha/year]	Max	6934.0
		Mean	5272.8
		Min	3477.0
		SD	700.4

Figure 6.21. Estimated crop growing season and seasonal CWR for each tomato plot. On the CWR histogram are reported the average and the standard deviation (respectively the dashed and dotted lines).

The seasonal CWR estimated for tomatoes field ranges between 6,934.0 and 3,477.0 m^3/hectare with a mean value of 5,272.8 m^3/hectare. These values are in line with the standard CWR for tomato provided from the SIAR which for 2017, estimated for a standard growing season started the 1st of May (Day Of the Year - DOY 121) and ended the 30th of September (DOY 273), was equal to 6,132 m^3/hectare. Since the retrieved crop growing season is different for each plot, any other correlation at the plot scale between standard and modelled CWR over a shorter temporal scale was not possible.

The retrieved crop growing season for the 67 fields considered, started on average on the DOY 141 (141.6 ±13.7 days) and was long 101 days (101.1 ± 8.6 days) with an average end on the DOY 243 (242.7 ±16.6 days). Therefore, it is possible to conclude that the procedure for the delimitation of the growing season based on the FVC trend is valid for tomato.

6.5.4. Maize

The seasonal CWR estimated for maize ranges between 4,886.0 and 8,130.0 m^3/hectare with a mean value of 6,877.4 m^3/hectare. These values are in line with the standard CWR for grain and fodder maize provided from the SIAR value respectively 8,025 and 5,630 m^3/hectare. However, from the available crop map was not possible to distinguish among these varieties, and therefore it was not possible any other correlation for variety. Moreover, since the retrieved crop growing season is different for each plot any other correlation at plot scale between standard and modelled CWR over a shorter temporal scale was not possible.

The retrieved crop growing season for the 19 fields considered, started on average on the DOY 126 (126.4 ±10.2 days) and was long 140 days (139.7 ± 10.2 days) with an average end on the DOY 265 (265.0 ± 11.0 days).

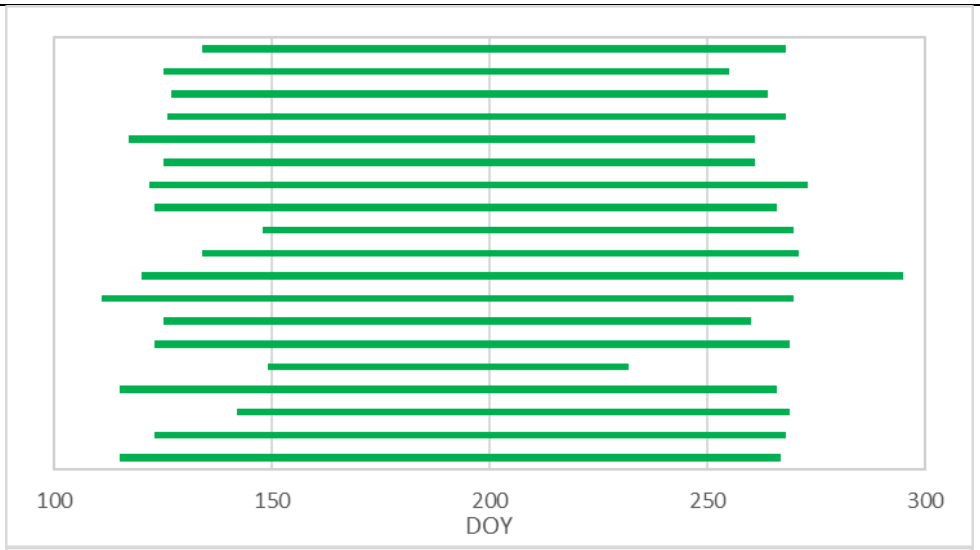

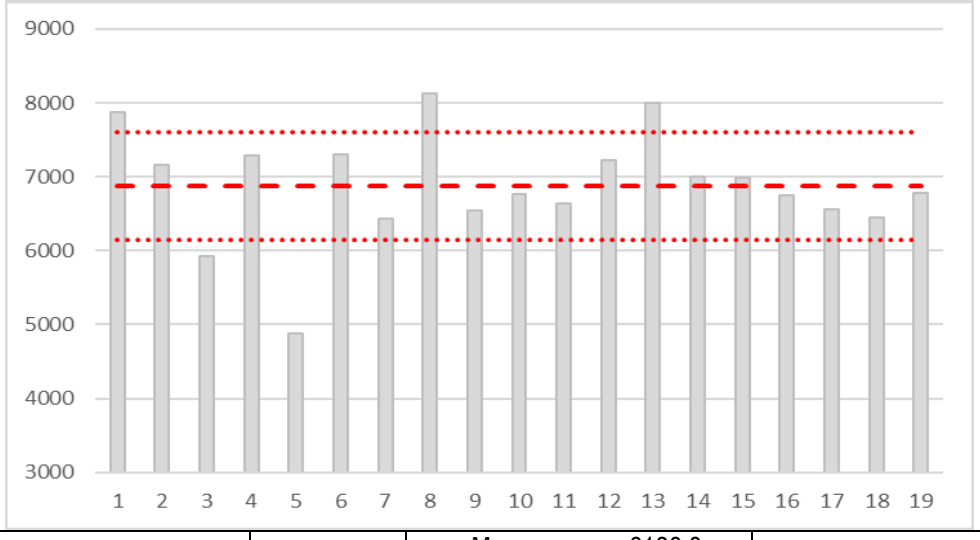

	CWR [m³/ha/year]	Max	8130.0	
		Mean	6877.4	
		Min	4886.0	
		SD	723.5	

Figure 6.22. Estimated crop growing season and seasonal CWR for each maize plot. On the CWR histogram are reported the average and the standard deviation (respectively the dashed and dotted lines).

6.6. CWR estimation at the irrigation district scale

6.6.1. CWR of "Sinistra Ofanto" Irrigation Scheme

Since the crop map for the Sinistra Ofanto scheme was available, it was possible to estimate the CWR for the "Sinistra Ofanto" irrigation Scheme. The CWRs of each district were estimated on daily basis using the classical "two-steps" FAO-PM approach. According to the land cover map, the average value of the crop coefficient for each irrigation district was estimated as the weighted mean of the crop coefficients:

$$Kc = \frac{\sum_{i=1}^{N} Kc_i \, A_i}{A} \tag{52}$$

Since the land cover map available is not updated every year, it does not provide a distinction between winter and summer crops which are reported in the unique crop class *"annual crops".* Therefore, summer crops were identified year by year as the residuals cropped field excluding the perennial crops (assumed stable during the three irrigation seasons). The crop pattern of each irrigation district was reported in Table 5-2. The adopted Kc values were retrieved from the FAO-56 guidelines and are graphically reported in Figure 6.23. To define the Kc values for the summer crops was assumed as a unique representative summer crop the tomato. Another simplification was introduced grouping into a unique crop class vineyard and stone fruit threes since they are characterized by a similar Kc temporal pattern and values.

The CWRs were estimated starting from the 1st of April to the 15th of September, corresponding to the core of the irrigation season.

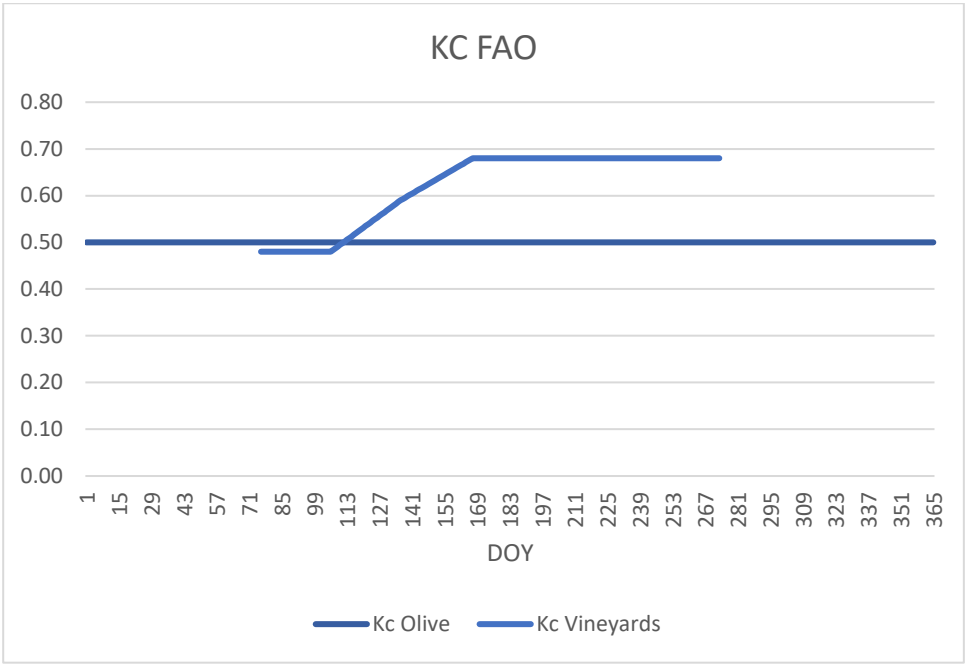

Figure 6.23. Temporal evolution along the year of the used Kc value for the estimation of CWR.

Looking at the seasonal CWRs values reported in Table 6-5, it is possible to notice as the CWR estimated with the Kc-FAO approach is always greater than the one retrieved with the EO-based FAO-56 method. This could be a further confirmation of the fact that the FAO-Kc approach leads to estimate the potential (maximum) and not the actual evapotranspiration. The overestimation is significantly higher for the dry years 2017 and 2019, while it is moderate for the rainier irrigation season 2018.

It is also interesting to notice as the total estimated CWR for the three years results to be a constant while, using the classical FAO-Kc approach, it is highly variable and influenced by the climatic conditions. Once again this demonstrates as the classical FAO-Kc approach leads to estimate the potential (maximum) evapotranspiration which is not representative of the Mediterranean contexts where water availability is the main limiting factor to the evapotranspiration process.

Table 6-5. Comparison between seasonal CWR estimated at irrigation district-scale using the EO-based FAO-56 method and the potential CWR retrieved from the classical Kc-FAO approach.

Irrigation District	CWR EO-based FAO 56		
	2017	2018	2019
11	12,429,312	12,064,661	12,140,099
12	5,959,955	6,095,646	5,971,049
12	4,877,243	5,529,286	5,616,974
14	4,551,633	4,732,743	4,370,227
Total	27,818,143	28,422,336	28,098,349

Irrigation District	CWR FAO-Kc		
	2017	2018	2019
11	18,299,993	13,440,549	14,415,231
12	8,617,818	6,714,727	7,388,554
12	7,781,496	5,696,723	6,408,350
14	5,623,828	4,333,069	6,295,459
Total	40,323,135	30,185,068	34,507,594

Irrigation District	CWR EO-based FAO 56 / CWR FAO-Kc		
	2017	2018	2019
11	67.9%	89.8%	84.2%
12	69.2%	90.8%	80.8%
12	62.7%	97.1%	87.7%
14	80.9%	109.2%	69.4%
Average	69.0%	94.2%	81.4%

6.6.2. CWR of "Canal del Zujar Irrigation District"

For the CZID the information about the crops cultivated during 2017 covers only 60.38% of the total extension area. Moreover, as most of the crop are annuals, characterized by a different crop pattern for each plot, even in presence of a detailed crop map the comparison with the standard FAO-56 CWR values is difficult and limited to a qualitative assessment since the standard Kc curve follows a theoretical pattern that does not consider the effective crop phenology which is affected by the specific meteorological conditions for the considered growing season and the farmers' choices as the sowing date.

Even if the direct comparison with the standard kc-FAO CWR is not possible, the obtained retrieved EO-based CER is in the following reported and qualitatively discussed.

The total estimated cropped area estimated using the FVC dataset following the procedure reported in Paragraph Masking no cropped areas3.3 covers about 96 per cent of the entire extension of the CZID. It is also possible to follow the temporal pattern of the extension of the cropped areas (Figure 6.24). The biggest development of the vegetated areas, as retrieved from the FVC trend at pixel-level, happened from April, reaches its maximum during the summer, and fall again since the end of August.

In the same way, it is possible to describe the spatial and temporal evolution of the CWR. The estimated annual reference evapotranspiration (estimated from the first to the last S2 overpass) results equal to 1,3422 mm. In the same period, the estimated average CWR value is 431 mm with very large spatial differences inside the CZID study are, as shown in Figure 6.26. The total seasonal CWR volume is estimated at 11,883,209 m^3. Lastly, in Figure 6.25 is reported the annual pattern of ETo and Rainfall compared with the estimated average ETc over the CZID for 2017.

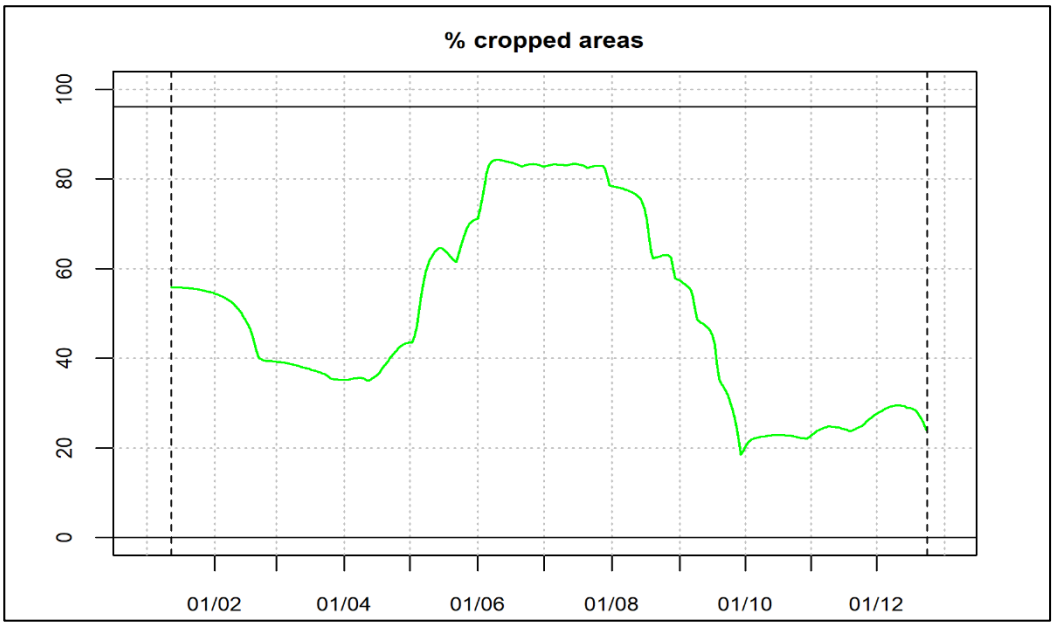

Figure 6.24. Temporal pattern of the extension of the cropped areas, based on the FVC trend.

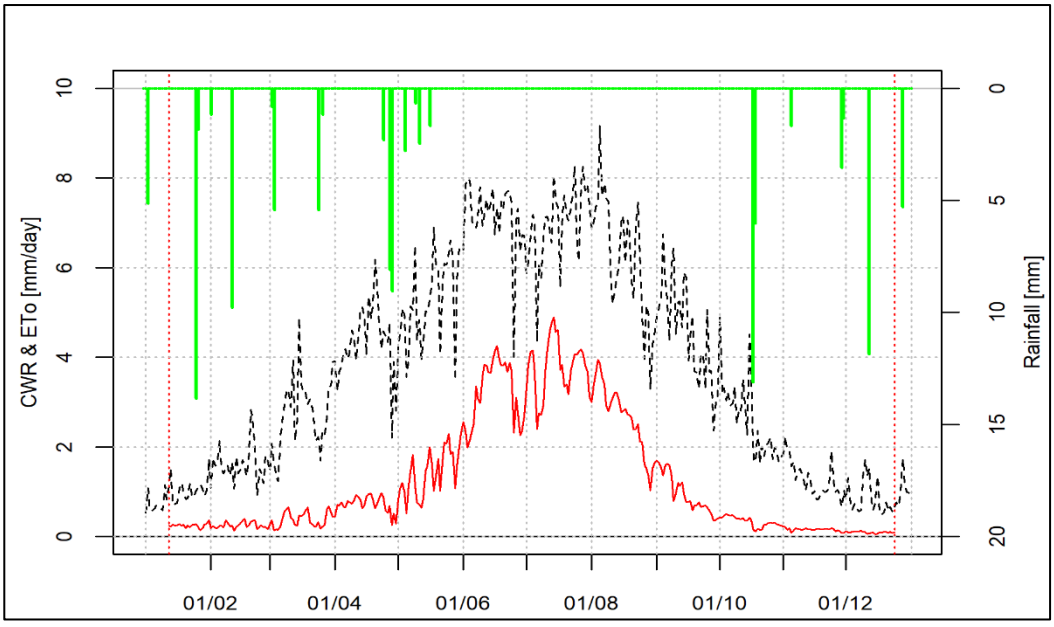

Figure 6.25. The annual pattern of ETo (dashed line), (estimated) average ETc and Rainfall over the CZID for 2017. The vertical red lines indicate respectively the first and last Sentinel-2 overpass.

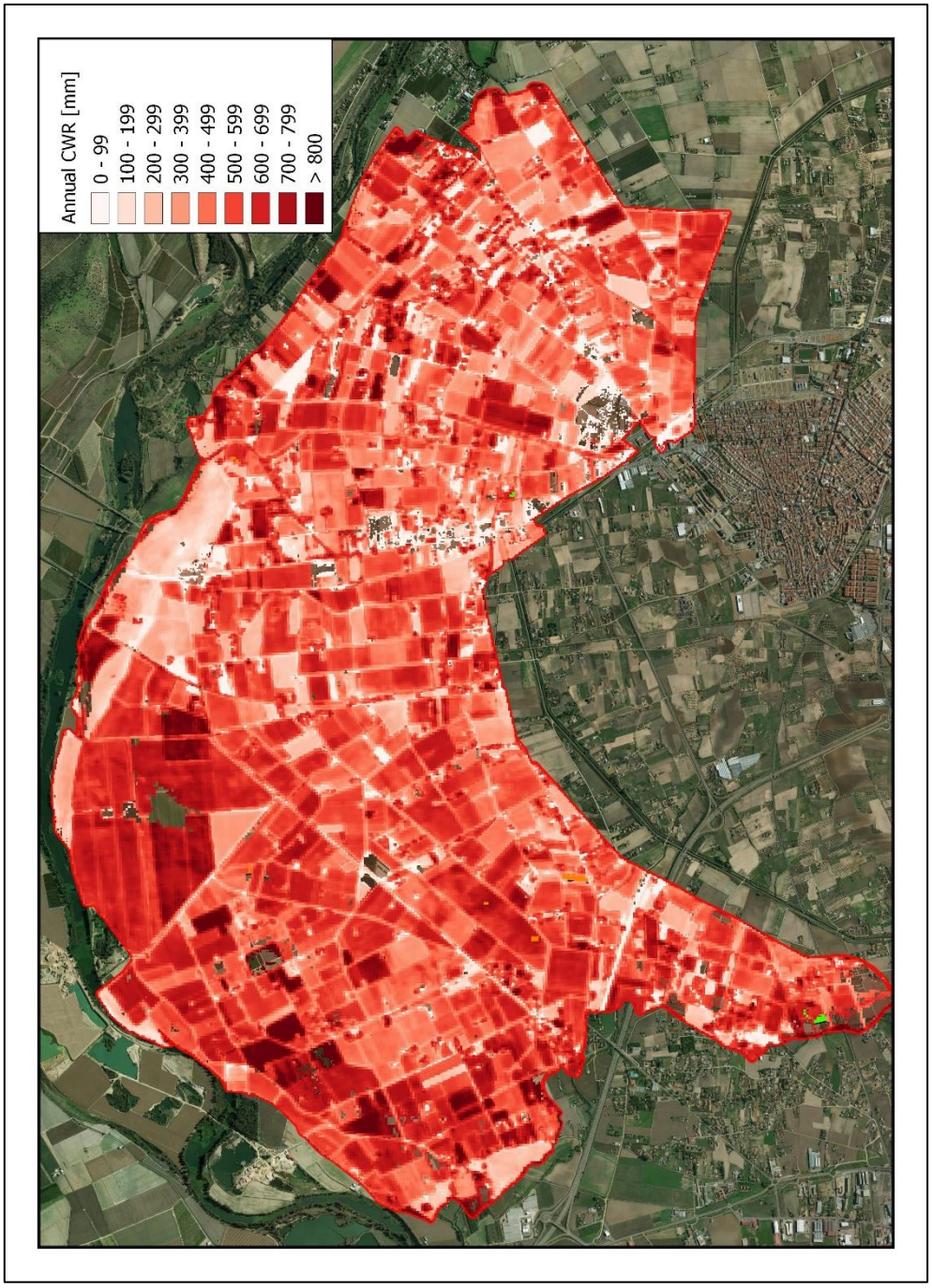

Figure 6.26. The spatial pattern of the estimated annual CWR over the CZID study area.

7. TEST THE EO-BASED "ONE-STEP" FAO-56 METHOD FOR IRRIGATION ACCOUNTING AND MONITORING

7.1. Methodological approach

As previously described in Paragraph 1.6.3 there are two mains possible way to estimate the IWR.

The first possibility is based on the identification of water deficit conditions which are presumably corresponding to irrigation, assuming implicitly that the water used for irrigation approximately correspond to the not-rainwater consumed by the crop. Under this hypothesis, which can be considered as reasonable in all cases where the cost of extracting and distributing irrigation requires the improvement of farmer's water use efficiency (as common in many Mediterranean regions), (net) IWR can be estimated as the difference between the Crop Water Requirements, represented by the actual ET (ETc) and the net rainfall (Rn) as reported in Equation (18). This approach can be easily applied for the IWR estimation of annual crops because farmers trying to avoid the condition of water deficits which lead to a reduction of plant transpiration and a decrease in the production of biomass. Indeed, usually, annual crops are being grown for its biomass (such as alfalfa or maize silage) or for its grains (like wheat, maize, and rice) and a water stress condition in such case lead to a decrease of biomass and grain yield and consequently of gross farmers' income.

A completely different scenario characterizes tree crops and vines (and for some annual crops, such as cotton) where the fruit is the economic product, a reduction in biomass production does not always result in a parallel reduction in fruit production (but can be affected negatively some quality parameters, such as fruit size or appearance). On the other hand, it has long been known that water deficits have beneficial effects on the production of trees and vines. Therefore, in addition to saving water, there are also other aspects and factors to be considered applying and managing water stress in perennial crops in terms of improving product quality and growers' revenues. Therefore, estimate the IWR for tree crops is more complex because irrigation is applied to avoid water deficits that are not compatible with management objectives. The usual

objective of the manager is to maximize net economic benefit, which does not always coincide with maximum yields, as when deficit irrigation can improve fruit quality and thus crop value.

Another great difference among annual and tree crops is represented by the deep of the root zone which for tree roots may reach several meters (however the effective depth of rooting for irrigation purposes is considered the maximum depth considered for water budget calculations ranges between 1.5 and 2 meters). In this case, therefore, the water storage capacity can sustain a relevant portion of the CWR. For this reason, it is not possible to consider the simplified equation of Equation (18) to estimate the IWR for tree crops, but it is necessary to apply the *water budget method* for irrigation scheduling. With this method, the tree root zone is considered a reservoir of soil water that is depleted as the ETc take place. The soil reservoir of available water that the tree depletes through ET is allowed to lose water until a soil water threshold (Allowable Depletion - AD) is reached, below which water stress starts to affect negatively crop production, quality or both. At this point, irrigation must be applied to refill the soil profile. This schematic representation follows the FAO-56 SWB method (Equation (2)) described in detail in Paragraph 1.1.

The water budget method requires also more input data regarding:

- The available soil water holding capacity or *Total Available Water* (TAW), defined as the difference between field capacity and permanent wilting point. It varies according to soil texture between 50 to 200 mm/m.
- Rooting depth.
- The Allowable Depletion (AD) usually varies between 50-70 per cent of TAW and represents the threshold level of the root zone storage capacity below which the level of water deficit in the tree is undesirable and therefore, at this point, irrigation is applied.

Moreover, it is important to know the farmers' behavior to reproduce it into the irrigation module of the SWB under the form of frequency and amount of every irrigation event.

In general, the way to cope with water scarcity is to modify the horticultural practices also by reducing the application of irrigation water. *Deficit irrigation* (DI) is defined as a regime where the irrigation water applied is less than the orchard ET requirements to induce the extraction of water from the soil reservoir. Two situations may then develop:

1. if sufficient water is stored in the soil and transpiration is not limited by soil water, the consumptive use (ET) is unaffected even though the volume of irrigation water was reduced.
2. if the soil water supply is insufficient to meet the ET demand, crop water deficits lead to a reduction in growth and transpiration and therefore DI reduces ET below its maximum potential.

There are many approaches to designing a DI program, but they follow two different principal strategies, reported graphically in Figure 7.1:

1. the continuous or *Sustained DI* (SDI), in which a constant fraction of the crop ET is applied at regular intervals. If the soil profile is full at the start of the season, the trees take up soil water to compensate for the deficits; as the season progresses, the soil is progressively depleted, and the water deficits increase with time in the absence of rainfall.

2. the *regulated DI* (RDI), defined as a regime that purposely stresses the trees or vines at specific developmental stages of the crop that are considered to be the least sensitive to water deficits. The goal of RDI, when water supplies are relatively high, is to have little if any, negative impact on the yield of marketable products and on gross profits. It should be emphasized that under RDI, the trees are subjected to irrigation deficits only at certain stages of development (normally when reproductive growth is relatively low) but they generally receive full irrigation outside

these periods. The RDI concept can also be used in drought years, where available irrigation supplies are limited

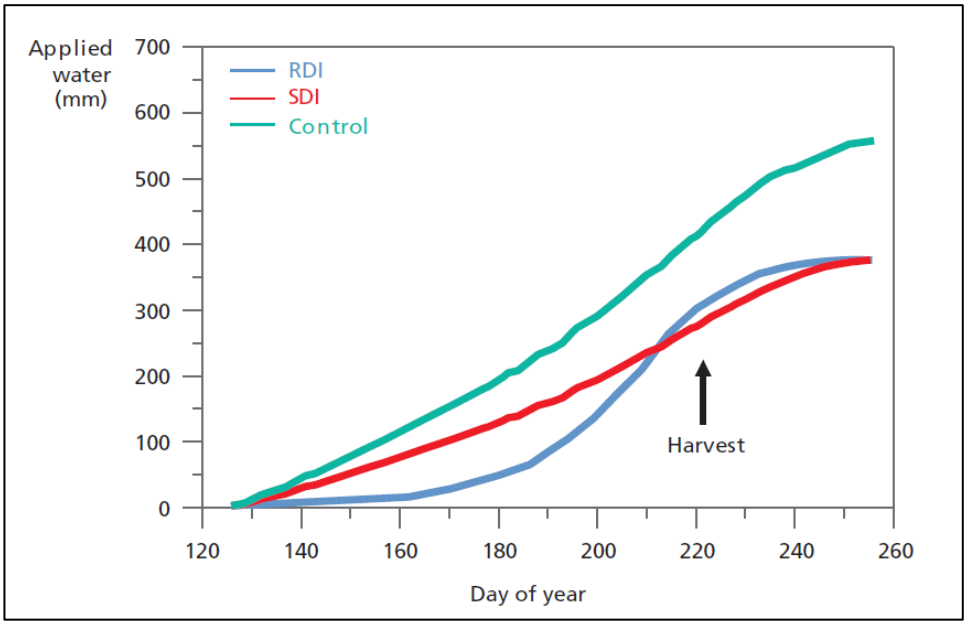

Figure 7.1. Patterns of seasonal applied water to an orchard under full irrigation (Control) and regulated (RDI) and sustained (SDI) deficit irrigation. Source: (Steduto et al., 2012).

Since in the RDI strategy the manager must decide whether to impose more severe water deficits during the stress-tolerant periods (or begin to expand the stress into the less stress-tolerant stages of the season or a combination of both) playing with the timing, magnitude, and duration of the stress periods it is hardly forecasting because is a farmer dependent choice. Therefore, the developed irrigation module for the tree crops works under the hypothesis of sustained deficit irrigation (SDI).

7.2. Irrigation Accounting and Monitoring at the plot scale for tree crops

To estimate the IWR of tree crops, was settled an FAO-based SWB model, as described in Paragraph 1.1. Assuming that, as usual for agricultural applications:

- the water table is more than about 1 m below the bottom of the root zone, the capillarity rise term (CR) was assumed to be equal to zero.
- Deep Percolation (DP), as commonly assumed in dry regions, can be neglected.
- the impact of the runoff (RO) component can be ignored.

Under these hypotheses, the daily SWB assumes the expression yet reported in Equation (2):

$$D_{r,i} = D_{r,i-1} - P_i - I_i + ETc_i$$

The net precipitation term was estimated from the rainfall measurements from the considered rainfall stations working on the Sinistra Ofanto scheme, applying a double threshold procedure. The first was applied to exclude the first 4 mm of rainfall which here was considered not effective for the CWR's fulfilment; the second threshold was imposed to consider that the infiltration into the soil could not exceed its maximum daily infiltration capacity. This second term, which in theory depend on the status of the soil and on the characteristics of the de precipitation (its intensity) was here defined adopting cut-off threshold limits fixed to 45 mm. All the exceeding amount of the rainfall was considered lost.

The SWB's irrigation module follows the regulated DI (RDI) strategy. For the two considered crop class was necessary to define the crop dependant SWB's parameters, that are reported in Table 7-1.

Soil properties data, synthetically described by the water content at Field Capacity (FC) and Wilting Point (WP), were retrieved from the Maps of indicators of soil hydraulic properties for Europe database (Panagos et al., 2011). This database provides the water retention and the hydraulic conductivity of topsoil (saturated hydraulic conductivity) at the spatial resolution if 1 km for the entire EU, estimated using as input

the European Soil Database and the new pan-European soil hydraulic pedotransfer functions based on the modified FAO texture class.

Table 7-1. Crop dependent SWB's parameters used for the IWR of tree crops (olive and vineyard)

		Olive	Vineyard
Rooting depth	[m]	2,00	1.50
Allowable depletion (p)	[-]	0.65	0.50

In the following two Paragraphs were analysed the results for each crop class, while the detailed outputs of the SWB are reported in Annex 3.

7.2.1. Olive

The IWE estimated for the olive plots is highly variable along with the three irrigation seasons and, during the same year, among the different plots. The number of the considered plot is different year by year due to the preliminary selection of the available irrigation volume registration finalized to exclude the time series incomplete or affected by errors.

The irrigation season 2017 was the only for which the SWB was able to estimate the IWRs. Indeed, not only the average IWE (992,1 m^3/ha) it is close to the average IWA (1.188,9 m^3/ha) but also the scatter plot demonstrates the goodness of the estimation because the points result equally distributed along the 1:1 line (Figure 7.2).

The irrigation season 2018 was strongly influenced by very cold days that occurred during the flowering phase which have compromised the entire yearly olive production. This can justify the fact that the farmers since the production was not able to pay back the cost of irrigation and thanks to the favourable rainfall pattern, decided to not irrigate. Indeed, the resulting average IWA (equal to 102.0 m^3/ha), was lower than the average estimated IWR (447.2 m^3/ha). The scatter plot confirms that this average data is valid for all the plots because all the points are located on the left of the 1:1 line (Figure 7.3).

Inversely, during the irrigation season 2019, was registered an average over-irrigation demonstrated on a global basis by the average IWA value significantly higher than the average IWE (respectively equal to 1,243.9 and 177.3 m^3/ha), and on the single plot by the scattergram which demonstrates as all the points are located on the left of the 1:1 line (Figure 7.4). Since the irrigation module of the SWB model was designed to replace the water stress condition, the IWE does not consider the economic aspects behind the adoption of an irrigation strategy which in this specific crop season can justify the application of more water than the amounts strictly necessary to avoid the water stress to improve the olive production.

The analysis of the results for the irrigation seasons 2018 and 2019 demonstrated as the IWR estimation for tree crops is more complex because:

- needs to consider not only the SWB equation but also the economic aspect which affect the farmers' irrigation strategy.
- is highly affected by the rainfall pattern and the soil water storage capacity.
- requires the knowledge of the spatial distribution of soil and crop characteristics.

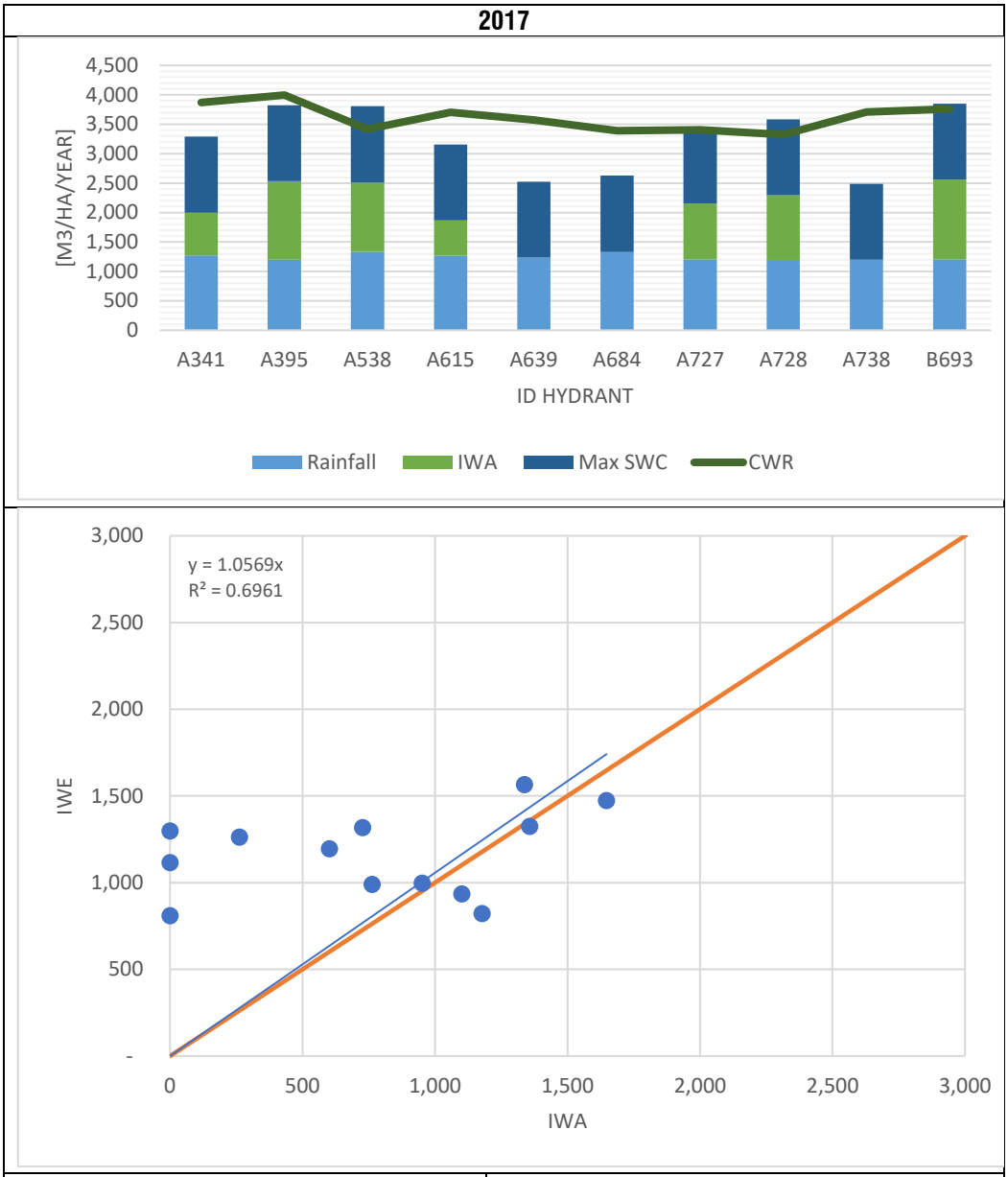

IWA [m^3/ha]		IWE [m^3/ha]	
Mean	992.1	Mean	1188.9
SD	476.5	SD	325.5

Figure 7.2. Seasonal SWB's components for each olive plot estimate during 2017 (upper plot) and scatter plot between Applied and Estimated Irrigation Water [m^3/ha].

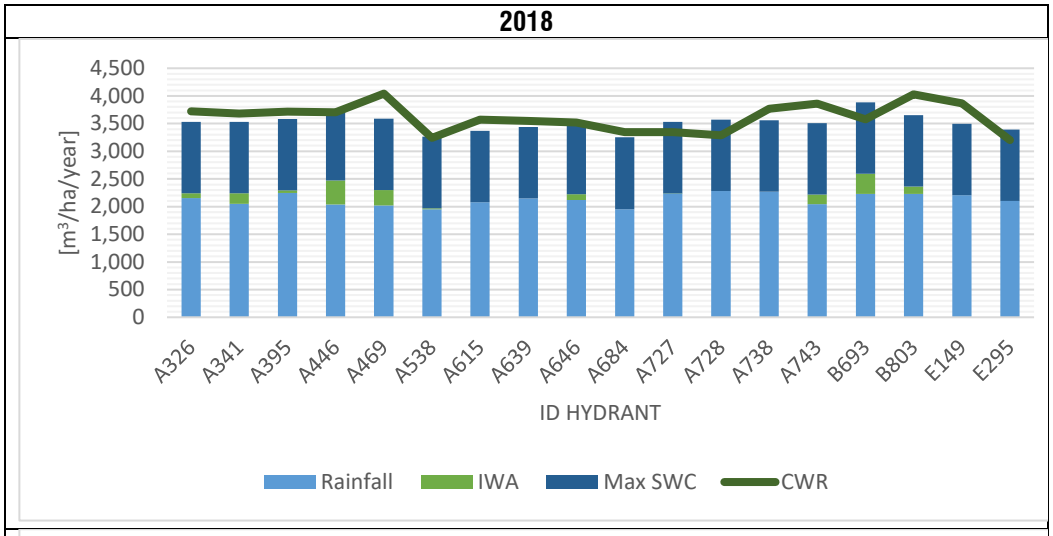

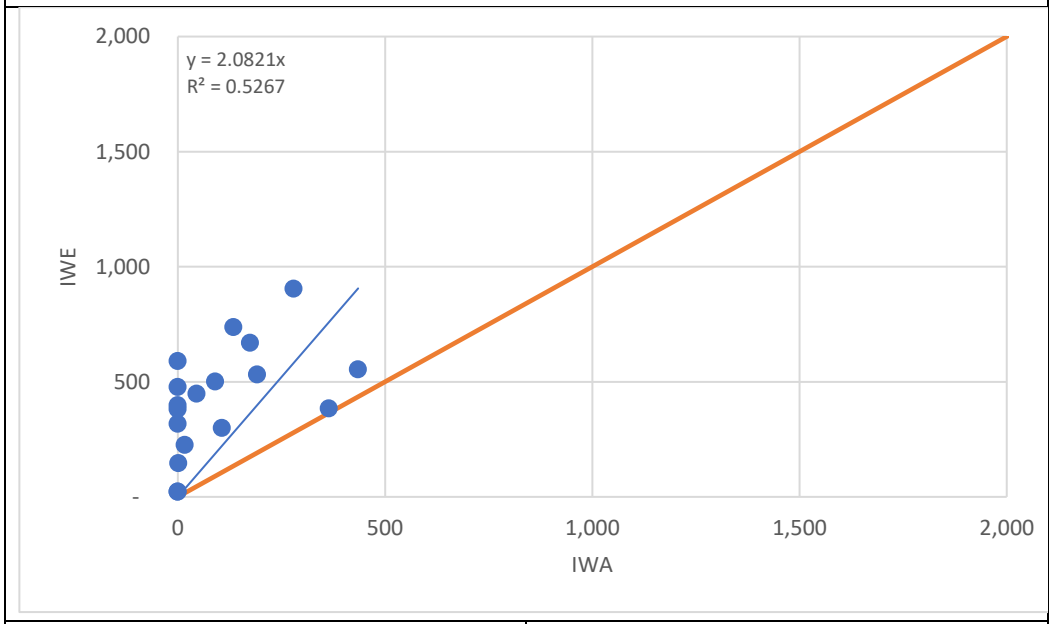

IWA [m³/ha]		IWE [m³/ha]	
Mean	102.0	Mean	424.3
SD	447.2	SD	418.8

Figure 7.3. Seasonal SWB's components for each olive plot estimate during 2018 (upper plot) and scatter plot between Applied and Estimated Irrigation Water [m³/ha].

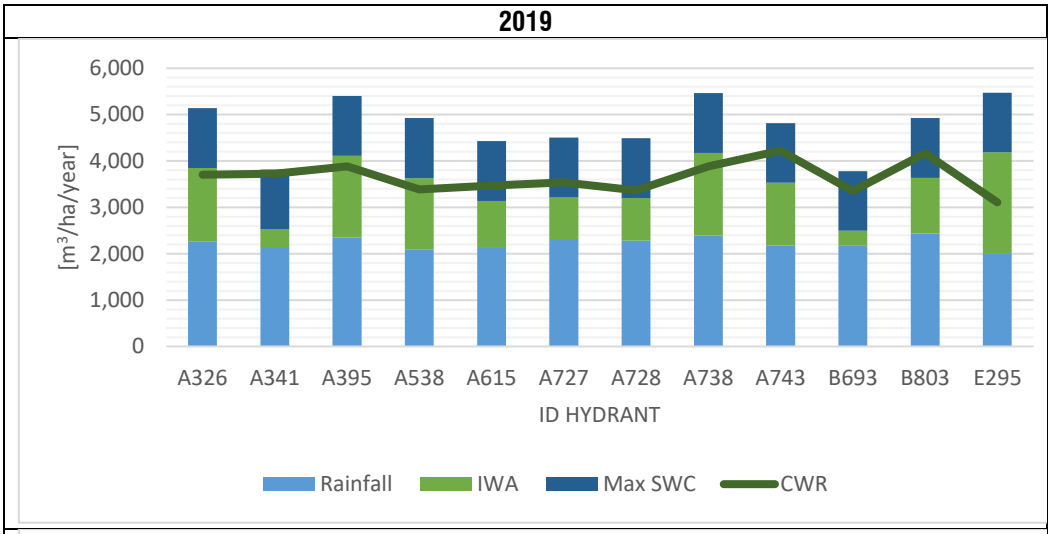

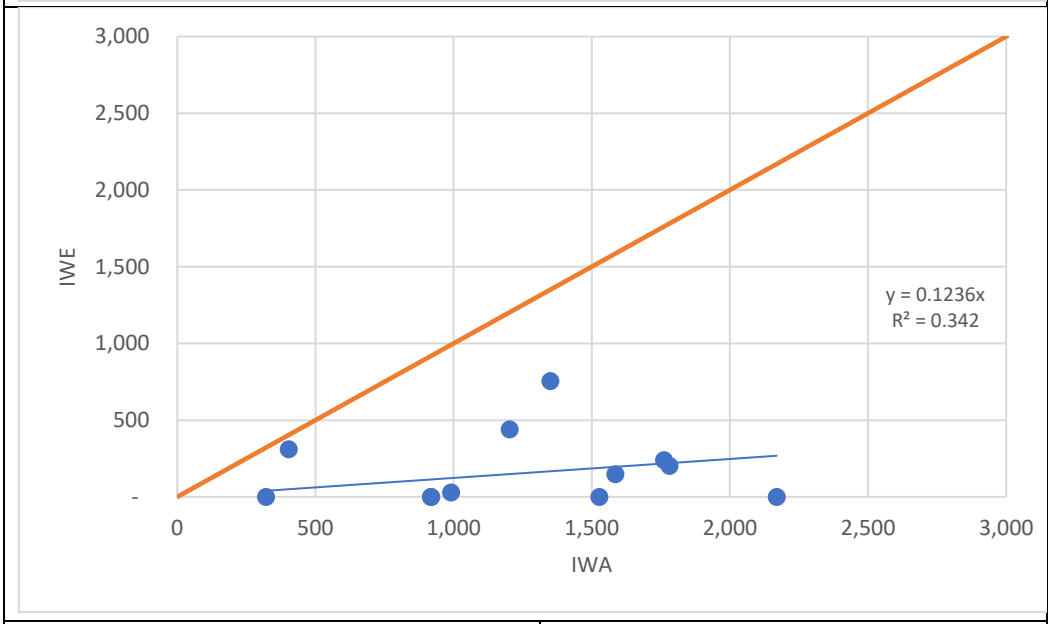

IWA [m³/ha]		IWE [m³/ha]	
Mean	1243.9	Mean	177.3
SD	555.4	SD	536.2

Figure 7.4. Seasonal SWB's components for each olive plot estimate during 2019 (upper plot) and scatter plot between Applied and Estimated Irrigation Water [m³/ha].

7.2.2. Vineyards

The comparison of estimated and applied IW volumes for the analysed vineyard plots shows clearer farmers behaviour than the observed for olive plots. Analysing the results for the three irrigation seasons considered, it is evident as the farmers usually not apply more water than the amount strictly necessary to avoid the onset of unsustainable water stress conditions which can affect grape production. Indeed, independently from the meteorological conditions in only one plot was retrieved IWE higher than the estimated.

For the irrigation season 2017 were available the data for only 4 hydrants which do not allow a deep statistical analysis of the results. However, for these hydrants the mean IWA, equal to 1,475 m^3/ha while the estimated IW was mostly double (2,389 m^3/ha).

The 2018 and 2019 irrigation season, thanks to the favourable rain condition, showed the lowest average IWE (equal respectively to 1,536 and 1,549 m^3/ha). However, while the 2019 average farmers' behaviour was clear and the scatter plot between IWE and IWA lies over the 1:1 line, 2018 was characterized by a general tendency to under-irrigate, in comparison with the optimal IWE which in average is equal to 1,091 m^3/ha.

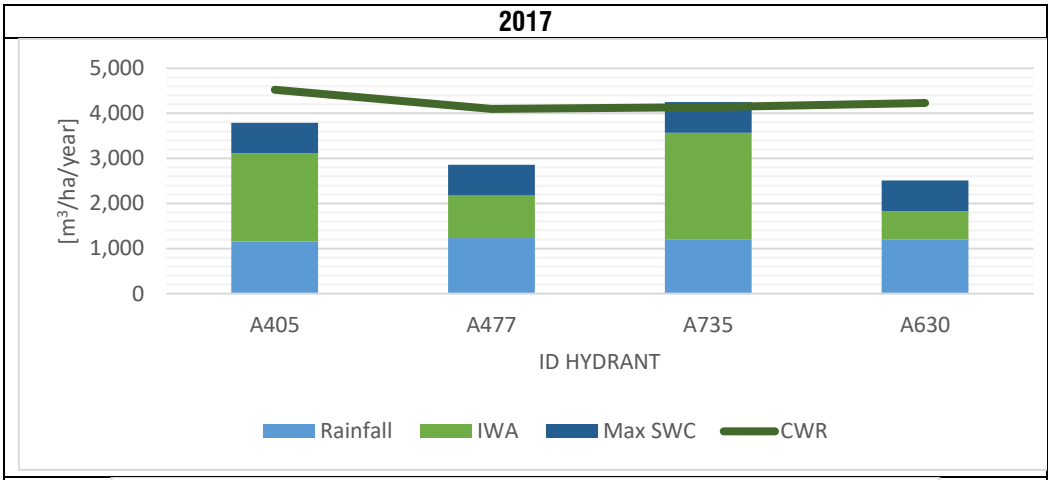

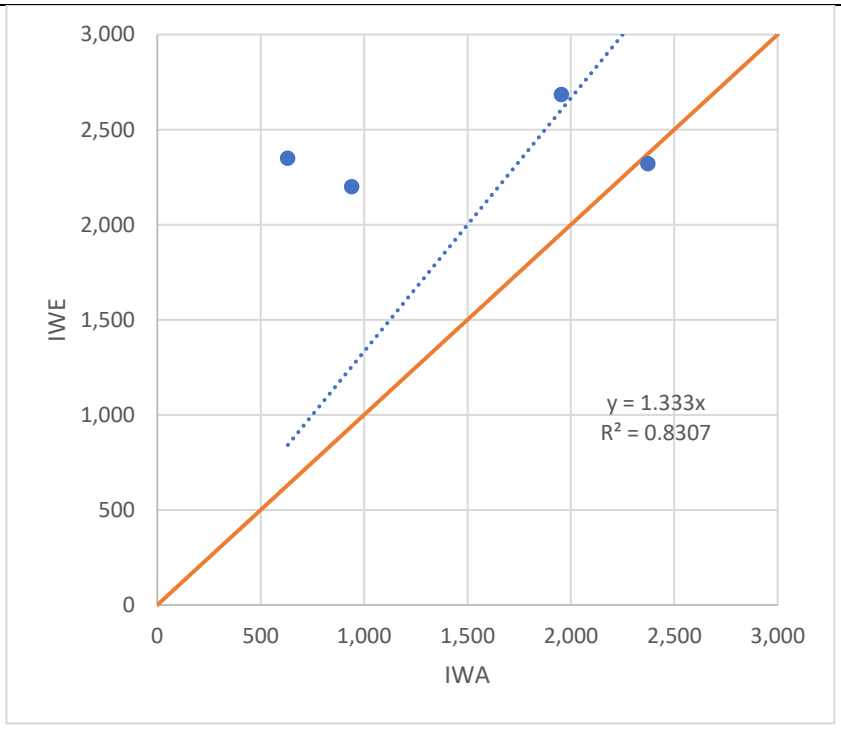

IWA [m³/ha]		IWE [m³/ha]	
Mean	1,475	Mean	2,389
SD	713	SD	180

Figure 7.5. Seasonal SWB's components for each vineyard plot estimate during 2017 (upper plot) and scatter plot between Applied and Estimated Irrigation Water [m³/ha].

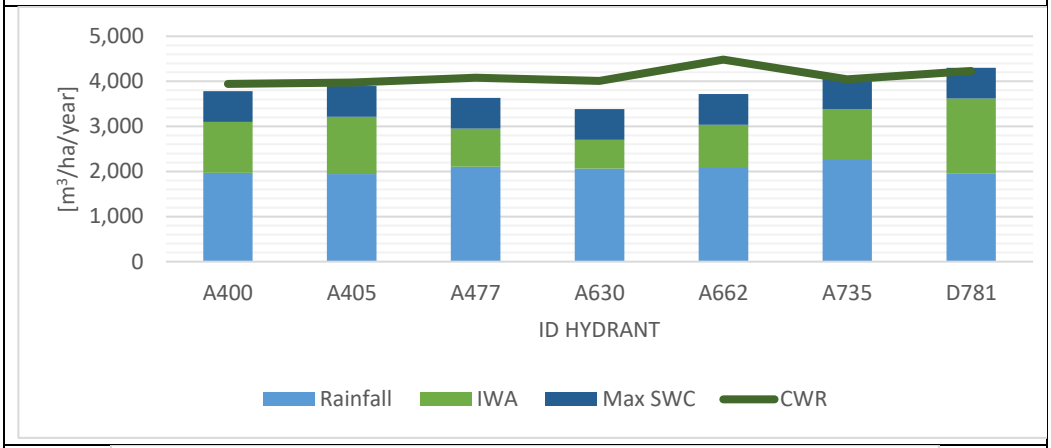

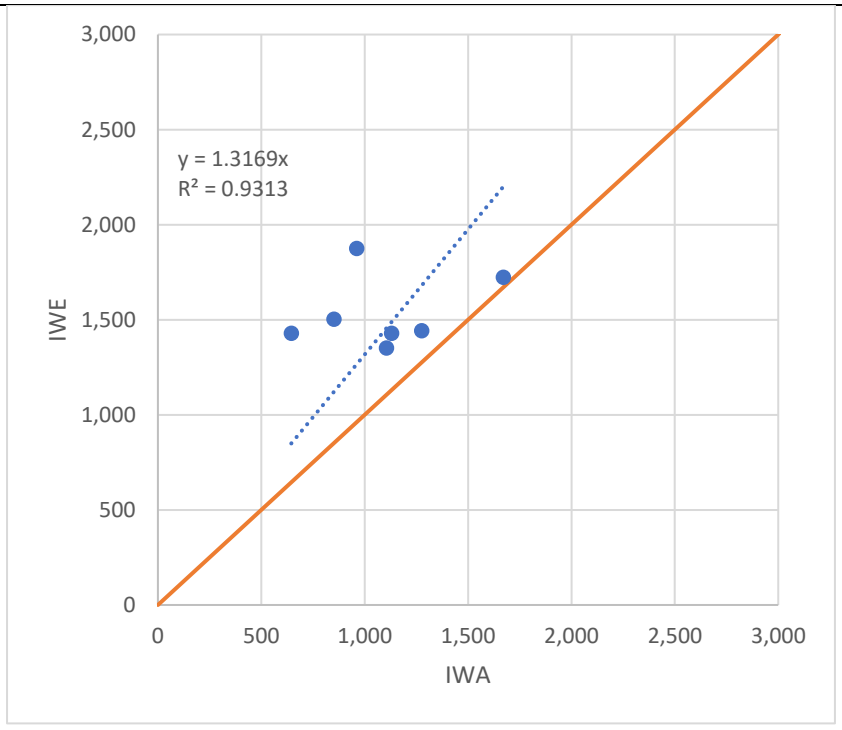

IWA [m³/ha]		IWE [m³/ha]	
Mean	1,091	Mean	1,536
SD	303	SD	176

Figure 7.6. Seasonal SWB's components for each vineyard plot estimate during 2018 (upper plot) and scatter plot between Applied and Estimated Irrigation Water [m³/ha].

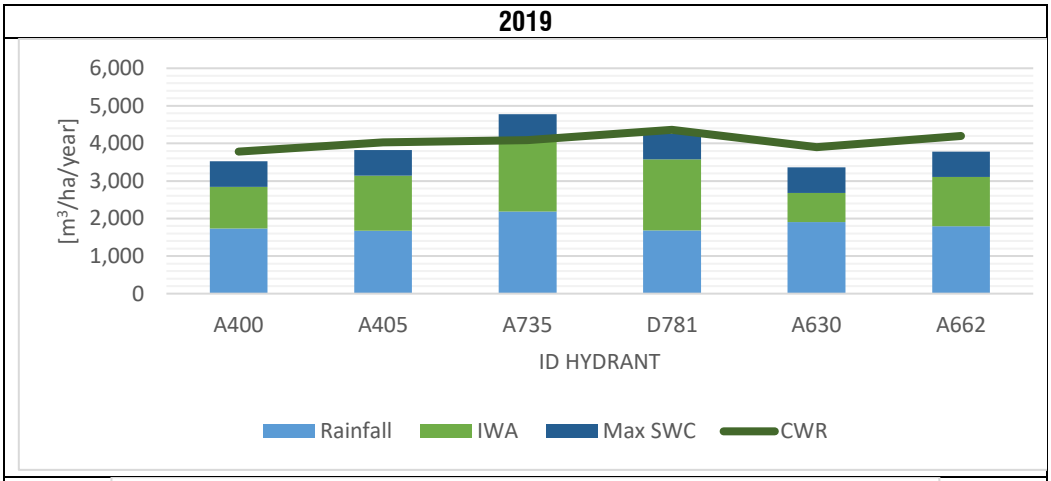

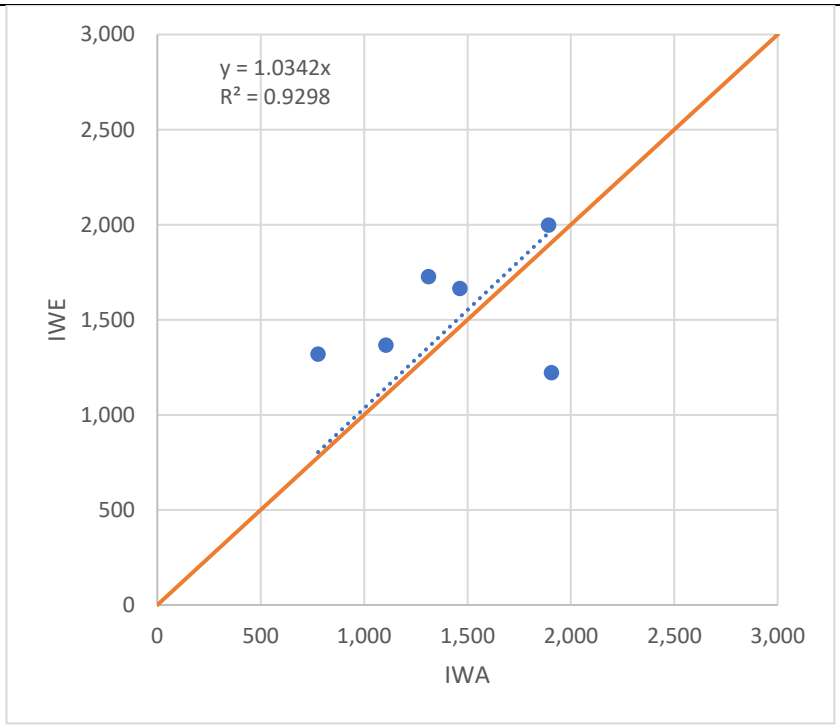

IWA [m³/ha]		IWE [m³/ha]	
Mean	1,409	Mean	1,549
SD	405	SD	271

Figure 7.7. Seasonal SWB's components for each vineyard plot estimate during 2019 (upper plot) and scatter plot between Applied and Estimated Irrigation Water [m³/ha].

7.3. Irrigation Accounting and Monitoring at the plot scale for annual crops

The irrigation estimation for the considered annual crops was conducted following the simplified approach described in Paragraph 7.1.

Since the IWE represent the water to be provided at the crop root, to be compared with the IWA it is necessary to consider losses that could happen at the field scale through the introduction of the irrigation efficiency. The value of the irrigation efficiency adopted, considering the irrigation system adopted and the farmers' behaviour for the CZID, was fixed to 95%.

7.3.1. Tomato

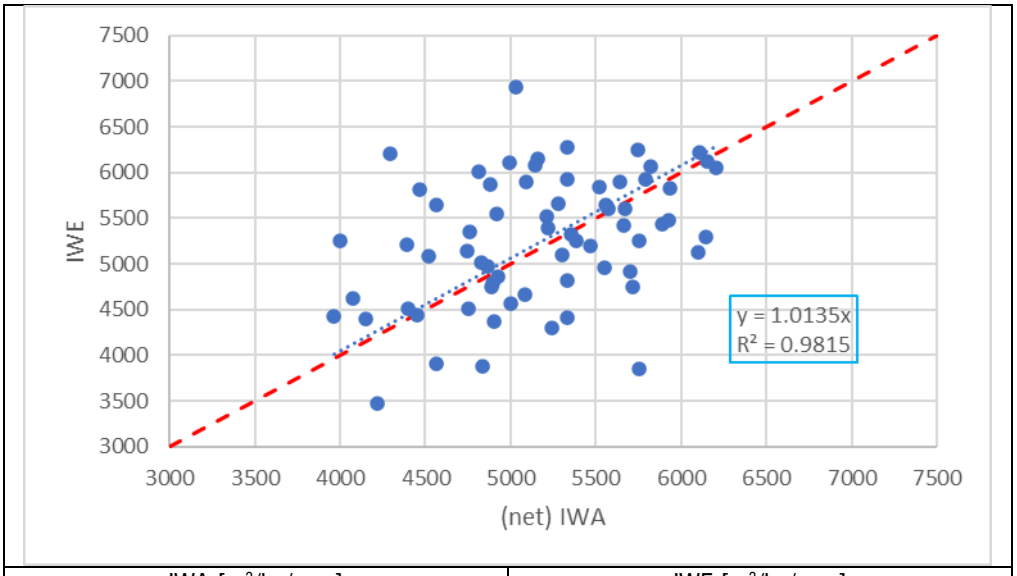

IWA [m³/ha/year]		IWE [m³/ha/year]	
Mean	5,439.9	Mean	5,272.8
SD	4,174.0	SD	3,477.0

Figure 7.8 Scatter plot between (net) Applied (Irrigation efficiency 0.95) and Estimated Irrigation Water retrieved for tomato [m³/ha/year].

7.3.2. Maize

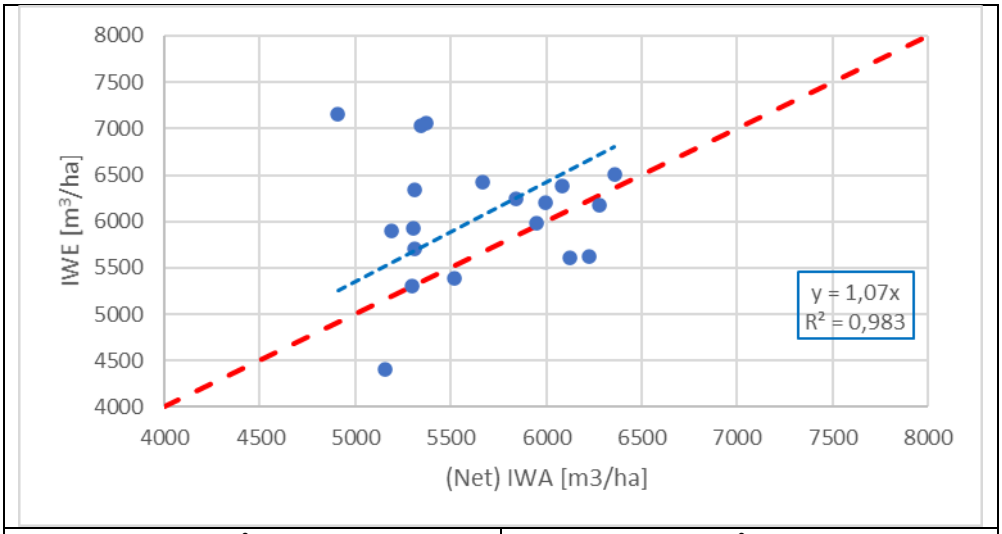

IWA [m³/ha/year]		IWE [m³/ha/year]	
Mean	5,940.8	Mean	6,134.7
SD	454.3	SD	685.7

Figure 7.9. Scatter plot between (net) Applied (Irrigation efficiency 0.95) and Estimate Irrigation Water retrieved for maize [m³/ha/year].

For tomato and maize, the scatter plot between IWA and IWE shows a clear regular trend. In the case of maize, framers usually apply under-irrigation due to the economic balance between the costs supported for irrigation and the increase of farmers' income. Tomato has and higher value which can justify the application of more water.

These two trends are clearly showed respectively in Figure 7.8 and Figure 7.9.

7.4. Irrigation Accounting and Monitoring at the irrigation district scale

7.4.1. IWR of "Sinistra Ofanto" Irrigation Scheme

The seasonal IWR of the "Sinistra Ofanto" Irrigation Scheme was assessed extending the FAO56-based SWB model proposed and described in Paragraph 7.2 to the whole irrigation scheme. The following Table 7-2 resumes the principal components of the SWB with a specific focus on rainfall and irrigation. To compare the IWA with the IWE, the net (net) IWE provided by the SWB was increased applying the irrigation efficiency coefficient. It was estimated and assumed equal to 0.95 since in the area is active a progressive volumetric water tariff which encourages the farmers to apply very efficient irrigation strategies.

Table 7-2. Resume of the principals seasonal positive SWB's components (rainfall and irrigation [m^3/year]) estimated at the irrigation district scale (ID).

	2017	2018	2019	2017	2018	2019
ID	**Rain Total**			**IWA CBC**		
11	3,778,194	7,174,039	11,121,281	5,933,796	3,734,173	5,251,241
12	2,219,545	3,530,948	5,212,899	2,911,394	1,402,125	2,637,765
13	1,760,976	3,469,004	5,187,063	2,885,511	1,231,693	2,466,225
14	1,265,277	2,304,044	4,021,909	2,869,103	2,034,221	2,461,412
Total	9,023,992	16,478,035	25,543,152	14,599,804	8,402,212	12,816,643
ID	**Rain Effective**			**(Gross) IWE**		
11	3,355,353	6,544,099	6,741,310	6,196,582	3,161,057	3,337,656
12	1,845,548	3,233,008	2,969,492	4,098,489	1,749,637	1,671,747
13	1,612,425	2,868,112	2,924,824	3,293,886	1,415,734	1,289,326
14	1,240,060	2,228,656	2,421,186	2,564,444	1,261,554	1,463,534
Total	8,053,386	14,873,876	15,056,812	16,153,402	7,587,981	7,762,263
ID	**Rain Effective / Rain Total**			**(Net) IWE / IWA**		
11	88.8%	91.2%	60.6%	104.4%	84.7%	63.6%
12	83.1%	91.6%	57.0%	140.8%	124.8%	63.4%
13	91.6%	82.7%	56.4%	114.2%	114.9%	52.3%
14	98.0%	96.7%	60.2%	89.4%	62.0%	59.5%
Total	89.2%	90.3%	58.9%	110.6%	90.3%	60.6%

It is important to notice as the temporal distribution of rainfall is crucial to estimate the IWR. Indeed, while 2018 and 2019 are characterized by a very different volume of rainfalls (respectively equal to 16.5 and 25.3 Mm^3), the estimated effective rainfall is very different and respectively equal to 14.9 and 15.1 Mm^3. This could be explained by looking at the meteorological characterization of the area, reported in Paragraph 5.1.2 which shows as the irrigation season 2019 was characterized by heavy and frequents rainfalls until July followed by the second part of the irrigation season relatively dry. For this reason, only 58.9% of the total rainfall volume (on average) was estimated as effective for 2019, while in the previous irrigation season the effectiveness of rainfall was higher and close to 90%.

The seasonal IWE for the 2017 and 2018 for the entire study area results to be close to the IWA provided by the Consortium with a 10% of overestimation during the dry year 2017 and vice versa an underestimation during 2018 highly influenced by the precipitation events. Even if these considerations are valid at the level of each irrigation district, the magnitude of the differences are variables for each district as a function of the specific crop patterns.

A different consideration is necessary to analyse the results for the irrigation season 2019. Hence, as experienced at the plot scale, the IWA for 2019 results higher than the estimated. However, the SWB model, and in particular the irrigation module, was designed to estimate the IWR strictly necessary to avoid the occurrence of water stress and cannot consider other factors that can affect the farmers' irrigation strategies.

Even if the SWB model can estimate the IWR at the daily scale, since for the Sinistra Ofanto the temporal distribution of the IWA is missing, was not possible to assess the performance of the SWB model during the irrigation season.

7.4.2. IWR of "Canal del Zujar Irrigation District"

The IWR for the CZID was estimated at a daily scale using the simplified approach of Equation (18). In this case, since the temporal pattern of the IWA by the farmers is available, was possible compare not only the seasonal total volume but also the temporal trends of the Applied and Estimated IWR over the entire area. The total IWA volume for 2017 is equal to 10,519,303 m^3 not equally distributed during the year. Indeed, almost half of the IWA is concentred during June and July (which account respectively the 30.75% and 17.54% of the total IWA). For the IWR estimation was therefore selected the period ranging from the 1st of April to the 30th of October, where almost the totality of IW was applied by farmers (98.16% corresponding to 10,325,613 m^3).

During the considered period the total effective rainfall, as retrieved from the SiAR, amount to 27.1 mm, occurring exclusively during April. For the rest of the period, no rainfall events were registered. The total effective rainfall, as reported in Paragraph 5.2.2 was equal to 104.2 mm.

Since the IWE represent the water to be provided at the crop root, to be compared with the IWA it is necessary to consider losses that could happen at the field scale introducing the Net IWA:

$$NIWA = \frac{IWA}{e} \tag{53}$$

The value of the irrigation efficiency adopted, considering the irrigation system adopted and the farmers' behaviour for the CZID, was fixed to 95%. Under this hypothesis, the Net IWA volume amounts to 9,809,332 m^3.

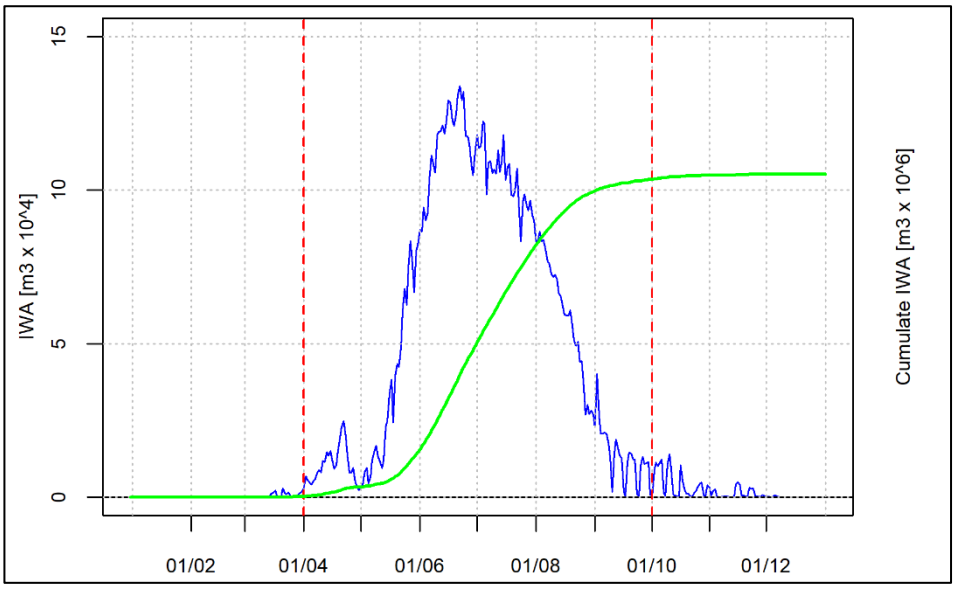

Figure 7.10. Temporal trend of the daily and cumulated IWA registered at the CZID during the year 2017.

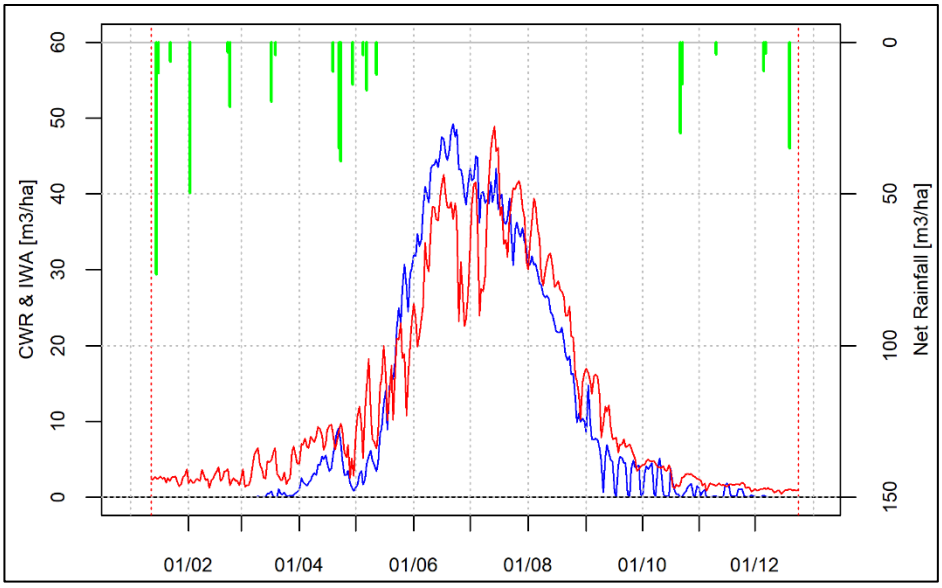

Figure 7.11. Temporal trend of the estimated CWR (red line), IWA (blue line) and effective rainfall.

The total estimated IWE is equal to 9,747,443 m^3 corresponding to an average IWE of 3,584 m^3 per hectare effectively cropped (excluding all the areas not cropped).

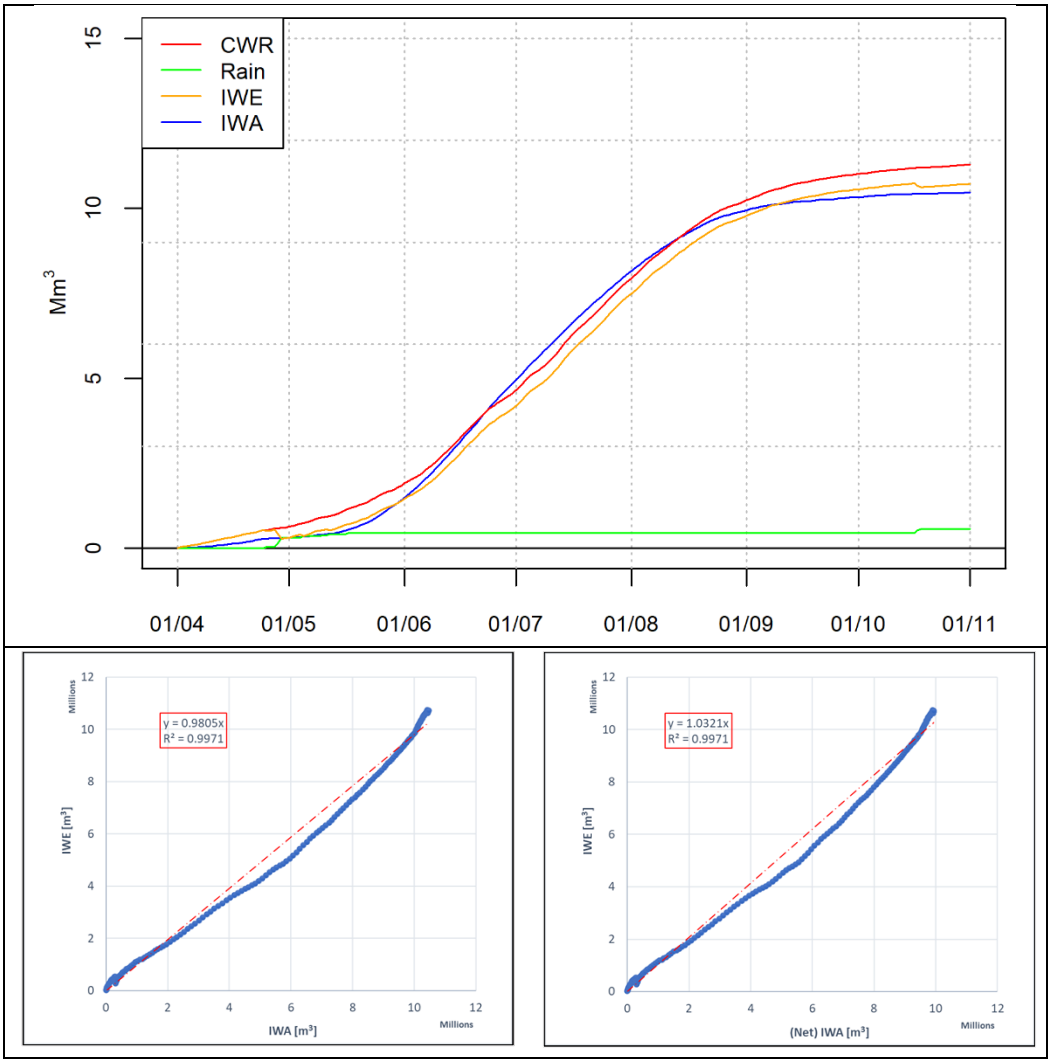

Figure 7.12. Comparison of the cumulated IWE and the gross (upper plot) and Net (bottom plot) IWA. The irrigation efficiency used was assumed equal to 95%.

The good agreement between estimated ad applied irrigation was confirmed also from the comparison of their temporal trends. In Figure 7.12 are reported the scatter plots between the cumulated IWE and net/gross IWA. The two datasets have a strong linear correlation and a low displacement from the 1:1 line. This displacement is better quantified both in terms of absolute and relative (reported to the total IWA) volumes in Figure 7.13.

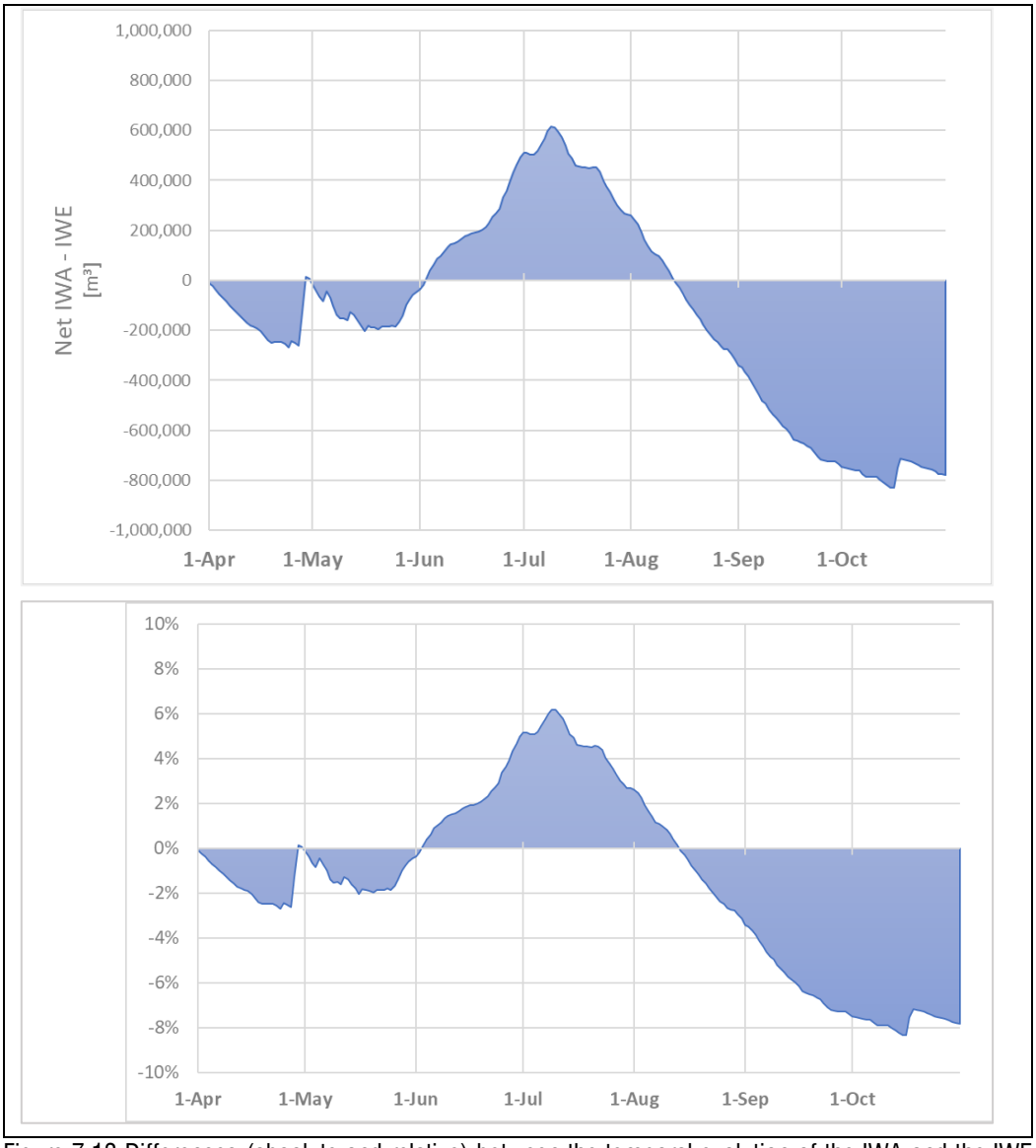

Figure 7.13 Differences (absolute and relative) between the temporal evolution of the IWA and the IWE cumulative curves.

The differences highlighted from Figure 7.13, assuming that the estimated CWR is correct, show the presence of three different possible phases of irrigation management:

1. During the first phase (April-May) the net IWA is smaller than the estimated, however, in this phase the water accumulated into the soil during the winter could be extracted and used by crops.
2. In the second phase (June – mid-August) the IWA is bigger than the expected. It could be justified assuming that this phase is the most delicate for the crop growing and therefore farmers applied more water than the strictly necessary.
3. In the last phase, coincident with the maturing and harvesting phase, the IWA is lower than the expected.

Since the Equation (18) was applied on the S2- pixel basis, it is possible to also retrieve the spatial distribution of the IWE at the selected temporal scale. In Figure 7.14 is reported the IWE estimated for the whole period considered (April to October). However, due to an incomplete spatial description of the IWA dataset, was not possible to perform a spatial correlation, between estimated and applied irrigation.

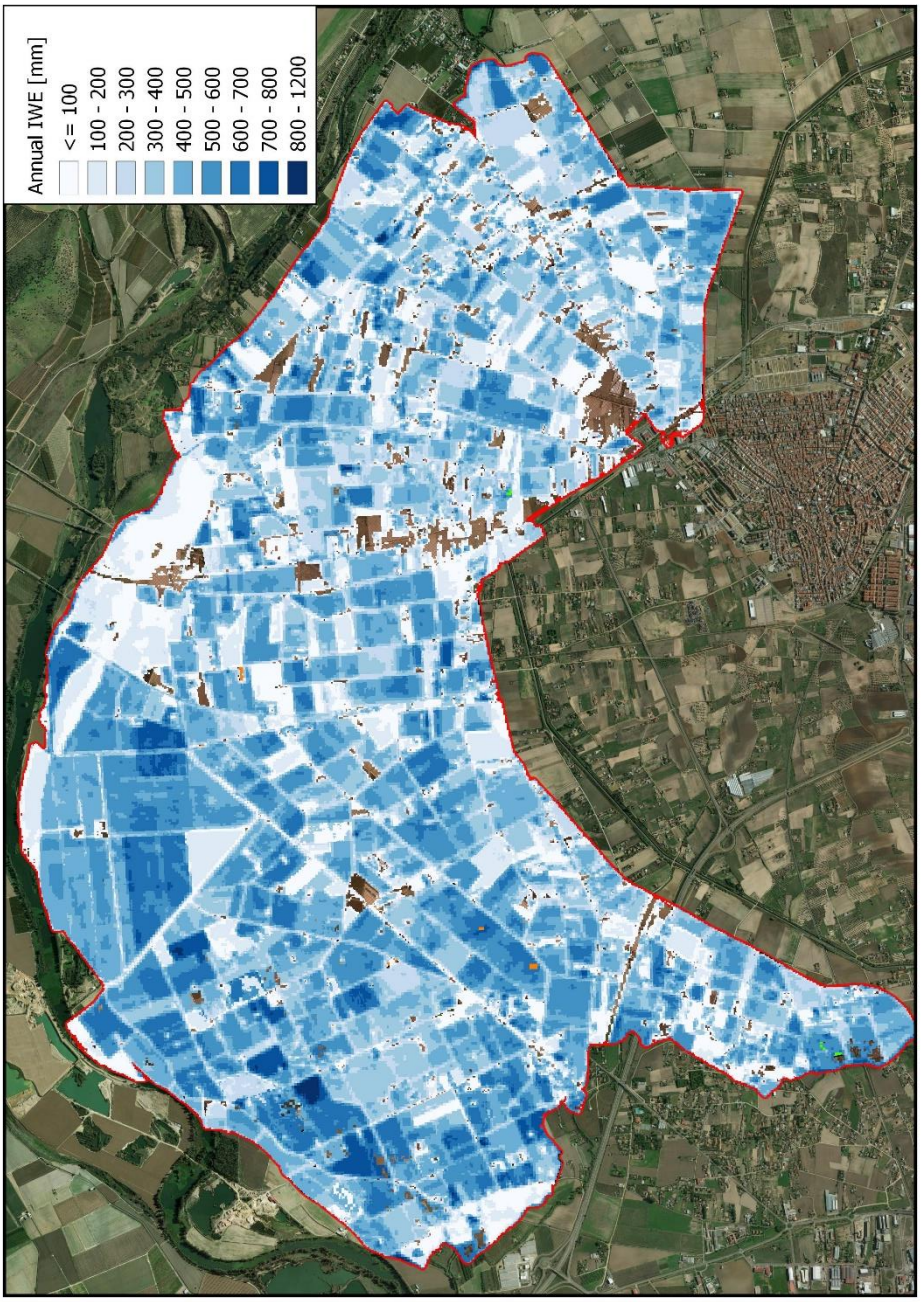

Figure 7.14. The spatial pattern of the estimated annual irrigation water requirement (IWE) [mm/year] over the CZID study area.

CONCLUSIONS

Major findings

Regarding the CWR estimation using EO-derived data:

- The EO-based FAO-PM approach in its original formulation, compared against the potential (maximum) CWR estimated using the classical Kc-FAO approach, lead to a high overestimate of the CWR for the trees crops analysed (olive and vineyard) and vice versa to underestimate the CWR for annual crops (tomato and maize).

- The modification of the resistance terms of the FAO-PM equation (particularly the surface resistance) leads to a better estimation of the CWR which result to be coherent with the FAO-Kc derived CWR. Moreover, the proposed modification allows:

    - to capture the water stress in dry years (as retrieved for the crop season 2017 over the Sinistra Ofanto test site).
    - to be applied also without the knowledge of the spatial distribution of the crop types since the parametrization is crop-independent.

Regarding the IWR estimation:

- identify irrigated agriculture is relatively simple in arid regions and for annual crops because, due to climatic conditions, the development and growth of agricultural crops would be impossible without irrigation. In these cases, irrigation can be assumed with a high degree of probability.

- IWR estimation for tree crops is more complex because:

- needs to consider not only the SWB equation but also the economic aspect which affect the farmers' irrigation strategy.
- is highly affected by the rainfall pattern and the soil water storage capacity.
- requires the knowledge of the spatial distribution of soil and crop characteristics.

Perspectives and future lines of investigation

The possible future lines of investigation could follow two principal pillars:

1. Consolidate the robustness of the method, due to:
    - use field ETc measurements to calibrate and validate quantitatively the "one-step" EO-based FAO-PM method.
    - Even if this work considered the major crop classes which characterize the Mediterranean agricultural system, it is necessary to extend the analysis over the remaining crops.
    - Testing and validating the procedure over the major possible number of study areas spread for the Mediterranean area.
    - Improve the RS-SWB especially for the woody crops, also including the socio-economic variables that could influence the framers' behaviour.

2. Apply the overall described procedure to agro-environmental studies finalized to:
    - *monitoring of the irrigated area*
    - *monitoring of groundwater use patterns*
    - *precision irrigation*
    - *Irrigation performance assessment*
    - *green-blue water accounting*
    - *Water-Energy-Food nexus analysis*

The spatial and temporal scale of these applications could be extremely variable since the procedure is modulable and scalable.

The spatial scales could range from the single plot scale to the Water User Association scale since to regional/watershed scale. The unique limitation of the procedure is represented by the increase, considering study areas even bigger, of the amount of data to be managed and stored. From the operative point of view, the proposed procedure is easily appliable.

The temporal scale and perspective could be very different. The procedure was tested and developed over data retrieved from previous crop season and therefore was demonstrated to be able to represent the *ex-post Crop and Irrigation Water Requirements,* but it can be applied also in a *near-real-time mode* feeding the model in continues with meteorological measurement and prevision and satellite-derived crop status information. In this way, it is possible to use the retrieved information as Decision Support Tools (DST) to take wise decisions on irrigation water-related management and governance issues. These previsions could be further extended looking to the mid-long-term period considering different possible scenarios as results of the effect of climate change (e.g., change in rainfall pattern) or socio-economic changes derived for example from the Common Agricultural Policy or from the change in customer needs and/or behaviours.

LIST OF FIGURES

LIST OF TABLES

REFERENCES

Aghdasi, F., 2010. Crop water requirement assessment and annual planning of water allocation. University of Twente Faculty of Geo-Information and Earth Observation (ITC).

Akdim, N., Alfieri, S.M., Habib, A., Choukri, A., Cheruiyot, E., Labbassi, K., Menenti, M., 2014. Monitoring of Irrigation Schemes by Remote Sensing: Phenology versus Retrieval of Biophysical Variables. Remote Sensing 6, 5815–5851. https://doi.org/10.3390/rs6065815

Allen, R.G., Howell, T.A., Pruitt, W.O., Walter, I.A., Jensen, M.E., 1991. Lysimeters for Evapotranspiration and Environmental Measurements 456–456.

Allen, R.G., Pereira, L.S., Raes, D., Smith, M., 1998. Crop evapotranspiration-Guidelines for computing crop water requirements-FAO Irrigation and drainage paper 56. Fao, Rome 300.

Anderson, M., Neale, C., Li, F., Norman, J., Kustas, W., Jayanthi, H., Chavez, J., 2004. Upscaling ground observations of vegetation water content, canopy height, and leaf area index during SMEX02 using aircraft and Landsat imagery. Remote Sensing of Environment 92, 447–464. https://doi.org/10.1016/j.rse.2004.03.019

Anderson, M.C., Allen, R.G., Morse, A., Kustas, W.P., 2012. Use of Landsat thermal imagery in monitoring evapotranspiration and managing water resources. Remote Sensing of Environment, Landsat Legacy Special Issue 122, 50–65. https://doi.org/10.1016/j.rse.2011.08.025

Bai, Y., Zhang, J., Zhang, S., Koju, U.A., Yao, F., Igbawua, T., 2017. Using precipitation, vertical root distribution, and satellite-retrieved vegetation information to parameterize water stress in a Penman-Monteith approach to evapotranspiration modeling under Mediterranean climate. Journal of Advances in Modeling Earth Systems 9, 168–192. https://doi.org/10.1002/2016MS000702

Balbontín, C., Campos, I., Odi-Lara, M., Ibacache, A., Calera, A., 2017. Irrigation Performance Assessment in Table Grape Using the Reflectance-Based Crop Coefficient. Remote Sensing 9, 1276. https://doi.org/10.3390/rs9121276

Barraza, V., Restrepo-Coupe, N., Huete, A., Grings, F., Beringer, J., Cleverly, J., Eamus, D., 2017. Estimation of latent heat flux over savannah vegetation across the North Australian Tropical Transect from multiple sensors and global meteorological data. Agricultural and Forest Meteorology 232, 689–703. https://doi.org/10.1016/j.agrformet.2016.10.013

Barraza, V., Restrepo-Coupe, N., Huete, A., Grings, F., Van Gorsel, E., 2015. Passive microwave and optical index approaches for estimating surface conductance and evapotranspiration in forest ecosystems. Agricultural and Forest Meteorology 213, 126–137. https://doi.org/10.1016/j.agrformet.2015.06.020

Bausch, W.C., 1995. Remote sensing of crop coefficients for improving the irrigation scheduling of corn. Agricultural Water Management 27, 55–68. https://doi.org/10.1016/0378-3774(95)01125-3

Blatchford, M., M. Mannaerts, C., Zeng, Y., Nouri, H., Karimi, P., 2020. Influence of Spatial Resolution on Remote Sensing-Based Irrigation Performance Assessment Using WaPOR Data. Remote Sensing 12, 2949. https://doi.org/10.3390/rs12182949

Bonan, G.B., 2008. Forests and Climate Change: Forcings, Feedbacks, and the Climate Benefits of Forests. Science 320, 1444–1449. https://doi.org/10.1126/science.1155121

Brocca, L., Tarpanelli, A., Filippucci, P., Dorigo, W., Zaussinger, F., Gruber, A., Fernández-Prieto, D., 2018. How much water is used for irrigation? A new approach exploiting coarse resolution satellite soil moisture products. International Journal of Applied Earth Observation and Geoinformation 73, 752–766. https://doi.org/10.1016/j.jag.2018.08.023

Brunsell, N.A., Ham, J.M., Arnold, K.A., 2011. Validating remotely sensed land surface fluxes in heterogeneous terrain with large aperture scintillometry. International Journal of Remote Sensing 32, 6295–6314. https://doi.org/10.1080/01431161.2010.508058

Calera, A., Campos, I., Osann, A., D'Urso, G., Menenti, M., 2017. Remote Sensing for Crop Water Management: From ET Modelling to Services for the End Users. Sensors 17, 1104. https://doi.org/10.3390/s17051104

Čermák, J., Deml, M., Penka, M., 1973. A new method of sap flow rate determination in trees. Biol Plant 15, 171–178. https://doi.org/10.1007/BF02922390

Cleugh, H.A., Leuning, R., Mu, Q., Running, S.W., 2007. Regional evaporation estimates from flux tower and MODIS satellite data. Remote Sensing of Environment 106, 285–304. https://doi.org/10.1016/j.rse.2006.07.007

Consoli, S., D'Urso, G., Toscano, A., 2006. Remote sensing to estimate ET-fluxes and the performance of an irrigation district in southern Italy. Agricultural Water Management 81, 295–314. https://doi.org/10.1016/j.agwat.2005.04.008

Courault, D., Seguin, B., Olioso, A., 2005. Review on estimation of evapotranspiration from remote sensing data: From empirical to numerical modeling approaches. Irrig Drainage Syst 19, 223–249. https://doi.org/10.1007/s10795-005-5186-0

Damm, A., Paul-Limoges, E., Haghighi, E., Simmer, C., Morsdorf, F., Schneider, F.D., van der Tol, C., Migliavacca, M., Rascher, U., 2018. Remote sensing of plant-water relations: An overview and future perspectives. Journal of Plant Physiology, From aquaporin to ecosystem: Plants in the water cycle 227, 3–19. https://doi.org/10.1016/j.jplph.2018.04.012

Doorenbos, J., Pruitt, W.O., 1977. FAO irrigation and drainage paper 24: crop water requirements. FAO, Roma 156.

Drusch, M., Del Bello, U., Carlier, S., Colin, O., Fernandez, V., Gascon, F., Hoersch, B., Isola, C., Laberinti, P., Martimort, P., Meygret, A., Spoto, F., Sy, O., Marchese, F., Bargellini, P., 2012. Sentinel-2: ESA's Optical High-Resolution Mission for GMES Operational Services. Remote Sensing of Environment, The Sentinel Missions - New Opportunities for Science 120, 25–36. https://doi.org/10.1016/j.rse.2011.11.026

Duchemin, B., Hadria, R., Erraki, S., Boulet, G., Maisongrande, P., Chehbouni, A., Escadafal, R., Ezzahar, J., Hoedjes, J.C.B., Kharrou, M.H., Khabba, S., Mougenot,

B., Olioso, A., Rodriguez, J.-C., Simonneaux, V., 2006. Monitoring wheat phenology and irrigation in Central Morocco: On the use of relationships between evapotranspiration, crops coefficients, leaf area index and remotely-sensed vegetation indices. Agricultural Water Management 79, 1–27. https://doi.org/10.1016/j.agwat.2005.02.013

D'Urso, G., 2010. Current Status and Perspectives for the Estimation of Crop Water Requirements from Earth Observation. Italian Journal of Agronomy 5, 107–120. https://doi.org/10.4081/ija.2010.107

D'Urso, G., Belmonte, A., 2006. Operative Approaches To Determine Crop Water Requirements From Earth Observation Data: Methodologies And Applications. AIP Conference Proceedings 852, 14–25. https://doi.org/10.1063/1.2349323

D'Urso, G., Menenti, M., 1995. Mapping crop coefficients in irrigated areas from Landsat TM images, in: Engman, E.T., Guyot, G., Marino, C.M. (Eds.), . Presented at the Satellite Remote Sensing II, Paris, France, pp. 41–47. https://doi.org/10.1117/12.227167

D'Urso, G., Richter, K., Calera, A., Osann, M.A., Escadafal, R., Garatuza-Pajan, J., Hanich, L., Perdigão, A., Tapia, J.B., Vuolo, F., 2010. Earth Observation products for operational irrigation management in the context of the PLEIADeS project. Agricultural Water Management 98, 271–282. https://doi.org/10.1016/j.agwat.2010.08.020

Dyer, A.J., 1961. Measurements of evaporation and heat transfer in the lower atmosphere by an automatic eddy-correlation technique. Quarterly Journal of the Royal Meteorological Society 87, 401–412. https://doi.org/10.1002/qj.49708737311

Er-Raki, S., Chehbouni, A., Guemouria, N., Ezzahar, J., Khabba, S., Boulet, G., Hanich, L., 2009. Citrus orchard evapotranspiration: Comparison between eddy covariance measurements and the FAO-56 approach estimates. Plant Biosystems - An International Journal Dealing with all Aspects of Plant Biology 143, 201–208. https://doi.org/10.1080/11263500802709897

Farg, E., Arafat, S.M., Abd El-Wahed, M.S., EL-Gindy, A.M., 2012. Estimation of Evapotranspiration ETc and Crop Coefficient Kc of Wheat, in south Nile Delta of Egypt Using integrated FAO-56 approach and remote sensing data. The Egyptian Journal of Remote Sensing and Space Science 15, 83–89. https://doi.org/10.1016/j.ejrs.2012.02.001

Fernández García, I., Lecina, S., Ruiz-Sánchez, M.C., Vera, J., Conejero, W., Conesa, M.R., Domínguez, A., Pardo, J.J., Léllis, B.C., Montesinos, P., 2020. Trends and Challenges in Irrigation Scheduling in the Semi-Arid Area of Spain. Water 12, 785. https://doi.org/10.3390/w12030785

Fisher, J.B., Tu, K.P., Baldocchi, D.D., 2008. Global estimates of the land–atmosphere water flux based on monthly AVHRR and ISLSCP-II data, validated at 16 FLUXNET sites. Remote Sensing of Environment 112, 901–919. https://doi.org/10.1016/j.rse.2007.06.025

Foken, T., 2008. The Energy Balance Closure Problem: An Overview. Ecological Applications 18, 1351–1367. https://doi.org/10.1890/06-0922.1

French, A.N., Hunsaker, D.J., Bounoua, L., Karnieli, A., Luckett, W., Strand, R., 2018. Remote Sensing of Evapotranspiration over the Central Arizona Irrigation Drainage District, USA. https://doi.org/10.20944/preprints201809.0501.v1

Gao, Y., Long, D., Li, Z.-L., 2008. Estimation of daily actual evapotranspiration from remotely sensed data under complex terrain over the upper Chao river basin in North China. International Journal of Remote Sensing 29, 3295–3315. https://doi.org/10.1080/01431160701469073

Garatuza-Payan, J., Tamayo, A., Watts, C., Rodriguez, J.C., 2003. Estimating large area wheat evapotranspiration from remote sensing data, in: IGARSS 2003. 2003 IEEE International Geoscience and Remote Sensing Symposium. Proceedings (IEEE Cat. No.03CH37477). Presented at the IGARSS 2003. 2003 IEEE International Geoscience and Remote Sensing Symposium. Proceedings (IEEE Cat. No.03CH37477), pp. 380–382 vol.1. https://doi.org/10.1109/IGARSS.2003.1293782

Garrido Rubio, J., Gonzalez-Piqueras, J., Campos, I., Osann, A., González-Gómez, L., Calera, A., 2020. Remote sensing-based soil water balance for irrigation water accounting at plot and water user association management scale. Agricultural Water Management 238. https://doi.org/10.1016/j.agwat.2020.106236

Glenn, E.P., Huete, A.R., Nagler, P.L., Hirschboeck, K.K., Brown, P., 2007. Integrating Remote Sensing and Ground Methods to Estimate Evapotranspiration. Critical Reviews in Plant Sciences 26, 139–168. https://doi.org/10.1080/07352680701402503

Glenn, E.P., Nagler, P.L., Huete, A.R., 2010. Vegetation Index Methods for Estimating Evapotranspiration by Remote Sensing. Surv Geophys 31, 531–555. https://doi.org/10.1007/s10712-010-9102-2

González-Dugo, M.P., Mateos, L., 2008. Spectral vegetation indices for benchmarking water productivity of irrigated cotton and sugarbeet crops. Agricultural Water Management 95, 48–58. https://doi.org/10.1016/j.agwat.2007.09.001

Gowda, P.H., Chavez, J.L., Colaizzi, P.D., Evett, S.R., Howell, T.A., Tolk, J.A., 2008. ET mapping for agricultural water management: present status and challenges. Irrig Sci 26, 223–237. https://doi.org/10.1007/s00271-007-0088-6

Guzinski, R., Nieto, H., 2019. Evaluating the feasibility of using Sentinel-2 and Sentinel-3 satellites for high-resolution evapotranspiration estimations. Remote Sensing of Environment 221, 157–172. https://doi.org/10.1016/j.rse.2018.11.019

Hemakumara, H.M., Chandrapala, L., Moene, A.F., 2003. Evapotranspiration fluxes over mixed vegetation areas measured from large aperture scintillometer. Agricultural Water Management, Agricultural Water Management on Remote Sensing and Water Resources Management 58, 109–122. https://doi.org/10.1016/S0378-3774(02)00131-2

Hu, G., Jia, L., 2015. Monitoring of Evapotranspiration in a Semi-Arid Inland River Basin by Combining Microwave and Optical Remote Sensing Observations. Remote Sensing 7, 3056–3087. https://doi.org/10.3390/rs70303056

Hu, G., Jia, L., Menenti, M., 2015. Comparison of MOD16 and LSA-SAF MSG evapotranspiration products over Europe for 2011. Remote Sensing of Environment 156, 510–526. https://doi.org/10.1016/j.rse.2014.10.017

Hu, X., Shi, L., Lin, L., Zhang, B., Zha, Y., 2018. Optical-based and thermal-based surface conductance and actual evapotranspiration estimation, an evaluation study in the North China Plain. Agricultural and Forest Meteorology 263, 449–464. https://doi.org/10.1016/j.agrformet.2018.09.015

Huete, A., Didan, K., Miura, T., Rodriguez, E.P., Gao, X., Ferreira, L.G., 2002. Overview of the radiometric and biophysical performance of the MODIS vegetation indices. Remote Sensing of Environment, The Moderate Resolution Imaging Spectroradiometer (MODIS): a new generation of Land Surface Monitoring 83, 195–213. https://doi.org/10.1016/S0034-4257(02)00096-2

Hunink, J.E., Contreras, S., Soto-García, M., Martin-Gorriz, B., Martinez-Álvarez, V., Baille, A., 2015. Estimating groundwater use patterns of perennial and seasonal crops in a Mediterranean irrigation scheme, using remote sensing. Agricultural Water Management 162, 47–56. https://doi.org/10.1016/j.agwat.2015.08.003

Hunsaker, D.J., Pinter, P.J., Barnes, E.M., Kimball, B.A., 2003. Estimating cotton evapotranspiration crop coefficients with a multispectral vegetation index. Irrig Sci 22, 95–104. https://doi.org/10.1007/s00271-003-0074-6

Irmak, S., Mutiibwa, D., 2010. On the dynamics of canopy resistance: Generalized linear estimation and relationships with primary micrometeorological variables. Water Resources Research 46. https://doi.org/10.1029/2009WR008484

Jackson, R.D., Moran, M.S., Gay, L.W., Raymond, L.H., 1987. Evaluating evaporation from field crops using airborne radiometry and ground-based meteorological data. Irrig Sci 8, 81–90. https://doi.org/10.1007/BF00259473

Jacquemoud, S., Verhoef, W., Baret, F., Bacour, C., Zarco-Tejada, P.J., Asner, G.P., François, C., Ustin, S.L., 2009. PROSPECT+SAIL models: A review of use for vegetation characterization. Remote Sensing of Environment, Imaging Spectroscopy Special Issue 113, S56–S66. https://doi.org/10.1016/j.rse.2008.01.026

Jarvis, P.G., Monteith, J.L., Weatherley, P.E., 1976. The interpretation of the variations in leaf water potential and stomatal conductance found in canopies in the field. Philosophical Transactions of the Royal Society of London. B, Biological Sciences 273, 593–610. https://doi.org/10.1098/rstb.1976.0035

Jayanthi, H., Neale, C.M.U., Wright, J.L., 2007. Development and validation of canopy reflectance-based crop coefficient for potato. Agricultural Water Management 88, 235–246. https://doi.org/10.1016/j.agwat.2006.10.020

Jia, L., Zheng, C., Hu, G.C., Menenti, M., 2018. 4.03 - Evapotranspiration, in: Liang, S. (Ed.), Comprehensive Remote Sensing. Elsevier, Oxford, pp. 25–50. https://doi.org/10.1016/B978-0-12-409548-9.10353-7

Jung, H.C., Getirana, A., Arsenault, K.R., Holmes, T.R.H., McNally, A., 2019. Uncertainties in Evapotranspiration Estimates over West Africa. Remote Sensing 11, 892. https://doi.org/10.3390/rs11080892

Kadam, S.A., Gorantiwar, S.D., Das, S.N., Joshi, A.K., 2017. Crop Evapotranspiration Estimation for Wheat (Triticum aestivum L.) Using Remote Sensing Data in Semi-Arid Region of Maharashtra. J Indian Soc Remote Sens 45, 297–305. https://doi.org/10.1007/s12524-016-0594-1

Kalma, J.D., McVicar, T.R., McCabe, M.F., 2008. Estimating Land Surface Evaporation: A Review of Methods Using Remotely Sensed Surface Temperature Data. Surv Geophys 29, 421–469. https://doi.org/10.1007/s10712-008-9037-z

Kamble, B., Kilic, A., Hubbard, K., 2013. Estimating Crop Coefficients Using Remote Sensing-Based Vegetation Index. Remote Sensing 5, 1588–1602. https://doi.org/10.3390/rs5041588

Karatas, B.S., Akkuzu, E., Unal, H.B., Asik, S., Avci, M., 2009. Using satellite remote sensing to assess irrigation performance in Water User Associations in the Lower Gediz Basin, Turkey. Agricultural Water Management 96, 982–990. https://doi.org/10.1016/j.agwat.2009.01.010

Kelliher, F.M., Leuning, R., Raupach, M.R., Schulze, E.-D., 1995. Maximum conductances for evaporation from global vegetation types. Agricultural and Forest Meteorology 73, 1–16. https://doi.org/10.1016/0168-1923(94)02178-M

Kullberg, E.G., DeJonge, K.C., Chávez, J.L., 2017. Evaluation of thermal remote sensing indices to estimate crop evapotranspiration coefficients. Agricultural Water Management, Special Issue on Improving Agricultural Water Productivity to Ensure Food Security under Changing Environments Overseen by: Brent Clothier 179, 64–73. https://doi.org/10.1016/j.agwat.2016.07.007

Kustas, W.P., Li, F., Jackson, T.J., Prueger, J.H., MacPherson, J.I., Wolde, M., 2004. Effects of remote sensing pixel resolution on modeled energy flux variability of croplands in Iowa. Remote Sensing of Environment, 2002 Soil Moisture Experiment (SMEX02) 92, 535–547. https://doi.org/10.1016/j.rse.2004.02.020

Kustas, W.P., Norman, J.M., 1996. Use of remote sensing for evapotranspiration monitoring over land surfaces. Hydrological Sciences Journal 41, 495–516. https://doi.org/10.1080/02626669609491522

Lamaddalena, N., Billi, A., Todorovic, M., Hamdy, A., Bogliotti, C., Quarto, A., 2004. Participatory water management in Italy: case study of the consortium" Bonifica della Capitanata". Options Méditerranéennes. Série B: Etudes et Recherches (CIHEAM).

Leuning, R., Zhang, Y.Q., Rajaud, A., Cleugh, H., Tu, K., 2008. A simple surface conductance model to estimate regional evaporation using MODIS leaf area index and the Penman-Monteith equation. Water Resources Research 44. https://doi.org/10.1029/2007WR006562

Li, J., Ju, W., He, W., Wang, H., Zhou, Y., Xu, M., 2019. An Algorithm Differentiating Sunlit and Shaded Leaves for Improving Canopy Conductance and Vapotranspiration Estimates. Journal of Geophysical Research: Biogeosciences 124, 807–824. https://doi.org/10.1029/2018JG004675

Li, Z.-L., Tang, R., Wan, Z., Bi, Y., Zhou, C., Tang, B., Yan, G., Zhang, X., 2009. A Review of Current Methodologies for Regional Evapotranspiration Estimation from Remotely Sensed Data. Sensors 9, 3801–3853. https://doi.org/10.3390/s90503801

Liou, Y.-A., Kar, S.K., 2014. Evapotranspiration Estimation with Remote Sensing and Various Surface Energy Balance Algorithms—A Review. Energies 7, 2821–2849. https://doi.org/10.3390/en7052821

Lu, X., Zhuang, Q., 2010. Evaluating evapotranspiration and water-use efficiency of terrestrial ecosystems in the conterminous United States using MODIS and AmeriFlux data. Remote Sensing of Environment 114, 1924–1939. https://doi.org/10.1016/j.rse.2010.04.001

Main-Knorn, M., Pflug, B., Louis, J., Debaecker, V., Müller-Wilm, U., Gascon, F., 2017. Sen2Cor for Sentinel-2, in: Image and Signal Processing for Remote Sensing XXIII. Presented at the Image and Signal Processing for Remote Sensing XXIII, International Society for Optics and Photonics, p. 1042704. https://doi.org/10.1117/12.2278218

Maselli, F., Battista, P., Chiesi, M., Rapi, B., Angeli, L., Fibbi, L., Magno, R., Gozzini, B., 2020. Use of Sentinel-2 MSI data to monitor crop irrigation in Mediterranean areas. International Journal of Applied Earth Observation and Geoinformation 93, 102216. https://doi.org/10.1016/j.jag.2020.102216

McCabe, M.F., Ershadi, A., Jimenez, C., Miralles, D.G., Michel, D., Wood, E.F., 2016. The GEWEX LandFlux project: evaluation of model evaporation using tower-based and globally gridded forcing data. Geoscientific Model Development 9, 283–305. https://doi.org/10.5194/gmd-9-283-2016

Minacapilli, M., Iovino, M., D'Urso, G., 2008. A distributed agro-hydrological model for irrigation water demand assessment. Agricultural Water Management 95, 123–132. https://doi.org/10.1016/j.agwat.2007.09.008

Mohan, M.M.P., Kanchirapuzha, R., Varma, M.R.R., 2020. Review of approaches for the estimation of sensible heat flux in remote sensing-based evapotranspiration models. JARS 14, 041501. https://doi.org/10.1117/1.JRS.14.041501

Monteith, J., Unsworth, M., 2013. Principles of Environmental Physics: Plants, Animals, and the Atmosphere. Academic Press.

Monteith, J.L., 1965. Evaporation and environment., in: Symposia of the Society for Experimental Biology. pp. 205–234.

Moran, M.S., Clarke, T.R., Inoue, Y., Vidal, A., 1994. Estimating crop water deficit using the relation between surface-air temperature and spectral vegetation index. Remote Sensing of Environment 49, 246–263. https://doi.org/10.1016/0034-4257(94)90020-5

Mu, Q., Heinsch, F.A., Zhao, M., Running, S.W., 2007. Development of a global evapotranspiration algorithm based on MODIS and global meteorology data. Remote Sensing of Environment 111, 519–536. https://doi.org/10.1016/j.rse.2007.04.015

Mu, Q., Zhao, M., Running, S.W., 2011. Improvements to a MODIS global terrestrial evapotranspiration algorithm. Remote Sensing of Environment 115, 1781–1800. https://doi.org/10.1016/j.rse.2011.02.019

Nagler, P.L., Glenn, E.P., Lewis Thompson, T., Huete, A., 2004. Leaf area index and normalized difference vegetation index as predictors of canopy characteristics and light interception by riparian species on the Lower Colorado River. Agricultural and Forest Meteorology 125, 1–17. https://doi.org/10.1016/j.agrformet.2004.03.008

Nagler, P.L., Glenn, E.P., Nguyen, U., Scott, R.L., Doody, T., 2013. Estimating Riparian and Agricultural Actual Evapotranspiration by Reference Evapotranspiration and MODIS Enhanced Vegetation Index. Remote Sensing 5, 3849–3871. https://doi.org/10.3390/rs5083849

Neugebauer, N., Vuolo, F., 2014. Crop Water Requirements on Regional Level using Remote Sensing Data – A Case Study in the Marchfeld Region. Photogrammetrie - Fernerkundung - Geoinformation 2014. https://doi.org/10.1127/1432-8364/2014/0230

Panagos, P., Jones, A., Bosco, C., Kumar, P.S., 2011. European digital archive on soil maps (EuDASM): preserving important soil data for public free access. International Journal of Digital Earth 4, 434–443.

Pasqualotto, N., D'Urso, G., Bolognesi, S.F., Belfiore, O.R., Van Wittenberghe, S., Delegido, J., Pezzola, A., Winschel, C., Moreno, J., 2019. Retrieval of Evapotranspiration from Sentinel-2: Comparison of Vegetation Indices, Semi-Empirical

Models and SNAP Biophysical Processor Approach. Agronomy 9, 663. https://doi.org/10.3390/agronomy9100663

Pereira, L.S., Allen, R.G., Smith, M., Raes, D., 2015. Crop evapotranspiration estimation with FAO56: Past and future. Agricultural Water Management, Agricultural Water Management: Priorities and Challenges 147, 4–20. https://doi.org/10.1016/j.agwat.2014.07.031

Pereira, L.S., Paredes, P., Melton, F., Johnson, L., Wang, T., López-Urrea, R., Cancela, J.J., Allen, R.G., 2020. Prediction of crop coefficients from fraction of ground cover and height. Background and validation using ground and remote sensing data. Agricultural Water Management 241, 106197. https://doi.org/10.1016/j.agwat.2020.106197

Piedelobo, L., Ortega-Terol, D., Del Pozo, S., Hernández-López, D., Ballesteros, R., Moreno, M.A., Molina, J.-L., González-Aguilera, D., 2018. HidroMap: A New Tool for Irrigation Monitoring and Management Using Free Satellite Imagery. ISPRS International Journal of Geo-Information 7, 220. https://doi.org/10.3390/ijgi7060220

Pôças, I., Calera, A., Campos, I., Cunha, M., 2020. Remote sensing for estimating and mapping single and basal crop coefficientes: A review on spectral vegetation indices approaches. Agricultural Water Management 233, 106081. https://doi.org/10.1016/j.agwat.2020.106081

Priestley, C.H.B., Taylor, R.J., 1972. On the assessment of surface heat flux and evaporation using large-scale parameters. Monthly weather review 100, 81–92.

Raine, S.R., Meyer, W.S., Rassam, D.W., Hutson, J.L., Cook, F.J., 2007. Soil–water and solute movement under precision irrigation: knowledge gaps for managing sustainable root zones. Irrig Sci 26, 91–100. https://doi.org/10.1007/s00271-007-0075-y

Reicosky, D.C., Peters, D.B., 1977. A Portable Chamber for Rapid Evapotranspiration Measurements on Field Plots1. Agronomy Journal 69, 729–732. https://doi.org/10.2134/agronj1977.00021962006900040051x

Rodriguez-Iturbe, I., 2000. Ecohydrology: A hydrologic perspective of climate-soil-vegetation dynamies. Water Resources Research 36, 3–9. https://doi.org/10.1029/1999WR900210

Rouse, J.W., 1974. Monitoring vegetation systems in the Great Plains with ERTS.

Sanchez, N., Martínez-Fernández, J., Calera, A., Torres, E., Pérez-Gutiérrez, C., 2010. Combining remote sensing and in situ soil moisture data for the application and validation of a distributed water balance model (HIDROMORE). Agricultural Water Management 98, 69–78. https://doi.org/10.1016/j.agwat.2010.07.014

Segarra, J., Buchaillot, M.L., Araus, J.L., Kefauver, S.C., 2020. Remote Sensing for Precision Agriculture: Sentinel-2 Improved Features and Applications. Agronomy 10, 641. https://doi.org/10.3390/agronomy10050641

Sellers, P.J., Berry, J.A., Collatz, G.J., Field, C.B., Hall, F.G., 1992. Canopy reflectance, photosynthesis, and transpiration. III. A reanalysis using improved leaf models and a new canopy integration scheme. Remote Sensing of Environment 42, 187–216. https://doi.org/10.1016/0034-4257(92)90102-P

Shuttleworth, W.J., 2006. Towards one-step estimation of crop water requirements. Transactions of the ASABE 49, 925–935.

Shuttleworth, W.J., Gurney, R.J., 1990. The theoretical relationship between foliage temperature and canopy resistance in sparse crops. Quarterly Journal of the Royal Meteorological Society 116, 497–519. https://doi.org/10.1002/qj.49711649213

Shuttleworth, W.J., Wallace, J.S., 1985. Evaporation from sparse crops-an energy combination theory. Quarterly Journal of the Royal Meteorological Society 111, 839–855. https://doi.org/10.1002/qj.49711146910

Smith, M., Nations, F. and A.O. of the U., 1992. CROPWAT: A Computer Program for Irrigation Planning and Management. Food & Agriculture Org.

Smith, R.C.G., Barrs, H.D., Fischer, R.A., 1988. Inferring stomatal resistance of sparse crops from infrared measurements of foliage temperature. Agricultural and Forest Meteorology 42, 183–198. https://doi.org/10.1016/0168-1923(88)90076-7

Steduto, P., Hsiao, T.C., Fereres, E., Raes, D., 2012. Crop yield response to water. FAO Irrigation and Drainage Paper.

Steinberg, S.L., Bavel, C.H.M.V., McFarland, M.J., 1990. Improved Sap Flow Gauge for Woody and Herbaceous Plants. Agronomy Journal 82, 851–854. https://doi.org/10.2134/agronj1990.00021962008200040037x

Thenkabail, P., 2015. Remote sensing of land resources: monitoring, modeling, and mapping: Advances of last 50 years and a vision for the future, Chapter 26.

Toulios, L., Spiliotopoulos, M., Papadavid, G., Loukas, A., 2020. Observation Methods and Model Approaches for Estimating Regional Crop Evapotranspiration and Yield in Agro-Landscapes: A Literature Review, in: Mirschel, W., Terleev, V.V., Wenkel, K.-O. (Eds.), Landscape Modelling and Decision Support, Innovations in Landscape Research. Springer International Publishing, Cham, pp. 79–100. https://doi.org/10.1007/978-3-030-37421-1_5

Toureiro, C., Serralheiro, R., Shahidian, S., Sousa, A., 2017. Irrigation management with remote sensing: Evaluating irrigation requirement for maize under Mediterranean climate condition. Agricultural Water Management 184, 211–220. https://doi.org/10.1016/j.agwat.2016.02.010

Ursitti, A., Giannoccaro, G., Prosperi, M., De Meo, E., De Gennaro, B.C., 2018. The Magnitude and Cost of Groundwater Metering and Control in Agriculture. Water 10, 344. https://doi.org/10.3390/w10030344

van Dijk, A.I.J.M., Renzullo, L.J., 2011. Water resource monitoring systems and the role of satellite observations. Hydrology and Earth System Sciences 15, 39–55. https://doi.org/10.5194/hess-15-39-2011

Vanino, S., Nino, P., De Michele, C., Falanga Bolognesi, S., Pulighe, G., 2015a. Earth Observation for Improving Irrigation Water Management: A Case-study from Apulia Region in Italy. Agriculture and Agricultural Science Procedia Volume 4, 99–107. https://doi.org/10.1016/j.aaspro.2015.03.012

Vanino, S., Nino, P., De Michele, C., Falanga Bolognesi, S., D'Urso, G., Di Bene, C., Pennelli, B., Vuolo, F., Farina, R., Pulighe, G., Napoli, R., 2018. Capability of Sentinel-2 data for estimating maximum evapotranspiration and irrigation

requirements for tomato crop in Central Italy. Remote Sensing of Environment 215, 452–470. https://doi.org/10.1016/j.rse.2018.06.035

Vanino, S., Pulighe, G., Nino, P., De Michele, C., Bolognesi, S.F., D'Urso, G., 2015b. Estimation of Evapotranspiration and Crop Coefficients of Tendone Vineyards Using Multi-Sensor Remote Sensing Data in a Mediterranean Environment. Remote Sensing 7, 14708–14730. https://doi.org/10.3390/rs71114708

Verstraeten, W.W., Veroustraete, F., Feyen, J., 2008. Assessment of Evapotranspiration and Soil Moisture Content Across Different Scales of Observation. Sensors 8, 70–117. https://doi.org/10.3390/s8010070

Vuolo, F., D'Urso, G., De Michele, C., Bianchi, B., Cutting, M., 2015. Satellite-based irrigation advisory services: A common tool for different experiences from Europe to Australia. Agricultural Water Management, Agricultural Water Management: Priorities and Challenges 147, 82–95. https://doi.org/10.1016/j.agwat.2014.08.004

Wang, H., Guan, H., Deng, Z., Simmons, C.T., 2014. Optimization of canopy conductance models from concurrent measurements of sap flow and stem water potential on Drooping Sheoak in South Australia. Water Resources Research 50, 6154–6167. https://doi.org/10.1002/2013WR014818

Wiernga, J., 1993. Representative roughness parameters for homogeneous terrain. Boundary-Layer Meteorol 63, 323–363. https://doi.org/10.1007/BF00705357

Xu, C.-Y., Singh, V.P., 2005. Evaluation of three complementary relationship evapotranspiration models by water balance approach to estimate actual regional evapotranspiration in different climatic regions. Journal of Hydrology 308, 105–121. https://doi.org/10.1016/j.jhydrol.2004.10.024

Yebra, M., Van Dijk, A., Leuning, R., Huete, A., Guerschman, J.P., 2013. Evaluation of optical remote sensing to estimate actual evapotranspiration and canopy conductance. Remote Sensing of Environment 129, 250–261. https://doi.org/10.1016/j.rse.2012.11.004

Yuan, W., Liu, S., Yu, G., Bonnefond, J.-M., Chen, J., Davis, K., Desai, A.R., Goldstein, A.H., Gianelle, D., Rossi, F., Suyker, A.E., Verma, S.B., 2010. Global estimates

of evapotranspiration and gross primary production based on MODIS and global meteorology data. Remote Sensing of Environment 114, 1416–1431. https://doi.org/10.1016/j.rse.2010.01.022

Zaccaria, D., Lamaddalena, N., Neale, C.M.U., Merkley, G.P., Palmisano, N., Passarella, G., 2013. Simulation of peak-demand hydrographs in pressurized irrigation delivery systems using a deterministic–stochastic combined model. Part I: model development. Irrig Sci 31, 209–224. https://doi.org/10.1007/s00271-011-0317-x

Zhou, M.C., Ishidaira, H., Hapuarachchi, H.P., Magome, J., Kiem, A.S., Takeuchi, K., 2006. Estimating potential evapotranspiration using Shuttleworth–Wallace model and NOAA-AVHRR NDVI data to feed a distributed hydrological model over the Mekong River basin. Journal of Hydrology 327, 151–173. https://doi.org/10.1016/j.jhydrol.2005.11.013

Annex 1. List of Sentinel-2 images selected for the "Zona Alta" test site

DOY	Date	Satellite	2017	2018	2019
63	4-Mar	S2B			x
68	9-Mar	S2A			x
83	24-Mar	S2B			x
88	1-Mar	S2A	x		
98	8-Apr	S2A	x	x	
103	13-Apr	S2B		x	
108	18-Apr	S2A			x
113	23-Apr	S2B		x	
133	13-May	S2B		x	
138	18-May	S2A	x		
153	2-Jun	S2B		x	
158	7-Jun	S2A	x		x
168	17-Jun	S2A			x
173	22-Jun	S2B		x	
178	27-Jun	S2A			x
183	2-Jul	S2B		x	x
188	7-Jul	S2A	x		x
193	12-Jul	S2B		x	x
198	17-Jul	S2A	x		
203	22-Jul	S2B		x	x
208	27-Jul	S2A	x	x	x
213	1-Aug	S2B		x	x
218	6-Aug	S2A	x		x
223	11-Aug	S2B		x	x
228	16-Aug	S2A	x		x
233	21-Aug	S2B		x	x
238	26-Aug	S2A	x		
243	31-Aug	S2B			x
248	5-Sep	S2A	x	x	x
258	15-Sep	S2A	x	x	
268	25-Sep	S2A		x	x
273	30-Sep	S2B		x	X
278	5-Oct	S2A	x		
283	10-Oct	S2B		x	x
288	15-Oct	S2A	x		x
293	20-Oct	S2B		x	
298	25-Oct	S2A		x	x
303	30-Oct	S2B		x	
N. images			14	21	24

Annex 2. List of Sentinel-2 images selected for the "Canal del Zujar" test site

Level	DOY	Date
L1C	12	12-Jan-2017
	52	21-Feb-2017
	92	2-Apr-2017
L2A	102	12-Apr-2017
	122	2-May-2017
	142	22-May-2017
	152	1-Jun-2017
	172	21-Jun-2017
	182	1-Jul-2017
	192	11-Jul-2017
	202	21-Jul-2017
	212	31-Jul-2017
	232	20-Aug-2017
	242	30-Aug-2017
	252	9-Sep-2017
	262	19-Sep-2017
	272	29-Sep-2017
	282	9-Oct-2017
	302	29-Oct-2017
	312	8-Nov-2017
	322	18-Nov-2017
	352	18-Dec-2017
	357	23-Dec-2017
	N. images	23

Annex 3. Soil water balance at plot scale for the "Sinistra Ofanto" case study

In the present Annex are reported the Soil Water balance outputs at the hydrant scale for the "Sinistra Ofanto" case study. Over the same plot are reported the Soil Water Content (SWC) in the soil simulated under 3 scenarios (as reported in the Figure below):

1. Scenario without irrigation (reported with the red line).
2. Scenario with the Irrigation really applied by the farmers, as metered by the Consortium (blue line, IWA).
3. Scenario with the Irrigation really applied by the farmers, as simulated by the irrigation module of the SWB adopted (green line, IWE).

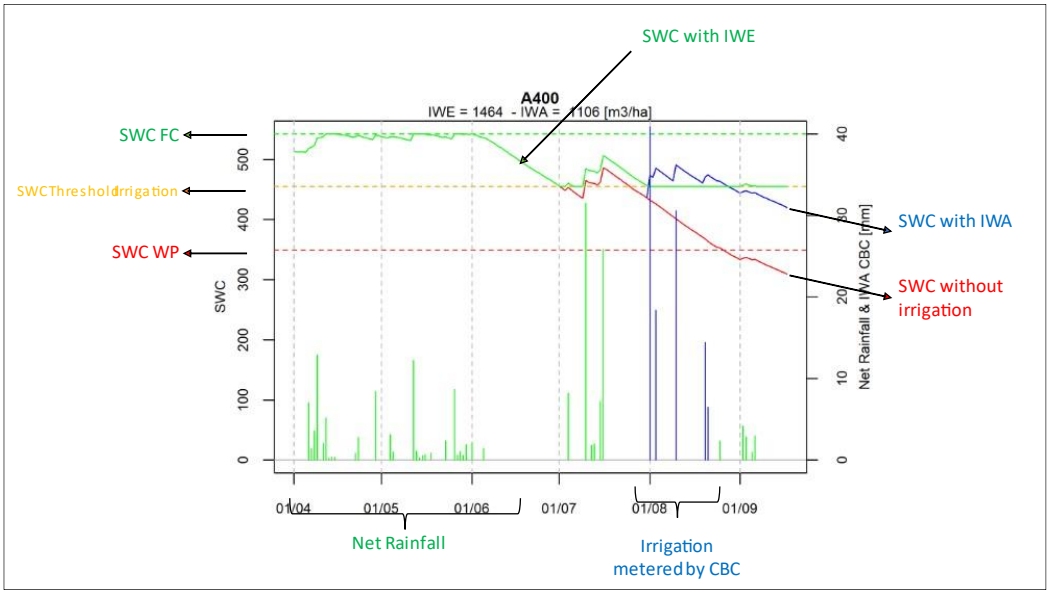

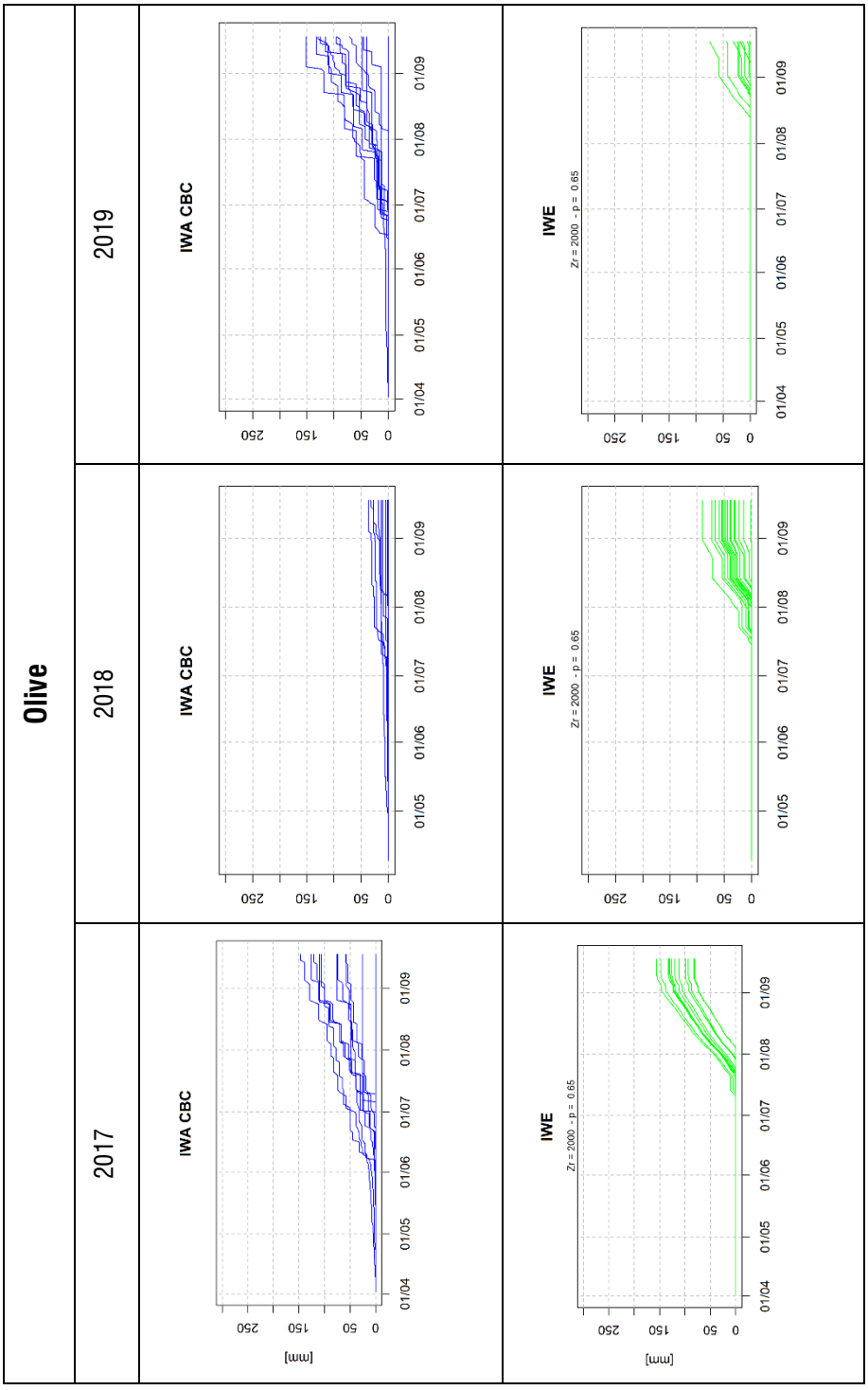
Olive
2017
2018
2019
IWA CBC
IWE
Zr = 2000 - p = 0.65
[mm]
0
50
150
250
01/04
01/05
01/06
01/07
01/08
01/09

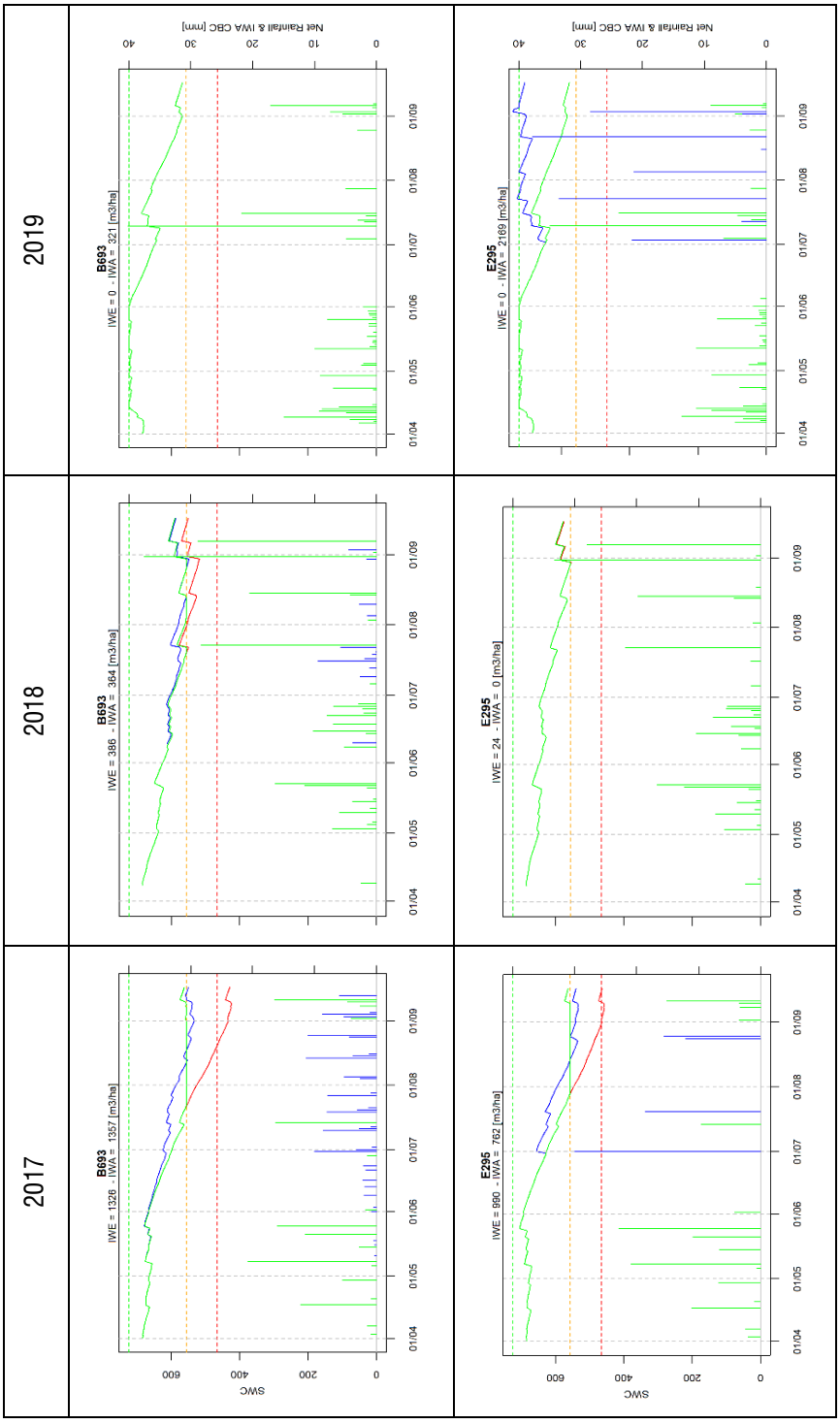
2017
2018
2019
B693
IWE = 1326 - IWA = 1357 [m3/ha]
B693
IWE = 386 - IWA = 364 [m3/ha]
B693
IWE = 0 - IWA = 321 [m3/ha]
E295
IWE = 990 - IWA = 762 [m3/ha]
E295
IWE = 24 - IWA = 0 [m3/ha]
E295
IWE = 0 - IWA = 2169 [m3/ha]
SWC
Net Rainfall & IWA CBC [mm]
01/04
01/05
01/06
01/07
01/08
01/09

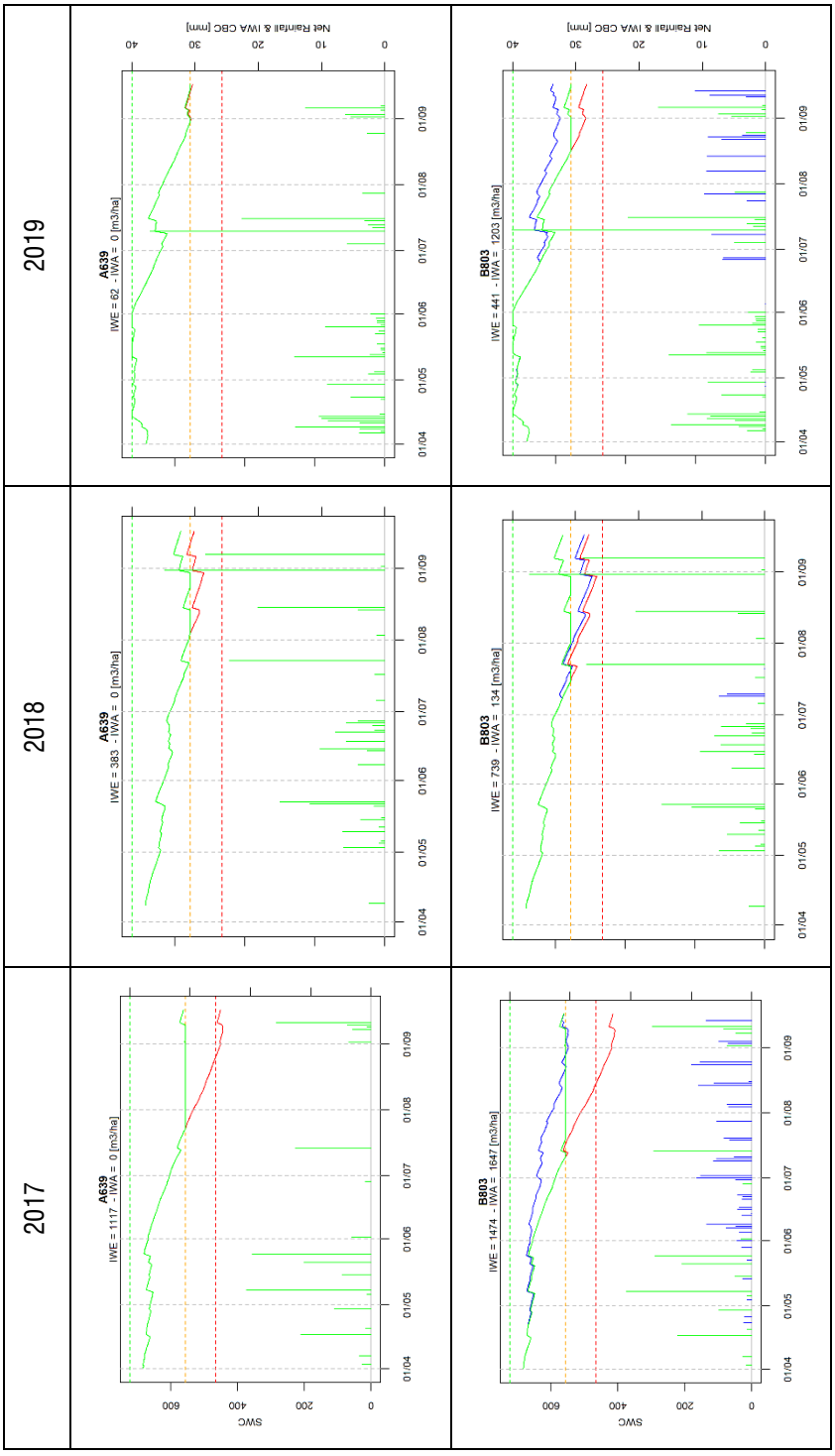
2019
2018
2017
A639
IWE = 62 - IWA = 0 [m3/ha]
B803
IWE = 441 - IWA = 1203 [m3/ha]
A639
IWE = 383 - IWA = 0 [m3/ha]
B803
IWE = 739 - IWA = 134 [m3/ha]
A639
IWE = 1117 - IWA = 0 [m3/ha]
B803
IWE = 1474 - IWA = 1647 [m3/ha]
Net Rainfall & IWA CBC [mm]
SWC
01/04
01/05
01/06
01/07
01/08
01/09

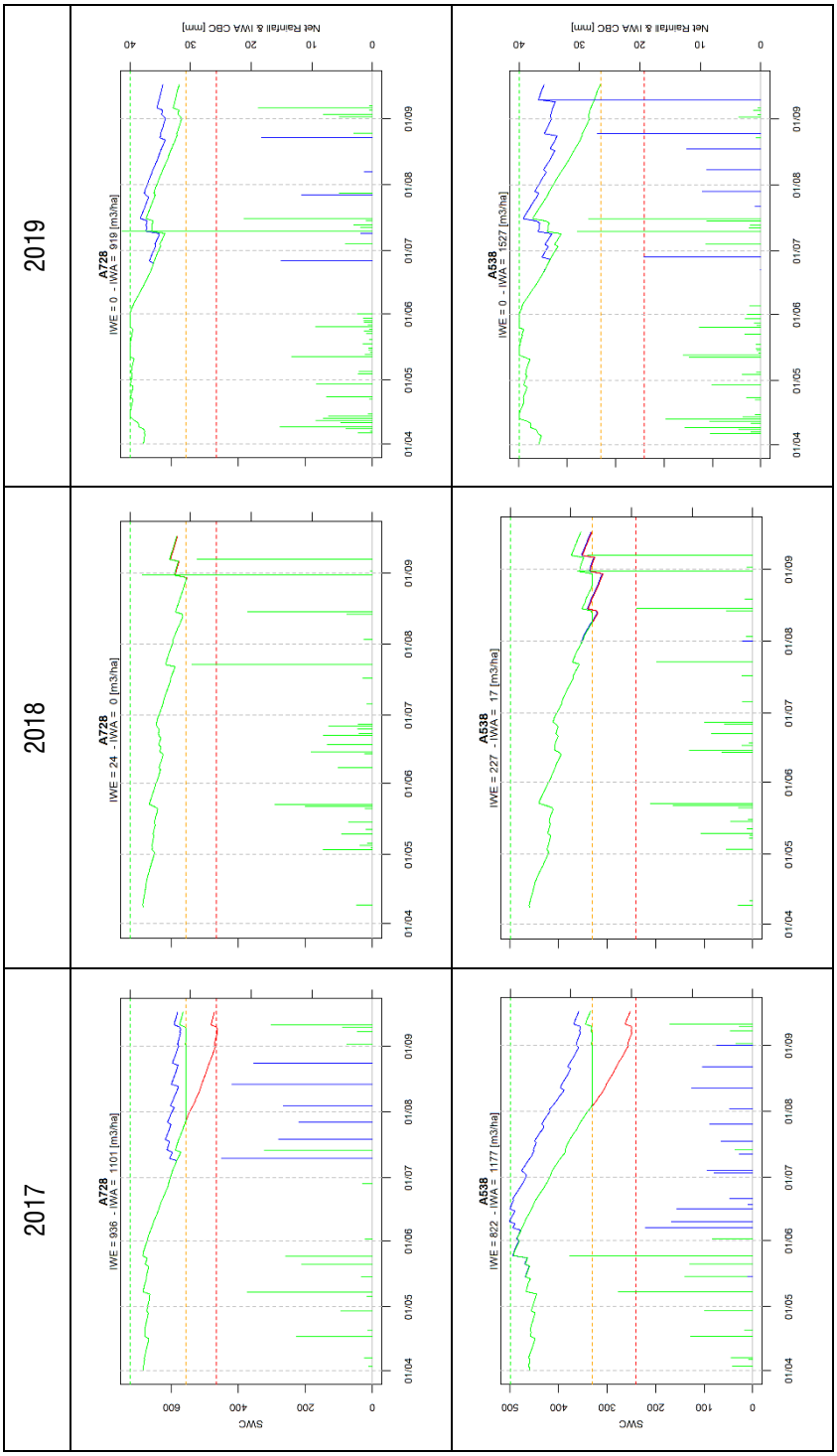
2017
2018
2019
A728
IWE = 936 - IWA = 1101 [m3/ha]
A728
IWE = 24 - IWA = 0 [m3/ha]
A728
IWE = 0 - IWA = 919 [m3/ha]
A538
IWE = 822 - IWA = 1177 [m3/ha]
A538
IWE = 227 - IWA = 17 [m3/ha]
A538
IWE = 0 - IWA = 1527 [m3/ha]
SWC
Net Rainfall & IWA CBC [mm]
01/04
01/05
01/06
01/07
01/08
01/09

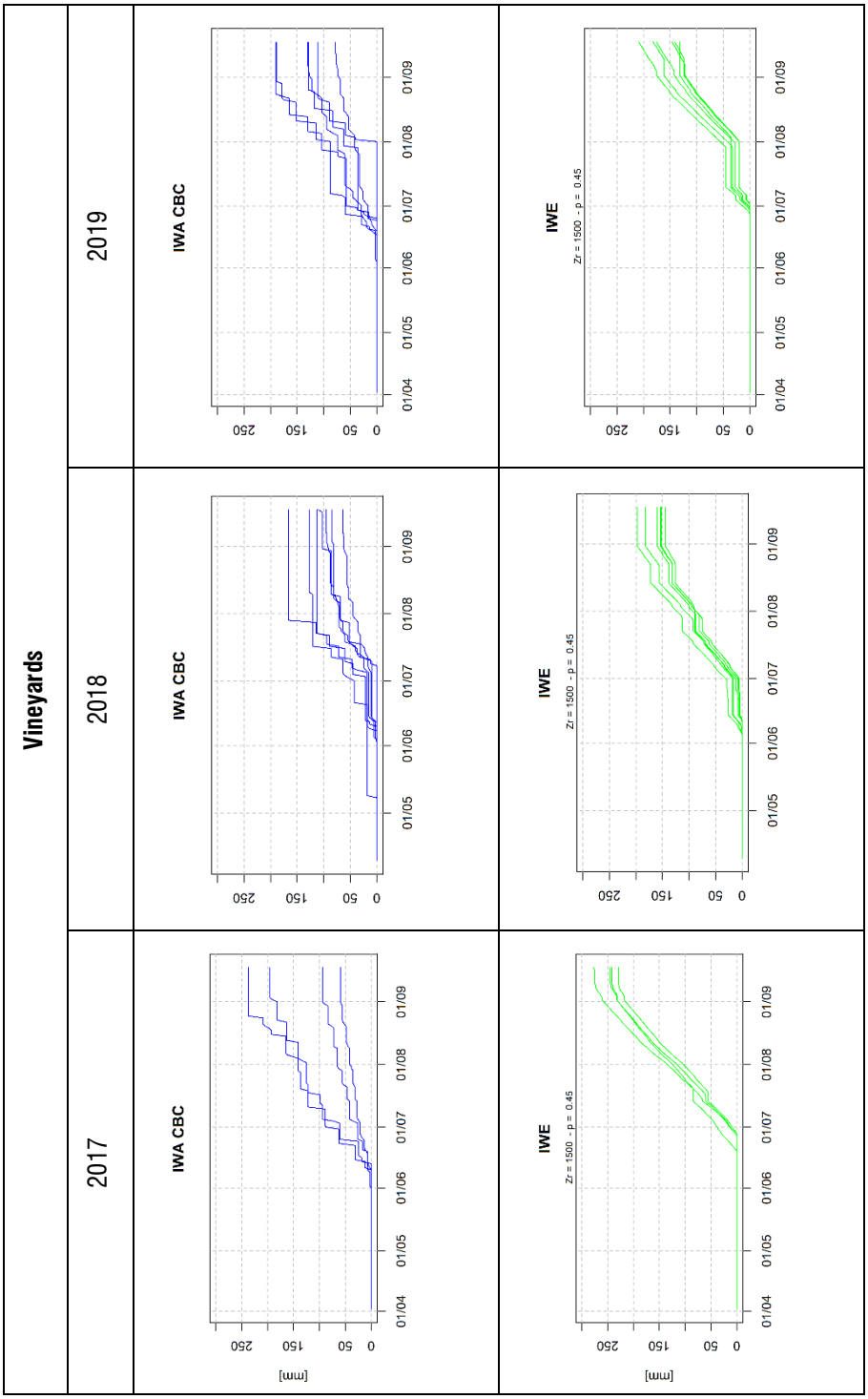
Vineyards
2017
2018
2019
IWA CBC
IWE
Zr = 1500 - p = 0.45
[mm]
0
50
150
250
01/04
01/05
01/06
01/07
01/08
01/09

2017
2018
2019
A735
IWE = 2418 - IWA = 2372 [m3/ha]
A735
IWE = 1448 - IWA = 1106 [m3/ha]
A735
IWE = 1318 - IWA = 1907 [m3/ha]
A400
IWE = 1525 - IWA = 1130 [m3/ha]
A400
IWE = 1464 - IWA = 1106 [m3/ha]
SWC
Net Rainfall & IWA CBC [mm]
01/04
01/05
01/06
01/07
01/08
01/09
0
100
200
300
400
500
10
20
30
40

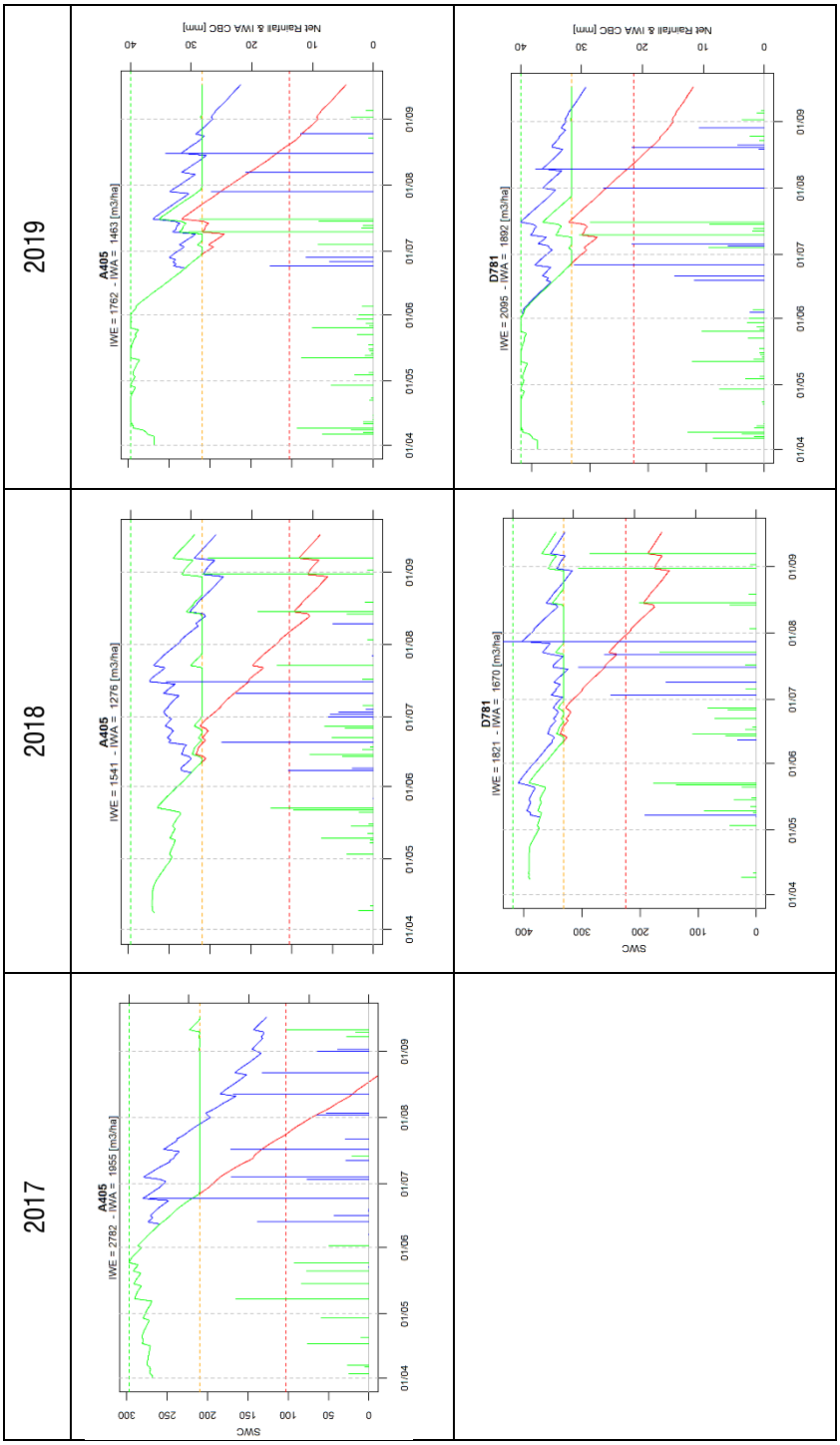
2019
2018
2017
A405
IWE = 1762 - IWA = 1483 [m3/ha]
D781
IWE = 2095 - IWA = 1892 [m3/ha]
A405
IWE = 1541 - IWA = 1276 [m3/ha]
D781
IWE = 1821 - IWA = 1670 [m3/ha]
A405
IWE = 2782 - IWA = 1955 [m3/ha]
Net Rainfall & IWA CBC [mm]
SWC
01/04
01/05
01/06
01/07
01/08
01/09